Protective and toxic antibodies in prion diseases

Dissertation

zur

Erlangung der naturwissenschaftlichen Doktorwürde
(Dr. sc. nat.)

vorgelegt der

Mathematisch-naturwissenschaftlichen Fakultät

der

Universität Zürich

von

Karl Joachim Frontzek

aus

Deutschland

Promotionskommission

Prof. Dr. Adriano Aguzzi (Vorsitz und Leitung der Dissertation)

Prof. Dr. Jean-Marc Fritschy

Prof. Dr. Fritjof Helmchen

Prof. Dr. Magdalini Polymenidou

Zürich, 2017

Table of contents

Summary

Prion diseases are as yet inexorably fatal diseases affecting the nervous system of humans and animals. They rely on the seeded propagation of the “scrapie” form of the prion protein (PrP^{Sc}) into its cellular counter-part PrP^{C}. PrP^{C} is indispensible for prion disease as animals lacking PrP^{C} do not succumb to the disease. Microscopically, prion diseases or transmissible spongiform encephalopathies (TSEs) are characterized by rapid neurodegeneration accompanied by astrogliosis, microglial activation, spongiform change and deposits of PrP^{Sc}. Recent research has exposed the dual nature of PrP^{C}: antibodies targeting the C-terminal, globular domain of PrP^{C} (PrP^{C}-GD) exert neurotoxic effects resembling genuine prion diseases. Antibodies targeting the N-terminal domain (denoted “flexible tail”, PrP^{C}-FT), especially those targeting the octapeptide region of PrP^{C} (PrP^{C}-OR), or interstitial deletions of PrP^{C}-OR are protective against both toxic PrP^{C}-GD antibodies and prions, suggesting an effector function of the N-terminus. However, the precise molecular mechanisms underlying PrP^{C}-mediated neurotoxicity remain largely unclear.

The aims of the experimental work presented in this thesis are threefold. My first goal was to establish a robust experimental assay to measure neurotoxicity. Current methodologies mainly rely on *post hoc* immunohistochemistry with neuronal markers resulting in large read-out variability that can mask experimental effects. Accordingly, I used organotypic slices from transgenic mice expressing fluorescence in neuronal subsets that were subjected to sequential confocal imaging *in vivo*. By taking into account baseline differences in slice size and viability, I was able to decrease the read-out variability derived from conventionally used *post hoc* analyses. Sequential time-lapse *in vivo* imaging was successfully employed in the neurotoxicity assessment of anti-prion compounds, which facilitated plotting precise dose-response curves that would not have been possible by traditional methods.

The second aim was to investigate the mechanisms of the neurotoxic, monoclonal PrP^{C}-GD antibody POM1 that recapitulates the key features of genuine prion diseases such as neuronal cells loss, astrogliosis and microglial activation. It is not known, however, whether

POM1 neurotoxicity is accompanied by the generation of prions. In fact, passaging of homogenates of POM1-treated cerebellar organotypic slice cultures (COCS) into the brains of PrP^C-overexpressing *Tga*20 indicator mice did not cause prion disease whereas inoculation of *Tga*20 mice with *bona fide* prions caused terminal disease after a few weeks. Histological examination of POM1-COCS inoculated mice did not show the typical signs of prion disease, nor did a real-time quaking induced conversion (RT-QuIC) assay induce the seeding of aggregates, leaving me to conclude that POM1 acts downstream of prion replication. In a next step, I aimed to determine whether simultaneous stabilization of both PrP^C-FT and PrP^C-GD through the bispecific, POM1/POM2-antibody LVp12 would be effective against prion disease. LVp12 exerted neuroprotective effects in prion-infected COCS even after first signs of prion pathology were detectable. In contrast, POM2 alone was only beneficial to neurons when given directly after prion inoculation, but not when given at later stages. To dissect the underlying molecular mechanisms of POM1-induced toxicity, I studied 11 different, mutated single chain variable fragments (scFv) of POM1 derived from alanine scanning of POM1 in complex with PrP^C. In this experiment, scFvPOM1^{Y57A} and scFvPOM1^{Y104A} showed neuroprotection in prion-infected COCS and further attenuated the activation of prion-induced toxic pathways such as the unfolded protein response and microglial activation. Molecular dynamics (MD) simulations showed that relaxation of the rigid loop of the prion protein upon wild-type POM1 binding was responsible for the induction of toxicity. These findings suggested that scFvPOM1^{Y57A} and scFvPOM1^{Y104A} represent dominant-negative immunoreagents of PrP^C.

In the final step, I addressed the effects of naturally occuring anti-PrP autoantibodies in human patients. Antibodies derived from human subjects frequently show superior safety profiles and affinity maturation compared to “humanized” hybridomas or synthetic libraries. On the other hand, patients suffering from idiopathic neurological disease have a dismal prognosis due to prolonged diagnostic work-up and delayed therapy. Considering both the detrimental effects of anti-PrP^C-GD targeting antibodies and the beneficial effects of anti-PrP^C-FT antibodies, I opted to isolate high-affinity, therapeutic anti-PrP-autoantibodies from humans without neurological disease and to screen human patients with neurological diseases of

unknown origin for the presence of toxic anti-PrP-autoantibodies. I was able to identify patients with highly anti-PrP reactive blood samples and to establish a bait-gated fluorescent-activated cell sorting (FACS) protocol for subsequent single cell sequencing to clone the variable heavy and light chain immunoglobulin genes from cognate memory B-cells. Furthermore, I identified that the blood of patients suffering from chronic demyelinating inflammatory polyneuropathy (CIDP) harbored a heightened anti-PrP response. As PrP deficient mice are prone to develop chronic demyelinating polyneuropathy, one might speculate that depletion of endogenous PrP in human CIDP patients through anti-PrP autoantibodies would lead to the observed nerve pathology.

The elucidation of the mechanisms of prion toxicity and the development of new and potentially therapeutic compounds against prion disease will open new paths to create effective therapy against this still fatal disease.

Zusammenfassung

Die Fehlfaltung des zellulären Prionproteins PrPC führt zu infektiösen und bis jetzt unheilbaren Hirnerkrankungen, sogenannten Prionenkrankheiten. Die Ursache von Prionenerkrankungen ist die Übertragung des pathologischen, „scrapie“ Prionproteins PrP^{Sc} auf das zelluläre Prionprotein PrP^{C}. PrP^{C} ist notwendig für die Ausbreitung von Prionenerkrankungen, da Tiere ohne PrP^{C} gegen Prionenerkrkanungen resistent sind. Mikrokopisch zeigen sich in Prionenerkrankungen oder transmissiblen, spongiformen Enzephalopathien (TSEs) charakteristischerweise spongiforme Veränderungen, Nervenzellverlust, Astro- und Mikrogliose, sowie pathologische Ablagerungen von PrP^{Sc}. Die Gruppe von A. Aguzzi hat den zweiseitigen Mechanismus des Prionproteins entdeckt – Antikörper gegen den flexiblen Schweif (*flexible tail*, PrP^{C}-FT) schützen vor Prionenerkrankungen, wohingegen solche gegen die globuläre Domäne (*globular domain,* PrP^{C}-GD) toxisch sind. Diese Ergebnisse suggerieren PrP^{C}-FT als Effektor von PrP^{C}-GD induzierter Toxizität, wobei die genauen, molekularen Ursachen weitgehend ungeklärt sind.

Die wissenschaftlichen Ziele dieser Arbeit bestehen aus drei Teilen. Mein erstes Ziel war es, eine robuste Methode zur Messung von Nervenzellverlust in Prionenerkrankungen zu entwickeln. Derzeitig verwendete Methoden nutzen vor allem *post hoc* Immunhistochemie mit neuronalen Markern, die in einer grossen Varianz resultieren, welche die experimentell gewonnenen Erkenntisse maskieren kann. Um eine spezifischere Messung zu erhalten, habe ich *in vivo* Konfokalmikroskopie in organspezifischen Scheibenkulturen von transgenen Mäusen, welche ein fluoreszentes Protein in einzelnen Nervenzellgruppen exprimieren, angewendet. Indem ich individuelle Unterschiede bei Beginn der Messungen, wie unterschiedliche Scheibengrösse und Viabilität, mit in die Auswertung eingeschlossen habe, konnte ich mit meiner neu entwickelten Methode die bisher beobachtete Variabilität signifikant vermindern.

Mein zweites Ziel war es, die Mechanismen des monoklonalen anti-PrP^{C}-GD Antikörpers POM1 genauer zu untersuchen. POM1 rekapituliert die histopathologischen Charakteristika von Prionenerkrankungen, jedoch ist unklar, ob Behandlung von Hirngewebe

mit POM1 auch zu Infektiosität führt. Ich habe Kleinhirnscheiben, welche mit POM1 behandelt wurden, in Gehirne von PrP^C-überexprimierenden *Tga*20 Mäuse injiziert. Während *Tga*20 Mäuse, welche mit *bona fide* Prionen infiziert wurden, innerhalb weniger Wochen charakteristische Zeichen der Prionenkrankheit entwickelten, blieben mit POM1-behandeltem Gewebe injizierte Mäuse über 200 Tage symptomfrei. Dies lies mich schlussfolgern, dass die Toxizität von POM1 unterhalb der Prionenreplikation agiert. Um die genauen Mechanismen von POM1-induzierter Toxizität zu untersuchen, habe ich genetisch modifizierte Varianten von POM1, sowie dessen Bindungsstellen an PrP^C untersucht. *Ex vivo* Versuche an Prionen-infizierten, organspezifischen Hirnscheiben zeigten, dass die selektive Mutagenese von einzelnen Bindungsresiduen der POM1-PrP^C Interaktion zur dominant-negativen Immunotherapie gegen Prionenerkankungen führte. Diese Therapie agierte unterhalb der Prionenreplikation und verbesserte neurotoxische Kaskaden, welche durch Prionenerkrankungen ausgelöst wurden.

In einem dritten Teil habe ich die Folgen und die Nutzbarkeit von humanen Autoantikörpern in ausgewählten Erkrankungen gegen das Prionenprotein untersucht. Patienten mit Mutationen im PrP^C-kodierenden Gen *PRNP* leiden an einer fatalen neurologischen Erkrankung, jedoch werden *PRNP*-Mutationsträger erst im hohen Alter klinisch manifest, obwohl sie ihr Leben lang ein krankheitsassoziertes Protein exprimieren. Dies ist hinweisend auf protektive Faktoren und ich glaube, diese Faktoren sind anti-PrP^C Autoantikörper. Sofern vorhanden, plane ich protektive, humane Autoantikörper aus Gedächtnis B-Zellen von *PRNP* Mutationsträgern zu klonieren und als mögiches, therapeutisches Agens gegen Prionenkrankheiten einzusetzen. Patienten mit chronisch-inflammatorischer, demyelinisierender Polyneuropathie (CIDP) leiden an einer bis jetzt ungeklärten Nervenerkrankung. Das Fehlen des Prionproteins in Mäusen führt zu einer chronisch-demyelinisierenden Erkrankung und ist heutzutage die einzige, mehrfach bestätige, physiologische Funktion von PrP^C. Erhöhte Autoantikörper gegen PrP^C könnten endogenes PrP^C abpuffern und einen „quasi-knock out“ hervorrufen. Ich habe eine sensitive und reliable Methode entwickelt, mit der sich humane Autoantikörper gegen PrP^C detektieren und aus

Gedächtnis B-Zellen extrahieren lassen. *PRNP*-Mutationsträger weisen keine signifikant gesteigerte Prävalenz von anti-PrP^C Autoantikörpern im Vergleich zu gesunden Familienmitgliedern auf. Interessanterweise lässt sich im Alter von *PRNP*-Mutationsträgern eine verminderte Anzahl von anti-PrP^C Autoantikörpern feststellen, welche nicht in gesunden Familienmitgliedern auftritt. Diese könnte eine Erklärung der späten, klinischen Manifestation von *PRNP*-Mutationsträgern liefern. Des Weiteren zeigten CIDP Patienten eine kräftige und spezifische Autoantikörperreaktion gegen PrP^C, welche das immunologische Substrat der chronischen Demyelinisierung liefern kann.

Abbreviations

+/-	In the presence and in the absence of
aa	Amino acid
AAV	Adeno-associated virus
AD	Alzheimer's disease
AICc	Akaike Information Criteria values adjusted for finite sample sizes
APECED	Autoimmune Polyendocrinopathy-Candidiasis-Ectodermal Dystrophy
APP	Amyloid precursor protein
APPPS1	Double transgenic mice expressing mutated APP and PS1
APS	Autoimmune Polyendocrine Syndrome
AscA	Ascorbic acid
BLI	Bioluminiscence imaging
bPrP^{C}	bovine PrP^{C}
BSA	Bovine serum albumin
BSE	Bovine spongiforme encephalopathy
BV421-SA	BrilliantViolet421-Streptavidin
Ca^{2+}	Calcium ions
cAMP	Cyclic adenosine monophosphate
CC2	Charged cluster 2 region of PrP^{C}
CDP	Chronic demyelinating polyneuropathy
CGL	Cerebellar granule layer
CHO	Chinese hamster ovary
CIDP	Chronic inflammatory demyelinating polyneuropathy
CJD	Creutzfeldt-Jakob's disease (umbrella term for sCJD, vCJD, iCJD, gCJD)
CLSM	Confocal laser scanning microscopy
COCS	Cerebellar organotypic slice cultures
CRISPR	Clustered Regularly Interspaced Short Palindromic Repeats
DIV	days *in vitro*
DNA	Deoxyribonucleic acid
dpe	Days post-exposure
dpi	Days post-infection
Dpl	Doppel
DTT	Dithiothreitol
Edbg	*Prnp*$^{0/0}$ mouse Edinburgh (Manson et al. 1994)
EDTA	Ethylenediaminetetraacetic acid
eGFP	Enhanced GFP
ELISA	Enzyme-linked immunosorbent assay
ER	Endoplasmic reticulum
FACS	Fluorescence-activated cell sorting
FBS	Fetal bovine serum
FDG-PET	F-fluorodeoxygluose positron emission tomography
FFI	Familial fatal insomnia
GBS	Guillain-Barré Syndrome
GdnHCl	Guanidine hydrochloride
GFAP	Glial fibrillary acidic protein
GFP	Green fluorescent protein
gCJD	Genetic Creutzfeldt-Jakob's disease
GPCR	G-protein coupled receptor
gPrD	Genetic prion disease (umbrella term for gCJD, FFI, GSS)
GSS	Gerstmann-Sträussler-Scheinker disease
H&E	Hematoxylin and eosin
H-bond	Hydrogen bond
HD	Huntington's disease

hIgG	Human IgG
HOCS	Hippocampal organotypic slice cultures
$hPrP\text{-}AT_{biotin}$	biotinylated human PrP-Avitag
$hPrP^{C}$	Human cellular prion protein
HRP	Horseradish peroxidase
iCJD	Iatrogenic Creutzfeldt-Jakob's disease
IgG	Immunoglobulin G
IL-2	Interleukin 2
IPTG	Isopropyl-β-D-thiogalactopyranosid
IQR	Inter-quartile range
IRB	Institutional review board
KEK-ZH	Cantonal Ethics Committee of Zurich (Kantonale Ethikkommission Zürich)
LB	Lysogeny broth
Luc	Luciferase
MDS	Molecular dynamics simulations
MEMRI	Manganese-enhanced magnetic resonance imaging
mIgG	Murine IgG
$mPrP^{C}$	Murine cellular prion protein
MRI	Magnetic resonance imaging
mRNA	Messenger RNA
NAc	*N*-acetyl cysteine
NADPH	Nicotinamide adenine dinucleotide phosphate hydrogen
NBH	Non-infectious brain homogenate
NeuN	Neuronal nuclei
Ngsk	$Prnp^{0/0}$ mouse Nagasaki (Sakaguchi et al. 1996)
Ni-NTA	Ni-Nitrilotriacetic acid
NIR	Near-infrared
NIR-VAD-fmk	Near-infrared Valin-Alanine-Aspartate-fluoromethylketone
NOX2	NADPH oxidase 2
OCS	Organotypic slice cultures
OGB-1	Oregon Green 488 BAPTA-1 AM
ORF	Open reading frame
PCR	Polymerase chain reaction
PD	Parkinson's disease
PE	R-phycoerythin
$pE_{3\text{-}17}$	Pyroglutamylated $Aβ_{3\text{-}17}$
PerCP	Peridinin Chlorophyll Protein Complex
PERK	Protein kinase-like endoplasmic reticulum kinase
PET	Positron emission tomography
PK	Proteinase K
PNGase F	Peptide -N-Glycosidase F
PPS	Pentosan polysulphate
PS1	Presenilin 1
Prnp	Prion protein gene (murine)
PRNP	Prion protein gene (human)
PrP	Prion protein
PrP^{C}	Cellular prion protein
$PrP^{C}\text{-}FT$	Flexible tail of PrP^{C}
$PrP^{C}\text{-}GD$	Globular domain of PrP^{C}
$PrP^{C}\text{-}OR$	Pctapeptide region of PrP^{C}
PrP^{Sc}	Scrapie prion protein
PTFE	Polytetrafluorethylen
recPrP	Recombinant PrP ($rhPrP_{23\text{-}231}$ + $rmPrP_{23\text{-}230}$)
$rhPrP_{23\text{-}231}$	Recombinant, full-length human PrP, aa 23-231
RML6	Passage 6 of the Rocky Mountain Laboratory strain mouse-adapted scrapie prions

ROI	Region of interest
$rmPrP_{23-230}$	Recombinant, full-length murine PrP, aa 23-230
RNA	Ribonucleic acid
ROS	Reactive oxygen species
RT-QuIC	Real-time quaking induced conversion
SBDP	Spectrin breakdown products
ScFv	Single chain fragment, variable
sCJD	Sporadic Creutzfeldt-Jakob's disease
S.D.	Standard deviation
SDM	Site-directed mutagenesis
SDS-PAGE	Sodium dodecyl sulfate polyacrylamide gel electrophoresis
sgRNA	Single guide RNA
sFI	Sporadic fatal insomnia
SLE	Systemic lupus erythematodes
SPR	Surface plasmon resonance
TALEN	Transcription activator-like effector nuclease
TLR	Toll-like receptor
TMB	3,3', 5,5;-tetramethylbenzidine
TOF MS ES	Time-of-flight mass spectrometry electrospray
TSE	Transmissible spongiforme encephalopathy
UHZ	University Hospital Zurich
UPR	Unfolded protein response
UPS	Ubiquitin proteasome system
VAD-fmk	Valin-Alanine-Aspartate fluoromethylketone
vCJD	Variant Creutzfeldt-Jakob's disease
WT	Wild-type
YFP	Yellow fluorescent protein
ZH1	*Prnp*$^{0/0}$ mouse Zurich I (Büeler et al. 1992)
ZH3	*Prnp*$^{0/0}$ mouse Zurich III (Nuvolone et al. 2016)

Declaration

Parts of this thesis are either reproduced or quoted verbatim from data published on September 29th 2016 in the following article in PLOS ONE

Neurotoxic Antibodies against the Prion Protein Do Not Trigger Prion Replication

Karl Frontzek, Manuela Pfammatter, Silvia Sorce, Assunta Senatore, Petra Schwarz, Rita Moos, Katrin Frauenknecht, Simone Hornemann, Adriano Aguzzi

https://doi.org/10.1371/journal.pone.0163601

Further parts are adapted or reproduced from the following manuscripts in press or in preparation:

Towards Therapy of Human Prion Diseases

Adriano Aguzzi, Asvin K. K. Lakkaraju, Karl Frontzek

Annual Reviews of Pharmacology and Toxicology (58), 2018

A bispecific immunotweezer prevents soluble PrP aggregates and abolishes prion toxicity

Marco Bardelli, Karl Frontzek, Luca Simonelli, Simone Hornemann, Mattia Pedotti, Adriano Aguzzi, Luca Varani

Manuscript in preparation

Introduction

The discovery of prions

Historically, prion disease was first observed in merino sheep in the 18th century. Excessive inbreeding of sheep in an attempt to improve the quality of wool led to an increased number of sheep suffering from a disease, in which the animals repeatedly scraped off their fleece against fences or rocks, hereafter termed *scrapie* (Leopoldt 1759; Brown and Bradley 1998). In the beginning of the twentieth century, two German neurologists, Hans-Gerhard Creutzfeldt and Alfons Maria Jakob, independently coined the term *spastic pseudosclerosis* to describe a neurological syndrome that did not fit into consensus diagnostic criteria (Creutzfeldt 1920; Jakob 1921). Their histopathological observations on post-mortem brain tissue, that is, neuronal loss and gliosis, are still considered hallmarks of prion diseases (Aguzzi, Barres, and Bennett 2013). In recognition of this seminal work, the most commonly observed human prion disease is eponymously called Creutzfeldt-Jakob's disease (*Figure* 1, CJD).

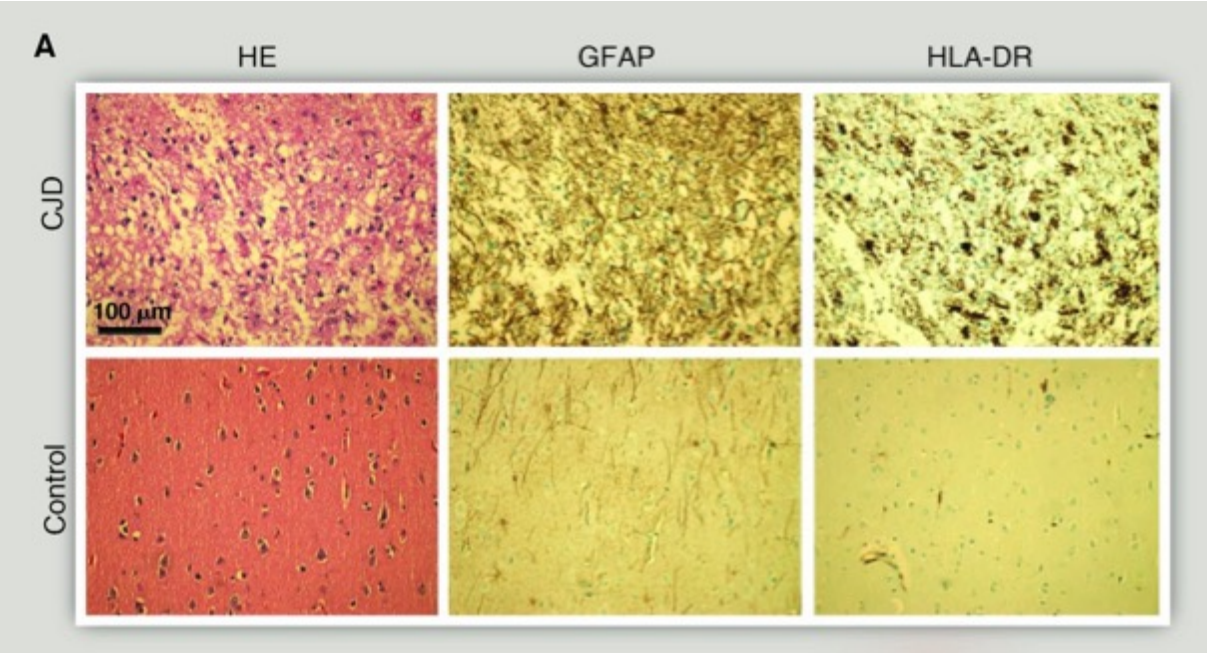

***Figure* 1**. Microscopically, Creutzfeldt-Jakob's disease is characterized by marked spongiform change and neuronal loss (HE, *upper panel, left image*), reactive gliosis (GFAP, *upper panel, middle image*) and microglial activation (HLA-DR. *upper panel, right image*). Bottom images are control histographs from a patient without neurological disease. Reprint with permission from (Aguzzi, Barres, and Bennett 2013), Rightslink license number 4127060736524.

.

The first experiments demonstrating the disease's transmissibility were performed by the French veterinarians Jean Cuillé and Paul-Louis Chelle, who intracerebrally inoculated healthy sheep with brain homogenates of scrapie-infected sheep, which led to disease onset, thus confirming the transmissible properties of the scrapie agent (Cuillé and Chelle 1936). Vincent Zigas and Carleton Gajdusek (Gajdusek and Zigas 1957) described a distinct neurological syndrome, similar to scrapie and CJD in the *Fore* tribe in Papua New Guinea, who practiced ritual cannibalism. Only a few years later the authors were able to successfully transmit the disease to chimpanzees using brain tissue from patients with either Kuru or CJD (Gibbs et al. 1968; Beck et al. 1969; Gajdusek, Gibbs, and Alpers 1966).

What is the exact nature of the infectious agent? The long incubation time of scrapie and scientific reports on disease-causing, viral nucleic acids (Fraenkel-Conrat and Williams 1955) led to the emergence of the *slow virus* (Sigurðsson 1954) hypothesis. However, attempts to inactivate the scrapie agent either by formalin (Gordon 1946) or high-dose ultra-violet light (Alper et al. 1967) were unsuccessful. In 1967, J.S. Griffith applied a mathematical approach to the "protein-only" hypothesis of prion replication, which proved to be pivotal (Griffith 1967). Stanley Prusiner, recognizing the significance of Griffith's hypotheses, concluded that the scrapie agent lacked nucleic acid and coined the term prion, a portmanteau derived from protein and infection (Prusiner 1982). In fact, Prusiner and co-workers were able to extract a relatively proteinase K-resistant protein from scrapie-infected hamster brain (Bolton, McKinley, and Prusiner 1982). Shortly thereafter, Patricia Merz and colleagues performed ultrastructural investigations on a variety of prion-diseased brains from different mammals and found so-called "scrapie-associated fibrils" (Merz et al. 1983). Only a few weeks after Merz' discovery, Prusiner and colleagues published their results about the presence of a single protein,the prion protein, PrP with rod-shaped, birefringent particles morphologically similar to amyloid in scrapie brains (Prusiner et al. 1983). The birefringent rods consisted of a multitude of PrP molecules leading them to the conclusion that amyloid plaques observed in transmissible, degenerative neurological diseases might contain prions.

Throughout this manuscript, I will use the following terminology: PrP^{C} for the cellular prion protein, which is physiologically expressed in tissue; PrP^{Sc}, the Proteinase K (PK)-resistant, disease associated prion protein found in human prionopathies such as CJD and other prionopathies such as scrapie; PrP, refers to PrP^{C} and PrP^{Sc}, whenever applicable, for both forms. *Prnp* is the genetic designation for the murine gene, *PRNP* for the respective human gene encoding the prion protein.

The prion protein is indispensable for prion disease

According to the *Central Dogma of Molecular Biology*, biological information is sequentially transferred from DNA to RNA to protein (Crick 1970). In search of the genetic basis of prion disease, Charles Weissmann and co-workers isolated a PrP-related gene encoding for the scrapie agent (Oesch et al. 1985), while Chesebro almost simultaneously described the messenger RNA of PrP (Chesebro et al. 1985). Additionally, no evidence of nucleic acids was found in the purified preparations of scrapie prions, strengthening the “protein-only” hypothesis (Oesch et al. 1985).

Transgenic mice lacking the prion protein gene *Prnp* were generated, yielding the first $Prnp^{0/+}$ and $Prnp^{0/0}$ mice (Zurich I, ZH1 (Büeler et al. 1992)). Primary behavioral analyses up to an age of seven months did not reveal an overt phenotype (Büeler et al. 1992). When challenging $Prnp^{0/0}$ (ZH1) with prions, $Prnp^{0/0}$, but not $Prnp^{+/+}$ or $Prnp^{0/+}$ were resistant to prion disease, strongly arguing in favor of the prion protein as indispensable for prion disease (Bueler et al. 1993). Interestingly, serial passaging of brain and spleen homogenates from prion-inoculated $Prnp^{0/0}$ (ZH1) mice into $Prnp^{+/+}$ CD1 indicator mice showed an almost complete loss of infectivity, except when the inoculum was not heated prior to inoculation, albeit only very low levels of infectivity could be observed (Bueler et al. 1993).

The pivotal experiments of Weissmann and colleagues (Bueler et al. 1993) precluded a loss-of-function of PrP^{C} as the cause of prion diseases; however, it was unclear whether PrP^{Sc} exerted toxic effects or neurotoxicity was induced by another mechanism. Moreover, up

to 10-fold overexpression of PrP^C compared to wild-type levels in *Tga*20 animals did not lead to a neurological phenotype, making a toxic gain-of-function of PrP^C unlikely. Upon grafting of $Prnp^{+/+}$ neural tissue into $Prnp^{0/0}$ mice and subsequent prion inoculation, a sharply demarcated border between pathologically altered $Prnp^{+/+}$ and unaffected $Prnp^{0/0}$ tissue was seen (Brandner et al. 1996). Moreover, $Prnp^{0/0}$ host tissue adjacent to $Prnp^{+/+}$ grafts showed widespread PrP^{Sc} deposits with no overt pathology suggesting that neurotoxicity is exerted by prions in the presence of PrP^C through activation of hitherto unspecified intracellular cascades (Brandner et al. 1996).

The physiological role of PrP^C

The $Prnp^{0/0}$ (ZH1) mouse was the first transgenically modified animal for studying the physiological effects of the prion protein (*Figure* 2), with pilot behavioral analyses showing no overt phenotype (Büeler et al. 1992). Using $Prnp^{0/0}$ (ZH1) animals, it became clear that prion protein is necessary for prion disease, as $Prnp^{0/0}$ (ZH1) mice did not succumb to the disease (Bueler et al. 1993). Later generated $Prnp^{0/0}$ mice included, but were not limited to the $Prnp^{0/0}$ (Edbg) mice, on a pure 129/Ola background (Manson et al. 1994) and the $Prnp^{0/0}$ (Ngsk) mice, on a mixed 129/Bl6 background (Sakaguchi et al. 1996).

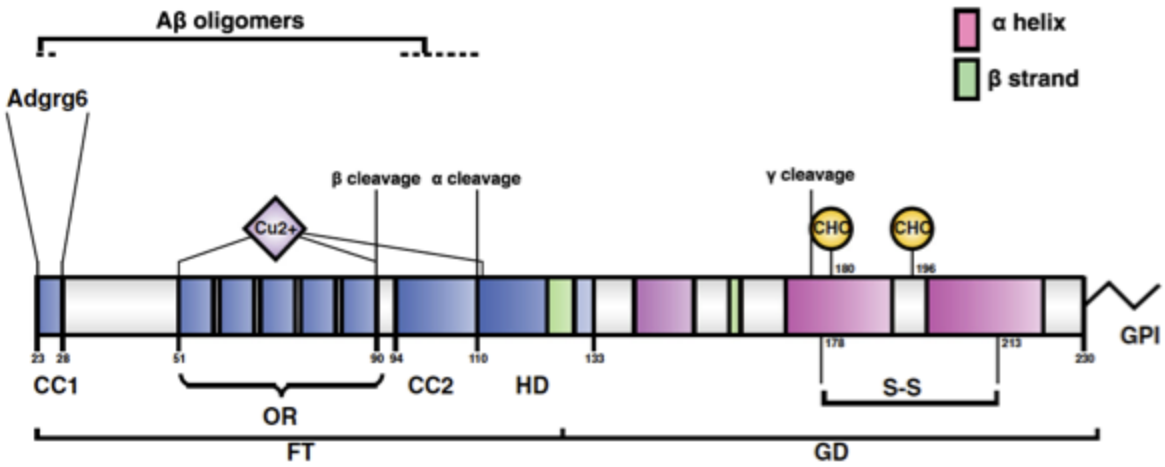

***Figure* 2.** Structure of PrP^C (nomenclature of residues according to murine PrP^C). *Adgrg6* denotes residues involved in binding of *Adgrg6*, Cu^{2+} denotes copper binding sites, interaction regions of PrP^C with *Aβ oligomers* are indicated above. *CHO* denotes glycosylation stes. Graph modified according to the Creative Commons Attribution Licence 4.0 from (Wulf, Senatore, and Aguzzi 2017).

One inherent lack of studying physiological protein function on the bases on knock-out animals was the technique used for generation of *Prnp*$^{0/0}$ transgenic mice at that time: typically, *Prnp*$^{0/0}$ mouse embryonic stem cells were derived from the 129 strain of *Mus musculus* and implanted into pseudopregnant foster mothers from the C57BL/6 strain of *Mus musculus* (Steele, Lindquist, and Aguzzi 2007). Although resulting mixed Bl6129 mice were backcrossed > 10 times to (mostly) Bl6 mice to generate Bl6.129 congenic animals, genes flanking *Prnp* may co-segregate during meiotic recombination and lead to mixing of polymorphisms in genes additional to *Prnp* (Gerlai 1996).

What is the true phenotype of the *Prnp*$^{0/0}$ mouse? Susceptibility to prion disease was repeatedly reported to be independent of the *Prnp*$^{0/0}$ animal's host strain. According to the prevailing consensus, it is now considered to represent a genuine function of PrP^{C} (Steele, Lindquist, and Aguzzi 2007). The possibility of misleadingly observed phenotypes due to genetic confounders in knock-out animals of mixed genetic background was already mentioned during the characterization of the first *Prnp*$^{0/0}$ (ZH1) mouse (Bueler et al. 1993; Büeler et al. 1992). Nonetheless, numerous publications emerged that attributed a plethora of diverse, e.g. electrophysiological, immunological, neurological phenotypes to the *Prnp*$^{0/0}$ mice irrespective of genetic bias (Steele, Lindquist, and Aguzzi 2007). The olfactory bulb shows strong PrP^{C} expression and *Prnp*$^{0/0}$ mice showed abnormal olfactory behavior resembling anosmic mice: this altered behavior was observable in mice bred in different genetic backgrounds, both pure and congenic (ZH1, Edbg, Ngsk), suggesting a genuine function of PrP^{C} (Le Pichon et al. 2009).

A chronic demyelinating polyneuropathy (CDP) was seen in animals lacking PrP^{C} at around 10 weeks of age (Bremer et al. 2010). This phenotype was confirmed in four different *Prnp*$^{0/0}$ mouse strains, e.g. ZH1, Edbg, Ngsk and *Prnp*$^{GFP/GFP}$, suggesting an authentic *Prnp*$^{0/0}$ phenotype independent of flanking gene polymorphisms (Bremer et al. 2010; Heikenwalder et al. 2008). A strictly co-isogenic *Prnp*$^{0/0}$ C57BL/6 mouse (termed Zurich III, ZH3) was created by means of transcription activator-like effector nucleases (TALEN) (Nuvolone et al. 2016). *Prnp*$^{0/0}$ (ZH3) animals authentically recapitulated CDP and a polybasic, N-terminal fragment of

PrP^C was found to be a promyelinating agonist of the G-protein coupled receptor (GPCR) Gpr126 (Nuvolone et al. 2016; Kuffer et al. 2016). Development of CDP in *Prnp*$^{0/0}$ mice represents the best characterized phenotype of animals lacking PrP^C to date.

A seeding/nucleation model for prion propagation

What is the disease-causing agent and how do prions replicate? As stated, experimental evidence worked against either loss-of-function or gain-of-function of PrP^C (Büeler et al. 1992; Bueler et al. 1993), intrinsic toxicity of PrP^{Sc} was unlikely as well (Brandner et al. 1996). Until the beginning of the twenty-first century, the only known molecular differences between PrP^C and PrP^{Sc} were the higher β-sheet content of PrP^{Sc} and resistance to PK digestion (Aguzzi and Heppner 2000). Historically, prion propagation was believed to occur through a so-called „template-assisted“ or „refolding“ conversion of PrP^C to PrP^{Sc} whereby PrP^{Sc} „imposes“ its pathological tertiary structure onto PrP^C (Aguzzi and Heppner 2000). The conversion reaction was anticipated to involve another molecule, provisionally designated “protein X” (Telling et al. 1995). In the light of the relative innocuousness of PrP^{Sc} (Collinge and Clarke 2007), Collinge and Clarke postulated the presence of an alternative, smaller and neurotoxic protein, designated “PrP-lethal” (PrP^L) as the cause of prion-induced neurodegeneration .To date, however, no physical definition of either protein X or PrP^L exists. Most likely, these proteins are non-existent in nature (Aguzzi and Falsig 2012).

Besides disease-associated protein aggregation in prion disease, ordered protein aggregation is considered harmless in physiological processes such as protein crystallization (Senisterra and Finerty 2009). In view of the positive correlation of slow clinical manifestation with the gradual increase in PrP^{Sc} aggregates, Jarrett and Lansbury postulated a model of “nucleation-dependent polymerizations” of the prion protein (Jarrett and Lansbury 1993). Indeed, a plethora of scientific data has accumulated in favor of disease-causing, small toxic oligomers that are generated by nucleation from monomeric proteins (Arosio et al. 2014). In the case of prions, mathematical modelling of fragmentation and elongation of PrP^{Sc}

aggregates precisely align with gathered *in vivo* data showing a dose-dependent (i.e. PrP^C expression levels of the host) disease onset (*Figure* 3, (Knowles et al. 2009; Fischer et al. 1996)).

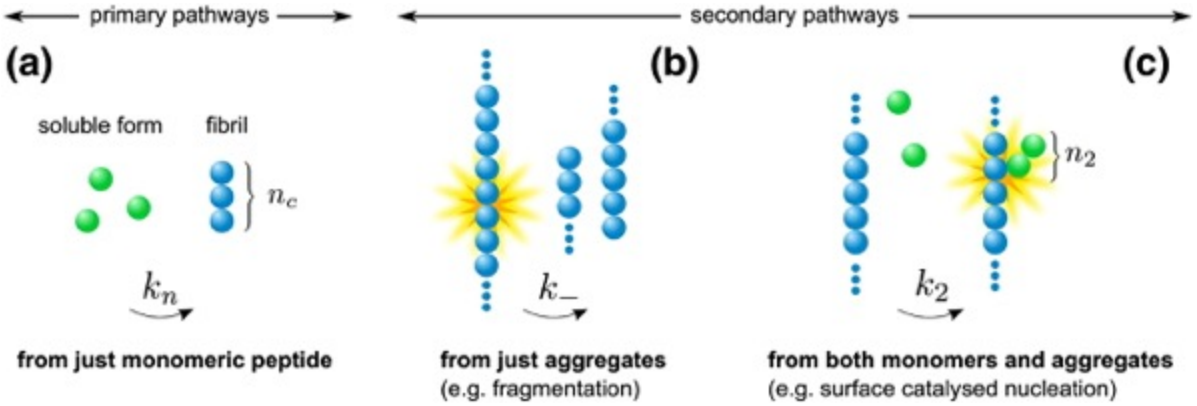

***Figure* 3**. Graphic illustration of reaction pathways leading to the generation of protein aggregates, e.g. in neurodegenerative disorders. (A) Soluble monomers reacting with each other define primary nucleation pathways. (B) Monomer-independent aggregation, e.g. by fragmentation or (C) monomer-dependent aggreagation delineate secondary aggregation pathways. Reprint with permission from (Cohen et al. 2012), Rightslink license number 4127071484123.

This model, however, is not *per sé* restricted to PrP^{Sc}: inoculation of brain extracts from human AD patients successfully induced cerebral β-amyloidosis (Meyer-Luehmann et al. 2006), intracerebral inoculation of synthetic α-synuclein into wild-type mice induced Lewy pathology (Luk et al. 2012) and different Tau-strains reproducibly showed prion-like propagation upon re-introduction into naïve cells and animals (Sanders et al. 2014). Although β-amyloid, α-synuclein and Tau showed cell-to-cell propagation, they were not the causes of epidemic diseases such as bovine spongiform encephalopathy (BSE) or Kuru – hence the term “prionoids” was coined to better separate them from genuine prions (Ashe and Aguzzi 2013).

Autoimmunity in human prion diseases

In humans, prion diseases are mostly of sporadic origin (sporadic Creutzfeldt-Jakob disease, sCJD and rarely, sporadic Fatal familial insomnia, sFI), and in 10-15%, of genetic origin (genetic CJD, gCJD; genetic Fatal familial insomnia, gFI and Gerstmann-Sträussler-Scheinker disease, GSS). Prion diseases acquired through an iatrogenic or dietary update represent a

third group of cases (iatrogenic CJD, iCJD; Kuru; variant CJD, vCJD) (Capellari et al., 2011). As previously noted, human prion diseases are recognized by the histopathological hallmarks of spongiform change, neuronal cell loss, astrogliosis, microglial activation and deposits of PrP^{Sc} (Aguzzi and Falsig 2012). Genetic prion diseases are characterized by mutations in the PrP^{C} encoding human gene *PRNP* (Takada and Geschwind 2013). Two families have been reported with several family members affected by CJD but without *PRNP* mutation, suggesting possible risk genes outside of *PRNP* to be responsible for disease susceptibility (Frontzek et al. 2015; Webb et al. 2008). Large genome-wide association studies, however, hitherto failed to identify potential risk genes (Mead et al. 2012).

Naturally occurring autoantibodies have been proposed to play a protective role in a variety of neurodegenerative diseases such as Alzheimer's disease or Parkinson's disease (Bach and Dodel, 2012; Neff et al., 2008). Herein, autoantibodies are suggested to inhibit the formation of toxic species of disease-causing proteins amongst others beta-Amyloid and alpha-Synuclein (Neff et al., 2008). Genetic prion diseases are exclusively attributed to mutations of the prion protein-coding gene *PRNP* following an autosomal-dominant trait. As in their sporadic counterpart, patients show accumulations of aggregated and misfolded PrP^{Sc} (Mastrianni, 2010). Interestingly, albeit mutation bearers express this pathological protein throughout their whole life, clinical symptoms occur almost exclusively in advanced age (Takada and Geschwind, 2013). This observation is indicative of protective factors. To this end, one study has proposed the presence of autoantibodies against a fragment of the common, PrP^{C}_{A117V} mutation in commercially available, pooled plasma preparations (Wei et al., 2012). The subsequently isolated autoantibodies were suggested to exert neuroprotective effects against the artificial fragment $PrP(106\text{-}126)_{A117V}$ (Roettger et al., 2013). However, $PrP^{A117V}_{106–126}$ does not exist in nature, and therefore, such speculations are implausible.

The mechanisms of prion toxicity

What is responsible for neuronal death in prion diseases? Pathologically, brains from humans and animals with terminal prion disease show a typical spongiform degeneration that is accompanied by widespread neuronal death, astrogliosis, microglial activation and PrP^{Sc} deposits (Kovacs and Budka 2008). When PrP^{C} is depleted during the early phase of prion-induced neurodegeneration, a reversal of spongiform changes was observed (Mallucci et al. 2003). Shmerling and co-workers investigated the phenotypes of animals with mutants of the flexible tail of PrP^{C} (PrP^{C}-FT) and observed a cerebellar syndrome with neuronal death in the cerebellar granule layer (CGL) in mutants lacking the residues 32-121 (denoted $PrP^{\Delta E}$) and 32-134 (denoted $PrP^{\Delta F}$), but not in shorter deletions (Shmerling et al. 1998). Re-introduction of a functional PrP^{WT} allele restored neurotoxicity in $PrP^{\Delta E}$ and $PrP^{\Delta F}$ mutants pointing to the important role of PrP^{C}-FT in mediating PrP^{C}-dependent neurotoxicity (Shmerling et al. 1998).

In one study, prion infection was reported to cause dysfunction of the ubiquitin proteasome system (UPS) causing a reduction of protein degradation (Kristiansen et al. 2007). Mallucci and colleagues observed abrupt cessation in synaptic protein expression in prion-infected mice when synapse numbers were already decreasing (Moreno et al. 2012). They hypothesized that accumulation of unfolded proteins in the endoplasmic reticulum (ER) leads to a decrease in translation and observed an increase in expression of BiP/Grp78 (BiP), which detects rising protein levels and initiates the unfolded protein response (UPR) (Moreno et al. 2012). BiP leads to auto-phosphorylation of protein kinase-like endoplasmic reticulum kinase (PERK); phosphorylated PERK (PERK-P) phosphorylates eukaryotic translation initiation factor, eIF-2α; eIF-2α-P induces expression of ATP4 and CHOP and eventual activation of GADD34, which acts in a negative feedback loop to end UPR signaling (Moreno et al. 2012). Lentoviral vector-mediated overexpression of GADD34 and oral administration of the PERK inhibitor GSK2606414 resulted in a decrease of UPR activation and amelioration of prion disease (Moreno et al. 2012; Moreno et al. 2013).

When testing a panel of putative anti-prion compounds in cerebellar organotypic slice cultures (COCS) (Falsig and Aguzzi 2008), Congo red, pentosan polysulphate (PPS),

amphotericin B, porphyrin, suramin, imatinib and E64d conferred neuroprotection against passage 6 of the Rocky Mountain Laboratory strain mouse-adapted scrapie prions (RML6) prions (Falsig et al. 2012). Congo red was already demonstrated to confer protection against prion disease (Caspi et al. 1998), possibly due to hyperstabilization of PrP^{Sc} aggregates. Furthermore, PPS, porphyrin, amphotericin B, suramin and imatinib also exerted neuroprotection through counter-acting prion replication (Falsig et al. 2012). Although treatment of prion-infected COCS with the calpain inhibitor E64d led to minimally increased PrP^{Sc} levels and infectivity, neuroprotection was seen, implying inhibition of pathways downstream of prion replication, as was the case in two other calpain inhibitors, e.g. calpeptin and MDL-28170 (Falsig et al. 2012). Calpains are cytoplasmic, calcium-dependent proteases (Suzuki et al. 2004). Calpain activation leads to cleavage of αII-spectrin (α-fodrin) with characteristic spectrin breakdown products (SBDP) of 150 and 145 kDa (SBDP150 and SBDP145) (Wang 2000). In prion-infected COCS, but not in COCS inoculated with non-infectious brain homogenate, SBDP150 and SBDP145 can be observed, indicative of calpain activation (Falsig et al. 2012). Anti-prion antibodies, first and foremost those targeting PrP^{C}-GD, lead to rapid neurodegeneration with histomorphological features resembling genuine prion diseases, such as neuronal cell loss, astrogliosis and microglial activation (Sonati et al. 2013). Interestingly, treatment of COCS with the murine monoclonal anti-PrP^{C}-GD antibody POM1 also leads to activation of calpains and subsequent α-fodrin cleavage yielding SBDP150 and SBDP145 – as was shown in *bona fide* prions (Sonati et al. 2013; Herrmann et al. 2015). Scavengers of reactive oxygen species (ROS) such as ascorbic acid, and *N*-acetyl cysteine ameliorate POM1-induced toxicity, suggesting that ROS production contributes to cell toxicity (Sonati et al. 2013). Both cell-permeable and cell-impermeable ROS inhibitors were protective in POM1-induced neurodegeneration, indicating extracellular superoxide to be the responsible ROS species. Indeed, inhibition of the nicotinamide adenine dinucleotide phosphate hydrogen (NADPH) oxidase 2 (NOX2) through the NOX2 inhibitor diphenyleneiodonium chloride led to an amelioration of POM1-induced superoxide production (Sonati et al. 2013). Are anti-PrP^{C}-GD antibody-mediated pathways also seen in mammalian prion diseases? NOX2 activity was

observable predominantly around spongiform vacuoles in human brains from CJD patients, significantly stronger than in AD controls (Sorce et al. 2014). Mice lacking both copies of Nox2 showed a delay in prion disease compared to wild-type animals (Sorce et al. 2014), pointing to an important role of ROS in mammalian prion diseases.

Neuronal cell loss in prion diseases

The histological hallmarks of prion pathology are characterized by spongiform change, neuronal cell loss, astrogliosis, microglial activation and deposits of PrP^{Sc} (Aguzzi and Heppner 2000). Early reports suggested morphological alterations resembling apoptosis following prion-infected cell lines (Schatzl et al. 1997). Conversely, tissue microarrays on a variety of chronically infected cell lines did not show an observable cellular reaction (Julius et al. 2008). A wealth of controversy prevails regarding the role of caspase-3 in prion-induced neuronal cell death. Punctual activation of caspase-3 was reported in immunohistochemical studies of cerebella in human CJD patients (Puig and Ferrer 2001) and scrapie-infected mice (Siso et al. 2002), while another study failed to see activation of caspase-3 in neurons from scrapie-affected sheep brains (Lyahyai et al. 2006). Thorough biochemical investigations and treatment with caspase-3 inhibitors in scrapie-infected mice and RML6-infected COCS; however, did not reveal a role of activated caspase-3 in prion disease (Falsig et al. 2012).

Further, mainly immunohistochemical studies on *post mortem* tissue from sCJD patients suggested a complex interplay of a variety of apoptosis-related proteins depending on the molecular subtype of sCJD (Kovacs and Budka 2010). Inconclusive results have been found when correlating mediators of neural degeneration to brain regions of different sCJD subtypes (Llorens et al. 2014). Exhaustive studies on the complement system and prions revealed a protective effect of a lack of the components C1q, Bf/C2 and C3, as well as complement receptors on prion pathogenesis (Klein et al. 2001). Genetic depletion of complement receptors was beneficial in a mouse model of chronic wasting disease (CWD) (Michel et al. 2012). Accordingly, a subsequently published study suggested that the presence of neuronal depositions of activated, terminal complement fragments in human sCJD brains

had a similar effect (Kovacs et al. 2004). As complement deposition inhibited the accumulation of PrP^{Sc}, one can conclude that the protective effect is mediated at the level of prion infectivity and propagation, but not on downstream effects such as cell toxicity.

As previously stated, activation of calpains, calcium-dependent proteases followed by cleavage of α-fodrin and generation of ROS through NOX2 was shown to mediate of toxicity of *bona fide* prions as well as "prion-mimetic", toxic anti-PrP^{C}-GD antibodies (Sorce et al. 2014; Falsig et al. 2012; Herrmann et al. 2015; Sonati et al. 2013). Furthermore, translational repression in prion diseases through activation of BiP, PERK and eIF2α is another well-characterized mechanism of prion-induced toxicity as described above (Moreno et al. 2012; Moreno et al. 2013). Taken together, pharmacological and genetic inhibition of the latter two pathways, e.g. through ablation of PrP^{C}-FT or antibodies against PrP^{C}-FT, calpain inhibitors, ROS scavengers, $NOX2^{0/0}$ mice, PERK inhibitors, overexpression of GADD etc., are effective in delaying prion diseases. In addition, they represent the most widely studied and faithfully reproducible routes of prion-induced neurotoxicity.

Antibodies against the prion protein

A pivotal experiment in antibody immunotherapy of prion disease was performed by mixing prion protein-specific antiserum with purified prions, which led to reduced prion infectivity (Gabizon et al. 1988). Further studies on the effects of antibodies in prion disease were mostly limited to *in vitro* experiments that investigated whether the administered compounds are able to abrogate the generation of PrP^{Sc}. Subsequently, a plethora of positively tested antibodies were tested with the goal of halting the generation of PrP^{Sc} – e.g. the monoclonal anti-PrP^{C} antibodies (or fragments thereof) D13, D18, 6H4, R1, R2, SAF32, SAF61 (Enari, Flechsig, and Weissmann 2001; Peretz et al. 2001; Perrier et al. 2004; Feraudet et al. 2005). These PrP^{Sc}-clearing antibodies were usually administrated to prion-infected cell lines, which posed two major obstacles. Firstly, prion replication has to be at least as fast as cell division in chronically prion-infected cells, as slower replication rates will lead to cessation of infectivity over time.

Secondly, prion infection can decrease the cell's fitness, again leading to non-infected cells (Li et al. 2010).

The Aguzzi lab was the first to describe the protective effects of systemic expression of antibodies against prion disease *in vivo* (Heppner et al. 2001). Herein, the µ chain of the anti-PrP^C antibody 6H4 was expressed by transgenesis in *Prnp*$^{0/0}$ mice – the 6H4 clone was previously shown to successfully and persistently ablate prion infectivity (Enari, Flechsig, and Weissmann 2001). Transgenic antibody expression prevented prion disease after intraperitoneal inoculation without affecting expression of PrP^C suggesting successful passive immunotherapy (Heppner et al. 2001). Further reports have confirmed the protective action of systemic antibody levels in prion diseases (White et al. 2003; Goni et al. 2005). D13, a monoclonal antibody directed against a linear motif between the PrP^C-OR and the charged cluster 2 region of PrP^C (PrP^C-CC2) was initially claimed to induce neurotoxicity (Solforosi et al. 2004). A second study that established minimal toxic antibody concentrations of anti-PrP^C antibodies *in vivo* was also able to recapitulate D13-induced toxicity (Reimann et al. 2016). Of concern, however, was another study that concluded that D13 was innocuous, probably due to the low-dose regimen tested (Klöhn et al. 2012). D18, a monoclonal anti-PrP^C antibody targeting regions proximal to and within the α1-helix of PrP^C-GD did not show toxic effects in a primary study. A subsequent investigation of adenoviral-mediated expression of a single chain variable fragment of D18 (AAV-scFvD18) in prion-inoculated mice showed beneficial effects of AAV-scFvD18 by delaying disease onset (Solforosi et al. 2004; Moda et al. 2012).

***Figure* 4**. Overview of epitope specificities of the POM1 monoclonals. Reprinted from (Polymenidou et al. 2008) under the Creative Commons Attributed Licence 4.0.

The immunization of *Prnp*$^{0/0}$ mice with PrP^C yielded a comprehensive set of monoclonal anti-PrP^C antibodies, termed POM antibodies (*Figure* 4, (Polymenidou et al. 2008)). Thorough investigations of anti-PrP^C antibody toxicity showed a bimodal nature of PrP^C – eight out of

twelve anti-PrP^C-GD antibodies showed profound neurotoxicity compared to one out of four anti-PrP^C-FT antibodies. Of note, anti-PrP^C-GD-mediated toxicity could be ablated by pre-incubation with anti-PrP^C-OR antibodies or in interstitial deletion mutant mice lacking PrP^C-OR, pointing to an important role of the PrP^C-OR in mediating neurotoxity (Sonati et al. 2013). Transcriptional analyses showed changes in similar pathways in anti-PrP^C-GD and prion toxicity (Herrmann et al. 2015). Highly controversial results were observed when a therapeutic effect was attributed to ICSM18, a monoclonal anti-PrP^C-GD antibody targeting a conformational epitope on the α1-α3 helices of PrP^C-GD (Klöhn et al. 2012). ICSM18 targets PrP^C-GD in close proximity to the epitope of the severly neurotoxic antibody POM1 (Baral et al. 2012; Antonyuk et al. 2009). Klöhn et al. reported no drug-related side effects of up to 2 µg of ICSM18 upon stereotaxic injections in the brain (Klöhn et al. 2012). Rigorously performed dose escalation studies, however, revealed the neurotoxic nature of ICSM18 (Reimann et al. 2016), which was later confirmed by another group (Wu et al. 2017). Recent reports on the preparation of a humanized version of ICSM18 – PRN100 – for use in clinical trials against prion and Alzheimer's disease are unsettling (Klyubin et al. 2014).

Screening techniques for the discovery of novel prion therapeutics

In spite of intense ongoing research targeting different aspects of prion disease, no effective therapy is in sight. A major limiting factor is the dearth of cell lines exhibiting cell-autonomous cytotoxicity upon prion infection. Prion-specific phenotypes were described after prion inoculation of the neuronal cell line GT-1, resembling spongiform pathology (Schatzl et al. 1997). Other studies however failed to detect perceivable changes in a panel cultured neuronal cells (Julius et al. 2008). A recent work shows early synaptotoxicity in prion-infected hippocampal cells expressing PrP^C, but not in prion-infected cells from $PrP^{0/0}$ mice (Sevigny et al. 2016). Artificially engineered cell lines bearing interstitial deletion mutants of PrP^C such as $PrP_{\Delta 105\text{-}125}$ present an antibiotics-induced hypersensitivity that could be restored by the small molecule LD7 (Imberdis et al. 2016). The most potent derivative of LD7 was also suggested to ameliorate prion-induced synaptotoxicity in hippocampal cells described in (Fang et al. 2016)

and to lower PrP^{Sc} levels *in vitro*. Future research has to show whether these changes observed *in vitro* can be successfully translated to cure prion disease *in vivo*. The Aguzzi lab has described an *ex vivo* slice culture system for cerebellar organotypic slice cultures (COCS) that is easily amendable to prion infections and pharmacological manipulation (Falsig et al. 2008b). Of note, typical prion-induced changes such as the accumulation of PrP^{Sc} , astro- and microgliosis, spongiform change and neuronal loss can be studied in COCS. What is more, compounds conferring neuroprotection *ex vivo* successfully ablated toxicity *in vivo* as well (Sonati et al. 2013).

Certain cell types permit efficient prion replication *in vitro* (Mahal et al. 2007). In order to find an inhibitor targeting prion replication, pharmacophores were selected from a computer-based algorithm to exert a dominant-negative effect onto the alleged PrP^{C}-"Protein X" binding site (Perrier et al. 2000). A lead molecule, Cp-60, was shown to efficiently cure cells from PrP^{Sc} at a half-maximal inhibitory concentration (IC_{50}) of around 20 µM (Perrier et al. 2000). Compounds consisting of a tricyclic scaffold such as acridines and phenothiazines have demonstrated a favorable blood-brain-barrier penetration and were shown to reduce PrP^{Sc} levels (Korth et al. 2001). Fittingly, drugs like Quinacrine (derived from acridine) and Chlorpromazine (a phenothiazine) that were already established as anti-psychotic drugs and anti-malarials were immediately transferred to clinical trials in prion disease (see below). Second-generation compounds of the ladder groups were joined via linkers of variable length and molecular composition resulting in so-called bis-acridines (May et al. 2003). Optimal covalent linkage resulting in the most efficient PrP^{Sc} reduction with acceptable cytotoxicity was achieved at a spacer distance of 10 Å with half-maximal effective concentrations (EC_{50}) of around 25 nM, yielding a EC_{50} reduction of one log when compared to first-generation compounds such as Quinacrine (May et al. 2003). STI571 (also known as Gleevec or imatinib mesylate) emerged as lead compound from a screen targeting several pathways activated in prion disease and was later suggested to delay disease onset in prion-infected mice albeit lacking the potential to clear PrP^{Sc} (Yun et al. 2007; Ertmer et al. 2004).

Taking a so-called “dynamics-based drug discovery” approach, a cavity created by several residues in helices B and C of PrP^{C} that demonstrated relatively lower stability during high-pressure NMR was targeted by small molecules in order to stabilize the PrP^{C} conformation (Kuwata et al. 2007). The most promising candidate from the screen, GN8, showed PrP^{Sc} reduction in a dose-dependent manner with dissociation constant (K_D) of around 4 µM. A comparison of NMR spectra after chemical shift perturbation showed a connection of distant PrP^{C} residues by GN8 suggesting the exclusion of large conformational shifts (Kuwata et al. 2007). Conversely, in experiments from another group using equilibrium dialysis of known compounds described to bind to PrP^{C}, neither GN8 was able to bind to a human PrP_{91-231} fragment, nor did Quinacrine or tetracycline bind to human PrP_{91-231} after two days of equilibration time (Nicoll et al. 2010). The cationic porphyrin Fe(III)-TMPyP [Fe(III) *meso*-tetra (*N*-methyl-4-pyridyl) porphine], however, was retained in the PrP-containing chamber and provided a reduction of 50% of amplified protease-resistant PrP^{Sc} during the protein-misfolding cycling amplification (PMCA) assay (Nicoll et al. 2010).

Rather than aiming at reduction of total PrP^{Sc} levels, another study screened 32 compounds for their propensity to catalyze the formation of larger-order PrP^{Sc} species that would by themselves reduce the amount of toxic and aggregation prone monomers (Ayrolles-Torro et al. 2011). One compound, P30, increased the formation of PrP^{Sc} dimers and trimers *in vitro* and led to increased survival in prion-infected mice, albeit no higher-order PrP^{Sc} species were detectable *in vivo,* leaving the anti-prion mechanism of P30 elusive (Ayrolles-Torro et al. 2011). In the PrP-fluorescence resonance energy transfer (FRET)-enabled high throughput assay (PrP-FEHTA), two antibodies targeting distinct, non-overlapping epitopes on PrP^{C} were labelled with either a fluorescence donor or acceptor leading to FRET upon binding to PrP^{C} on the cell surface (Karapetyan et al. 2013). Using PrP-FEHTA, the effects on PrP^{C} cell surface levels of 1,280 drugs approved for use in humans were screened. Herein, Tacrolimus (a widely used immunosupressant) and Astemizole (an antihistamine) were found to efficiently reduce PrP^{Sc} levels. In prion-infected mice, Astemizole, but not Tacrolimus, led to a strong, but non-significant extension (p=0.06) of survival time (Karapetyan et al. 2013). Interestingly, when

testing a panel of PrP^{Sc} lowering drugs, one study did not find any measurable, direct interaction between the compounds and PrP^{C} or a direct capacity to disaggregate PrP^{Sc} suggesting all PrP^{Sc} clearing effects to be indirect (Poncet-Montange et al. 2011). 2-aminothiazoles, another group of PrP^{Sc} lowering compounds, showed initial success in extending the life-span of prion-infected mice, but eventually led to a fatal neurodegenerative syndrome in prion-infected animals treated with the lead compound IND24 . Subpassages of their brain homogenates in mice and cells demonstrated drug resistance to IND24. Drug sensitivity to IND24 was restored after a treatment pause with vehicle control (Berry et al. 2013). This study could have a broader implication for monotherapies in prion disease patients.

Live imaging approches in models of neurological diseases

Neuronal cell death is a commonly shared feature of several neurodegenerative diseases, amongst others Alzheimer's disease (AD), Parkinson's disease (PD), Huntington's disease (HD) and prion disease (Bredesen, Rao, and Mehlen 2006). The precise, experimental determination of neuronal cell loss is important when asking scientific questions addressing pathogenetic mechanisms. Robust and sensitive assays are also needed for screening putatively neuroprotective or neurotoxic compounds. In AD, pathologically aggregated forms of β-amyloid protein and hyperphosphorylated τ (Tau)-Protein are considered causative factors of the disease (Scheltens et al. 2016). To date, no effective therapy has been developed for patients suffering from AD, emphasizing the acute need for tools that can reliably predict neuronal outcome (Sevigny et al. 2016). F-fluorodeoxygluose positron emission tomography (FDG-PET) and PET with β-amyloid-specific ligands has gained importance in the clinical assessment of diseases from the AD spectrum (Scheltens et al. 2016). A combination of the plethora of available transgenic AD mouse and rat models with miniaturized PET, so-called microPET, allows precise assessment of plaque load and can be used to monitor therapeutic efficacy of novel anti-AD drugs, to date, several novel radiotracers for AD diagnostics have been established using microPET (Zimmer et al. 2014).

Double transgenic APPPS1 mice bear mutations in both the amyloid precursor protein (APP) and presenilin 1 (PS1) leading to overexpression in pathological β-amyloid depositions (plaques) and subsequent neuronal dysfunction (Radde et al. 2006). Two different, fluorescent reporter proteins expressing animals were used to study the kinetics of β-amyloid plaque deposition, neuroinflammation and neuritic dystrophy. Mice bearing APPPS1 mutations and expressing of yellow fluorescent protein (YFP) in a subset of cortical neurons (B6C3-YFP mice) and mice bearing an APP mutation crossed to mice expressing green fluorescent protein (GFP) in microglia were longitudinally imaged *in vivo* using multiphoton microscopy (Meyer-Luehmann et al. 2008). Interestingly, after rapid onset of plaques, microglial activation and recruitment to β-amyloid plaques were observed and subsequently, neurites became dysmorphic, providing unique insights into the temporal evolution of AD neuropathology (Meyer-Luehmann et al. 2008). In APPPS1 mice, depositions of β-amyloid plaques preceded loss of dendritic spines as was visualized by *in vivo* two-photon imaging with computational reconstruction (Bittner et al. 2012).

Lipophilic, fluorescent dyes such as Oregon Green 488 BAPTA-1 AM bind to intracellular calcium (Ca^{2+}) and shifts in their fluorescence intensity can be used as surrogate markers of calcium load (Tada et al. 2014). *In vivo* two-photon imaging of animals harboring AD-causing mutations in APP and PS1 showed reduced spiking, as visualized by OGB-1 traces. In addition, “hyperactive”, increasingly spiking neurons, especially in close proximity to β-amyloid plaques, revealed the bimodal effects of β-amyloid aggregates on neuronal excitability (Busche et al. 2008). Live imaging through a cranial window of animals expressing GFP under the Thy1 promoter in neocortical neurons (strain GFP-M) was used to study the effects of seizures on dendritic morphology (Rensing et al. 2005; Feng et al. 2000). After chemically induced seizures through administration of 4-aminopyridine, only minimal alterations in dendritic spine morphology could be found (Rensing et al. 2005). Using kainate injections for modelling seizures and the same imaging techniques from the aforementioned study, contrary results were obtained, i.e., widespread dendritic spine degeneration in the acute seizure phase (Zeng et al. 2007).

Bioluminiscence imaging (BLI) refers to the detection of light emitted from a bioluminiscent source, most commonly generated by an enzyme (e.g., luciferase, luc) and its substrate (e.g., luciferin) (Hochgrafe and Mandelkow 2013). Transgenic mice were created that contained an inducible, bidirectional expression system for stoichiometric expression of human Tau protein mutants and luciferase (Sydow et al. 2011). The tau burden of neurons positively correlated with BLI signal and interestingly, when production of Tau protein and luminensce was ceased, pathological synaptic alterations induced by pathological Tau mutants could be ameliorated (Sydow et al. 2011). Bigenic mice expressing luc under the glial fibrillary acidic protein (GFAP) promoter and expressing mutants of human APP were used to study reactive gliosis in AD (Watts et al. 2011). BLI signals showed an age-dependent increase in β-amyloid plaques overexpressing mice and intracerebral inoculation of AD brains from old mice to young mice resulted in an accelerated disease onset, as could be measured through rapid elevations of BLI (Watts et al. 2011). Toll-like receptor 2 (TLR2) is strongly upregulated in microglial cells upon injury, hence a dual luc/GFP reporter system under the control of a murine TLR2 promoter was implemented into a transgenic mouse to study microglial activation in brain ischemia *in vivo* (Lalancette-Hebert et al. 2009). Surprisingly, the authors observed biphasic findings, i.e. acute and chronic, microglial response after brain ischemia. Of note they could also observe an activation of microglial cells in the olfactory bulb upon brain injury, additional to the site of injury, suggesting the recruitment of olfactory bulb microglial cells in ischemic conditions (Lalancette-Hebert et al. 2009).

Imaging prion neurotoxicity *in vivo*

Early attempts to investigate prion-induced toxicity by means of live imaging were attempted by Negro an co-workers. Specifically, human epithelial carcinoma (HeLa), murine neuroblastoma (N2a) and Chinese hamster ovary (CHO) cells expressed bovine PrP^C ($bPrP^C$) and bovine orthologs of the pathogenic human PrP^C mutations D178N/129M and E200K fused to GFP (Negro et al. 2001). When comparing the subcellular distribution of the mutant proteins

to wild-type, PrP^C mutants exhibited a higher fraction of retention in the ER, and to a lesser degree in the Golgi apparatus (E200K). However, bovine PrP^C mutants did not alter significantly from their human counterparts (Negro et al. 2001).

In mammalian prion diseases and other neurodegenerative diseases, neuropathology is marked by pronounced reactive gliosis, i.e., astrocytes develop a protoplasmic phenotype accompanied by a strongly eosinophilic cytoplasm representing the morphological correlate of increased protein expression of GFAP and vimentin and others (Singh and Joshi 2017). GFAP is not required for prion pathogenesis as mice devoid of GFAP do not exhibit altered disease incubation times or deposition patterns of PrP^{Sc} upon prion infection compared to their wild-type counterparts (Tatzelt et al. 1996). A transgenic mouse expressing luciferase (luc) under the GFAP promoter, i.e. Tg(*Gfap*-luc), bioluminescence imaging (BLI, see above) was used to determine the kinetics of GFAP activiation in intercerebrally prion-inoculated animals (Tamguney et al. 2009). Accumulation of PrP^{Sc} could be detected as early as 42 days post-infection (dpi) while GFAP was detectable at the mRNA level and by BLI at 55 dpi, in accordance with prior reports on the temporal evolution of prion disease (Jendroska et al. 1991). BLI signal was inversely proportional to the infectivity titers used for inoculation and assessing prion pathology in Tg(*Gfap*-luc) mice provided an increase in sensitivity as signals on BLI markedly preceded neurological dysfunction. On the other hand, GFAP activation is not restricted to prion-induced pathology but also encountered in other pathological processes such as trauma, e.g., intracerebral inoculation with dull needles, which results in decreased specificity of measuring prion pathology in Tg(*Gfap*-luc) mice (Singh and Joshi 2017; Tamguney et al. 2009). Testing of Compound B, an amyloidophilic compound against prion disease in Tg(*Gfap*-luc) mice showed efficient neuroprotection against mouse-adapted prions, but not against human CJD prions, as measured by BLI (Lu et al. 2013).

A cyanine, near-infrared (NIR) autofluorescent contrast agent was conjugated to Valine-Alanine-Aspartate-fluoromethylketone (VAD-fmk, yielding NIR-VAD-fmk), which binds to the active site of caspases and allows for live imaging of apoptosis *in vivo*, (Lawson et al. 2010; Morita-Fujimura et al. 1999). After intracerebral inoculation with the M1000 prion strain,

*Tga*20 mice were injected with NIR-VAD-fmk and subjected to fluorescence reflectance imaging. After 45 dpi, a strong autofluorescence signal was observed in prion-inoculated, but not in sham-inoculated animals. On the other hand, although injection of 2 subsequent doses of NIR-VAD-fmk did not show observable toxicity, the potential of the compound for repetitive imaging was not demonstrated (Lawson et al. 2010). The YFP-H mouse line (Feng et al. 2000) expressing YFP predominantly in hippocampal and cortical neurons, has been used for studying synaptic spine dynamics in prion disease (Fuhrmann et al. 2007). Repetitive imaging through a chronically implanted, cortical window facilitated investigations of early synaptic changes in prion-infected mice. Computational modelling of spines yielded unprecedented insights into spine dynamics in prion disease, although this *in vivo* approach is not suitable for medium-to high-throughput screenings of putatively neuroprotective anti-prion compounds (Fuhrmann et al. 2007).

In vivo, manganese-enhanced magnetic resonance imaging (MEMRI) impressively demonstrated the effects of anti-PrP^C antibody-mediated toxicity (Sonati et al. 2013). Monoclonal anti-PrP^C antibodies targeting the globular domain of PrP^C (PrP^C-GD) showed widespread and rapid neurotoxicity closely resembling genuine prion diseases. Stereotaxic injection of the anti-PrP^C-GD antibody POM1 demonstrated rapid formation of brain edema and subsequent cerebellar atrophy within a few days as was seen by MEMRI (*Figure* 5, (Sonati et al. 2013; Reimann et al. 2016)). Contralateral injection of POM1 pre-incubated with recombinant, full-length murine PrP^C ($rmPrP_{23-230}$) was innocuous. Moreover, anti-PrP^C-GD antibody-mediated toxicity was dependent on the presence of a functional flexible tail of PrP^C (PrP^C-FT), since genetic or pharmacological ablation of PrP^C-FT was neuroprotective (Sonati et al. 2013).

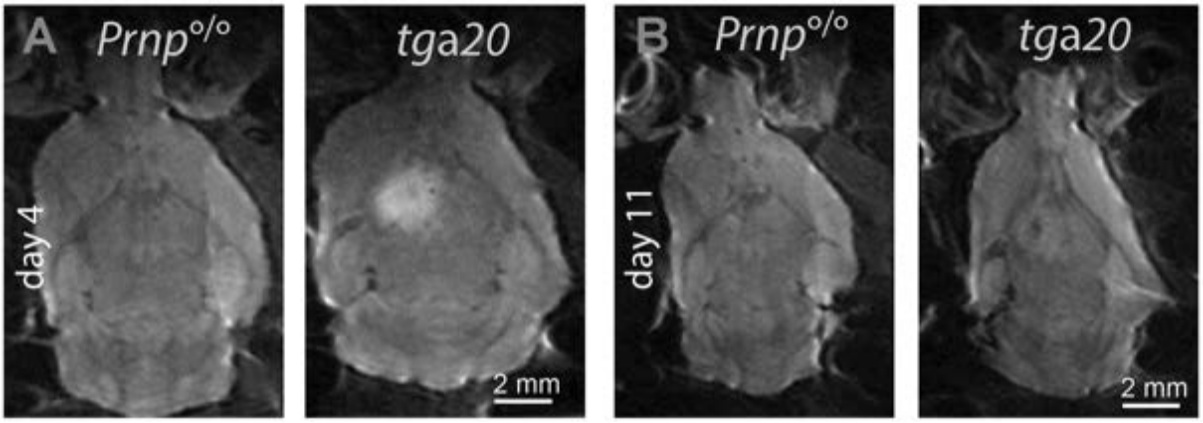

***Figure* 5.** (A) Injection of the neurotoxic anti-PrP^{C} antibody POM1 into the brain of PrP^{C}-overexpressing *Tga*20 mice leads to a diffusion restriction 4 days after injection as visualized by the hyperintense signal. POM1 injection into *Prnp*$^{0/0}$ (ZH1) mice does not elicit toxicity. (B) The same animals were re-imaged 11 days post-injection: no diffusion restriction is no longer visible, indicating resorption of the acute injury.

When assessing the dose-dependent toxicity of a variety of anti-PrP^{C} monoclonal antibodies, dose-escalation of the anti-PrP^{C}-GD targeting antibody ICSM18 showed hyperintense lesions on MEMRI corresponding to pathologically altered hippocampal neurons as observed on H&E histology, putting the therapeutic potential of ICSM18 as a potential anti-prion and anti-AD therapeutic in question (Klyubin et al. 2014; Reimann et al. 2016).

Part I – Novel *in vivo* assays to measure prion-induced neurodegeneration

Aims of the study

My goal is to establish a reliable, *in vivo* live-imaging assay to study neuronal cell loss in prion disease. As laid out before, currently available techniques are limited to low-throughput methods (MEMRI, imaging of spine dynamics through chronic windows) that do not allow medium- to high-throughput screening of putatively neuroprotective compounds (Reimann et al. 2016). Furthermore, current screening methods rely mainly on post hoc immunohistochemistry using neuronal markers such as neuronal nuclei (NeuN) resulting in a large read-out variability (Sonati et al. 2013; Falsig et al. 2012). By exposing hippocampal and cerebellar organotypic slice cultures expressing fluorescent reporter proteins in a subset of neurons to repeated *in vivo* confocal laser scanning microscopy (CLSM), I have reduced read-out variability by taking into account pre-treatment slice viability and inter-slice variability.

Results

Time-lapse confocal imaging of YFP^{+} CA1 pyramidal neurons in YFP16 HOCS confirms neurotoxicity of PrP^{C}-GD targeting antibodies

In a first step, I determined the contributing background values of my imaging setup (i.e. YFP16 HOCS on PFTE membranes in slice culture medium) to EYFP reference spectra by recording lambda stacks of individual culture components without YFP16 HOCS, herein, when measuring cell bodies, background fluorescent did not contribute more than 5% of the total recorded signal (*Figure* 6A).

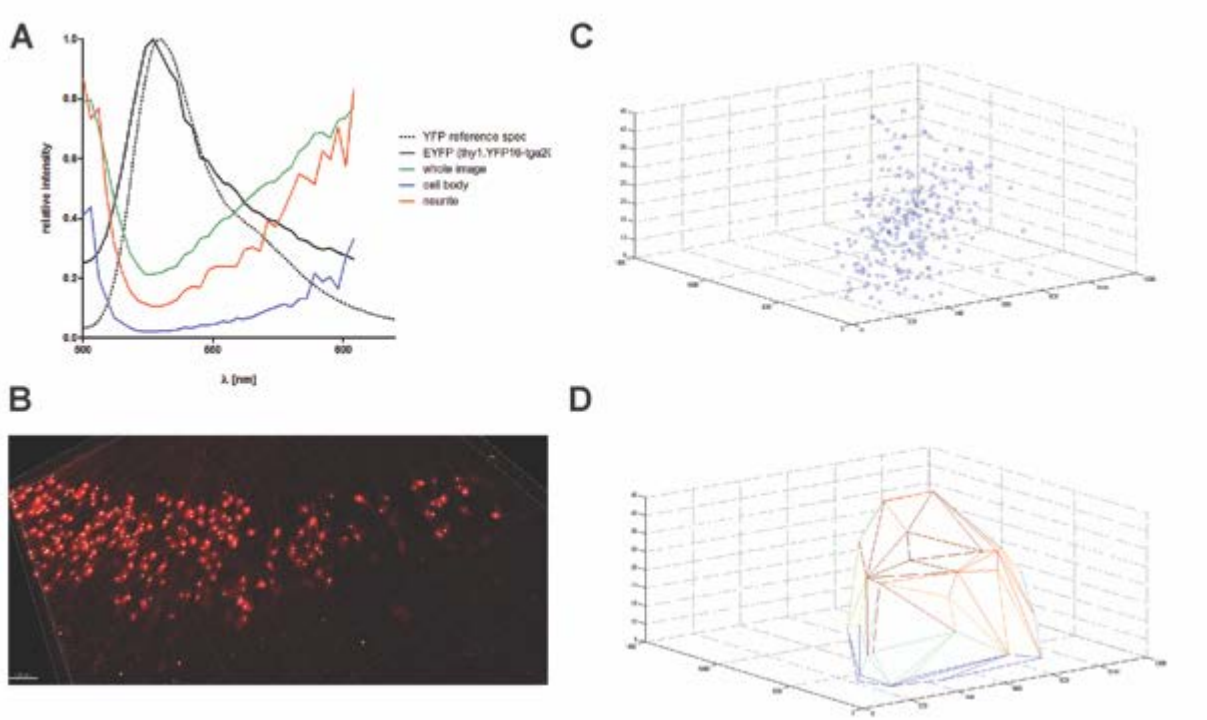

***Figure* 6.** (A) Lambda stacks of YFP16 HOCS show a contributory noise level of less than 5% for assessing cell bodies (blue line) in peak fluorescence spectrum from YFP reference spectrum (dashed line, Invitrogen/Life Technologies, Grand Island, NY, USA) and enhanced YFP (solid black line, fluorophore used in these experiments). Enhanced noise ratios are observed for imaging of neurites (red line); green line denotes unspecific background region of interest. Semiautomatic identification of neuronal cell bodies through IMARIS Spots (C) and graphical visualization of spots (D) and computation of encompassing volume through a convex hull (E); axes = [pixel]. Scale bar = 100 µm.

Neurons were counted semi-automatically using IMARIS spots function (*Figure* 6B) and the encompassing volume of counted neurons was calculated using MATLAB *convhull* function (*Figure* 6C, D). Fluorescent protein expression in YFP16 HOCS was exclusively limited to a

subset of CA1 pyramidal neurons as was confirmed by YFP-NeuN double staining on immunohistochemistry (mean Pearson's r=0.58 ± 0.09 for colocalized $YFP^+/NeuN^+$ pixel, n=7, *Figure 7*A).

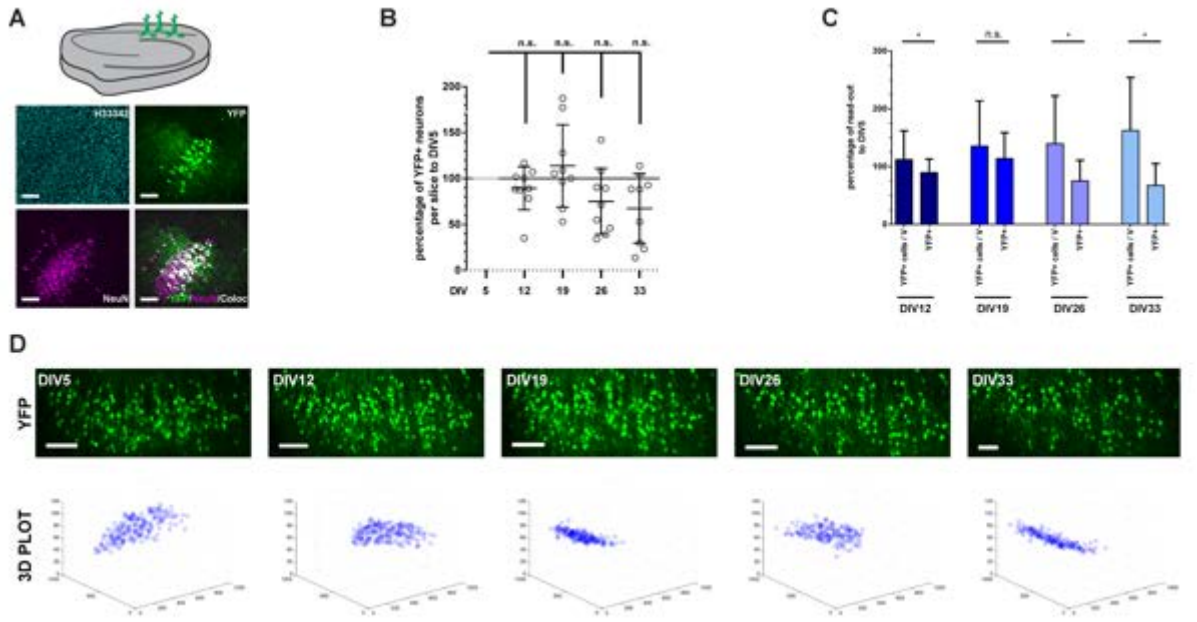

Figure 7. (A) *Upper drawing*: Schematic depiction of YFP^+ CA1 pyramidal neurons in YFP16 HOCS. *Lower panel*: Post hoc immunostainings for cell nuclei (H33342) and neuronal nuclei (NeuN) of YFP16 HOCS with subsequent colocalization analysis for $YFP^+/NeuN^+$ positive pixels showed a high correlation (grey pixels, lower right image, Pearson's r=0.58 ± 0.09). Scale bar = 100 µm. (B) Time-course analysis of untreated YFP16 HOCS showed no significant spontaneous neurodegeneration over 5 weeks (one-way ANOVA with Dunnett's post-test, n.s. [not significant]). (C) Counting of absolute neurons showed significantly reduced read-out variability than YFP^+ neurons-to-encompassing volume ratio ($p<0.05$ in 3 of 4 comparisons, F-test of equality of variances). (D) YFP16 HOCS allowed for re-tracing of identical neuronal populations and individual neurons in confocal imaging (maximum intensity projections from the same YFP^+ slice, *upper panel*) as well as in three-dimensional point reconstruction (*lower panel*). *Upper panel*: scale bar = 100 µm, *lower panel*: axes are given in [µm].

To determine long-term viability of repeated recordings of YFP16 HOCS, slices were imaged during 5 weeks after dissection starting from 5 days *in vitro* (DIV5). Semi-automated counts of absolute YFP^+ neurons per slice obtained throughout the recorded time period were normalized to baseline YFP^+ neuron counts of each corresponding slice (i.e. DIV5). YFP^+ neurons did not significantly decrease throughout the recorded time period when compared to baseline (*Figure 7*B) and semi-automated counting of YFP^+ hippocampal CA1 pyramidal neurons showed less read-out variability than the ratio of cell to total YFP^+ encompassing volume ($p<0.05$ in 3 of 4 comparisons, F-test of equality of variances, *Figure 7*C). Repetitive imaging allowed re-tracing of the same neuronal population over several time points (*Figure*

*7*D*, upper panel*). Also, three-dimensional neuronal cell distribution was reconstructed using MATLAB that also allowed re-tracing of single neurons from reconstructed point clouds (*Figure* 1D*, lower panel*).

I have crossed YFP16 mice (harboring 2 wild-type alleles of *Prnp*) to PrP^{C} overexpressing *Tga*20 mice, yielding $YFP16^{Tga20/-}$ mice that allow for sensitive investigation of neurotoxic anti-PrP^{C}-GD antibodies (Fischer et al. 1996). $YFP16^{Tga20/-}$ HOCS were treated with a full-length ([67 nM], 10 days) or a Fab_1-fragment ([67 nM], 6 days), respectively, of the PrP^{C}-GD targeting antibody POM1. Anti-prion protein antibodies pre-incubated with $rmPrP_{23\text{-}230}$ at molar excess ([134 nM]) were used as negative controls.

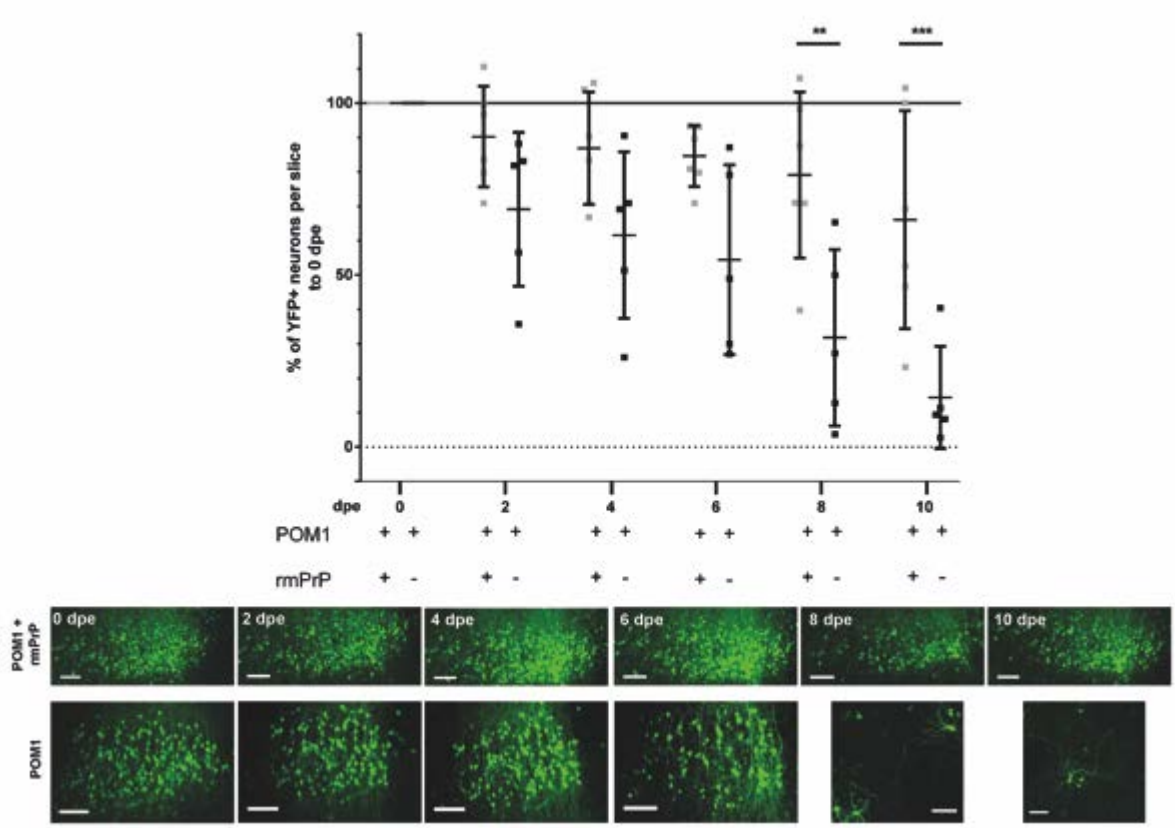

***Figure* 8**. *Upper graph*: Time-lapse confocal imaging of $YFP16^{Tga20/-}$ HOCS treated with POM1 in the presence and absence (+/-) of $rmPrP_{23\text{-}230}$ shows significantly reduced YFP^{+} CA1 pyramidal neurons from 8 dpe, $p<0.01$ (one-way ANOVA with Sidak's post hoc test). Treatment was initiated after recording of baseline (i.e. dpe 0) and then re-added on days 2, 4, 6 and 8. *Lower panel:* Maximum intensity projections of imaged z-stacks demonstrate significant neurotoxicity of full-length POM1. Scale bars = 100 µm.

Slices were always imaged once at baseline and then every other day (full-length POM1, POM1) or every day (Fab_1-fragment of POM1, Fab_1POM1) using confocal time-lapse

microscopy. Treatment of YFP16$^{Tga20/-}$ with the PrP^{C}-GD targeting monoclonal antibody POM1 (*Figure 8*) and its Fab$_1$ fragment (*Figure* 4) showed severe neurotoxicity after only a few days

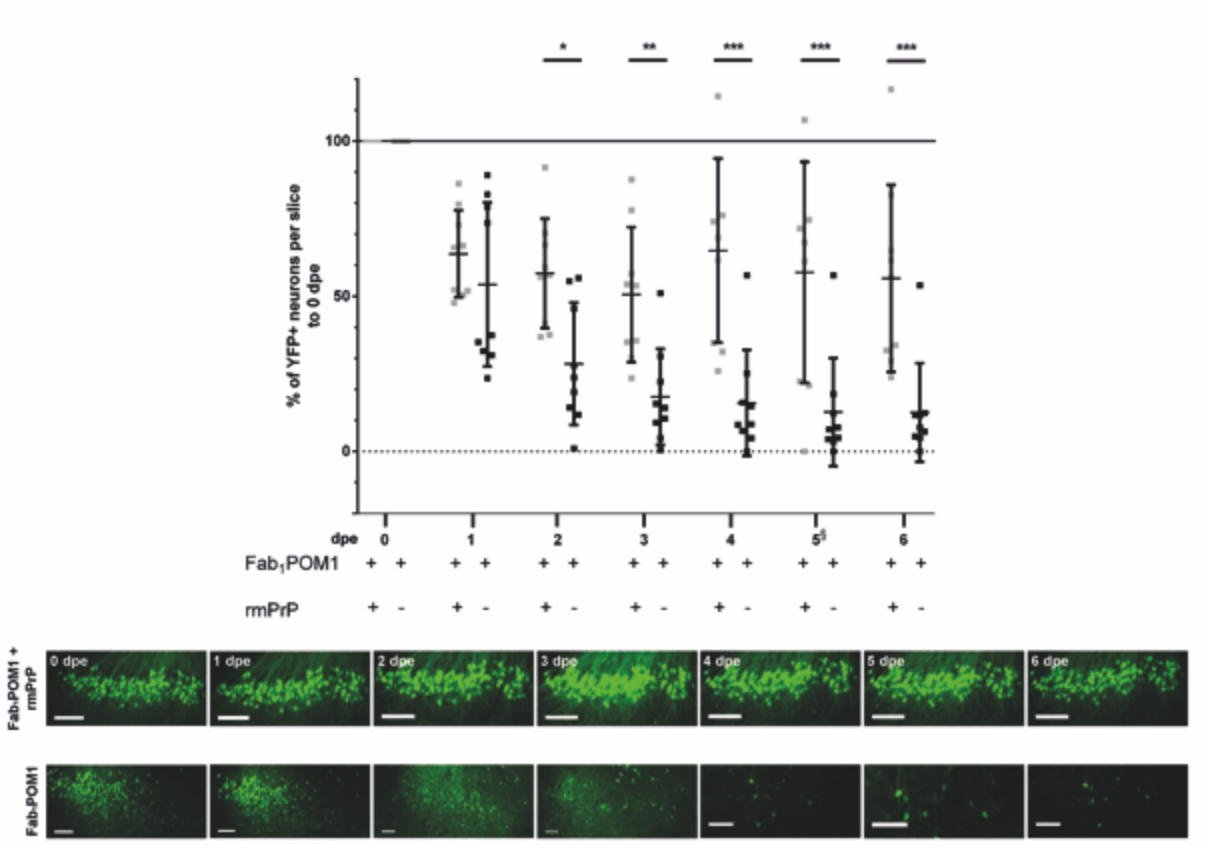

***Figure* 9**. *Upper graph:* Time-lapse confocal imaging of Tg(YFP16:tga20$^{tg/wt}$) HOCS treated with a Fab$_1$-fragment of POM1 +/- rmPrP shows markedly accelerated neurotoxicity, as soon as 2 dpe ($p<0.05$, one-way ANOVA with Sidak's post hoc test) that was sustained until the end of the imaged time-frame, i.e. 6 dpe. Treatment was initiated after recording of baseline (i.e. dpe 0) and then re-added on days 2, 4, 6 and 8. *Lower panel:* Maximum intensity projections of imaged z-stacks demonstrate significant neurotoxicity of Fab$_1$POM1 Scale bars = 100 µm. §: 1 HOCS was not readable on 5 dpe due to a technical error.

of treatment initiation ($p<0.01$ on day 8 for POM1, n=5, vs. POM1+ rmPrP, n=6, and $p<0.05$ on day 2 for Fab$_1$POM1 vs. Fab$_1$POM1 + rmPrP, n=9 for both treatment groups) that was sustained in both treatment schemes until the end of the imaged period.

Slice-based reconstruction of neuronal loss in YFP16 HOCS treated with PrP^{C}-GD targeting antibodies

Best curve estimates for reconstruction of single-slice based neuronal cell loss during the recorded time-course were assessed by the calculation of Akaike Information Criteria values adjusted for finite sample sizes (AICc) in 9 different curve estimation models (*Table* 1).

***Table* 1. Curve estimation equations used for modelling neurodegeneration** (*k = regression constant, λ = regression coefficient, t = time constant, u = upper boundary value*).

Linear	$y = k + \lambda * t$
Logarithmic	$y = k + \lambda * \ln(t)$
Inverse	$y = k + \lambda / t$
Compound	$y = k * \lambda^t$
Power	$y = k * t^\lambda$
S-curve	$y = e^{k+\lambda/t}$
Growth	$y = e^{k+\lambda*t}$
Exponential	$y = k * e^{\lambda*t}$
Logistic	$y = \frac{1}{1/u + k * \lambda^t}$

***Table* 2. Modeling neurodegeneration in YFP16 HOCS by comparison of Δ_i from different AICc values (*see Methods*).**

Table 2a. Δ_i values from control treated (i.e. (Fab_1)-POM1 + $rmPrP_{23-230}$) slices (k=2 for every model, RSS = residual sum of squares, n=14).

Model	*RSS*	Δ_i
Linear	622.556	771.3091
Logarithmic	593.521	748.9662
Inverse	654.746	749.5849
Compound	0.232	0
Power	0.353	4.719
S-curve	0.520	23.3895
Growth	0.228	0
Exponential	0.745	0
Logistic	1.608	233.3304

Table 2b. Δ_i values for (Fab_1)-POM1 treated slices (n=13).

Model	*RSS*	Δ_i
Linear	835.849	654.2637
Logarithmic	862.468	634.1705
Inverse	1090.613	660.4375
Compound	0.442	0
Power	0.789	47.036
S-curve	1.215	89.9362
Growth	0.438	0
Exponential	1.198	0
Logistic	2.038	100.9743

Strikingly, both groups showed the lowest AICc values for compound, growth and simple exponential equations, so we chose neuronal loss to be modeled by a compound function with a simple equation (*Tables* 1+2). This resulted in a good fit of the model as expressed through the root mean square error RMSE = 0.26 ± 0.2 (n=29). Individualized slopes of neuronal loss were reconstructed using a compound fit (*Figure 10*).

The regression coefficients showed a significant difference when comparing (Fab_1-)POM1 treated slices and their control treated counterparts (POM1+rmPrP 0.95 ± 0.04, n=6, versus

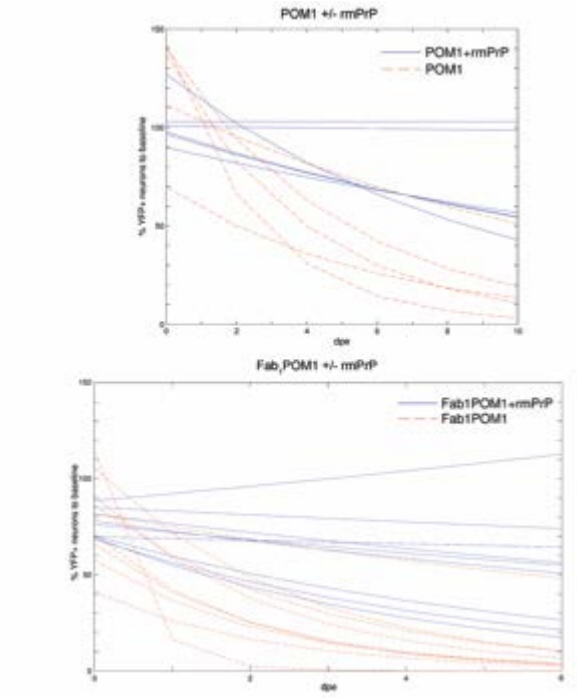

***Figure* 10**. Individualized slice-based slopes of neuronal loss were reconstructed using a compound fit for both POM1 in the presence or in the absence of $rmPrP_{23-230}$ (+/- rmPrP, *upper graph*) and Fab_1POM1 +/- rmPrP (*lower graph*) treated slices.

POM1 0.81 ± 0.09, n=5, p<0.05; Fab_1POM1+rmPrP 0.92 ± 0.08, n=9, versus Fab_1POM1 0.68 ± 0.10, n=8, p<0.001; one-way ANOVA with Sidak's post hoc test, *Figure* 11). Interestingly, a significant difference was observed when comparing the regression coefficients between HOCS treated with POM1 and Fab_1POM1 (p<0.05) while regression coefficents between (Fab1-) POM1+rmPrP treated HOCS did not differ significantly (one-way ANOVA with Sidak's post hoc test, *Figure* 11). These findings also point towards an accelerated neurodegeneration through the Fab_1-fragment of POM1 when compared to the whole antibody.

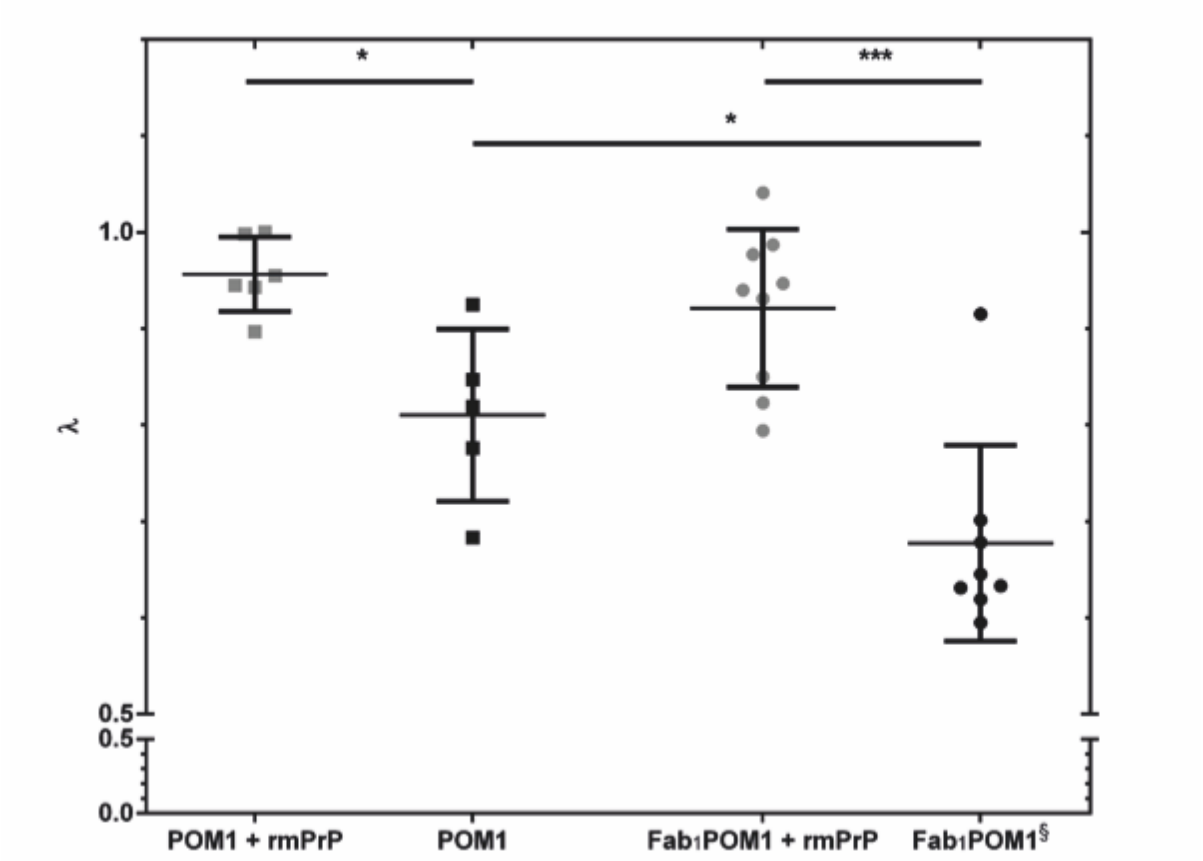

***Figure* 11.** Regression coefficients from curve estimation models showed a significant difference when comparing (Fab_1-)POM1 treated slices to their control treated counterparts (i.e. through pre-incubation with $rmPrP_{23-230}$). Regression coefficients of neuronal cell loss in Fab_1POM1 treated HOCS were also significantly reduced when compared to treatment with the whole antibody. * p<0.05, *** p<0.001; one-way ANOVA with Sidak's post hoc test.

Time-lapse imaging of YFP16 HOCS reduces read-out variability compared to post hoc morphometry

In order to compare the newly established *in vivo* imaging of YFP16 slices to the commonly employed *post hoc* NeuN morphometry, I challenged non-fluorescent HOCS from *Tga*20 mice with an identical treatment regimen, fixed and stained HOCS at defined time points (*Figure 12*). As previously reported, the NeuN-immunopositive area of (Fab_1-)POM1 treated HOCS

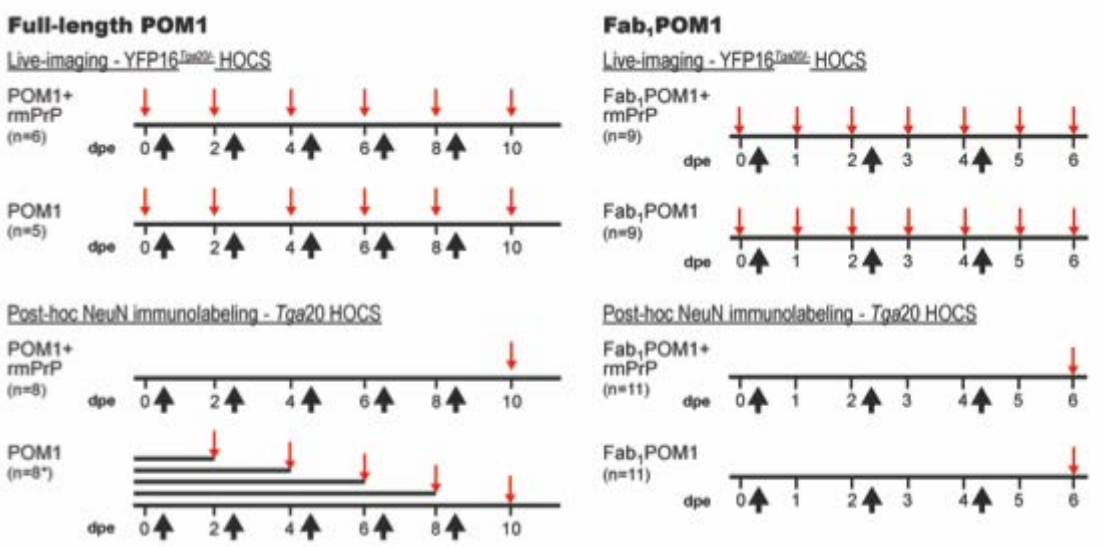

Figure 12. Treatment schemes used for read-out comparison of live-imaging versus post hoc NeuN immunolabeling. Black horizontal lines denote 1 treatment group, red arrows indicate imaged time points, and black arrows administration of treatment. *Here for all treatment groups n=8, except for POM1 treatment for 6 days, n=10 (*middle bar*).

was normalized to the average of control-treated slices, here (Fab_1-)POM1 treated HOCS with pre-incubated full-length $rmPrP_{23-230}$ (Falsig et al. 2012). *Tga*20 HOCS treated three times with Fab_1POM1 showed significant neurotoxicity after 6 days on NeuN morphometry when compared to those with pre-incubated $rmPrP_{23-230}$ ($p<0.01$, Fab_1POM1+$rmPrP_{23-230}$ [n=10] vs. Fab_1POM1 [n=11], paired two-tailed t-test, *Figure 13*A). *Tga*20 HOCS treated with POM1 +/- $rmPrP_{23-230}$ did not show any significant neuronal cell loss after 10 days of treatment comparing to the whole treatment course (one-way ANOVA with Dunnett's post hoc test). In contrast,

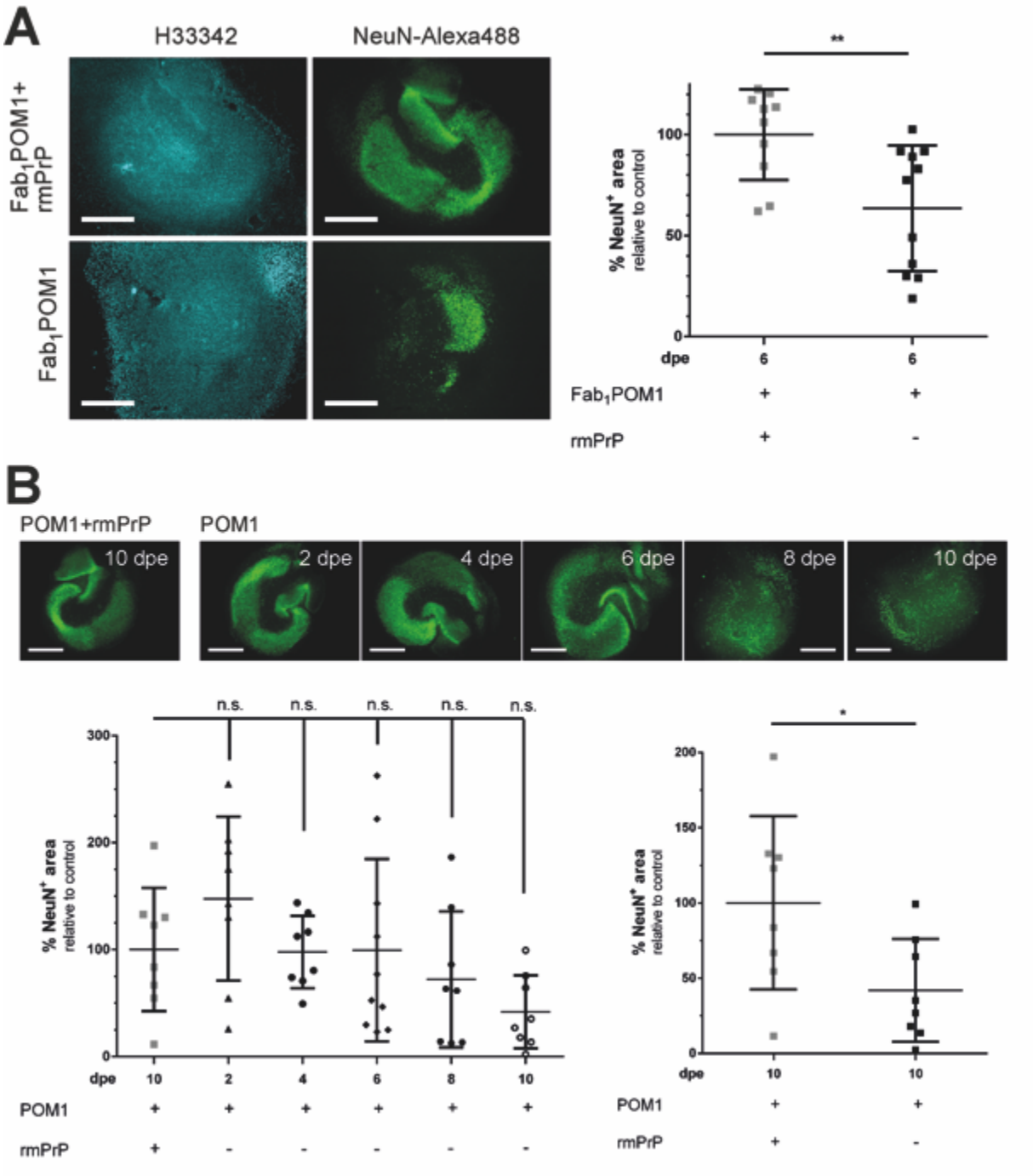

Figure 13. (A) Treatment of *Tga*20 HOCS with Fab$_1$POM1 for 6 days resulted in significantly decreased NeuN$^+$ cells as determined by NeuN morphometry ($p<0.01$, Fab$_1$POM1+rmPrP, n=10, vs. Fab$_1$POM1, n=11, paired two-tailed t-test). *Left panel*: representative fluorescent micrographs of NeuN immunolabeled HOCS counterstained with Hoechst 33342, 6 dpe. Scale bars = 500 µm. (B) Fluorescent micrographs (*top panel*) of POM1 +/- rmPrP treated *Tga*20 HOCS showing post hoc NeuN immunolabeling (scale bars = 500 µm). NeuN morphometry of the recorded time-course resulted in high read-out variability and did not show a significant neurotoxic effect of POM1-induced neurotoxicity (*lower left graph*) although an end-point based comparison (i.e. after 10 days) resulted in significantly decreased NeuN$^+$ area in treated HOCS ($p<0.05$, paired two-tailed t-test) (*lower right graph*).

YFP16$^{Tga20/-}$ animals showed a significant neurotoxicity after 8 dpe (days post-exposure) (*Figure 13*). The discrepancy of this finding seems noteworthy since PrP^C protein levels in *Tga*20 mice are around 10-fold higher when compared to wild-type mice than those of *Tga*20$^{+/-}$

showing around 6- to 7-fold higher expression levels of PrP^C than wild-type animals, pointing towards an increased sensitivity of YFP16 HOCS (Fischer et al. 1996). A post hoc two-group endpoint comparison (i.e. 10 dpe only) between POM1 and POM1+rmPrP did in prion protein levels show a significant neurotoxic effect ($p<0.05$, paired two-tailed t-test, *Figure 13*B).

Prnp$^{0/0}$ mice do not succumb to prion disease or anti-PrP^C-GD antibody-mediated toxicity (Sonati et al. 2013; Bueler et al. 1993). I crossed YFP16 mice with *Prnp*$^{0/0}$ (ZH1) mice, yielding YFP16$^{ZH1/ZH1}$. 14 days of treatment with a single-chain fragment of the variable domains (scFv) of POM1 (scFvPOM1) showed profound toxicity in YFP16$^{Tga20/-}$ ($p<0.01$, scFvPOM1 [n=8] vs. scFvPOM1+rmPrP$_{23-230}$ [n=8], one-way ANOVA with Dunnett's post hoc test), but not in YFP16$^{ZH1/ZH1}$ HOCS ($p<0.01$, scFvPOM1 in YFP16$^{Tga20/-}$ [n=8] vs. scFvPOM1 in YFP16$^{ZH1/ZH1}$ [n=9], one-way ANOVA with Dunnett's post hoc test, *Figure 14*A). Likewise, on *post hoc* NeuN immunohistochemistry, scFvPOM1 showed neurotoxicity in YFP16$^{Tga20/-}$ ($p<0.01$, scFvPOM1 [n=8] vs. scFvPOM1+rmPrP$_{23-230}$ [n=8], one-way ANOVA with Dunnett's post hoc test), but not in YFP16$^{ZH1/ZH1}$ HOCS ($p<0.001$, scFvPOM1 in YFP16$^{Tga20/-}$ [n=8] vs. scFvPOM1 in YFP16$^{ZH1/ZH1}$ [n=9], one-way ANOVA with Dunnett's post hoc test, *Figure 14*B).

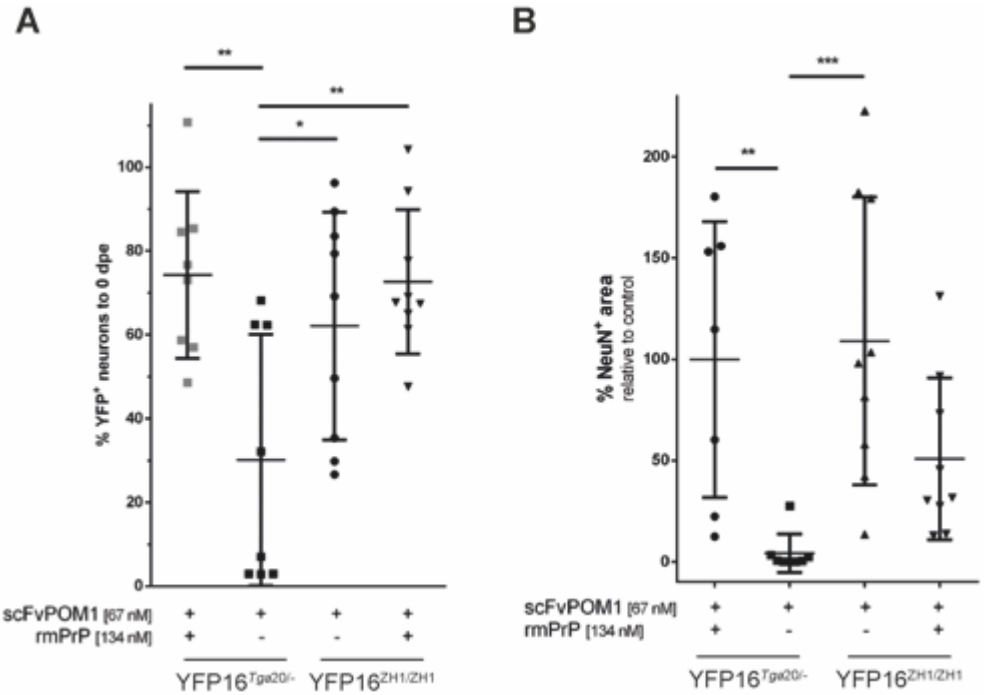

Figure 14. (A) Treatment with scFvPOM1 leads to significant neurotoxicity in YFP16$^{Tga20/-}$, but not in YFP16$^{ZH1/ZH1}$ HOCS. (B) Post hoc staining of YFP16$^{Tga20/-}$ and YFP16$^{ZH1/ZH1}$ HOCS with NeuN shows PrP^C-dependent toxicity of scFvPOM1, as YFP16$^{ZH1/ZH1}$ HOCS do not show a reduction of NeuN+ area when compared to YFP16$^{Tga20/-}$ HOCS. * $p<0.05$, ** $p<0.01$, *** $p<0.001$; one-way ANOVA with Dunnett's post hoc test.

To further test read-out variability of YFP16 HOCS, I tested compounds known to ablate anti-PrP^C-GD mediated toxicity, such as the anti-PrP^C-FT antibody POM2, the ROS scavenger ascorbic acid (AscA) and the calpain inhibitor calpeptin (Herrmann et al. 2015). Treatment for 12 days of $YFP16^{Tga20/-}$ with scFvPOM1 in combination with scFvPOM2 resulted in amelioration of neurotoxicity ($p<0.05$, scFvPOM1 [n=8] vs. scFvPOM1+scFvPOM2 [n=8], one-way ANOVA with Dunnett's post hoc test, *Figure 15*A), while post hoc NeuN stainings of the same slices did not reveal a significant difference ($p>0.05$, scFvPOM1 [n=8] vs. scFvPOM1+scFvPOM2 [n=8], one-way ANOVA with Dunnett's post hoc test, *Figure 15*B).

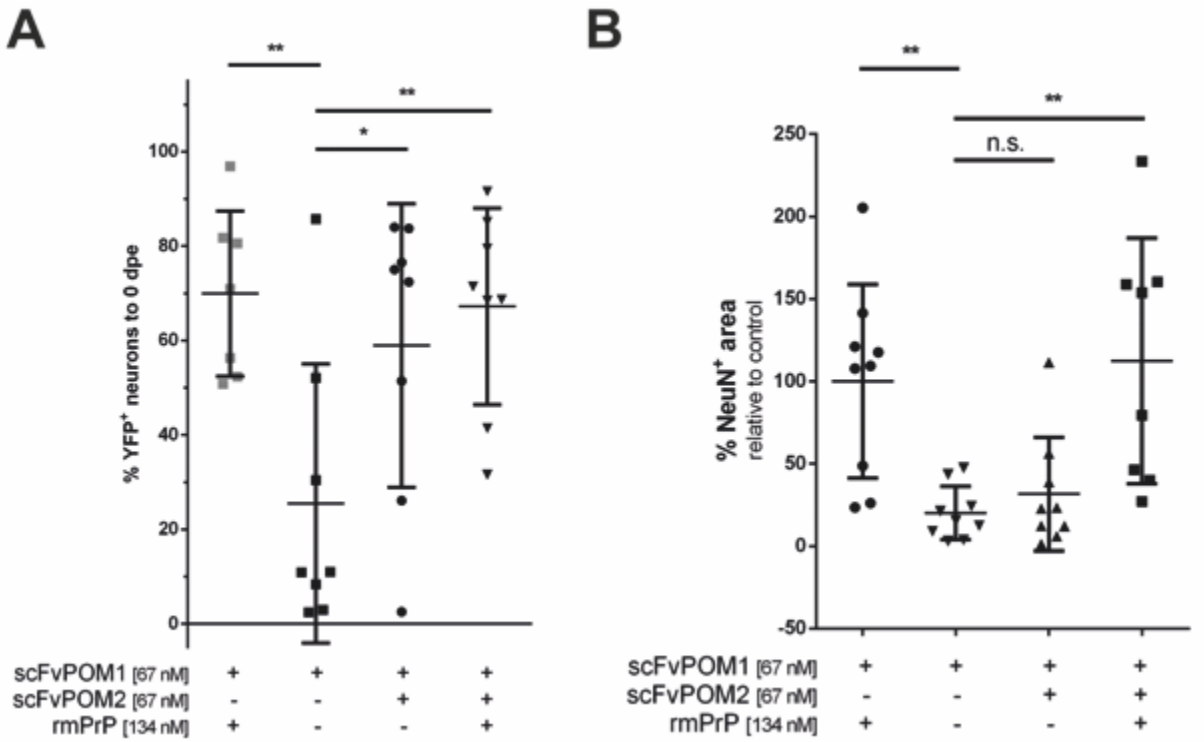

Figure 15. Treatment with scFvPOM2 ablates scFvPOM1-induced toxicity in time lapse imaged $YFP16^{Tga20/-}$ HOCS (A), but not in post hoc NeuN stained HOCS (B). * $p<0.05$, ** $p<0.01$, *** $p<0.001$; one-way ANOVA * $p<0.05$, ** $p<0.01$, *** $p<0.001$; one-way ANOVA with Dunnett's post hoc test. with Dunnett's post hoc test

Likewise, treatment with 50 µM calpeptin ($p<0.001$, scFvPOM1 [n=12] vs. scFvPOM1+Calpeptin [n=9], one-way ANOVA with Sidak's post hoc test, *Figure 16*A) or 2.5 M ascorbic acid ($p<0.001$, scFvPOM1 [n=10] vs. scFvPOM1+AscA [n=10], one-way ANOVA with Sidak's post hoc test, *Figure 16*C) demonstrated ablation of scFvPOM1-mediated toxicity as was observed by live imaging of YFP16 HOCS (*Figures* 16A+C), but not post hoc NeuN staining (*Figures* 16B+D).

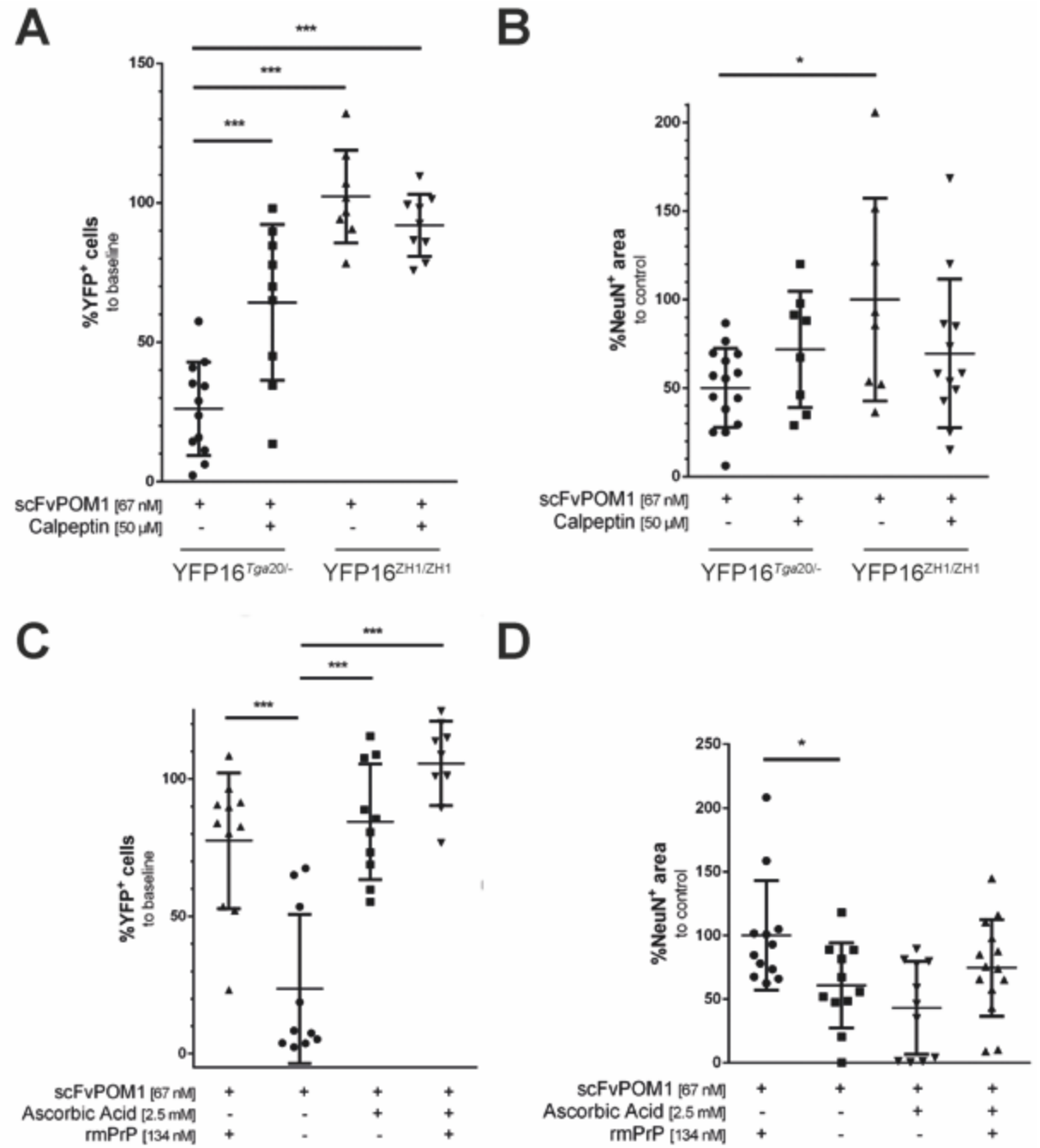

***Figure* 16**. Treatment with the calpain inhibitor calpeptin (A), as well as with the ROS scavenger AscA (C) ameliorates scFvPOM1-induced toxicity in time lapse imaged YFP16$^{Tga20/-}$ HOCS (A), but not in post hoc NeuN stained HOCS (B+D). * p<0.05, ** p<0.01, *** p<0.001; one-way ANOVA * p<0.05, ** p<0.01, *** p<0.001; one-way ANOVA with Sidak's (A+B) / Dunnett's (C+D) post hoc test.

OCS have been shown to faithfully replicate prion pathology (Falsig et al. 2012). In a last step, I investigated the read-out variability of the neuroprotective agent ascorbic acid in RML6-infected YFP16$^{Tga20/-}$ HOCS. As early as 28 days post inoculation (dpi), I could observe significantly increased YFP+ neurons when comparing RML-inoculated slice alone to RML

plus AscA-treated HOCS. This treatment effect was sustained until the end of the investigated time-period ($p<0.05$, RML [n=7] vs. RML+AscA [n=8], one-way ANOVA with Dunnett's post hoc test, *Figure 17*A). Conversely, post-hoc staining of imaged YFP16$^{Tga20/-}$ HOCS on 48 dpi with NeuN did not reveal any treatment effect (*Figure 17*B).

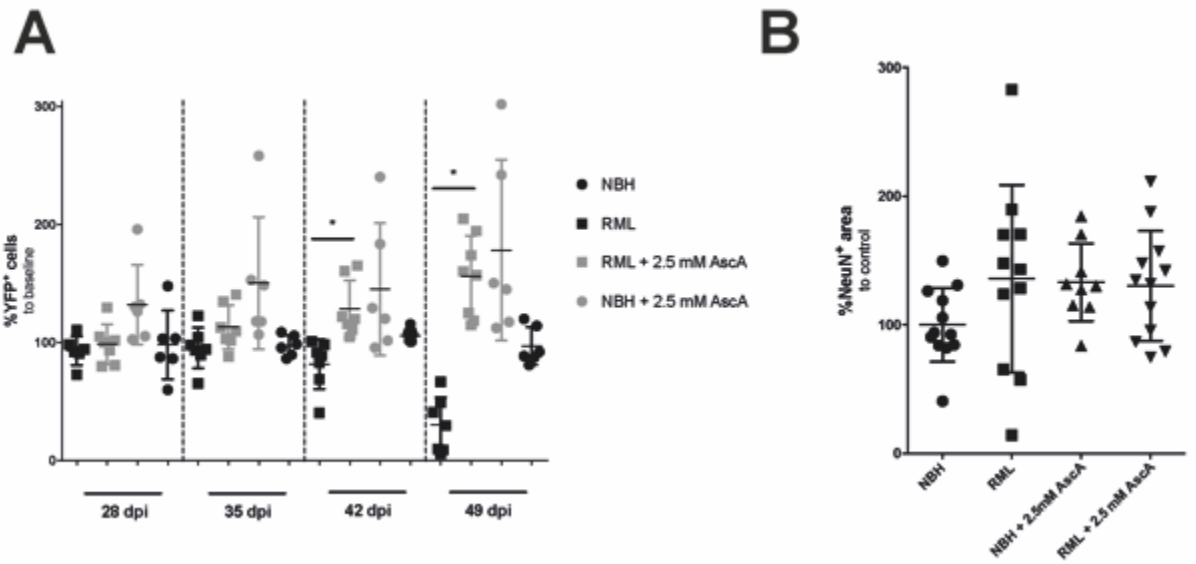

Figure 17. Treatment of RML-infected and NBH control HOCS with the ROS scavenger ascorbic acid showed significant disease amelioration in YFP16$^{Tga20/-}$ HOCS on 42 and 49 dpi ($p<0.05$, RML [n=7] vs. RML+AscA [n=8], one-way ANOVA with Dunnett's multiple comparison test) while post hoc NeuN morphometry on YFP16$^{Tga20/-}$ HOCS stained on 49 dpi did not show any observable treatment effects (B). * $p<0.05$, one-way ANOVA with Dunnett's post hoc test.

What is the overall performance of the live-imaging assay when compared to NeuN morphometry? A statistical evaluation of differences of variance between all n=28 treatment groups showed superiority of live imaging in YFP16 HOCS to NeuN morphometry in n=15 comparisons, equal read-out variability in n=12 and inferiority of YFP16 HOCS live imaging in n=1 comparisons, showing significantly reduced read-out variability of my novel live imaging assay in over 50% of cases.

Discussion and outlook

In this current study I present a novel fluorescence-based live-imaging assay for long-term imaging of a small neuronal subset in hippocampal organotypic slice cultures. I show that this assay reliably reproduced the previous findings of neurotoxic antibodies targeting the globular domain of the cellular prion protein, PrP^{C}-GD, with increased read-out sensitivity in over 50%

of the compared groups. The cerebellar organotypic slice culture (COCS) assay was shown to faithfully reproduce prion pathology *ex vivo.* This discovery allowed convenient pharmacological manipulation and eventually paved the way to demonstrate that PrP^C-antibody induced neurotoxicity is mediated through its flexible tail (Falsig et al. 2008a; Falsig et al. 2012). These observations in PrP^C-dependent neuronal cell death have been complicated through heightened read-out variability using NeuN morphometry from post-hoc immunolabeled COCS. Due to the lack of a suffiently labeled number of YFP^+ neurons in COCS from YFP16 mice, I chose HOCS as an *ex vivo* model for PrP^C-dependent POM1-induced neurotoxicity (Feng et al. 2000).

I crossed YFP16 mice with PrP^C-overexpressing, *Tga*20 mice that serve as a sensitive indicator of prion-induced pathology (Fischer et al. 1996), yielding $YFP16^{Tga20/-}$ mice. Treatment of $YFP16^{Tga20/-}$ with the monoclonal anti-PrP^C-GD antibody POM1 showed significant toxicity after 8 dpe (*Figure 13*), while longitudinal assessment with post hoc, immunohistochemical stainings in HOCS did not show any significant effects (*Figure 13*). High read-out variability in NeuN stained HOCS did not show significant results in multiple testing since an end-point comparison reached statistical significance (*Figure 13*). Further comparisons of POM1 in PrP^C-overexpressing versus $Prnp^{0/0}$ HOCS, as well as rescue of POM1 toxicity through POM2, calpeptin and ascorbic acid showed significantly reduced read-out variability in YFP16 HOCS in over 50% of all treatment groups. Significant inferiority of YFP16 COCS to post hoc morphometry was seen in 3.6% of cases.

What is the reason for the inferiority of post hoc NeuN morphometry in terms of read out variability? In the experiments performed here, large read-out variability obscures significant differences in multiple testing regimens. Furthermore, the downside of repetitive imaging of YFP16 HOCS is its increased toxicity. In addition, re-staining of HOCS after several rounds of imaging might obscure the true effects of gene knock-outs and pharmacological compounds. On the other hand, lowered read-out sensitivity in $YFP16^{Tga20/-}$ HOCS was unrelated to relatively lower expression levels of cellular prion protein: brains from $YFP16^{Tga20/-}$ mice show 6- to 7-fold higher PrP^C expression levels when compared to wild-type, while *Tga*20

mice show around 10-fold higher PrP^C expression levels compared to wild-type. I believe this observation underscores the sensitivity of my assay and suggests that the CA1 area is an early target in PrP^C-mediated neurotoxicity (Fischer et al. 1996).

Consistent with previous findings, Fab_1 and Fab_2-fragments of globular domain targeting PrP^C-antibodies showed more accelerated neurotoxicity than their full-length immunoglobulin counterparts (Sonati et al. 2013). I was able to reproduce this finding in hippocampal slices by showing that treatment of $YFP16^{Tga20/-}$ HOCS with Fab_1POM1 resulted in significant neuronal loss after only 2 dpe when compared to treatment with full-length POM1 (*Figures* 3+4). Since YFP-expression was limited to a small subset of hippocampal CA1 pyramidal neurons, those areas could be re-traced during each imaging time point. This in turn allowed the construction of neurodegenerative slopes with a high goodness of fit assuming an compound equation (*Tables* 1+2*, Figures* 5+6). Lastly, the comparison of computed neuronal loss decay rates further underlined the accelerated neurodegeneration induced by Fab_1-fragments of POM1 and added valuable information to the mechanisms of PrP^C-antibody dependent neurotoxicity (*Figure 16*). When screening putatively neuroprotective or -toxic compounds in neurodegenerative diseases, high read-out variability may stall efforts to identifyinteresting drugs that may broaden knowledge about deregulated pathways during disease. I show here that the semi-automated counting of time-lapse imaged YFP^+ HOCS adds 50% to read-out sensitivity when compared with identical treatment schemes using already established methods such as post-hoc NeuN morphometry.

Neuronal cell death is a commonly shared and pathognomonic hallmark amongst several neurodegenerative diseases such as amyotrophic lateral sclerosis, Parkinson's, Huntington's and prion disease (Bredesen, Rao, and Mehlen 2006). To assess neuronal loss in an experimental setup, a variety of commercially available tools and reagents exist; for instance through the addition of (not necessarily neuron-specific) chemicals that are either taken up or excluded by the cells depending on their viability in the culture system of interest, i.e. primary neuronal cultures, organotypic slice cultures etc. These compounds, including Trypan blue and Propidium iodide, are then quantified using conventional light or fluorescent

microscopy (Giordano et al. 2011). Although they are widely established and their application is rather cheap, they are always end-point based and lack the ability to directly measure the kinetics of cell death over a longer time span. Another - but also indirect - approach to study neuronal cell death by pre-labeling the cells with cell-permeable acetoxymethylester (AM)-conjugated dyes such as calcein AM. However, interpretation may be hampered by spontaneous cellular release of the dye after incorporation leading to reduced read-out sensitivity (Giordano et al. 2011).

Previous live imaging techniques to evaluate neurodegeneration in prion diseases entail bioluminescence imaging (BLI) using Tg(*Gfap*-luc) animals expressing luciferase under the GFAP promoter, i.e., exploiting reactive gliosis as a surrogate marker of prion pathology (Tamguney et al. 2009). BLI is a non-invasive method to longitudianally study neurodegeneration that has been shown to provide a sensitive, preclinical readout in prion-inoculated Tg(*Gfap*-luc) mice. On the other hand, reactive gliosis is a non-specific reaction of the central nervous system to a variety of injuries and can lead to false-positive results (Singh and Joshi 2017). High-resolution imaging of dendritic spine turnover dynamics through a cranial window in mice expressing fluorescently marked neurons yielded unprecedented insights into early prion pathogenesis. However, the invasive nature of animal surgery and imaging, is unlikely to be suitable for parallel screening of several compounds (Fuhrmann et al. 2007). Manganese-enhanced magnetic resonance imaging (MEMRI) was demonstrated to be a sensitive indicator of toxic anti-PrP^C antibodies allowing calculation of dose-response curves (Sonati et al. 2013; Reimann et al. 2016). A major drawback of MEMRI, however, are the side effects of chronic Mn^{2+} administration leading to PD-like symptoms questioning the suitability of MEMRI for longitudinal studies (Silva and Bock 2008). Admittedly, my novel live-imaging based assay may be more expensive and more time-consuming than previous end-point based assays with the need for intercrosses with the genotype of interest, organotypic slice cultures, repetitive imaging, and high-resolution microscopes for live-imaging. Conversely, I believe that this approach may provide valuable information on neurotoxicity screening applications by gathering pharmacokinetic data and reduction of false-negative

results through increased read-out sensitivity. Further optimizations of the assay might include minituarization of the assay, e.g., by using fragments of fluorescent OCS to increase throughput, since I have already shown that a small subset of neurons is enough for sentitive screening.

PART II - The globular domain of the prion protein induces prion neurotoxicity through increased relaxation of its β2α2 loop

Aims of the study

Antibodies and single-chain variable fragment (scFv) targeting certain epitopes of the prion protein PrP^C are acutely neurotoxic. Transcriptional and proteomic analyses indicate that their toxicity closely recapitulates that of prion infections, suggesting that these antibodies mimic the docking of prions to PrP^C. Toxicity is mediated by the flexible tail of PrP^C, implying that antibody binding triggers an allosteric transition within PrP^C. Here I report that POM1 firstly does not induce prion replication and secondly imposes a strict spatial constraint on the flexibility of the β2-α2 loop of PrP^C without appreciably distorting its overall structure. To assess the functional consequences of this constraint, each one of the POM1 residues interacting with PrP^C was replaced with alanine. Single chain variable fragments of the resulting 11 individual mutants were found to be toxic (S32A, D52A, W94A, Y101A), innocuous (D55A), or protective (Y57A, Y104A) to naïve and prion-infected cerebellar organotypic slice cultures (COCS). Toxic mutants induced acute neuronal loss and astrogliosis that, as with their parental antibody POM1, was prevented by antibody scFvPOM2 against the amino terminus of PrP^C. Protective mutants attenuated microgliosis and activation of the unfolded protein response, and suppressed the toxicity of both scFvPOM1 and infectious prions. Molecular dynamics simulations showed that protective mutations led to a relaxation of the β2-α2 loop. Besides implying loop rigidity as a mediator of prion toxicity, these investigations have led to the discovery of dominant-negative immunoreagents binding to PrP^C and quenching prion toxicity. These structural insights provide a well-defined pathway towards the development of efficacious antiprion drugs.

Results

The neurotoxic anti-PrP^{C} antibody POM1 does not elicit prion replication

In order to investigate the possible generation of prions by the neurotoxic, anti-PrP^{C}-GD targeting antibody POM1, I treated PrP^{C}-overexpressing *Tga*20 COCS with either scFvPOM1 (400 nM) or with scFvPOM1 (400 nM) preincubated with a molar excess of rmPrP$_{23\text{-}230}$ (600 nM) for control. This treatment was maintained over 10 days with three medium changes per week; scFvPOM1 was replaced with each medium change. NeuN immunofluorescent stainings, which identify neurons, showed widespread neuronal degeneration in COCS treated with scFvPOM1, but not in COCS treated with antibody that had been preemptively blocked with rmPrP$_{23\text{-}230}$ (*Figure 18*A). To clarify whether this effect was induced by the aggregation of PrP, I analyzed pooled COCS homogenates treated with either scFvPOM1 (n=8) or

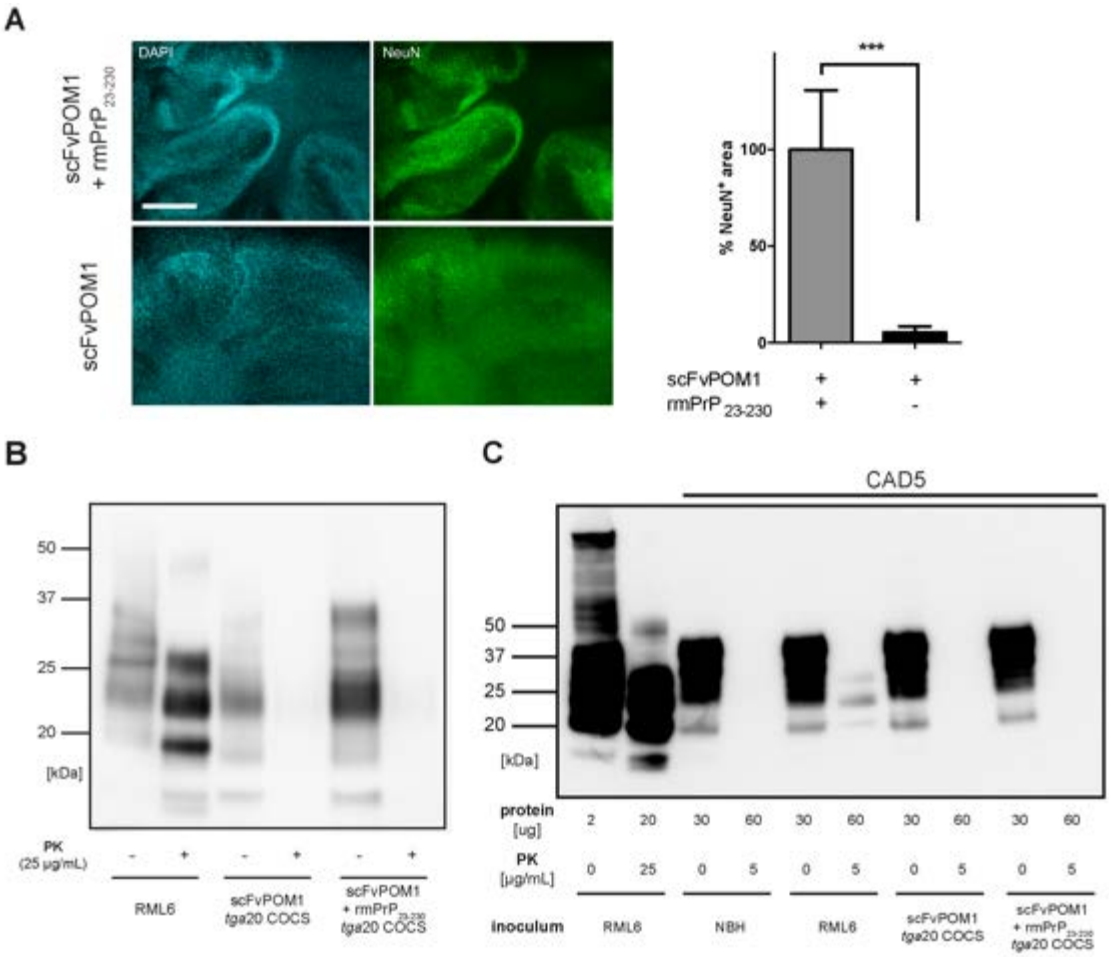

***Figure* 13 (*page 56*).** (A) Chronic treatment of COCS with scFvPOM1 induced profound neurodegeneration. Instead, no neurodegeneration was observed in COCS exposed to scFvPOM1 pre-incubated with rmPrP$_{23-230}$. *** p<0.001, unpaired, two-tailed T-test. Scale bar = 500 µm. (B) Pooled slice homogenates of scFvPOM1-treated (n=8 slices) or (scFvPOM1+ rmPrP$_{23-230}$)-treated *Tga*20 COCS (n=5 slices) did not show PK-resistant species after digestion as is typically observed in RML6 brain homogenate (n=1). (C) No PrP^{Sc} was observed after inoculation of the highly PrP^{Sc}-susceptible cell line CAD5 with pooled scFvPOM1-treated COCS homogenates. CAD5 cells were successfully infected with RML6 as shown by the typical "diagnostic shift" of PK-digested RML6 with un-, mono- and diglycosylated PrP^{Sc} bands. RML6 brain homogenate served as a positive control (left band pair).

scFvPOM1 + rmPrP$_{23-230}$ (n=5) for PrP^{Sc}, an isoform of PrP that is partially resistant to proteinase K (PK) and is universally employed as a surrogate marker for prion infectivity (*Figure 18*B). Pooled slice homogenates from scFvPOM1-treated (n=8) and (scFvPOM1+rmPrP$_{23-230}$)-treated (n=5) *Tg*a20 COCS were analyzed by Western blotting and were found to be devoid of PrP^{Sc}. In contrast, PK digestion of prion-containing brain homogenate (RML6 = passage 6 of the Rocky Mountain Laboratory strain mouse-adapted scrapie prions), which served as positive control, showed the typical diagnostic shift towards a smaller PK-resistant core with un-, mono- and diglycosylated PrP^{Sc}.

The murine neuroblastoma cell line CAD5 is highly susceptible to prion infection and serves as a sensitive bioassay for prion propagation (Enari, Flechsig, and Weissmann 2001). I therefore spiked cell culture media of exponentially growing CAD5 cells with RML6 prions, non-infectious brain homogenate (NBH), or homogenates from COCS that had been exposed to scFvPOM1 or scFvPOM1+rmPrP$_{23-230}$- (6–12 ng protein of total homogenate in 1 mL of cell culture media). After 4 days of culture, I lysed the CAD5 cells and assessed PrP^{Sc} by Western blotting. No PrP^{Sc} was detectable in CAD5 cells inoculated with COCS homogenates exposed to either scFvPOM1 or scFvPOM1+rmPrP$_{23-230}$. In contrast, RML6 prion-infected CAD5 cells displayed the typical pattern of PrP^{Sc} on Western blots (*Figure 18*C).

To investigate the possible presence of prions in POM1-treated COCS in more detail, Manuela Pfammatter (Institute of Neuropathology, University Hospital Zurich) assessed the prion propagation activity of antibody-treated *Tg*a20 COCS homogenates using the real-time quaking induced conversion assay (RT-QuIC) (Atarashi et al. 2011). The RT-QuIC allows sensitive detection of PrP^{Sc} based on prion-catalyzed cyclic amplification of misfolded PrP. Homogenates of COCS treated with scFvPOM1 or scFvPOM1+rmPrP$_{23-230}$ as well as COCS

homogenates treated with NBH- and RML6 were spiked into the RT-QuIC reaction mixture and amplified for 70 hours. Neither scFvPOM1-treated nor (scFvPOM1+rmPrP$_{23-230}$)-treated COCS homogenates induced *de novo* PrP aggregate formation in the RT-QuIC assay. In contrast, RML6-treated COCS homogenates induced aggregation after an initial lag phase of about 24 hours (*Figure 19*A).

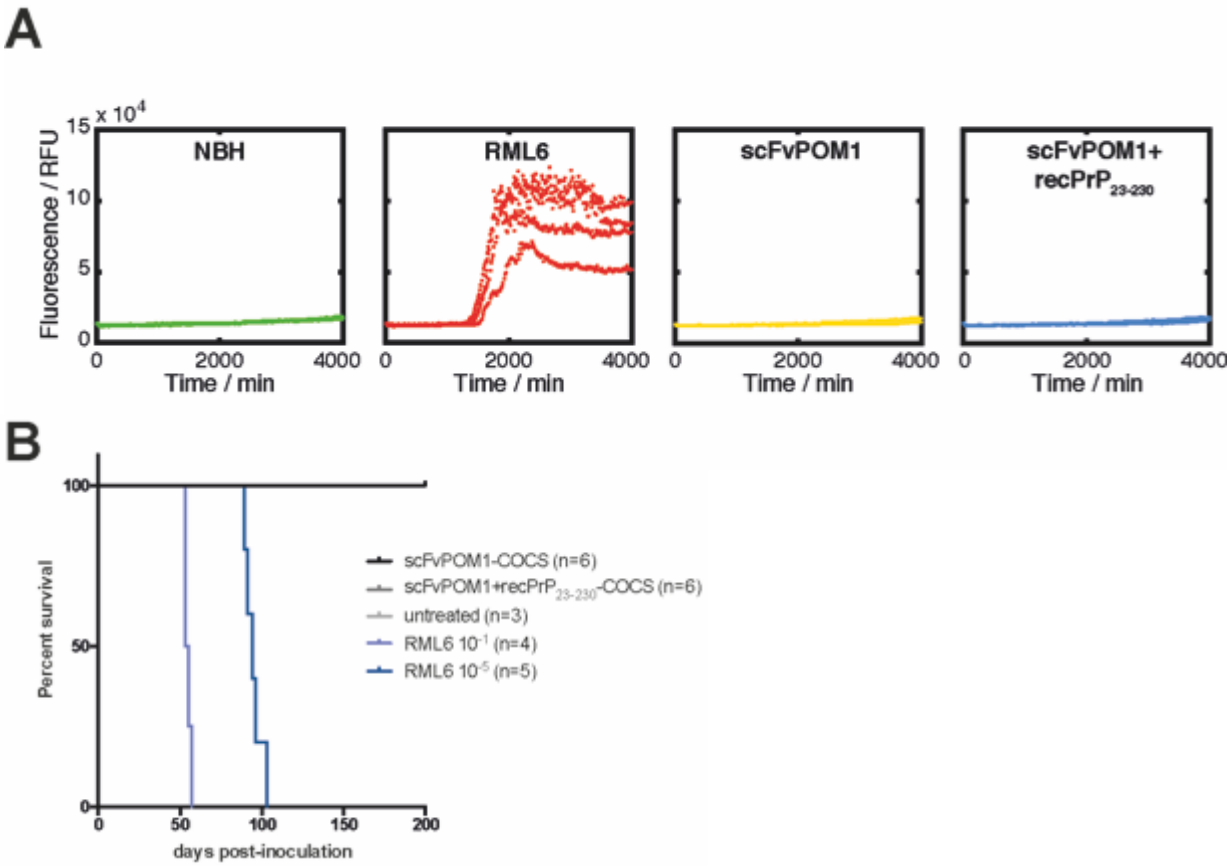

Figure 19. (A) RT-QuIC analyses failed to reveal de novo PrP^{Sc} aggregation when seeded with scFvPOM1 or (scFvPOM1+rmPrP$_{23-230}$)-treated *Tga*20 COCS homogenates. NBH- and RML6-treated *Tga*20 COCS homogenates were used as negative and positive controls for prion-catalyzed amplification of aggregated PrP, respectively. RT-QuIC reactions were performed in quadruplicates for each sample. (B) *Tga*20 mice inoculated with pooled slice homogenates of scFvPOM1-treated (n=6 mice) or (scFvPOM1+rmPrP$_{23-230}$)-treated tga20 COCS (n=6 mice) stayed healthy for at least 200 days after inoculation. tga20 mice infected at high dose (n = 4 mice) or low dose (n = 5 mice) with RML6 succumbed to prion disease at 55 ± 2 (mean ± s.d., high dose) and 95 ± 5 (high dose) days, respectively.

The failure to detect PrP^{Sc} suggests that exposure to toxic GD ligands does not induce PrP aggregation. However, the sensitivity of the assays employed is not very high. Moreover, GD ligands may conceivably induce PK-sensitive PrP aggregates which may still be infectious (Head et al. 2013). Finally, cell-based assays suffer from the differential susceptibility of

individual cell lines to specific prion strains, which is unpredictable and may lead to false-negative results (Mahal et al. 2007).

To overcome these limitations, I tested the transmissibility of pathology from antibody-treated COCS to PrP^{C}-overexpressing *Tga*20 mice that serve as sensitive indicators of prion infectivity (Fischer et al. 1996; Blattler et al. 1997). COCS treated with scFvPOM1 or scFvPOM1+rmPrP$_{23-230}$ (1%, 18 µg total brain homogenate in 30 µl) were inoculated intracerebrally (i.c.) into *Tga*20 mice. In control experiments (performed non-synchronously with mice of the same genotype and age), *Tga*20 mice were i.c. inoculated with RML6 at high dose (1%, 36 µg total brain homogenate, corresponding to 3 x 10^6 median lethal dose [LD_{50}] units and low dose (0.0001%, 3.6 pg total brain homogenate, corresponding to 3 x 10^2 LD_{50} units). RML6-infected mice showed the characteristic clinical signs of terminal prion disease (e.g. progressive ataxia, rolling gait) at 55 ± 2 (high dose) and 95 ± 5 days (low dose, *Figure 19*B). *Tga*20 mice inoculated with homogenates from scFvPOM1 or scFvPOM1+rmPrP$_{23-230}$ treated COCS, as well as non-inoculated control mice, did not develop any signs of disease within an observation period of 200 days (*Figure 19*B).

Immunohistochemical analysis of brain sections from RML6-inoculated mice showed prominent and classical signs of prion disease, such as spongiform changes, neuronal cell loss, astrogliosis, and microglial activation (*Figure 20*). In contrast, none of these signs were observed in mice treated with scFvPOM1 COCS homogenate, scFvPOM1+rmPrP$_{23-230}$ COCS homogenate, or non-inoculated mice (*Figure 20*). Western blots of brain homogenates from RML6-infected mice showed the molecular weight shift typical of PrP^{Sc} after PK digestion (*Figure 21*). No PrP^{Sc} was detected by Western blotting in brain homogenates from mice inoculated with scFvPOM1-COCS, (scFvPOM1+recPrP$_{23-230}$)-COCS, or NBH.

***Figure* 20 (*page 55*).** Brain sections from terminally sick mice (high dose RML6, lowest row) revealed typical signs of prion disease such as spongiform change (H&E), astrogliosis (GFAP), microgliosis (IBA1) and PrP^{Sc} deposition (SAF84). None of these features were observed in *Tga*20 mice inoculated with scFvPOM1-COCS, (scFvPOM1+rmPrP$_{23-230}$)-COCS, or in untreated mice. Scale bar = 50 µm.

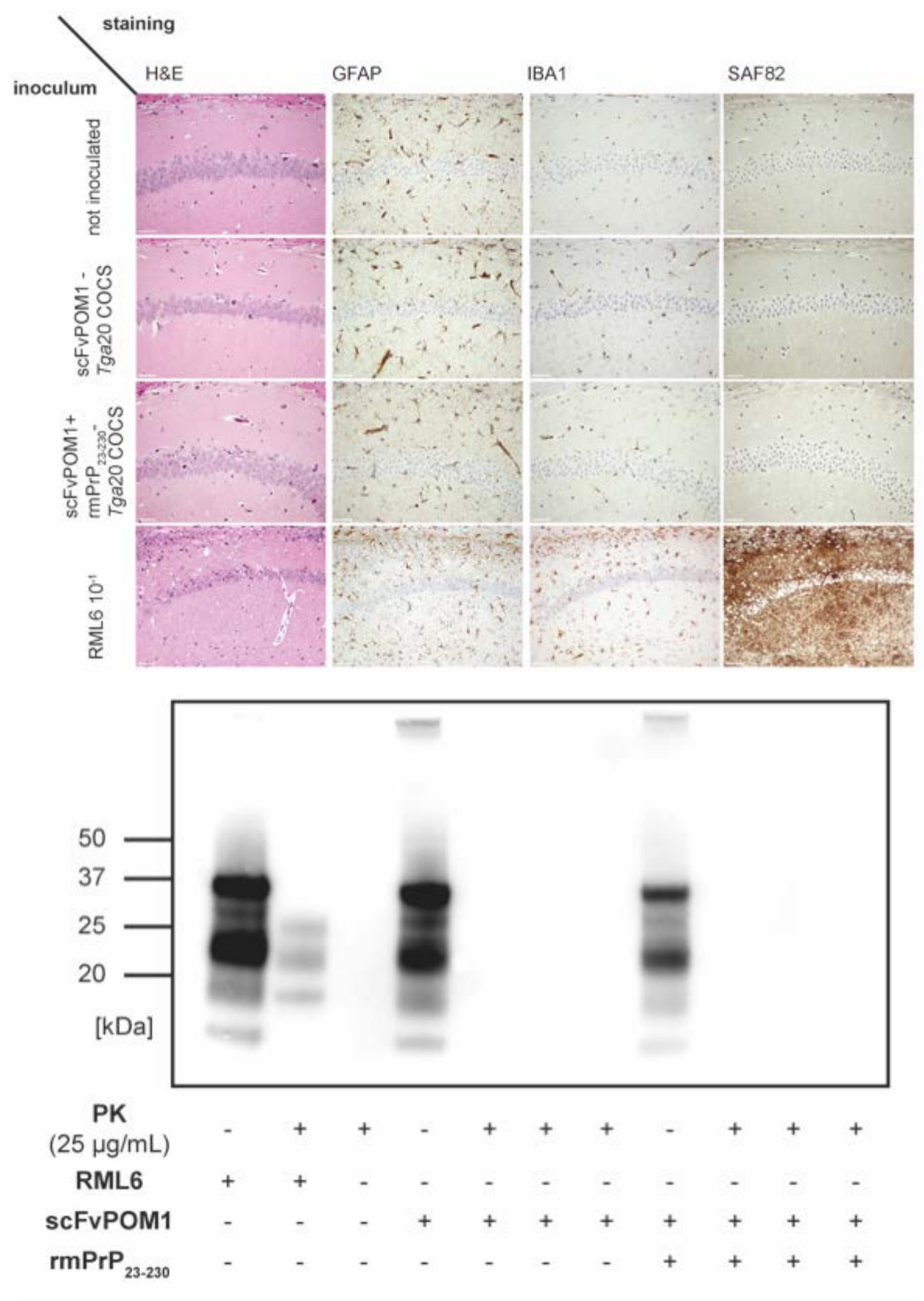

Figure 21. PK-digestion of brain homogenate from a terminally sick *Tga*20 mouse revealed relative protease resistance. The residual PrP^{Sc} showed a typical diagnostic shift in its molecular weight. Neither untreated, scFvPOM1-COCS inoculated (n=3 brain homogenates) nor (scFvPOM1+rmPrP$_{23-230}$)-COCS inoculated (n=3 brain homogenates) *Tga*20 mice showed detectable PrP^{Sc}.

Generation and binding studies of scFvPOM1 mutants

X-ray crystallography of Fab_1POM1 in complex with human PrP^C resulted in precise determination of binding sites (*Table* 3, (Baral et al. 2012)). In order to dissect the toxic effects of the PrP^C globular domain (PrP^C-GD) binding antibody POM1 the Luca Varani lab (IRB Bellinzona) has performed single-alanine scanning mutagenesis of all known binding sites resulting in 11 individual mutants that were subsequently expressed as single-chain variable fragments and purified, mutagenized scFvPOM1 antibodies ($scFvPOM1^{Mut}$) migrated as a single band around 25 kDa in SDS-PAGE (scFv, *Table* 4 and *Figure 22*, (Baral et al. 2012)). Mutagenesis of $POM1^{Asn92}$ was omitted since alanine scanning did not yield a significant impact on binding energy.

Human PrP^C	**Fab_1POM1**	**Human PrP^C**	**Fab_1POM1**
Fab_1POM1 light chain		**Fab_1POM1 heavy chain**	
Gly142	Tyr96	**His140**	Trp33
Ser143	Asn92	**His140**	Tyr101
Asp144	Ser32	**Gly142**	Tyr104
Asp144	Ser91	**Asp147**	Tyr104
Asp144	Tyr50	**Lys204**	Tyr57
Asp144	Asn92	**Arg208**	Asp52
Tyr145	Asn92	**Arg208**	Asp55
		Gln212	Asp55

***Table* 3**. Interaction sites of Fab_1POM1 in complex with human PrP^C, as determined by X-ray crystallography, modified from (Baral et al. 2012)

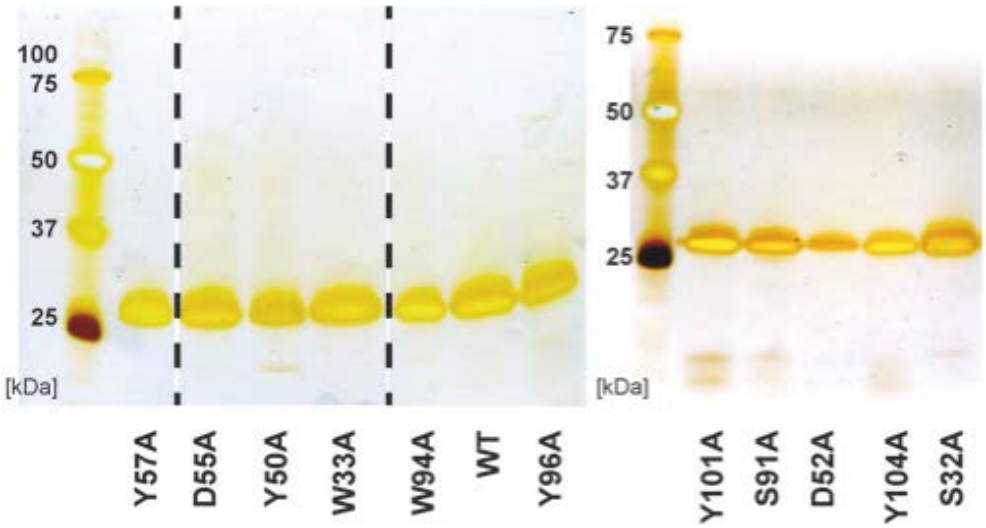

Figure 22. Silver staining of purified $scFvPOM1^{Mut}$ (expressed as mutated amino acids) and $scFvPOM1^{WT}$ (*WT*) shows migration of scFv antibodies at around 25 kDa in SDS-PAGE. Dashed bars indicate cropping of gel.

Surface plasmon resonance (SPR) measurements performed by Marco Bardelli (Group Luca Varani, IRB Bellinzona) yielded binding characteristics of scFv parental antibodies and scFvPOM1^{Mut} (*Table* 4). Herein, no or low-affinity binding in W33A and S91A mutants (K_D > 1µM), medium-affinity binding in D52A, D55A, Y57A, Y50A, W94A and Y96A mutants (K_D = 100 nM – 1 µM) and high-affinity binding (K_D < 100 nM) in Y101A, Y104A and S32A mutants was observed (*Table* 4).

scFvPOM1 antibody	*K_a [1/nMs]*	*K_d [1/s]*	*K_D [nM]*	*location on POM1*	*hPrP^C binding site*
Wild-type	4.78 x 10^4	3.16 x 10^{-4}	5.08		
W33A	no binding	no binding	no binding	CDR_H1 loop	H140
D52A	3.34 x 10^5	4.56 x 10^{-2}	103	CDR_H2 loop	R208
D55A	1.05 x 10^5	3.67 x 10^{-2}	372		R208, Q212
Y57A	7.7 x 10^4	3.15 x 10^{-2}	406		K204
Y101A	6.26 x 10^4	7.14 x 10^{-4}	11.5	CDR_H2 loop	H140
Y104A	3.61*10^4	2.09*10^{-4}	8.79		G142, D147
S32A	6.36 x 10^4	5.95 x 10^{-4}	9.98	CDR_L1 loop	D144
Y50A	5.7 x 10^4	8.17 x 10^{-3}	313	CDR_L2 loop	D144, Y145
S91A	1.34 x 10^4	1.85 x 10^{-2}	1430	CDR_L3 loop	D144
W94A	3.08 x 10^5	2.7 x 10^{-2}	201		hydrophobic enviroment[§]
Y96A	6.24 x 10^4	7.4 x 10^{-3}	123		G142

***Table* 4**. Binding characteristics of scFvPOM1 and scFvPOM2 parental antibodies and scFvPOM1 mutants as determined through SPR. K_a = association rate constant, K_d=dissociation rate constant, K_D = equilibrium dissociation (binding) constant, CDR = complementary-determining region, L/H 1-3 = CDR 1-3 of antibody light/heavy chains. [§] Trp94 was described to create a hydrophobic environment for POM1-hPrP^C binding.

To determine whether scFvPOM1^{Mut} could effectively inhibit binding of the wild-type maternal antibody (scFvPOM1^{WT}) to rmPrP$_{23-230}$, Tiziana Sonati (Institute of Neuropathology, University Hospital Zurich) performed Förster Resonance Energy Transfer (FRET) using recombinant, full-length mouse PrP$_{23-230}$ (rmPrP$_{23-230}$), the allophycocyanin (APC) labelled, monoclonal anti-PrP antibody POM3 (APC-POM3, binding residues aa 95-100 (Polymenidou et al. 2008)) and an europium (Eu) labelled scFvPOM1^{WT} (Eu-scFvPOM1^{WT}). All scFvPOM1^{Mut} antibodies, as well as scFvPOM1^{WT}, but not the off-target small molecule 400-B1 (Lilly) successfully showed binding to $_{rmPrP23-230}$, as was seen by a dose-dependent decrease of maximal NET FRET signal (*Figure 23*A). The concentration needed for half-maximal displacement (half-maximal inhibitory dose ID$_{50}$) signifcantly correlated with antibody affinity as measured by SPR (Spearman r=0.86, p<0.01, *Figure 22*B).

Toxic scFvPOM1^{Mut} antibodies faithfully recapitulate scFvPOM1^{WT} toxicity that can be ablated by the PrP^{C}-OR binding antibody POM2

At 400 nM, the Aguzzi lab has shown scFvPOM1^{WT} to induce severe neurotoxicity in PrP^{C}-overexpressing, *Tga*20 cerebellar organotypic slices cultures (COCS), conversely, COCS derived from Zurich 1 *Prnp* knock-out mice are resistant to POM1-induced toxicity (Sonati et al. 2013). Initial toxicity assessment of the mutagenized scFvPOM1 variants was performed through exposure of COCS derived from both *Tga*20 and *Prnp*$^{0/0}$ (ZH1) at a concentration of 400 nM for 14 days (*Figure 23*A). Expectedly, scFvPOM1^{WT} led to rapid and profound neurodegeneration as reflected by low levels of cells stained positive for neuronal nuclei (NeuN, *Figures* 24A+B). ScFvPOM1^{WT}-like toxicity, i.e. a rapid decrease of NeuN^{+} area

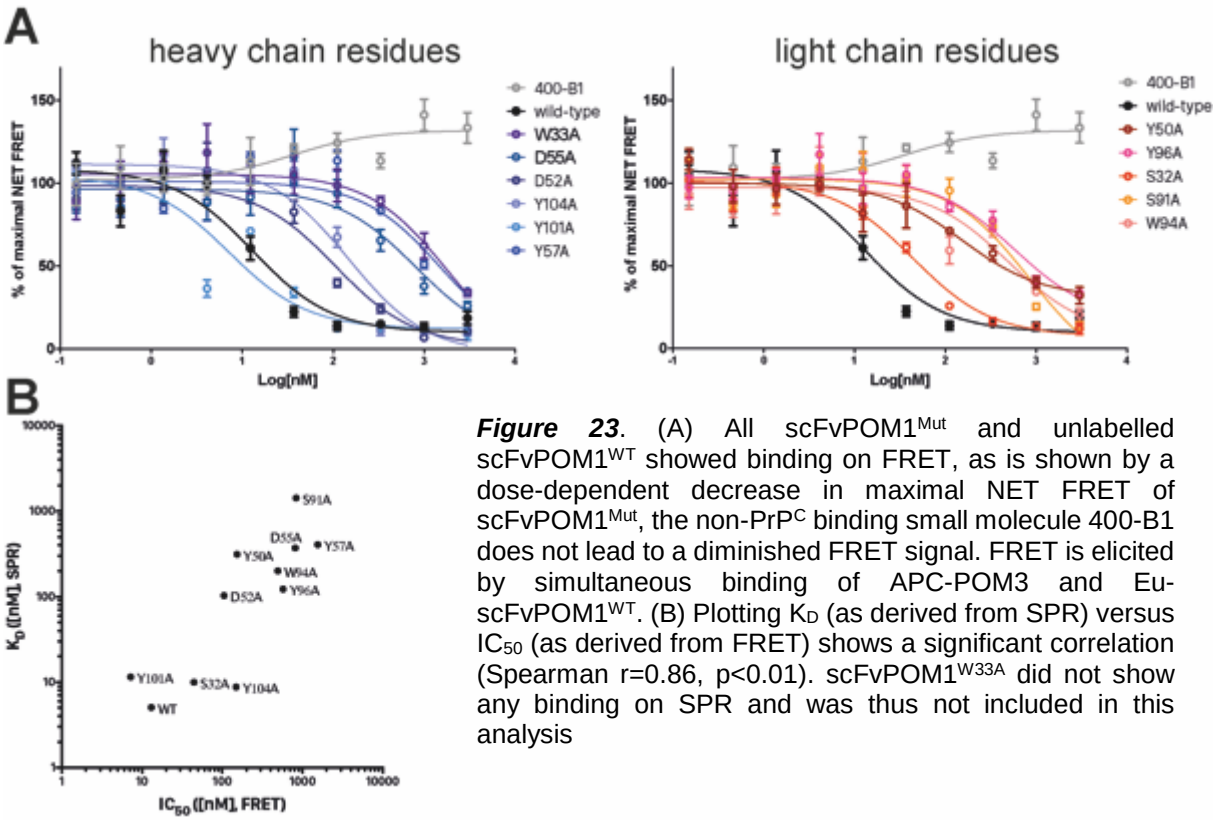

Figure 23. (A) All scFvPOM1^{Mut} and unlabelled scFvPOM1^{WT} showed binding on FRET, as is shown by a dose-dependent decrease in maximal NET FRET of scFvPOM1^{Mut}, the non-PrP^{C} binding small molecule 400-B1 does not lead to a diminished FRET signal. FRET is elicited by simultaneous binding of APC-POM3 and Eu-scFvPOM1^{WT}. (B) Plotting K_D (as derived from SPR) versus IC_{50} (as derived from FRET) shows a significant correlation (Spearman r=0.86, p<0.01). scFvPOM1^{W33A} did not show any binding on SPR and was thus not included in this analysis

compared to untreated *Tga*20 COCS, was also observable in scFvPOM1^{S32A}, scFvPOM1^{Y50A}, scFvPOM1^{D52A}, scFvPOM1^{S91A}, scFvPOM1^{W94A}, scFvPOM1^{Y96A} and scFvPOM1^{Y101A} (*Figures* 18A+B). Innocuity, i.e. unchanged levels of NeuN^{+} area, was observed in scFvPOM1^{W33A}, scFvPOM1^{D55A}, scFvPOM1^{Y57A} and scFvPOM1^{Y104A} (*Figures* 24A+B) although I believe the findings to be irrelevant in the case of scFvPOM1^{W33A} as it does not show any measurable biophysical binding on SPR (*Table* 4).

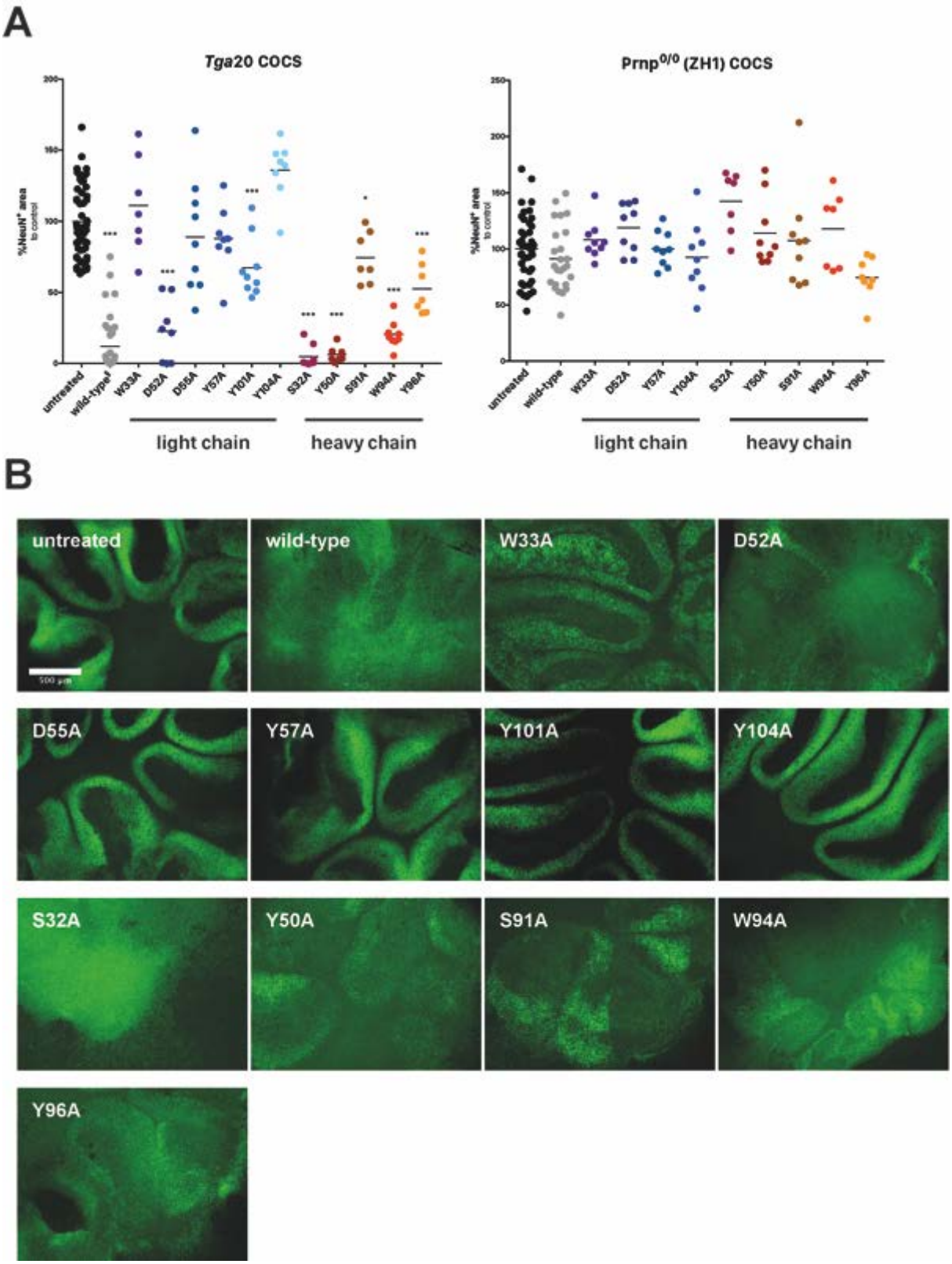

Figure 24. (A) *Left panel:* Treatment of *Tga*20 COCS with scFvPOM1^{WT}, scFvPOM1^{D52A}, scFvPOM1^{Y101A}, scFvPOM1^{S32A}, scFvPOM1^{Y50A}, scFvPOM1^{S91A}, scFvPOM1^{W94A} and scFvPOM1^{Y96A} leads to rapid and significant neurodegeneration when compared to untreated COCS, while treatment with scFvPOM1^{W33A}, scFvPOM1^{D55A}, scFvPOM1^{Y57A} and scFvPOM1^{Y104A} do not show significant toxicity. *Right panel:* Neither scFvPOM1^{WT} nor scFvPOM1^{Mut} show significant toxicity in *Prnp*$^{0/0}$ (ZH1) COCS. * p<0.05, *** p<0.001, one-way ANOVA with Holm-Sidak's post-hoc test. (B) Representative micrographs of NeuN-stained *Tga*20 COCS treated with scFvPOM1 wild-type (*WT*) and scFvPOM1^{Mut} antibodies. Scale bar = 500 µM.

The toxicity of (scFv-) POM1^{WT} is dependent on the presence of PrP^{C}, as *Prnp*$^{0/0}$ mice do not show neurodegeneration and toxicity can be ablated by pre-incubation of the antibody with rmPrP$_{23-230}$ (Sonati et al. 2013). Furthermore, POM1^{WT}-induced neurotoxicity is histologically characterized by neuronal cell loss, astrogliosis and microglial activation (Sonati et al. 2013; Herrmann et al. 2015). In a next step, I was wondering whether the high-affinity and toxic scFvPOM1 mutants scFvPOM1^{S32A} and scFvPOM1^{Y101A} share similar pathways as their scFvPOM^{WT} counterpart. Pre-incubation of 400 nM of scFvPOM1^{WT}, as well as scFvPOM1^{S32A} and scFvPOM1^{Y101A} with molar excess (600 nM) of rmPrP$_{23-230}$ significantly ameliorated neuronal cell loss, as was illustrated by increased NeuN^{+} area (*Figure* 25A+B).

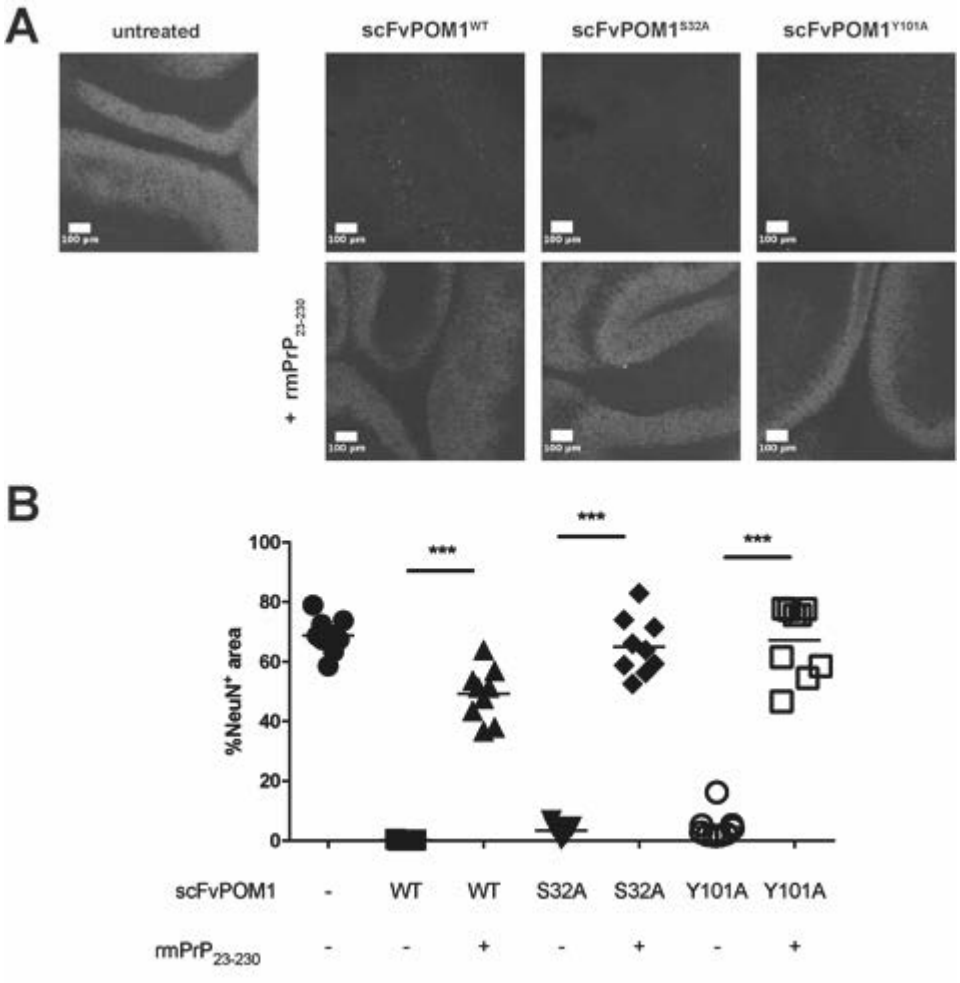

***Figure* 25**. The toxicity of the high-affinity scFvPOM1^{Mut} antibodies scFvPOM1^{S32A} and scFvPOM1^{Y101A} is PrP^{C}-dependent, as pre-incubation of antibodies with rmPrP$_{23-230}$ leads to amelioration of NeuN^{+} cell number ((A) confocal fluorescent micrographs of NeuN-Alexa^{488} stained *Tga*20 COCS, (B) statistical assessment). Scale bar = 100 µm, *** p<0.001, one-way ANOVA with Sidak's post hoc test.

Also, pre-incubation of scFvPOM1^{WT} and high-affinity scFvPOM1^{Mut} with molar excess of rmPrP$_{23-230}$ led to ablation of reactive gliosis (as was assessed by post hoc GFAP

immunohistochemistry, *Figure* 26A+C) and microgliosis (as assessed by post hoc F4/80 immunohistochemistry, *Figure* 26B+D) as was induced by the toxic antibodies.

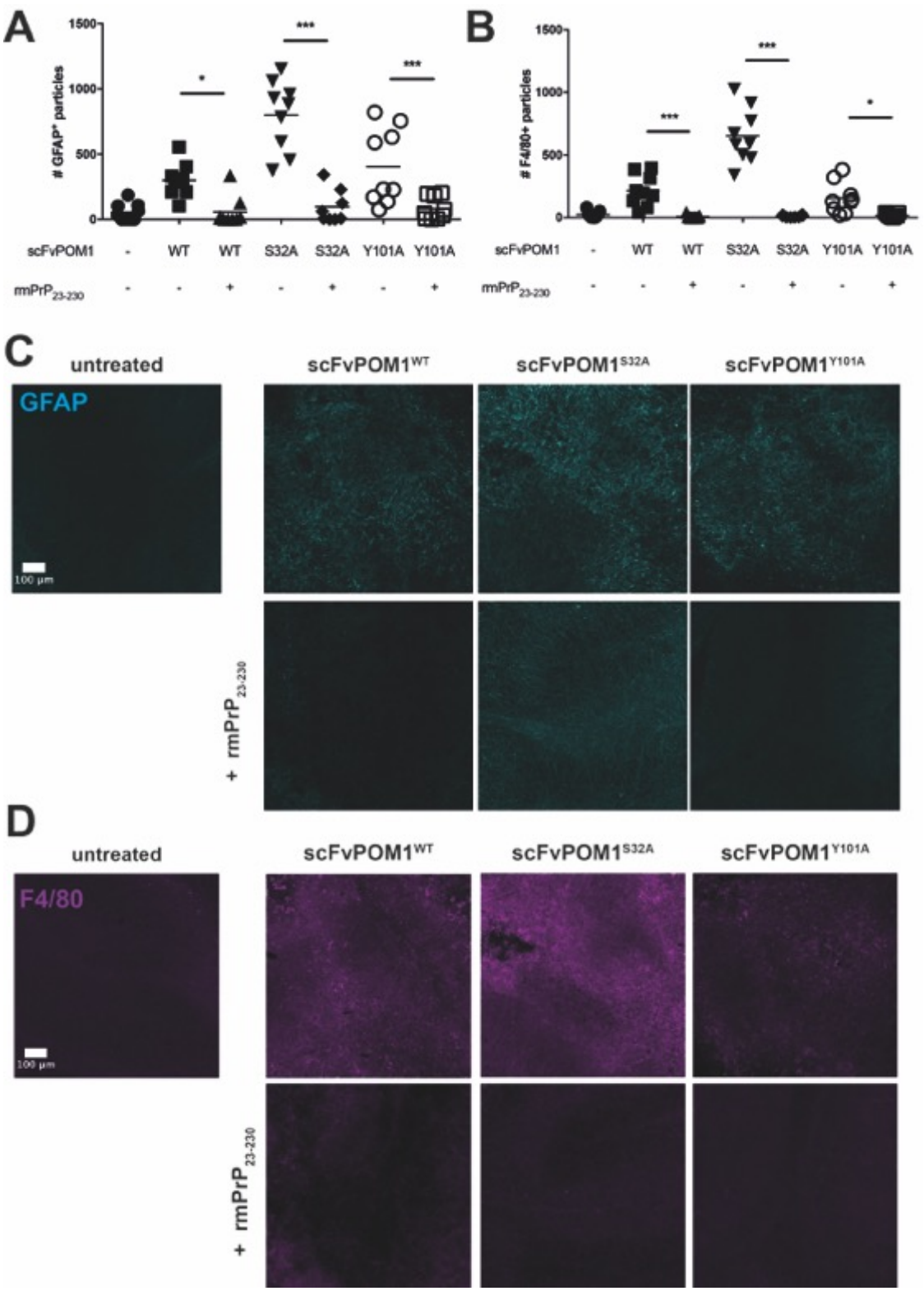

***Figure* 26**. ScFvPOM1^{WT}, as well as the high-affinity scFvPOM1^{Mut} antibodies scFvPOM1^{S32A} and scFvPOM1^{Y101} induce reactive gliosis (GFAP, (A) and (C)) and microgliosis (F4/80, (B) and (D)) that can be ablated by pre-incubation of antibodies with $_{rmPrP23-230}$. Scale bar = 100 µm, * $p<0.05$, *** $p<0.001$, one-way ANOVA with Sidak's post hoc test.

The neurotoxicity of POM1^{WT} is dependent on a functional PrP^{C}-OR, as genetic ablation of PrP^{C}-OR or anti-PrP^{C}-OR antibodies, such the monoclonal mouse antibody POM2 inhibit POM1^{WT}-induced toxicity (Sonati et al. 2013). When I added 400 nM scFvPOM2 to 200 nM of scFvPOM1^{S32A}, neurotoxicity after 10 dpe was significantly ablated ($p<0.05$, scFvPOM1^{S32A} [n=9] vs. scFvPOM1^{S32A} + scFvPOM2 [n=9], one-way ANOVA with Sidak's post hoc test, *Figure* 27). The same was observed for scFvPOM1^{WT} ($p<0.001$, scFvPOM1^{WT} [n=9] vs. scFvPOM1^{WT} + scFvPOM2 [n=9], one-way ANOVA with Sidak's post hoc test, *Figure* 27).

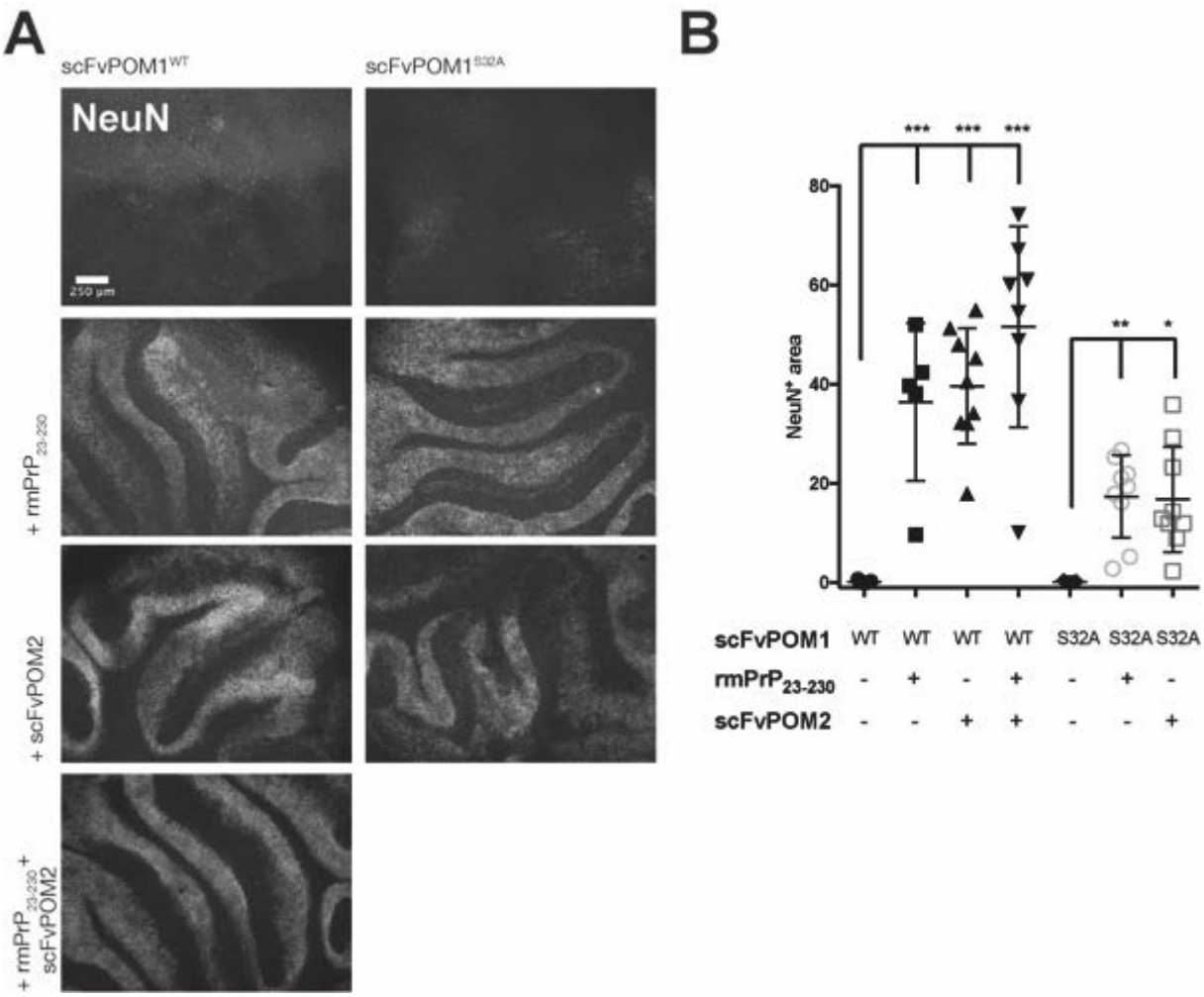

***Figure* 27**. Neurotoxicity of scFvPOM1^{WT}, but also scFvPOM1^{S32A} is ameliorated by pre-incubation with scFvPOM2 in *Tga*20 COCS. (A) Fluorescent micrographs of post hoc NeuN immunohistochemistry, (B) NeuN morphometry of (A). * $p<0.05$, ** $p<0.01$, *** $p<0.001$, one-way ANOVA with Sidak's post hoc test.

POM1^{Y57A} and POM1^{Y104A} are innocuous and neuroprotective mutants of POM1

During my initial screen of the 11 scFvPOM1^{Mut} antibodies, I observed innocuity of the mutants scFvPOM1^{W33A}, scFvPOM1^{D55A}, scFvPOM1^{Y57A} and scFvPOM1^{Y104A} (*Figure* 24), although scFvPOM1^{W33A} did not show any binding on SPR, and very weak binding on FRET measurements (*Table* 4, *Figure* 23), and hence was not followed up. To determine the minimal dosis of scFvPOM1^{WT} needed in *Tga*20 COCS to exert significant neurotoxicity, i.e. the optimal dosage to test whether scFvPOM1^{Mut} can ablate the toxic effects of scFvPOM1^{WT}, I exposed *Tga*20 COCS to 67, 33.5, 20 and 6.7 nM of scFvPOM1^{WT} over 2 weeks in the presence and absence of molar excess of rmPrP$_{23-230}$: on post-hoc NeuN morphometry, 67 nM of scFvPOM1^{WT} were needed to exert significant toxicity ($p<0.001$, scFvPOM1^{WT} [67 nM] vs. scFvPOM1^{WT} [67 nM] + rmPrP$_{23-230}$ [100 nM], *Figure* 28).

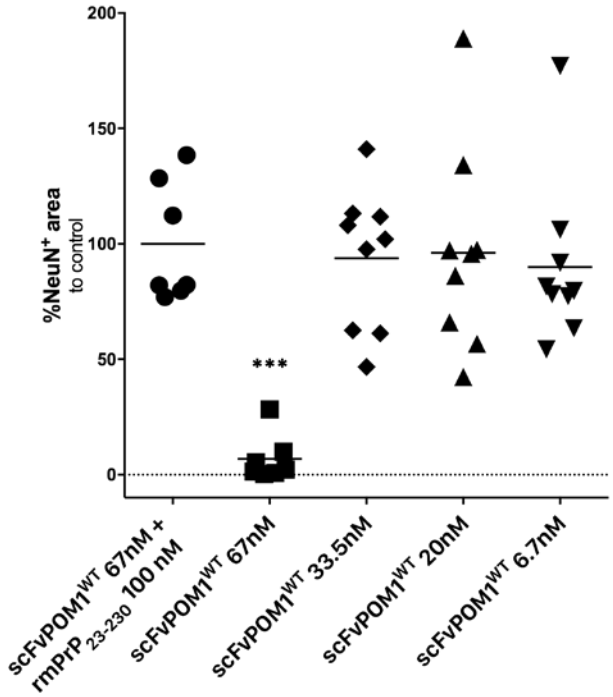

***Figure* 28.** 67 nM scFvPOM1^{WT} for 14 days are necessary to induce significant neurotoxicity in *Tga*20 COCS.

In order to investigate possible neuroprotective effects of the innocuous mutants, I inoculated *Tga*20 COCS with RML6 prions and non-infectious brain homogenate (NBH) and started treatment with scFvPOM1^{Mut} on 21 dpi, on 45 dpi, slices were formalin-fixed and stained with NeuN to assess neurodegeration. Treatment with scFvPOM1^{D55A} at 400 nM for 24 days was well tolerated, as was illustrated by unchanged NeuN^{+} cells in NBH-inoculated, *Tga*20 COCS,

treatment of RML-inoculated *Tga*20 COCS with scFvPOM1^{D55A}, however, did not result in rescue of RML-mediated neuronal cell loss (*Figure* 29).

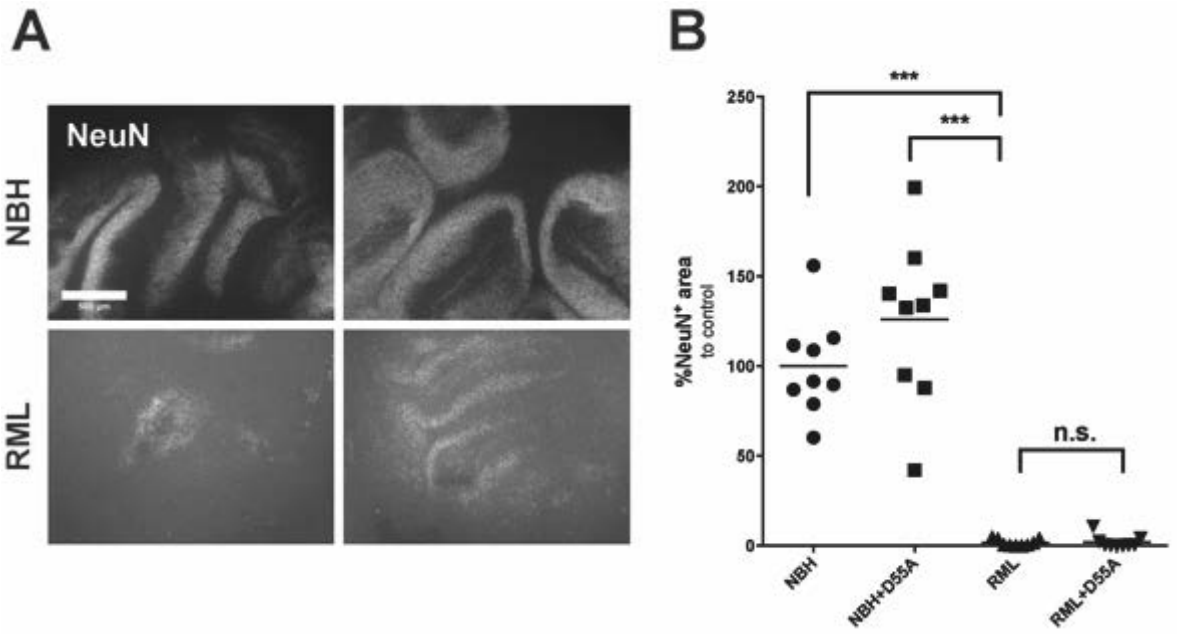

***Figure* 29**. Treatment of prion-infected, *Tga*20 COCS with scFvPOM1^{D55A} does not ameliorate prion-induced neurodegeneration. (A) Fluorescent micrographs of *Tga*20 COCS with post hoc NeuN immunohistochemistry, (B) NeuN morphometry of (A). n.s. not significant, *** p<0.001, one-way ANOVA with Dunnett's post-hoc test. Scale bar = 500 µm.

When adding scFvPOM1^{Y104A} to RML-infected, *Tga*20 COCS on 21 dpi at 400 nM, post hoc NeuN immunohistochemistry on 45 dpi showed a significant increase in prion-infected COCS treated with scFvPOM1^{Y104A} compared to untreated COCS (p<0.001, RML *Tga*20 COCS [n=6] vs. RML+scFvPOM1^{Y104A} [n=7], one-way ANOVA with Dunnett's post-hoc test, *Figure* 30A+B), also, chronic treatment with scFvPOM1^{Y104A} NBH-infected *Tga*20 for 24 days did not reveal observable toxicity (*Figure* 30A+B). Moreover, scFvPOM1^{Y104A} also ablated scFvPOM1^{WT} toxicity, albeit at threefold molar excess, i.e. 400 nM of scFvPOM1^{WT} versus 1200 nM of scFvPOM1^{Y104A} (p<0.01, scFvPOM1^{WT} [n=6] vs. scFvPOM1^{WT} + scFvPOM1^{Y104A} [n=6], one-way ANOVA with Dunnett's post hoc test, *Figure* 30C+D).

ScFvPOM1^{Y57A} was added to RML-infected *Tga*20 COCS on 10 and 21 dpi and slices were harvested on 45 dpi. On NeuN morphometry, addition of scFvPOM1^{Y57A} on both timepoints resulted in increased NeuN^{+} areas when compared to RML alone (*Figure* 31A+B).

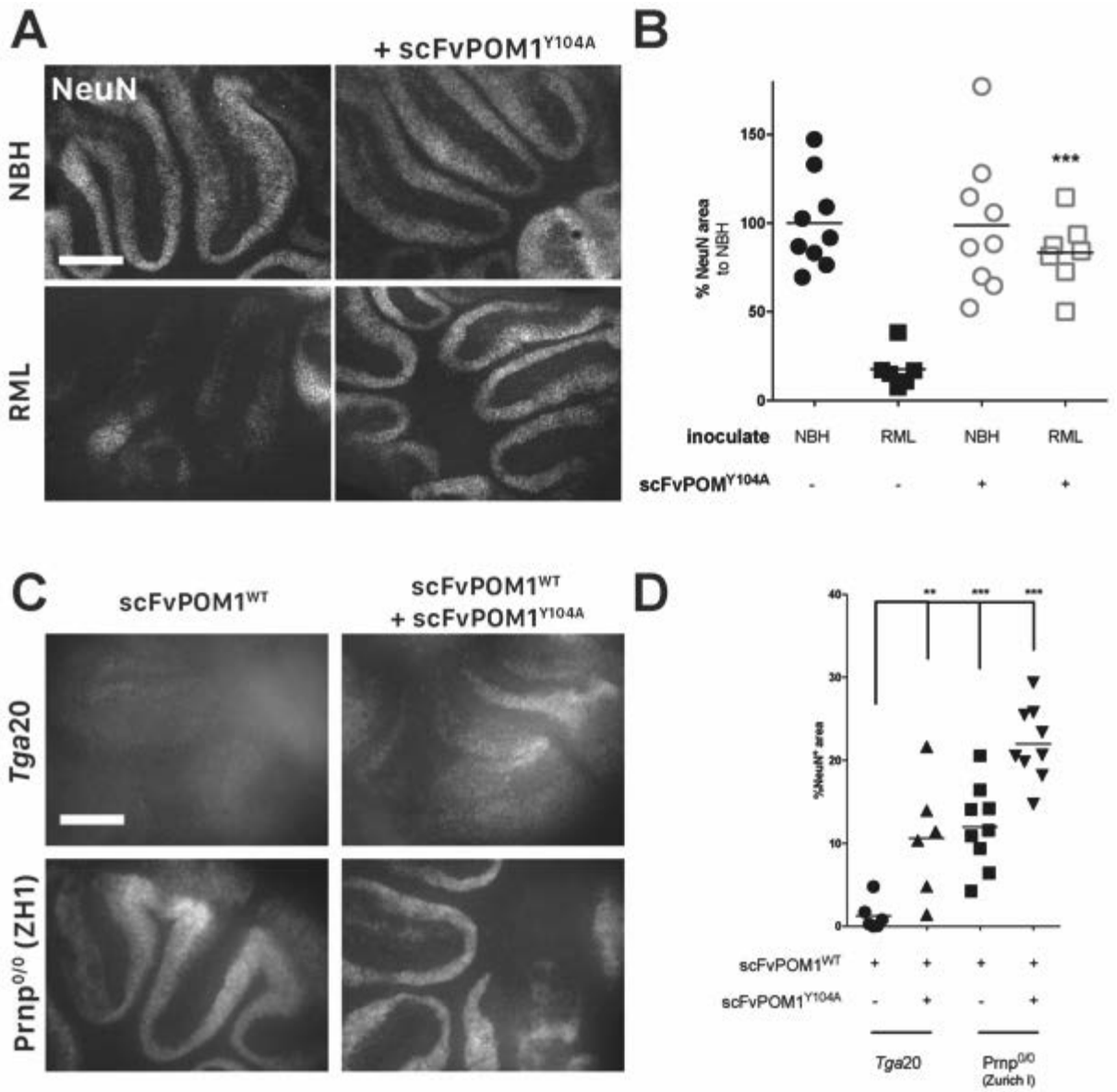

***Figure* 30.** (A+B) Treatment of RML-inoculated *Tga*20 COCS with scFvPOM1^{Y104A} leads to amelioration of neuronal cell loss. (C+D) Addition of scFvPOM1^{Y104A} ([1200 nM]) to scFvPOM1^{WT}-treated ([400 nM]) *Tga*20 COCS prevents neuronal loss. ** p<0.01, *** p<0.001, one-way ANOVA with Dunnett's post hoc test (A+B: all groups versus RML, C+D: all groups versus scFvPOM1^{WT}). Scale bar = 500 µm.

SPR measurements revealed the K_D of scFvPOM1^{Y57A} to be 79.9-fold weaker than the K_D of scFvPOM1^{WT} (5.08 nM scFvPOM1^{WT} vs. 406 nM scFvPOM1^{Y57A}, *Table* 4). Hence, any effective competition of scFvPOM1^{WT} by scFvPOM1^{Y57A} will need 79.9-fold molar increase of the latter compound, i.e., 5353.3 nM of scFvPOM1^{Y57A} at a minimal toxic concentration of scFvPOM1^{WT} 67 nM. I hence exposed *Tga*20 and *Prnp*$^{0/0}$ (ZH3) COCS to increasing concentrations of scFvPOM1^{Y57A} to assess the maximum tolerable dosis. A single treatment of 1200 nM already induced significant neurotoxicity in *Tga*20 COCS as was observable by

decreased NeuN levels on western blot (*Figure* 31C+D). 2400 nM of scFvPOM1^{Y57A} in *Prnp*$^{0/0}$ (ZH3) COCS did not result in observable toxicity making off-target effects unlikely (*Figure* 31C+D). I concluded that a competition experiment of scFvPOM1^{WT} with scFvPOM1^{Y57A} was not feasible to due unfavorable binding affinities.

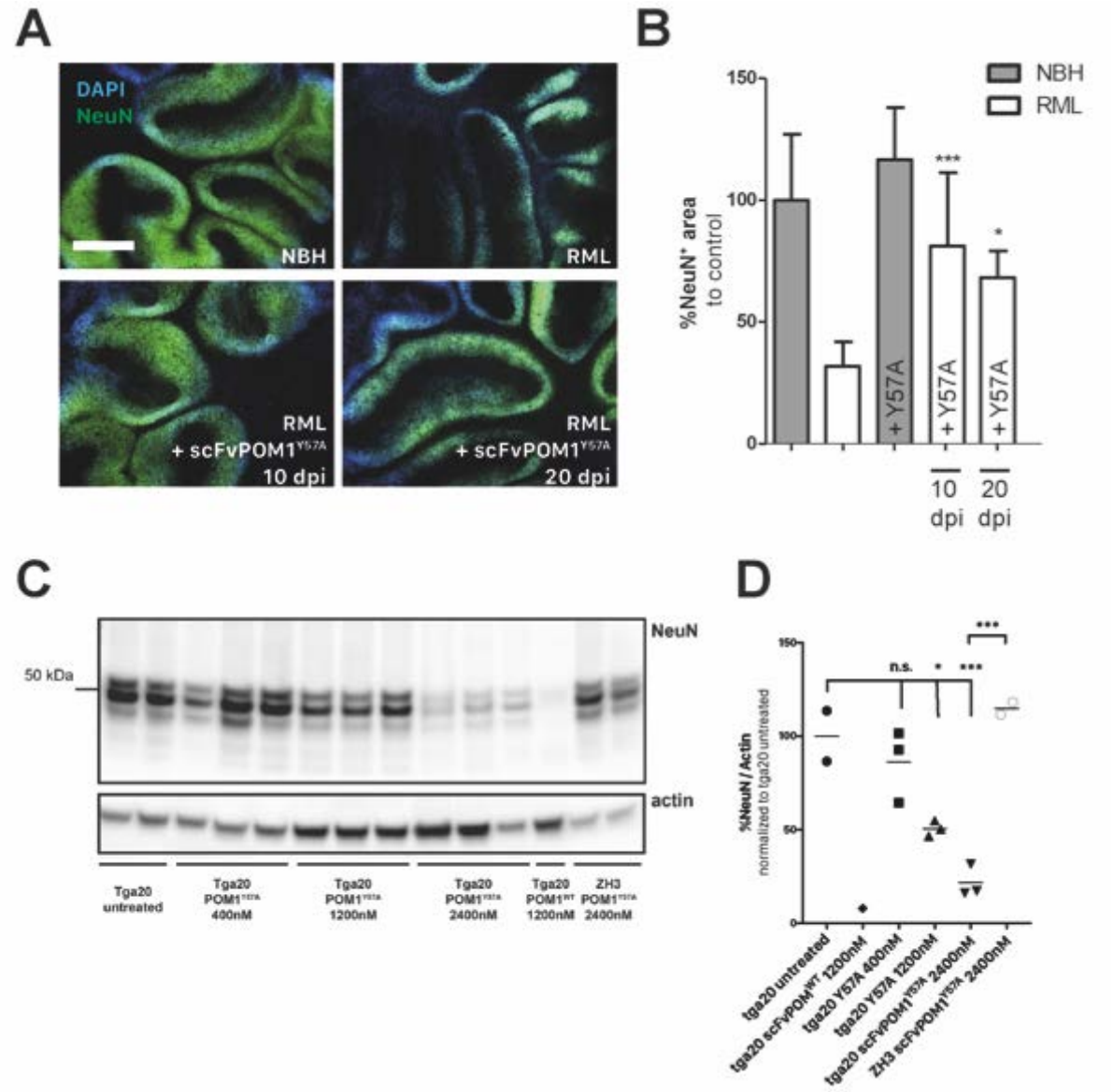

***Figure* 31.** (A+B) Fluorescence micrographs and NeuN morphometry quantification of *Tga*20 COCS, addition of scFvPOM1^{Y57A} was protective against RML when given both on 10 and 20 dpi. (C+D) Western blot and densitometric analysis of *Tga*20 and *Prnp*$^{0/0}$ (ZH3) COCS treated with increasing amounts of scFvPOM1^{Y57A} showing good tolerability of 400 nM, but not 1200 nM or 2400 nM in *Tga*20 COCS, while 2400 nM of scFvPOM1^{Y57A} in *Prnp*$^{0/0}$ (ZH3) COCS did not show toxicity, suggesting a PrP^{C}-specific effect. * p<0.05, ** p<0.01, *** p<0.001, one-way ANOVA with Sidak's post hoc test. Scale bar = 500 µm.

The neuroprotective scFvPOM1 mutants Y57A and Y104A restore levels of ROS enzymes and the UPR independent of PrP^{C} or PrP^{Sc} levels

As laid out before, prion infection leads to activation of reactive oxygen species and microglia activation(Sorce et al. 2014), when adding scFvPOM1^{Y104A} to prion-infected *Tga*20 COCS, a decrease in NOX2 levels can be seen (*Figure* 32A), also, when adding scFvPOM1^{Y57A}, microglial activation was attenuated as illustrated by lowered levels of Iba1 (*Figure* 32B).

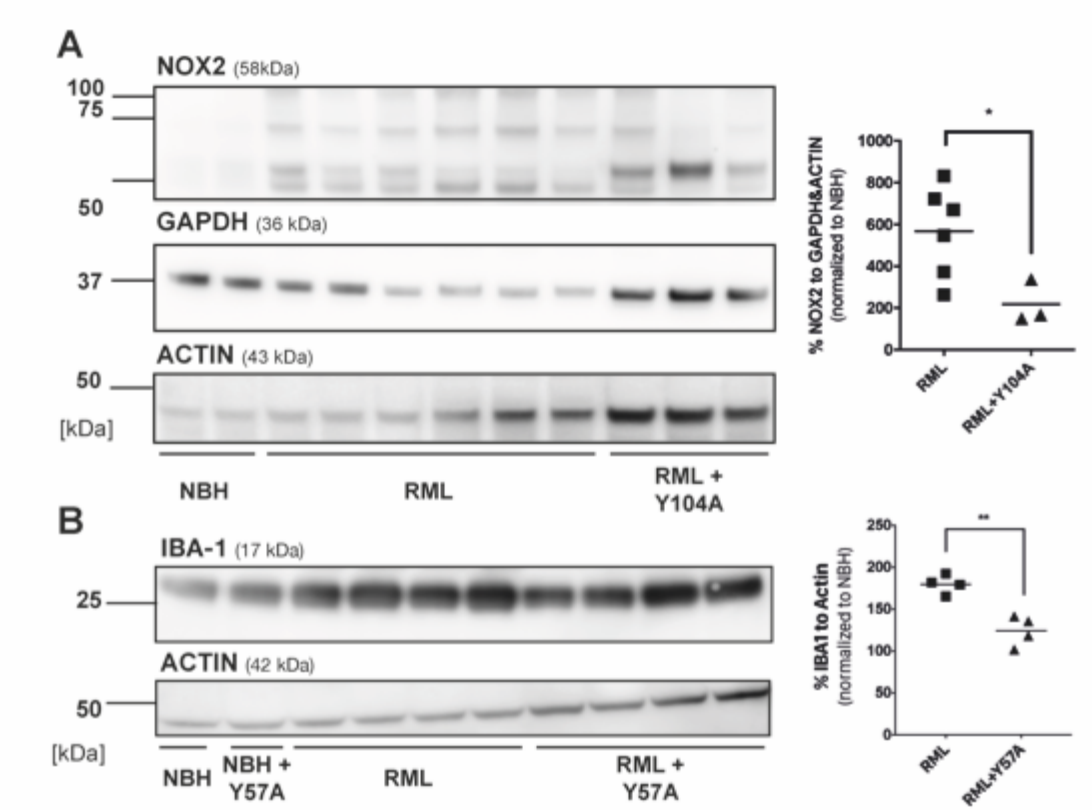

***Figure* 32**. (A) NOX2 levels are significantly reduced in RML-infected *Tga*20 COCS by 24 days of treatment with scFvPOM1^{Y104A}, when adding scFvPOM1^{Y57A} to RML-infected COCS, microglial activation is significantly reduced (B). * p<0.05, ** p<0.01, unpaired, two-sided T-test.

Activation of the unfolded protein response leading to translational repression is commonly observed in prion disease, as is the production of ROS and activation of microglia (Moreno et al. 2012; Aguzzi, Barres, and Bennett 2013; Sorce et al. 2014). To assess whether the aforementioned, neuroprotective scFvPOM1 mutants Y57A and Y104A ameliorated toxic cascades, NBH- and RML-inoculated *Tga*20 COCS were treated with either scFvPOM1^{Y57A} or scFvPOM1^{Y104A} (400 nM, starting at 21 dpi) until 45 dpi, then COCS were lysed and subjected to western blot. Upon activation of the unfolded protein response, phosphorylated eIF-2α leads to activation of ATF-4, which in turn leads to activation of CHOP (Moreno et al. 2012) –

treatment with protective scFvPOM1^{Mut} led to a restoration of ATF-4 levels (scFvPOM1^{Y57A}, *Figure* 33A, and scFvPOM1^{Y104A}, *Figure* 33B) and CHOP levels (scFvPOM1^{Y104A}, *Figure* 33C).

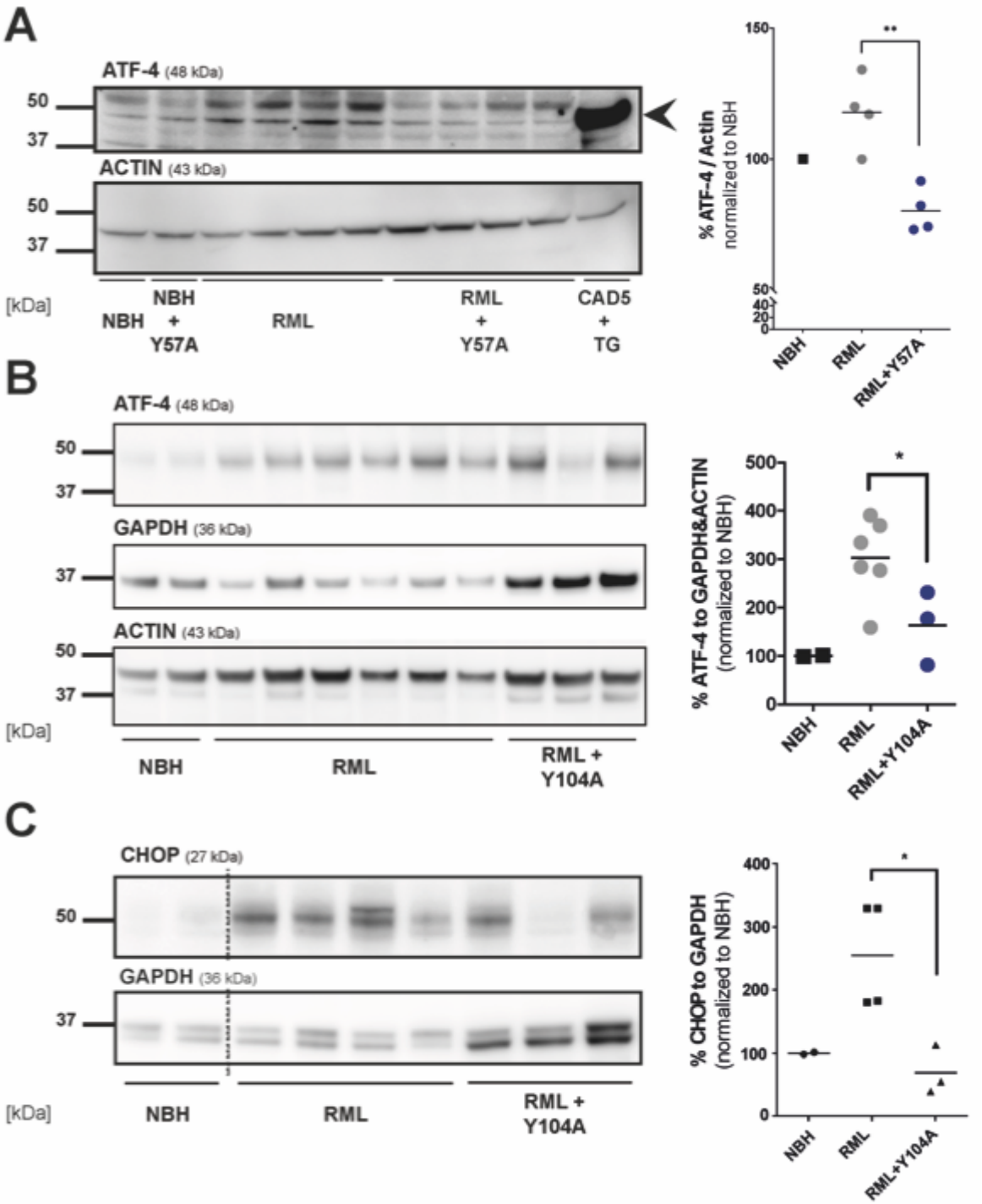

***Figure* 33**. (A) Treatment of RML-inoculated *Tga*20 COCS with the scFvPOM1^{Mut} Y57A leads to an attenuation of the UPR, as is reflected by lower ATF-4 levels. An arrow at 48 kDa denotes ATF-4, CAD5+TG: as a positive control, the murine neuroblastoma cell line CAD5 was treated with 0.5 M of Thapsigargin for 24h. (B+C) Treatment of RML-inoculated *Tga*20 COCS with scFvPOM1^{Y104A} leads to attenuated levels of ATF-4 (B) and CHOP (C). * $p<0.05$, ** $p<0.01$, unpaired, two-tailed T-test.

Binding of antibodies to surface receptors can lead to substantial receptor endocytosis and degradation (Yarden and Tarcic 2013).In the case of scFvPOM1^{Mut} , this could lead to a protective effect due to lowered PrP^{C} levels and not due to binding to a toxicity-inducing epitope on PrP^{C}. In order to assess whether the protective scFvPOM1^{Mut} antibodies Y57A and Y104A lead to a downregulation of PrP^{C} expression, *Tga*20 COCS were treated for 7 days with scFvPOM1^{Y57A} and scFvPOM1^{Y104A} in the presence and absence of molecular excess of rmPrP$_{23-230}$. COCS were lysed and a sandwich ELISA using POM19 (absorbed to a polystyrene plate) and biotinylated POM3 (for detection) was employed to measure total PrP^{C} levels - treatment with either scFvPOM1^{Mut} antibody did not lead to downregulation of PrP^{C} (*Figure* 34).

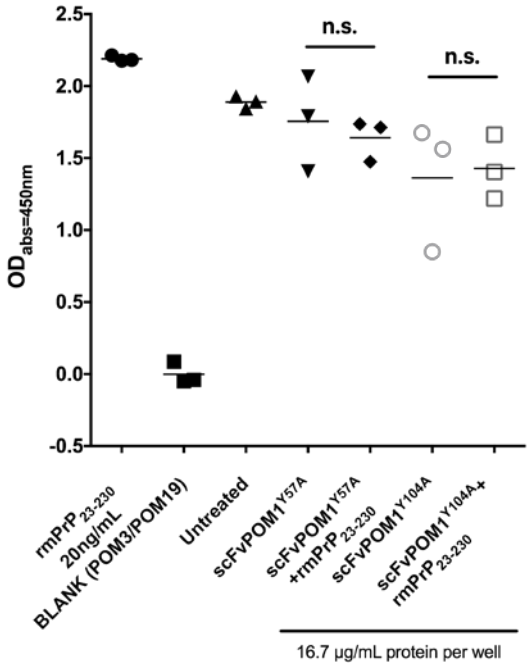

***Figure* 34**. Chronic treatment (7 days, 400 nM) of *Tga*20 COCS with either scFvPOM1^{Y57A} or scFvPOM1^{Y104A} in the absence or the presence of molar excess of $_{rmPrP23-230}$ did not lead to reduced PrP^{C} levels as was measured in a POM3/POM19 sandwich ELISA.

I then wanted to know whether neuroprotective scFvPOM1^{Mut} antibodies are protective due to reduction of PrP^{Sc} levels. I inoculated *Tga*20 COCS with NBH and RML, respectively, and added scFvPOM1^{Y57A} and scFvPOM1^{Y104A} on 21 dpi for 24 further days, on 45 dpi, I lysed the COCS and assessed PrP^{Sc} levels by proteinase K digestion of COCS lysates and western blot with the monoclonal anti-PrP^{C} antibody POM1. Densitometric analyses of PrP^{Sc} did not reveal a decrease in PrP^{Sc} after treatment with scFvPOM1^{Y57A} or scFvPOM1^{Y104A} suggesting protection through binding to an epitope not involved in prion replication (*Figure* 35).

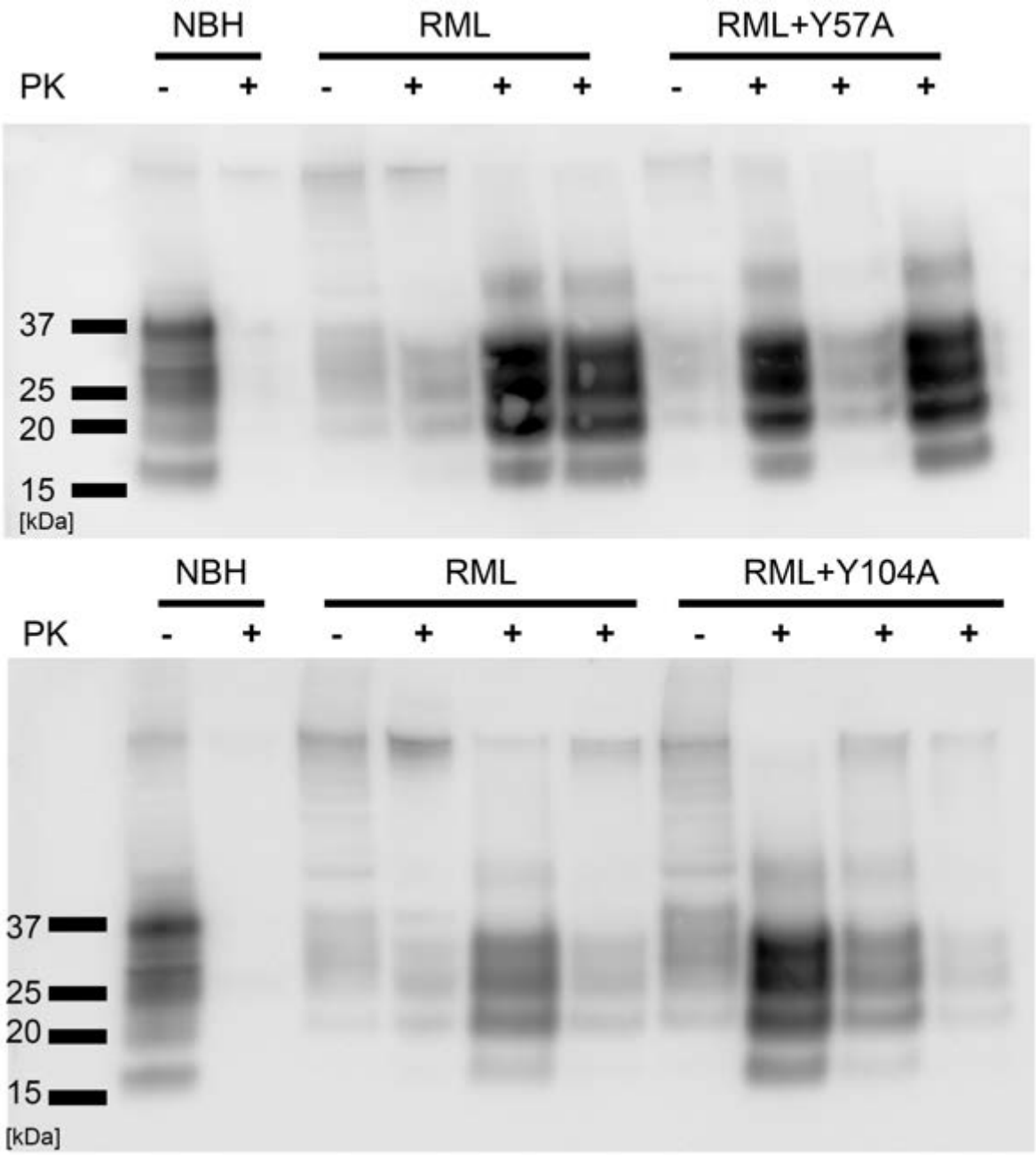

***Figure* 35**. Treatment of RML-inoculated *Tga*20 COCS with scFvPOM1^{Y57A} (A) or scFvPOM^{Y104A} (B) does not lead to decreased PrP^{Sc} levels.

Establishing models to study relaxation of the PrP^{C}-β2α2 loop

Molecular dynamics simulations (MDS) on POM1 mutants in complex with PrP^{C} performed by Marco Bardelli and Luca Varani (IRB Bellinzona) showed an almost complete overlap with the *in vivo* findings presented in this work. POM1^{WT}, when in complex with human PrP^{C} (hPrP^{C}),

POM1(Y57) forces the intercalation of a hydrogen bond (H-bond) between hPrP^{C}(R208) and hPrP^{C}(H140), leading to a relaxation of the β2α2 loop. When hPrP^{C} is free in solution, hPrP^{C}(R208) points towards hPrP^{C}(Q212). POM1 with a Y57A substitution (POM1^{Y57A}) does not form a H-bond at hPrP^{C}(R208-H140) in MDS, and as mentioned, abolished infectious prion toxicity *in vivo* (*Figure* 31). POM1^{D52A} was not able to disrupt binding of hPrP^{C}(R208-H140) in MDS resulting in neurotoxicity, a finding that was confirmed *in vivo* (*Figure* 24). On the contrary, another innocuous antibody mutant such as scFvPOM1^{D55A} also disrupted the H-bond formation in MDS, but was not protective against prions *in vivo* (*Figure* 29), probably due to insufficient dosage. The binding of the other protective mutant scFvPOM1^{Y104A} occurs via the more N-terminal residue hPrP^{C}(K204), although specific MDS have not been performed yet.

To study the effects of POM1 toxicity onto the β2α2 loop in mPrP^{C} (aa 165-175), I aimed to generate three PrP^{C} mutants.Firstly, alanine mutagenesis of mPrP^{C}(R207), corresponding to hPrP^{C}(R208), should abolish POM1 toxicity upon binding to PrP^{C}. Secondly, replacing glutamine mPrP^{C}(Q211) by a negatively charged residue, e.g., glutamate, was suggested to attract mPrP^{C}(R207) away from mPrP^{C}(H139) (the murine equivalents of hPrP^{C}(R208-H140)) in MDS. Thirdly, by forcing a disulfide bridge between mPrP^{C}(R207-H139) with a mPrP^{C}(C207-C139) mutant, I aimed to simulate the H-bond between mPrP^{C}(R207-H139) as created by POM1 in MDS.

In the first step, I assessed whether the intended mutants, i.e. mPrP^{R207A}, mPrP^{Q211E} and mPrP$^{I138C-R207C}$ showed correct membranal presentation, glycosylation and conformational orientation. To express the mutants on a pure *Prnp*$^{0/0}$ background, I first knocked-out *Prnp* in the murine neuroblastoma cell line CAD5 by means of CRISPR/Cas9. To avoid expression of abberant or truncated versions of PrP^{C} or deletion of the splice acceptor site that would lead

to pathological overexpression of Doppel (Dpl) mRNA (Moore et al. 1999), I used single-stranded guide RNA (sgRNA) cloned into the MLM3636 plasmid aiming at a protospacer adjacent motif (PAM) site in the signal peptide of *Prnp* (*Figure* 36A). Cells were co-transfected with MLM3636 and the hCas9 plasmid followed by transient antibiotic selection.

Subsequently, 7 clones were manually picked, expanded and subjected to further characterization. Cells were lysed and PrP^C levels were measured by POM1/POM2 sandwich ELISA. Herein, 7 CAD5 *Prnp*$^{0/0}$ candidate clones #A6, #C2, #C6, #C12, #H7, #H9 and #H12 all showed near-zero PrP^C levels comparable to the established *Prnp*$^{0/0}$ cell line HPL ($p>0.05$, one-way ANOVA with Dunnett's post hoc test, *Figure* 36B, (Kuwahara et al. 1999)). 5 clones were further assessed on western blot for detection of PrP^C, where no detectable PrP^C levels could be observed (*Figure* 36C), suggesting a successful knock-out of PrP^C in all 5 *Prnp*$^{0/0}$ candidate clones. DNA was extracted from expanded cells of clones #C2 and #C12 and the mutagenized region was sequenced by PCR amplification of the open reading frame (ORF) of *Prnp*. Amplified products were cloned into the pCR-Blunt II-TOPO plasmid (Invitrogen) and at 10 colonies per clone were studied by sanger sequencing. Herein, #C2 showed four different mutations, i.e., three deletions and one insertion, while #C12 showed two different deletions proximal to the PAM (*Figure* 36D). These results indicate multiploidy to be more likely in #C2 than in #C12, hence all further experiments are performed with the CAD5 *Prnp*$^{0/0}$ clone #C12.

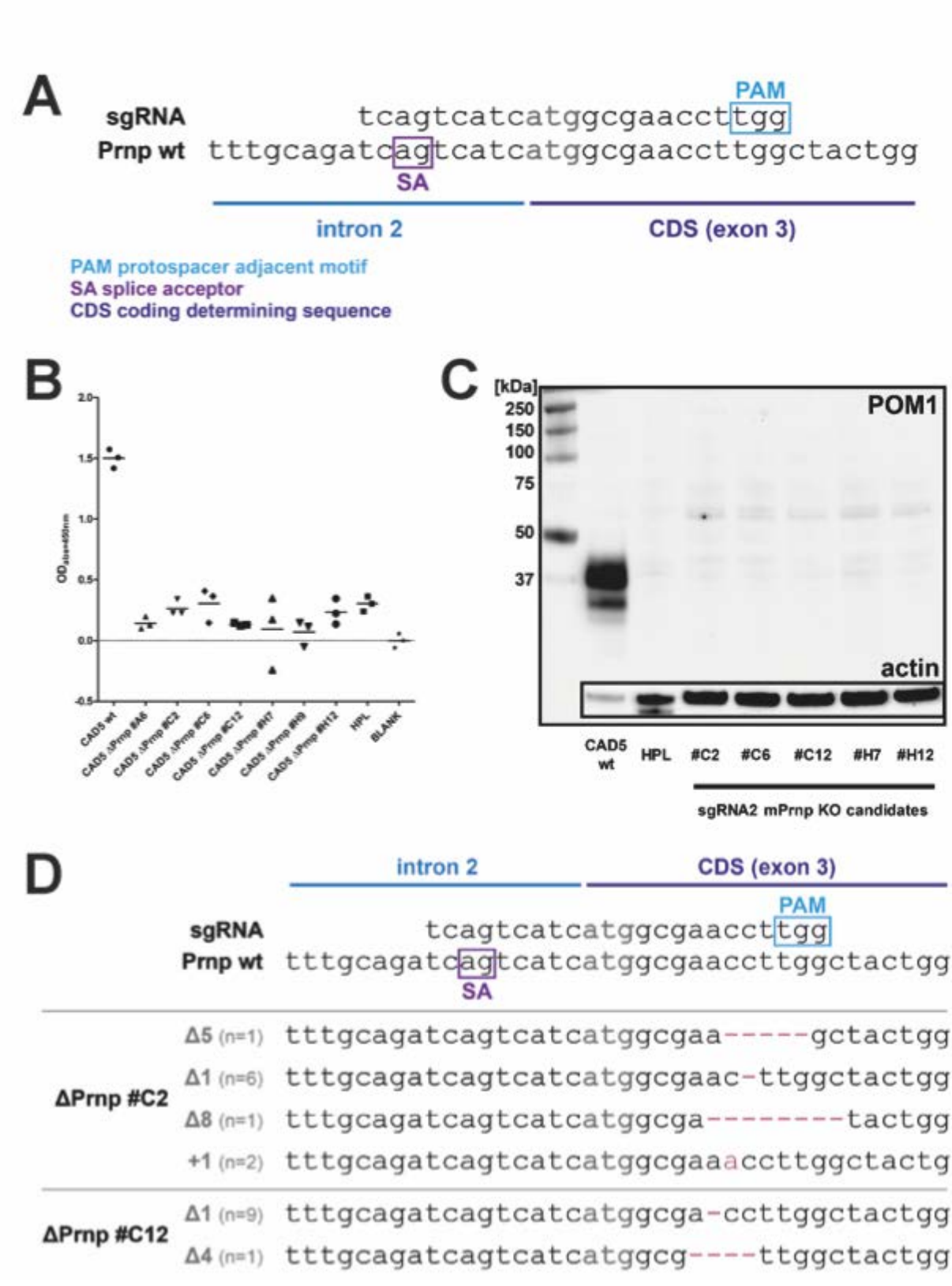

***Figure* 36**. (A) Design of sgRNA for CRISPR/Cas9 mediated generation of CAD5 *Prnp*$^{0/0}$ cells. A PAM in the coding sequence of the signal peptide was chosen. (B+C) ELISA of 7 candidate CAD5 *Prnp*$^{0/0}$ clones showed similar PrP^{C} levels compared to the established *Prnp*$^{0/0}$ cell line HPL, 5 of which were further assessed by PrP^{C} western blot, confirming lack of PrP^{C} expression (C). (D) Sanger sequencing of PCR amplified *Prnp* ORF showed n=4 different mutations in #C2 and n=2 different mutations, labelling according to (A). The splice acceptor site is unaffected in both of the constructs.

CAD5 *Prnp*$^{0/0}$ were stably transfected with empty plasmid (CAD5$^{0/0}$) and plasmids expressing mPrP^{WT} (CAD5^{WT}), mPrP^{R207A} (CAD5^{R207A}), mPrP^{Q211E} (CAD5^{Q211E}) and mPrP$^{R207C\text{-}I138C}$ (CAD5$^{R207C\text{-}I138C}$). In order to assess correct membranal expression of mutants I performed immunhistochemical analyses of CAD5 cells with POM1 and POM19, with the former expected to lose binding in *Prnp*^{Mut} and the latter to retain binding due to its more C-terminal epitope (Sonati et al. 2013). Expectedly, POM1 binding was only seen in CAD5^{WT} but not in the empty plasmid, mPrP^{R207A}, mPrP^{Q211E} and mPrP$^{I138C\text{-}R207C}$ expressing cells (*Figure* 37A). Conversely, POM19 binding was retained on the cell membrane in all cells except CAD5$^{0/0}$ (*Figure* 37B). These findings suggest that although the POM1 binding site is abolished, PrP^{Mut} is correctly presented on the membrane with preservation of the conformational, POM19 epitope.

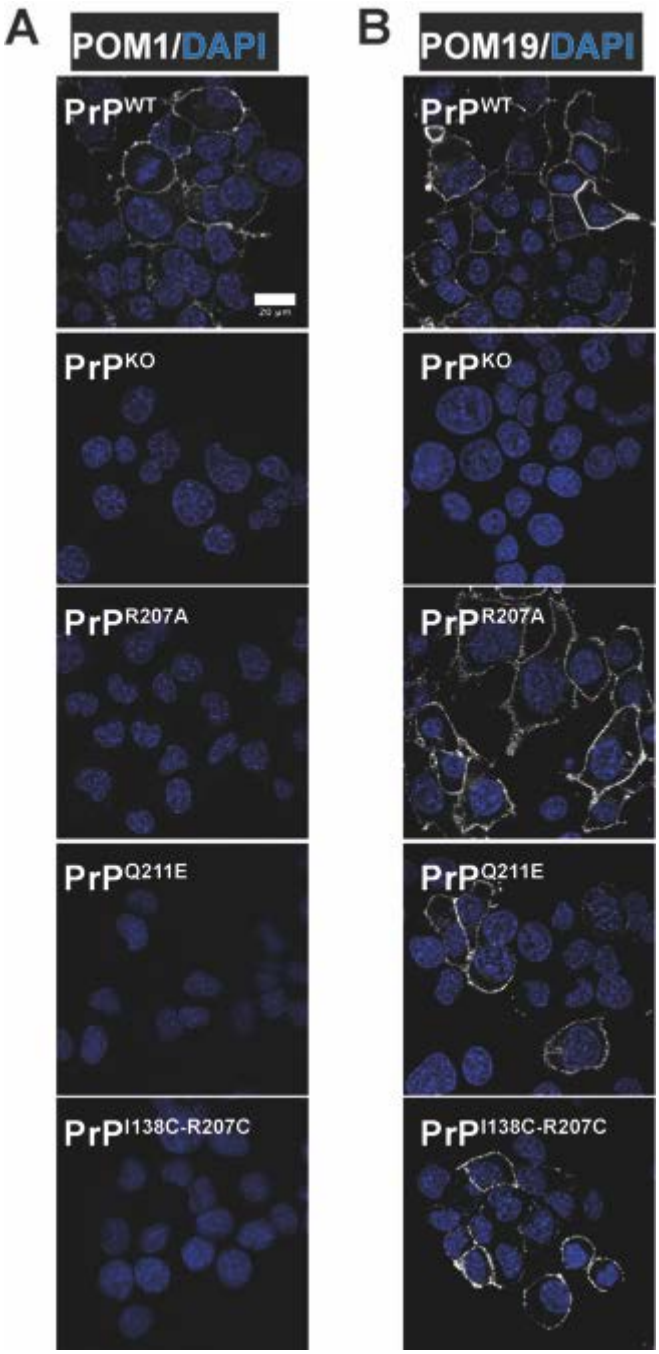

***Figure* 37**. The POM1 epitope is retained in CAD5^{WT}, but not in CAD5^{R207A}, CAD5^{Q211E} and mPrP$^{R207C\text{-}I138C}$ (A). Conversely, POM19 detects both PrP^{WT} and mutated isoforms (B). Scale bar = 20 µm.

PrP^C exists in di-, mono- and unglycosylated forms (Aguzzi, Baumann, and Bremer 2008). In order to assess whether mutated PrP variants are correctly glycosylated, I performed digestion of cell lysates with Peptide -N-Glycosidase F (PNGase F), cleaving N-linked oligosaccharides between the innermost GlcNAc and asparagine residues (Maley et al. 1989). Prion protein wild-type and mutants showed a shift from partially glycosylated to fully unglycosylated proteins after PNGase F digestion on western blot, indicating correct glycosylation (*Figure* 38).

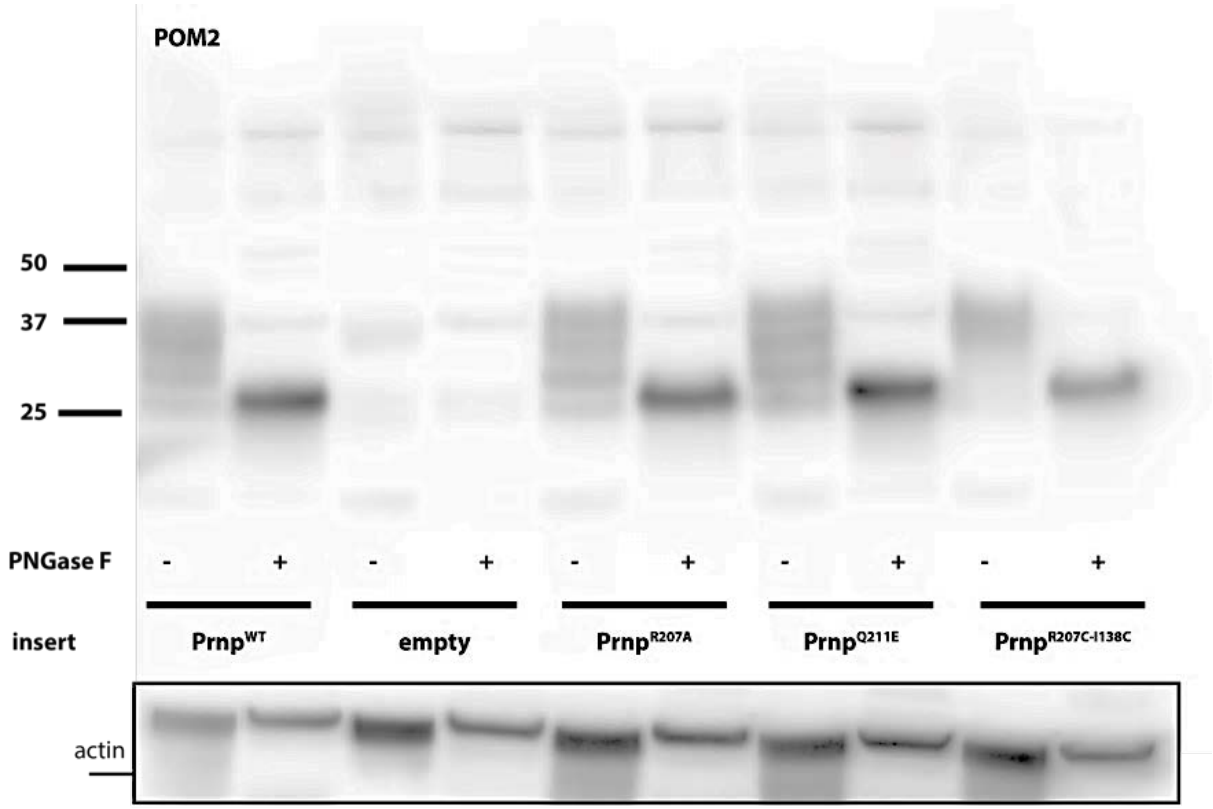

***Figure* 38**. Western blot with the anti-PrP^C antibody POM2 of cell lysates in the presence and in the absence of PNGaseF shows a shift from partially glycosylated (- PNGaseF) to fully unglycosylated (+ PNGaseF) prion protein in both wild-type and mutants, but not in control plasmid transfected CAD5 cells.

POM monoclonals target a variety of conformational epitopes on PrP^C (Polymenidou et al. 2008). Accordingly, I wanted to know whether I could further explore the conformational status of newly generated prion protein mutants, especially to study the alterations in rigidity of the $\beta2\alpha2$ loop of PrP^C as was seen in MDS. To this end I performed immunohistochemical stainings using the anti-PrP^C-$\beta2\alpha2$ loop targeting antibody POM5 and included a third PrP^C-GD antibody, i.e. POM8, to further elucidate the conformational stability of the mutants. POM1 and POM19 served as controls. On immunhistochemistry, $CAD5^{WT}$, $CAD5^{R207A}$, $CAD5^{Q211E}$ and $CAD5^{R207C\text{-}I138C}$ were detectable by POM19, as described before (*Figure* 37), further

membrane-associated immunopositivity was seen in all cells (except CAD5$^{0/0}$) by POM8, showing retention of the POM8 epitope on the α1-α2 helices of PrP^{C}-GD (*Figure* 39). Interestingly, POM5, which is a conformational antibody to the rigid β2α2 loop, did not bind to CAD5$^{R207C\text{-}I138C}$ strengthening the conformational alterations observed in MDS. Furthermore, the POM5 epitope was not detectable in CAD5^{Q211E} as well, suggesting conformational changes in CAD5^{Q211E} exceeding those seen in MDS (*Figure* 39).

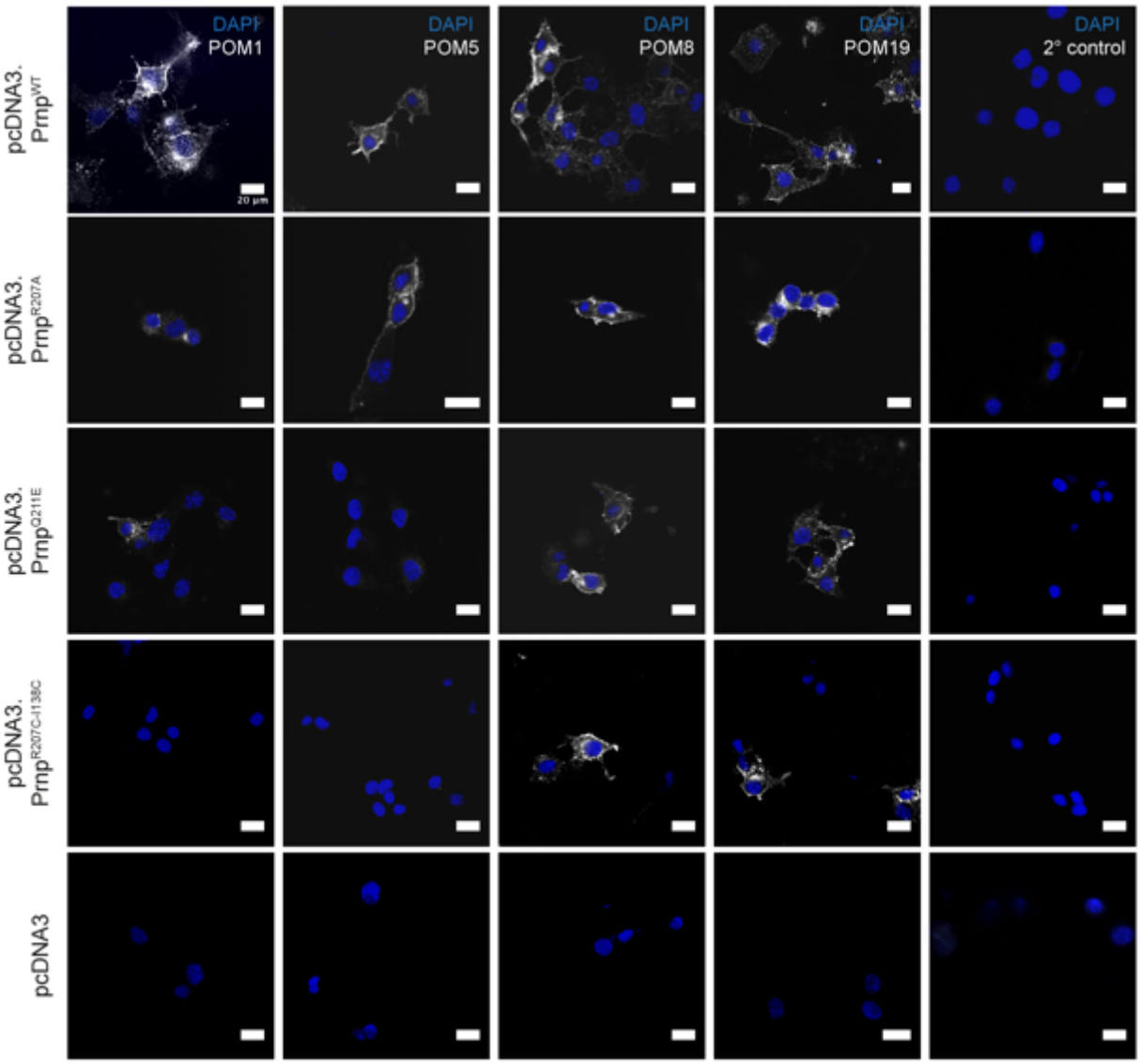

***Figure* 39**. Retention of the conformational POM1, POM5, POM8 and POM19 epitopes is only observable in CAD5^{WT}. The POM1 epitope is ablated in all prion protein mutants, while POM19 and POM8 epitopes are also retained in CAD5^{R207A}, CAD5^{Q211E} and CAD5$^{R207C\text{-}I138C}$. Conformational alterations in the β2α2 loop, as detected by loss of POM5 immunhistochemistry were seen in CAD5^{Q211E} CAD5$^{R207C\text{-}I138C}$. Scale bar = 20 µm.

In a last step, I was wondering whether I could chronically infect CAD5^{R207A}, CAD5^{Q211E} and CAD5$^{R207C-I138C}$ cells with RML prions as was described before (Enari, Flechsig, and Weissmann 2001) to study the effects of the mutants on prion propagation. I inoculated the cells with RML6 prions and split them three times every 3-4 days. I performed proteinase K digestion of cell lysates collected immediately before inoculation and after the last cell passaging. Herein, brain homogenate of RML6 infected mice showed the typical molecular "shift" towards the PK-resistant core (*Figure* 40). CAD5^{WT} cells were susceptible to chronic prion infection. CAD5$^{R207C-I138C}$ cells showed a faint PK-resistant band without the typical di-, mono- and unglycosylated prion protein isoforms before, but not after inoculation (*Figure* 40). Due to the variability of PK resistance at the low PK concentrations used, I believe this is rather due to protein aggregation than generation of PrP^{Sc}, which is usually resistant to concentrations of 100-500 µg/ml of PK (McKinley, Bolton, and Prusiner 1983).

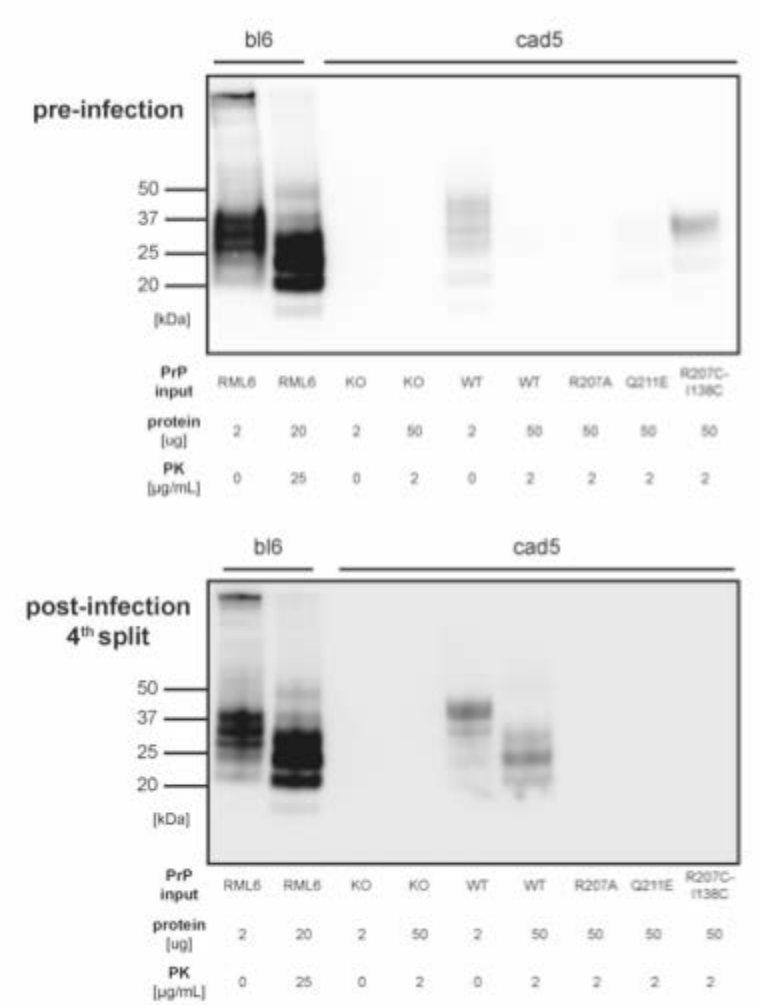

***Figure* 40**. CAD5^{WT}, but not CAD5^{R207A}, CAD5^{Q211E} or CAD5$^{R207C-I138C}$ cells are susceptible to chronic prion infection, as is illustrated by the presence of a PK-resistant "core" in CAD5^{WT} infected cell lysates (*lower panel*). CAD5$^{R207C-I138C}$ cells show a faint PK-resistant fraction in the pre-inculated lysates *(upper panel*), probably indicating moderate protein aggregation.

The bispecific POM1/POM2 antibody LVp12 is protective against prion diseases

In light of previous reports and the results shown in this chapter, I believe PrP^C-mediated toxicity is induced by an "inducing" site on PrP^C-GD and its execution is dependent on a functional PrP^C-FT (Reimann et al. 2016; Herrmann et al. 2015; Sonati et al. 2013). Conversely, a major drawback of the anti-PrP^C-FT antibody POM2 is its limited therapeutic potential, i.e. POM2 is only protective against prion disease when given directly after inoculation, but not when pathology is already visible (*Figure* 41).

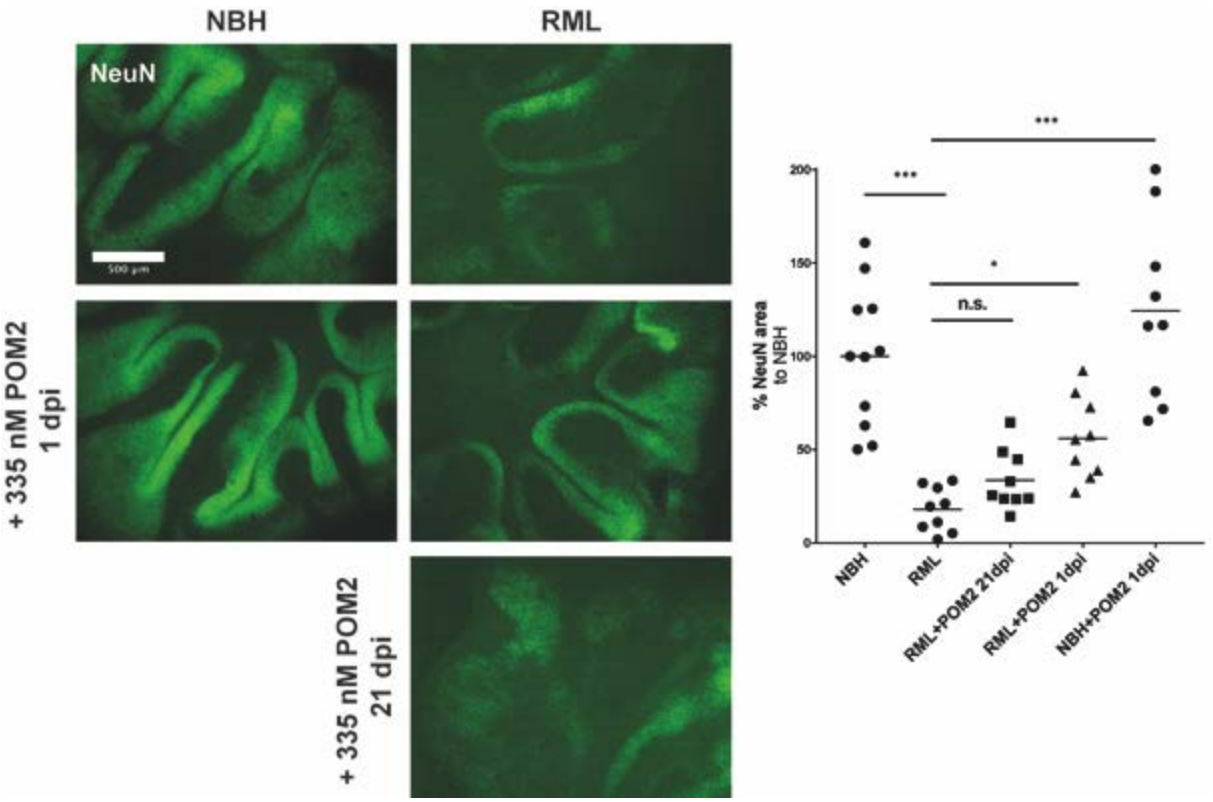

***Figure* 41**. Treatment of RML-infected *Tga*20 COCS with 335 nM of the anti-PrP^C-FT antibody POM2 leads to a significant amelioration of neuronal cell loss when given directly after inoculation, i.e. 1 dpi ($p<0.05$, one-way ANOVA with Dunnett's post hoc test), but not when pathology is already visible, i.e. 21 dpi. N.s. not significant, * $p<0.05$, *** $p<0.001$, one-way ANOVA with Dunnett's post hoc test.

To investigate whether concomitant blockage of PrP^C-FT and PrP^C-GD was beneficial against prion diseases, Marco Bardelli and Luca Varani (IRB Bellinzona) created a bispecific antibody consisting of both scFvPOM1 and scFvPOM2, termed LVp12 (*Figure* 42A). When adding LVp12 at 67 nM to RML-infected *Tga*20 COCS on 21 dpi, neuronal cell loss is significantly reduced, indicating higher efficacy of binding to both PrP^C-FT and PrP^C-GD than to PrP^C-FT alone (*Figure* 42B+C).

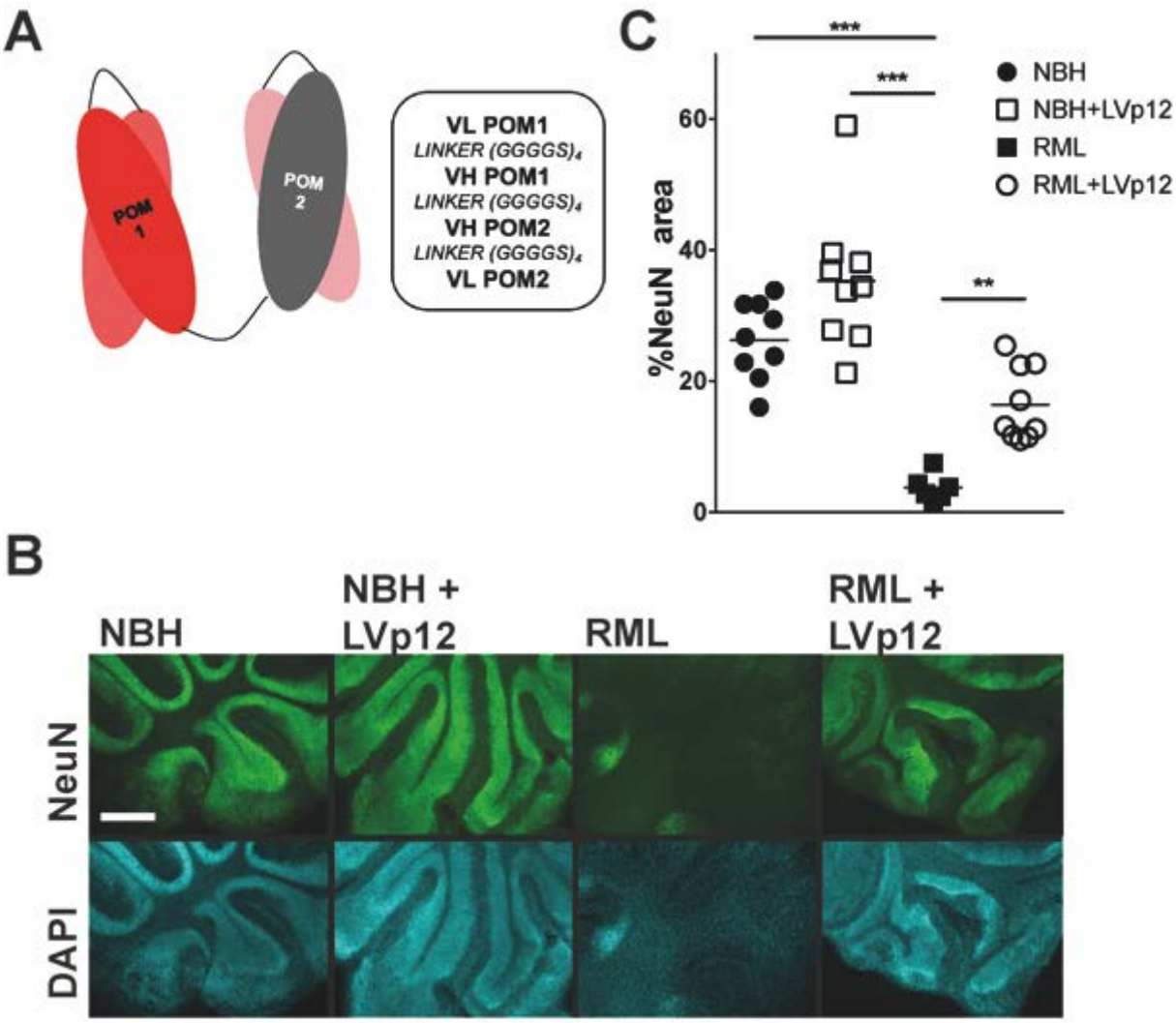

***Figure* 42**. (A) Scheme of LVp12: scFvPOM1 and scFvPOM2 are joined via $(GGGGS)_4$ linkers. (B) NeuN and DAPI histochemistry of LVp12 treated, *Tga*20 COCS showing rescue of RML-induced neurotoxicity by LVp12. Scale bar = 500 µm (C) NeuN morphometry of (B). ** $p<0.01$, *** $p<0.001$, one-way ANOVA with Dunnett's post hoc test.

Discussion and Outlook

The neurotoxic antibody POM1 mimics typical prion pathology with spongiform change, neuronal loss, astrogliosis, and microglial activation, and transcriptomic perturbations similar to those observed in prion diseases (Herrmann et al. 2015). It was shown before that prion toxicity or protection is dependent on the identity of the PrP^{C} epitopes recognized by each antibody (Sonati et al. 2013). Antibodies targeting the PrP^{C} globular domain are predominantly neurotoxic, whereas those targeting the flexible tail are largely protective (Sonati et al. 2013). FT-dependent protection through the OR-binding antibody POM2 is independent of prion replication, since it preserves neurons without reducing the accumulation of PK-resistant PrP^{Sc} (Herrmann et al. 2015). PrP^{C} mutants devoid of the octapeptide repeat domain do not confer POM1 susceptibility to *Prnp*-deficient COCS, confirming that the FT is a crucial effector of neurotoxicity (Sonati et al. 2013).

The scrapie prion protein PrP^{Sc} is defined through its resistance to enzymatic digestion by proteases and is commonly used as a surrogate marker for the presence of infectious prions (Aguzzi and Weissmann 1997).It is unclear, however, if and to what extent prion mimetics such as the monoclonal antibody POM1 are able to induce prions. I have shown in the first part of this chapter that POM1 treatment of COCS does not lead to the generation of infectious prions. In view of the pivotal importance of this question, I have employed a set of orthogonal methodologies including a cell bioassay, real-time quaking induced conversion (performed by Manuela Pfammatter), and a sensitive bioassay utilizing PrP^{C}-overexpressing transgenic mice.

Because of technological limitations, the docking of infectious PrP^{Sc} oligomers to membrane-resident normal PrP^{C} has never been observed directly. However, such docking represents a plausible basis for the phenomenon of prion toxicity. Accordingly, prions damage only neurons that express PrP^{C} on their surface, whereas *Prnp*-negative neurons do not undergo degeneration even after chronic, long-term exposure to prions (Brandner et al. 1996). I therefore submit that the docking of POM1 may mimic the process by which prions dock onto PrP^{C}. Consequently, I predict that compounds conferring protection against POM1 may have a high likelihood of being protective against infectious prions–a prediction that has been

verified experimentally with a number of compounds (Herrmann et al. 2015). By extension, POM1 toxicity seems to represent a promising model of prion toxicity that might allow for screening prion-protective compounds without the need of advanced biosafety measures.

The induction of toxicity independent of infectivity suggests the existence of a toxicity-inducing epitope of PrP^C that may be accessible to both neurotoxic antibodies and infectious prion seeds. The conformational POM1-epitope in the α1-α3 region of PrP^C could represent such a site, since additional monoclonal antibodies other than POM1 targeting residues in close proximity also induce neurotoxic effects (Reimann et al. 2016; Wu et al. 2017). To precisely pin down the important residues involved in PrP^C-GD mediated toxicity, I have assessed the effects of POM1 mutants carrying single alanine mutants of residues involved in PrP^C-binding as was observed in MDS (*Table* 4) resulting in 11 different scFvPOM1 mutants. Biophysical charaterization of the mutants has shown antibodies of different binding affinities, spanning K_D values of > 2 logs. High-affinity toxic antibodies showed activation of pathway similar to their wild-type, parental antibody, i.e., microgliosis and astrogliosis (*Figures* 25, 26) as well as execution of toxicity through PrP^C-FT, since scFvPOM1^{S32A} toxicity was ablatable by the anti-PrP^C-OR antibody POM2 (*Figure* 27).

I have found two mutants, scFvPOM1^{Y57A} and scFvPOM1^{Y104A} that ablated neurotoxicity induced by both the anti-PrP^C-GD antibody POM1 (scFvPOM1^{Y104A}) and prions (scFvPOM1^{Y57A} and scFvPOM1^{Y104A}, *Figures* 30, 31). Of note, treatment with scFvPOM1^{Y57A} and scFvPOM1^{Y104A} was successful when first signs of prion pathology were already visible, i.e. on 21 dpi in RML6-inoculated *Tga*20 COCS. This finding contrasts with the neuroprotective anti-PrP^C-OR antibody POM2, that is only therapeutic when given directly after prion inoculation, but not in later stages (*Figure* 41). Protective mutants attenuated the production of the reactive oxygen species producing enzyme NOX2 and microglial activiation (*Figure* 32), as well as the unfolded protein response (*Figure* 33). Low-binding affinity of scFvPOM1^{Y57A} and toxicity of scFvPOM1^{Y57A} at a dose of 1.2 µM precluded rescue experiments of anti-PrP^C-GD toxicity with scFvPOM1^{Y57A} (*Figure* 31).

How do anti-PrP^{C}-GD antibodies lead to protection against prion disease? Treatment of RML-infected COCS with either $scFvPOM1^{Y57A}$ or $scFvPOM1^{Y104A}$ does not lead to a reduction of PrP^{Sc}, hence their mode of action is most likely located downstream of prion replication (*Figure* 35). Chronic treatment with $scFvPOM1^{Y57A}$ or $scFvPOM1^{Y104A}$ does not lead to reduction of PrP^{C} levels, either, excluding lowered PrP^{C} "substrate" to be a cause of reduced toxicity (*Figure* 34). These findings point towards protective $scFvPOM1^{Mut}$ antibodies to act as dominant-negative immunoreagents binding to PrP^{C} and quenching prion toxicity.

Molecular dynamics simulations on human PrP^{C} showed that, when free in solution, R208 was free in solution, upon binding to POM1, R208 formed a H-bond with H140 leading to relaxation of the β2-α2 loop, implying loop rigidity as a mediator of prion toxicity. The β2-α2 loop ("rigid loop") spans aa 165-175 in the murine prion protein carrying a strictly conserved tyrosine at residue 169 (Kurt et al. 2014). Modification of as little as three amino acids in the rigid loop, was shown to profoundly alter the properties of interspecies transmission. In fact, transgenic mice carrying the a triple mutation of Y169G, S170N and N174T were completely resistant to mouse and chronic wasting disease prions (Kurt et al. 2014). I created $CAD5^{R207C-I138C}$ cells carrying a mutated form of PrP^{C} mimicking decreased β2-α2 rigidity, as observed in MDS (*Figure* 37). Indeed, binding of the monoclonal anti-PrP^{C}-β2-α2 antibody POM5 was ablated in $CAD5^{R207C-I138C}$, but not in $CAD5^{WT}$ cells, strengthening the observations made *in silico* (*Figure* 39). Furthermore, protection by $scFvPOM1^{Y57A}$ against prions and neurotoxicity of $scFvPOM1^{D55A}$ was predicted by MDS and has proven true *ex vivo* (*Figure* 24, 31).

Based on predictions made *in silico*, I further generated the allegedly protective $mPrP^{C}$ mutants PrP^{C}(R207A) and PrP^{C}(Q211E). Both mutations were intended to ablate binding to the supposed "toxicity inducer" domain of PrP^{C}-GD, i.e., the conformational epitope of POM1 and similar toxic anti-PrP^{C}-GD antibodies, amongst others ICSM18 and D18 (Wu et al. 2017; Reimann et al. 2016; Solforosi et al. 2004). Stable expressing PrP^{C} mutants showed correct membranal expression (*Figure* 37), correct glycosylation (*Figure* 38) and adequate conservation of the conformational POM8 and POM19 epitopes, as well as, the expected loss of POM1 recognition (*Figures* 37, 39). Unexpectedly, the prion protein mutant of $CAD5^{Q211E}$

was no longer recognizable by the anti-PrP^C-β2-α2 antibody POM5, suggesting conformational deregulation *in vitro* that was not predicted *in silico*, leaving the pathogenic significance of a mPrP(Q211E) elusive (*Figure* 39). Of note, stabilization of both PrP^C-FT and PrP^C-GD through a bispecific POM1/POM2 antibody had profound impact on amelioration of neuronal cell loss in RML-infected COCS and was efficient when given at low doses and in late stages of the disease (*Figure* 42). This observation contrasts with the anti-PrP^C-FT antibody POM2 that has to be applied directly after inoculation to exert significant, protective effects (*Figure* 41). These findings are of significance when translating protective anti-PrP^C antibodies into clinical trials, as the most commonly prevalent prion disease in humans, i.e. sporadic CJD, is usually only diagnosed when clinical symptoms appear – in contrast to lesser prevalent, inherited forms of prion disease (Takada and Geschwind 2013).

There are potential criticisms of my study. Firstly, I did not show the beneficial effects of any of the antibodies *in vivo*, e.g. in prion-infected mice. *In vivo* experiments with scFv antibodies are usually applicable when scFv are administrated locally, e.g. through a osmotic mini-pump, since they are cleared from the circulation after a few minutes after injection. As osmotic mini-pumps are implanted for several weeks into the animal's ventricles at 37°C, the aggregation-prone scFv will eventually lose their biological function (Tiziana Sonati and Uli Hermann, personal communication). Systemic administration of holo IgG antibodies is in my opinion the most feasible approach, although this has been hampered by as yet low antibody yields from recombinant protein production. Secondly, the mechanistic data presented is mostly derived from MDS *in silico.* In fact, some predicitions such conformational stability of $CAD5^{Q211E}$ and exertion of neuroprotective effects of $scFvPOM1^{D55A}$ (probably due to low dosage regimen) could not been reproduced *in vitro* or *ex vivo*, respectively. Furthermore, the allosteric changes upon POM1 and prion binding to PrP^C were not yet observed in NMR spectroscopy (Sonati et al. 2013), probably due to higher-order changes in tertiary and quarternary structure.

In the future, I am planning to confirm the neuroprotective effects of $POM1^{Y57A}$ and $POM1^{Y104A}$ *in vivo* by systemic administration of IgG_1 antibodies into prion infected mice.

Preliminary data by Marco Bardelli and Luca Varani have shown interaction of a N-terminal residue, i.e. Y127, with the C-terminal domain of PrP^{C} upon binding to POM1. I am currently cloning and producing 2 of 3 of the above-mentioned PrP-mutants (i.e. R207A and R207C-I138C) plus the mPrP(Y127F) mutant coupled to a fluorophore as adeno-viral expressed plasmids that can be used for transduction of *Prnp*$^{0/0}$ COCS to assess the impact of these mutations on POM1 and prion-induced toxicity. Further experiments include dose-escalation tests of the protective POM1-derivatives ($POM1^{Y57A}$, $POM1^{Y104A}$ and LVp12) to assess innocuity and test rescue of other downstream pathways by protective antibodies, such as calpains, cleavage of alpha-fodrin and reactive oxygen species. One could also speculate that a bispecific antibody consisting of both POM2 and $POM1^{Y57A}$ could provide a highly effective compound against prion disease.

Part III - Human autoantibodies against the prion protein in health and disease

Aims of the study

There is compelling evidence that anti-PrP^{C}-FT antibodies may be therapeutic in human prion diseases and eventually in other neurodegenerative diseases involving PrP^{C} such as AD (Herrmann et al. 2015; Chung et al. 2010). Furthermore, antibodies derived from human subjects frequently show superior safety profiles and affinity maturation compared to "humanized" hybridomas or synthetic libraries. They have already shown great therapeutic promise in the case of the anti-amyloid β antibody Aducanumab (Sevigny et al. 2016) and in a range of autoimmune and inflammatory diseases through naturally occurring interferon-gamma neutralizing autoantibodies (Meyer et al. 2016), among others.

Genetic prion disease patients express a pathological form of the prion protein throughout their entire life, clinical symptoms occur, however, almost exclusively in advanced age (Takada and Geschwind, 2013). This is indicative of protective factors. Here, I posit that such factors may consist of antibodies against prions that are responsible for the long clinically silent period of gPrD patients. Over time, however, the overproduction of PrP^{Sc} in *PRNP* mutation carriers may overwhelm the defense afforded by such antibodies.

CIDP is a rare, chronic neuropathy of uncertain etiology (Hanewinckel, Ikram, and Van Doorn 2016). $Prnp^{0/0}$ mice independent of the genetic background develop a chronic demyelinating polyneuropathy (CDP). After several months, $Prnp^{0/0}$ animals develop characteristic walking disturbances that manifest in typical demyelinating changes in peripheral nerves, such as macrophage invasion, breakdown of myelin proteins (Bremer et al. 2010). Recently, the G-protein coupled receptor Adgrg6/GPR126 has been demonstrated to depend on a functional PrP^{C}-FT signaling to maintain myelin integrity (Kuffer et al. 2016). I postulate that patients harboring anti-PrP^{C}-FT autoantibodies develop a chronic demyelinating neuropathy through sequestering of soluble PrP^{C}-FT by autoantibodies.

In search of both toxic and protective autoantibodies against PrP^C I will perform autoantibody screenings of gPrD and CIDP patient cohorts with subsequent clinical correlations and clone paired heavy and light chains of human antibodies from cognate memory B cells. Crucially, access to patient clinical history will ensure selection of autoantibodies for minimal toxicity and allow the correlation of clinical histories with autoantibody levels. Human-derived antibodies generated in this study will represent safe and efficacious new drug candidates compared to murine, humanized or human antibodies obtained by current immunization or peptide display approaches. Completion of the proposed activities will lead to the development of effective antibodies against these fatal disorders. Further, the discovery of toxic anti-PrP^C autoantibodies responsible for CIDP will vastly broaden our understanding of this still elusive disease and provide immediate treatment options for these patients.

Results

Establishing a screening platform to detect and extract anti-PrP^C autoantibodies in human blood

Enzyme-linked immunosorbent assays are sensitive assays that can be used in medium- and high-throughput screenings. I chose an indirect ELISA that would allow me to present the antigen of interest, i.e. human PrP^C, via a linker protein absorbed to the test plate, in order to reduce protein denaturation through direct absorption of the protein of interest resulting in reduced detection specificity and sensitivity (*Figure* 43A, (Kim and Herr 2013)).

In order to establish a robust positive control for anti-PrP^C autoantibody screenings, I created humanized versions of the monoclonal murine anti-PrP^C antibodies POM1 and POM2 (Polymenidou et al. 2008), hereafter termed HuPOM1 and HuPOM2 for human and MuPOM1 and MuPOM2 for murine counter-parts. To this end I have grafted their variable light and heavy chains onto human kappa (κ) and gamma (γ1) constant domains: light and heavy chains of POM1 and POM2 cloned into pFUSE2-CLIg-hK, for light chains, or pFUSE-CHIg-hG1 (both

Invivogen), for heavy chains, respectively. IgG_1 constant heavy chains were designed as L234A and L235A ("LALA") mutants to reduce Fcγ and complement binding (Hessell et al. 2007) (*Figure* 43B).

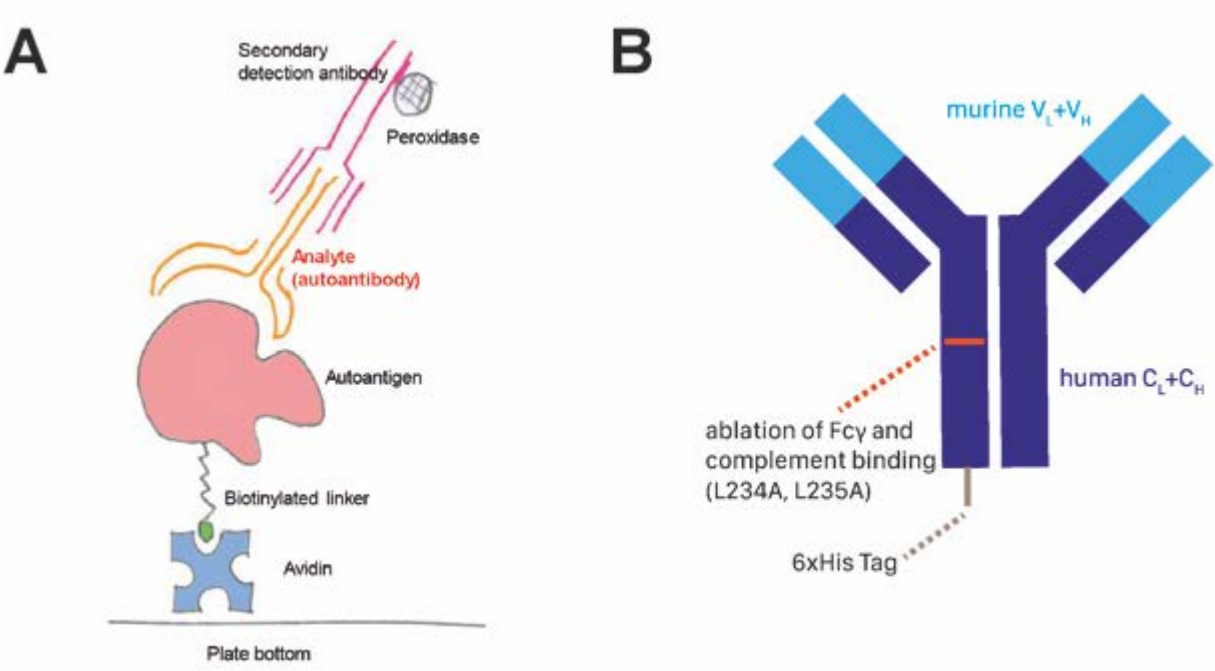

***Figure* 43**. (A) Schematic depiction of the anti-PrP^C autoantibody ELISA: avidin (here: Streptavidin) is adsorbed onto microtiter plates and bound by a site-specificbiotinylated antigen (here: $rhPrP_{23-231}$ C-terminally tagged with a biotinlyated *AviTag* peptide. Autoantibodies are bound to immobilized prion protein and detected via a horseradish peroxidase (HRP)-conjugated secondary antibody. Image courtesy of Adriano Aguzzi. (B) Scheme of humanized POM1 and POM2 antibodies, denoted HuPOM1 and HuPOM2, respectively. Murine, variable light and heavy chains are grafted onto their human constant light (κ) and gamma (γ1) counterparts. Constant heavy chains bear to L-to-A substitutions (L234, L235A; "LALA" mutation) to ablate complement and Fcγ binding. Constant heavy chains are tagged by 6x histidines.

HEK293 $PRNP^{0/0}$ #H1 cells were co-transfected with a ratio of 3:2 = light:heavy chain plasmids and stably selected with Blasticidin and Zeocin, cell supernatants were collected and purified by affinity chromatography using protein G sepharose (HuPOM1+HuPOM2) and Ni-NTA resin (HuPOM1, *Figure* 44A). Analyses of purified antibodies showed binding of both HuPOM1 and HuPOM2 to $rmPrP_{23-230}$ as well as to $rhPrP_{23-231}$ (*Figure* 44B). Expectedly, HuPOM1 bound to the PrP^C-GD fragment $rmPrP_{121-230}$, but not to $rmPrP_{23-120}$ and *vice versa* (*Figure* 44B).

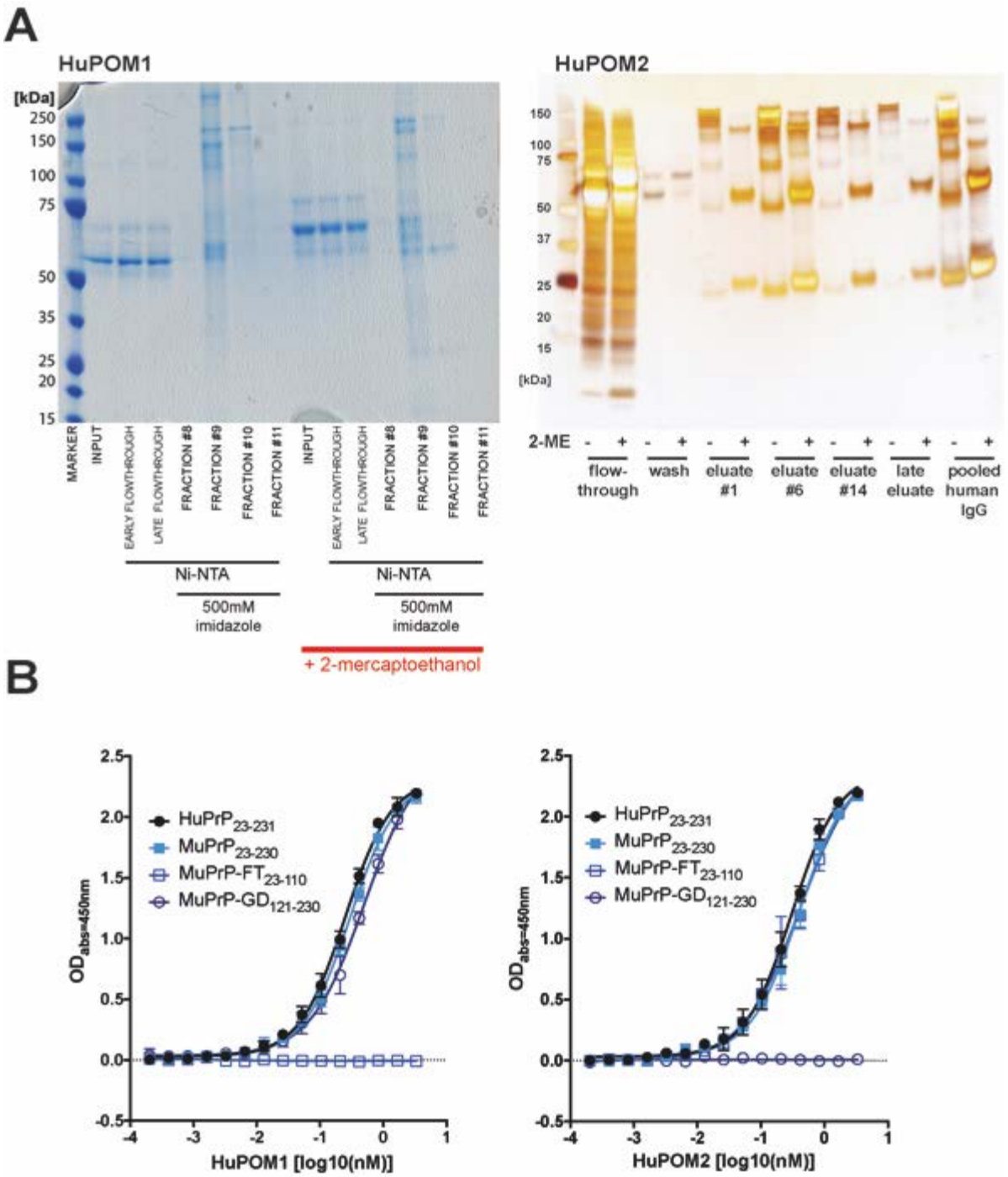

***Figure* 44** (A) SDS-PAGE of Ni-NTA purified HuPOM1 stained with InstaBlue (*left panel*) and silver stained SDS-PAGE of protein G sepharose purified HuPOM2 shows strong bands at 150 kDa under oxidative and heavy (50 kDa) and light (25 kDa) chain bands under reducing (+ 2-mercaptoethanol, 2-ME conditions). (B) Direct ELISA of HuPOM1/2 shows specific binding of HuPOM1 to $MuPrP_{121-230}$ without overt binding to $MuPrP_{23-110}$ and *vice versa*.

To test whether my assay would detect all human IgG (hIgG) isoforms, i.e. $hIgG_{1-4}$, I tested single $hIgG_{1-4}$ isoforms derived from multiple myeloma patients and pooled murine IgG (mIgG) against the HRP-conjugated anti-human IgG antibody. Herein, the anti-hIgG antibody

specifically reacted with all hIgG$_{1-4}$ isoforms, but not rabbit (*Figure* 45A) or murine IgG (*Figure* 45B).

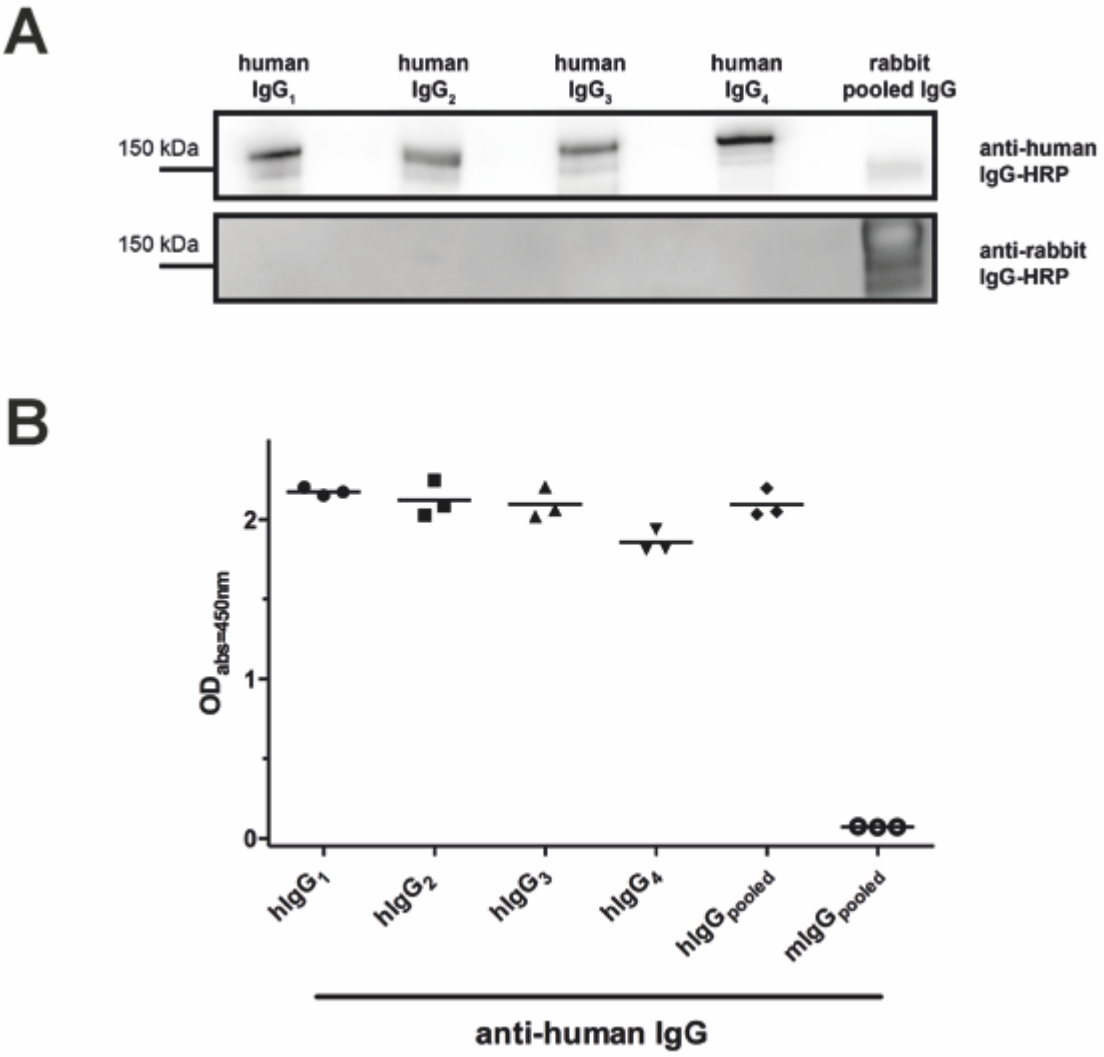

***Figure* 45**. All hIgG$_{1-4}$ isoforms are detected in the anti-PrP^{C} autoantibody ELISA. (A) Western blot of 10 ng of protein per lane shows specific reactivity of the anti-hIgG antibody to all hIgG$_{1-4}$ isoforms, but not to rabbit IgG. (B) Human IgG$_{1-4,}$ pooled hIgG and pooled mIgG were absorbed onto a polystyrene microtiter plate at c=20 µg/mL and detected using a anti-hIgG antibody, herein all hIgG$_{1-4}$ isoforms and pooled hIgG, but not mIgG were detected.

I have generated a full-length human PrP$_{23-231}$ with a C-terminal *AviTag*, a 15 aa linker tag with a central lysine, i.e. GLNDIFEAQ**K**IEWHE, which, upon co-transfection with the biotin ligase BirA in E. coli undergoes site-specific biotinylation *in vivo* (Fairhead and Howarth 2015) in order to facilitate native and conformationally correct presentation of hPrP^{C}. A *gBlock* (IDT) containing rhPrP$_{23-231}$, a GSGS linker and the *AviTag* was cloned into the *BamHI* and *EcoRI* sites of the pRST-Mini-T plasmid as described before (*Figure* 46A (Zahn, von Schroetter, and Wuthrich 1997; Sonati et al. 2013)). Co-transfection of E. coli with pRST-Mini-T.rhPrP$_{23-231}$-

AviTag and the pBirAcm plasmid containing BirA led to efficient *in vivo* biotinylation, yielding hPrP-AT$_{biotin}$ (*Figure* 46B). Proteomic analysis by time-of-flight mass spectrometry electrospray (TOF MS ES, performed by the Functional Genomics Center at the University of Zurich) showed two clear peaks according to the estimated molecular weight, namely native hPrP-AT and biotinylated hPrP-AT$_{biotin}$ (*Figure* 46C).

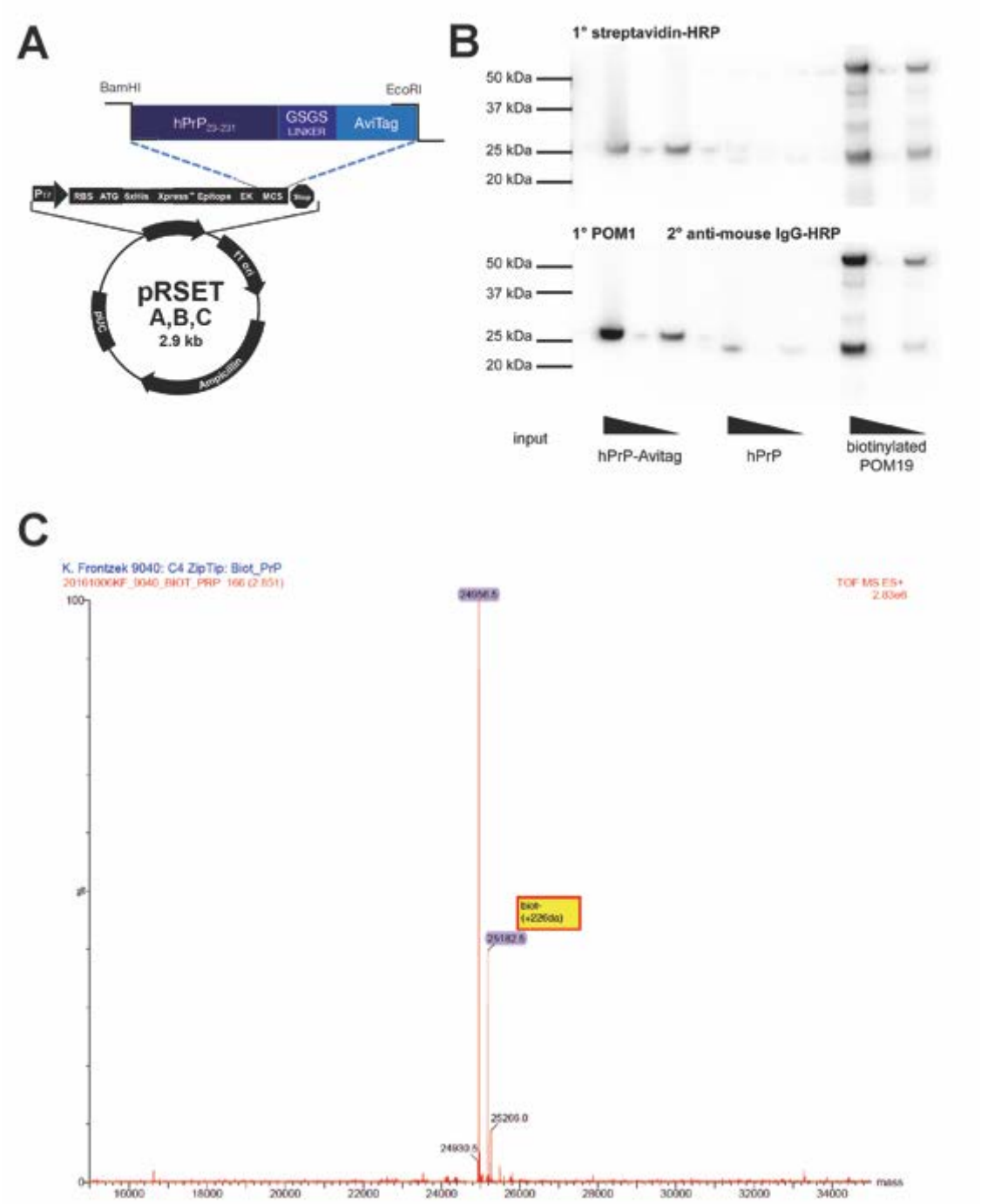

***Figure* 46**. (A) Scheme of the expression plasmid of hPrP-AT (B) Western blot of purified and *in vivo* biotinylated hPrP-AT$_{biotin,}$ native rhPrP$_{23-231}$ and biotinylated POM19 shows hPrP-AT$_{biotin}$, but rhPrP$_{23-231}$ is not detectable by both Streptavidin and POM1. Recombinant proteins are loaded at 300 ng (left band) and 100 ng (right band). (C) TOF MS ES shows the correct size of biotinylated and unbiotinylated hPrP-AT$_{biotin}$ after Ni-NTA resin purification of *in vivo* biotinylated hPrP-AT.

The magnitude of anti-PrP^C autoantibody reactivity is expressed as the negative decadic logarithm of the half-maximal inflection point of the binding curve [$-\log_{10}(EC_{50})$], as was calculated by an automated 4-point logistic regression fitter (by Georg Meisl, Cambridge). In order to test the specificity of my generated antibodies and further experimentally dervied hits from human plasma, I was wondering whether pre-incubation of $rhPrP_{23-231}$ with both HuPOM1 and HuPOM2 would lead to a decreased anti-PrP^C reactivity. Both HuPOM1 and HuPOM2 were pre-incubated with 300 nM of either $rhPrP_{23-231}$ or murine, scrambled PrP^C-N1 ($rmPrP_{23-110}$, see also (Kuffer et al. 2016)) in 1% TopBlock in 0.1% PBS-T at 4°C for 1 hour and then tested on the anti-PrP^C ELISA. A right-shift of the binding curve, i.e. weakend binding to hPrP-AT_{biotin} was observed upon pre-incubation with $rhPrP_{23-231}$, but not scrambled PrP^C-N1, suggesting successful competition (*Figure* 47).

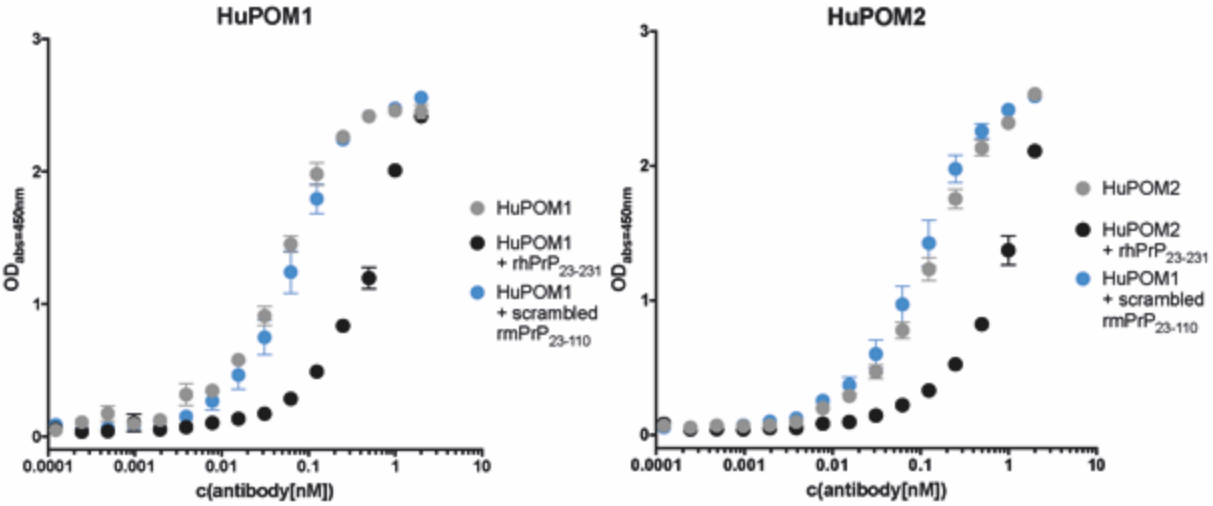

***Figure* 47**. Pre-incubation with 300 nM of $rhPrP_{23-231}$, but not scrambled PrP^C-N1 with HuPOM1 (*left panel*) or HuPOM2 (*right panel*) leads to a right-shift of the binding curve indicating specific competition of the soluble against the immobilized antigen.

In order to clone the cognate memory B-cell variable heavy and chain light repertoire, I established a protocol using bait-gated fluorescent activated cell sorting (FACS) in which hPrP-Avitag is tetramerized through binding to a Streptavidin-Fluorophore leading to increased avidity of B-cell binding (*Figure* 48A). Reportedly, a fraction of hybridoma cells not only secretes antibodies but also expresses membrane-bound antibodies (Seifert et al. 1992). To test the specificity of my bait-gated approach, I stained POM1 hybridoma cells (Polymenidou et al. 2008) with the lipophilic dye DiI (Invitrogen) and the anti-Cytokeratin 8/18 (CK8/18)

hybridoma cell line UCD/PR10-11 (ATCC) with the lipophilic dye DiO (Invitrogen) in a 1:1 ratio (*Figure* 48B) and incubated with a complex of hPrP-AT_{biotin} and Streptavidin-BV421. No $DiO^+/BV421^+$ cells, but a large fraction of $DiI^+/BV421^+$ cells were seen, indicating specific binding of the POM1 hybridoma cells to the hPrP-AT_{biotin}/Streptavidin-BV421 complex (*Figure* 48C).

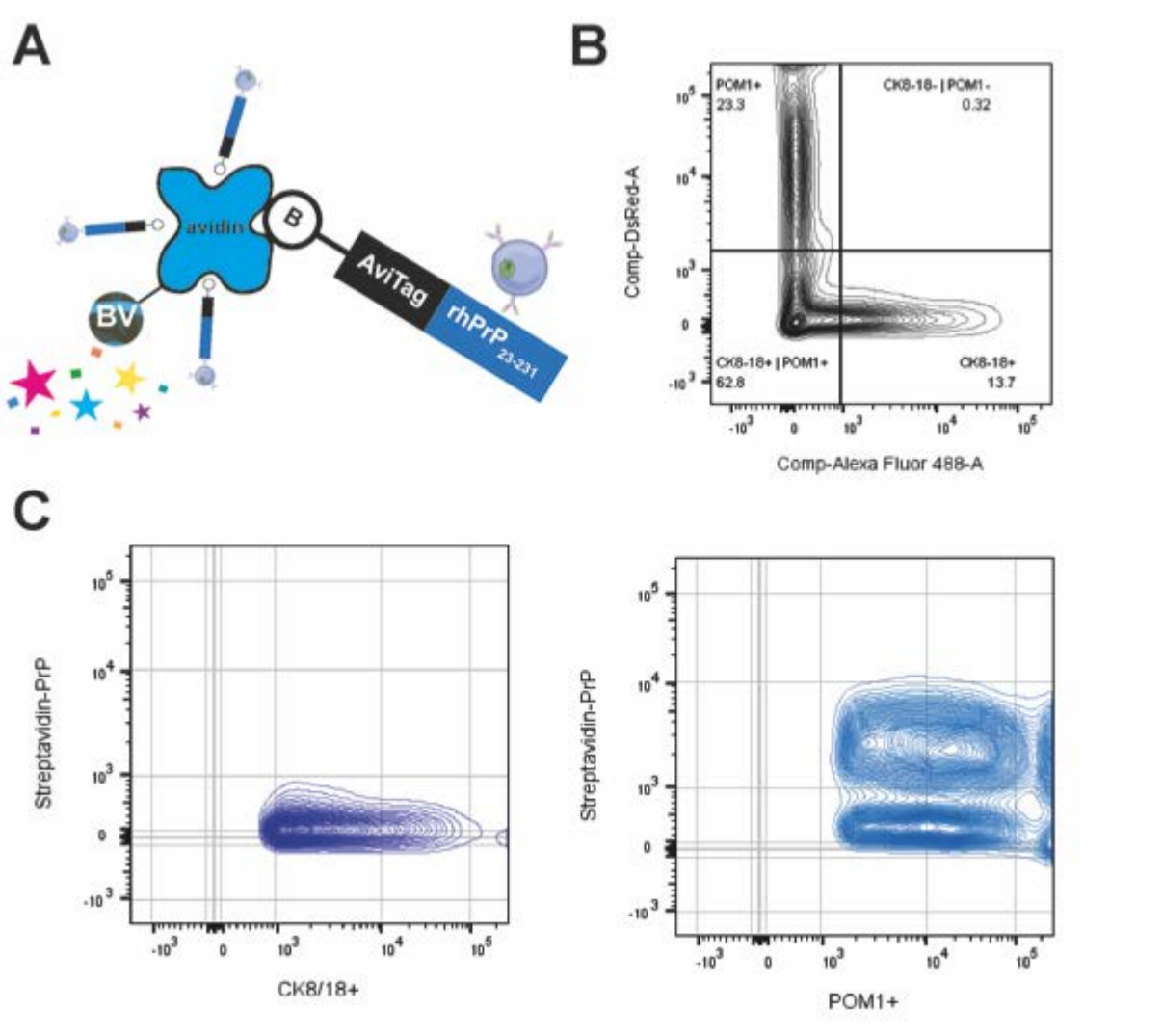

***Figure* 48**. (A) Scheme of tetrameric Streptavidin-BV421 bound to hPrP-AT_{biotin}. B= biotin, BV=brilliant violett 421. (B) Gating strategy for POM1 hybridomas stained with DiI and UCD/PR10-11 hybridomas stained with DiO. (C) Mixing of DiI^+ and DiO^+ cells with a complex of hPrP-AT_{biotin}/Streptavidin-BV421 complex shows specific binding in POM1, but not in anti-CK8/18 hybridoma cells.

Anti-PrP^C autoantibodies in genetic prion disease patients

Sequencing of the *PRNP* ORF from blood samples of genetic prion disease patients was performed using Sanger Sequencing at the Institute of Molecular Pathology (University

Hospital Zurich). Prior to sequencing, I established a protocol for the inactivation of prions from blood samples while maintaining DNA integrity (*Figure* 49).

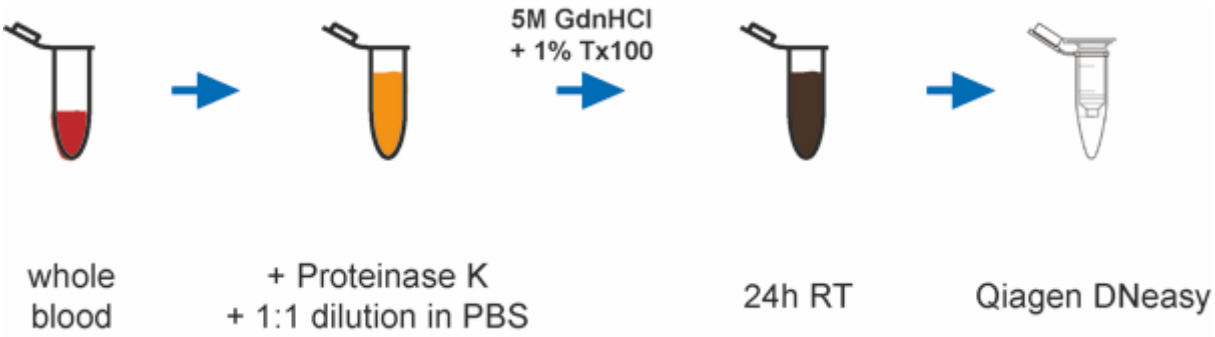

***Figure* 49**. For PRNP genotyping, whole blood was diluted in PBS and proteinase K was added to dissociate cells. To deactivate prions, 5M GdnGCl + 1% Triton X-100 (Tx100) at pH=5 were added and incubated for 24 hours at room temperature. Further DNA elution was performed using Qiagen's Blood and Tissue DNeasy kit.

A total of n=112 patients was genotyped in the frame of the study (detailed baseline characteristics, see *Table* 5). 54% (n=60) of individuals were *PRNP*^{WT}, i.e., unmutated family members, and 46% (n=52) of participants carried a non-synonymous *PRNP* mutation.

	Median (IQR)	n	Median (IQR)	n	data available in %	p-value
	***PRNP*^{WT}**		***PRNP*^{Mut}**			
# of patients		60		52	112	
demographics						
age [y]	36 (28-54)	51	43 (33-64.5)	49	89	0.12*
female		29		26	86	0.93§
p.129 polymorphism						
M/M		8		27	85	*<0.001§*
M/V		34		22		
V/V		4				
non-synonymous mutations						
E200K		-		48	100	
D178N		-		4		
clinical data						
gPrD symptoms				10	100	

***Table* 5**. Summary of the investigated gPrD cohort. IQR = inter-quartile range. * two-tailed, unpaired t-test § Chi-Square test

PRNP^{Mut} patients were almost exclusively E200K (92%, n=48) mutations and in a minor fraction D178N (8%, n=4) mutations. Nineteen percent (n=10) of *PRNP*^{Mut} patients were symptomatic when blood was drawn for the study. Demographic data provided by the participating institutions for all patients included age at phlebotomy (available for 89%, n=100) and gender (available for 89%, n=100). *PRNP*^{Mut} patients were significantly more likely to harbor Met/Met at p.129 that *PRNP*^{WT} individuals ($p<0.001$, 55% *PRNP*^{Mut} versus 17% *PRNP*^{WT}, Chi-square test, *Table* 5).

Screening of venous blood from n=103 genotyped patients for IgG autoantibody reactivity against PrP^{C} did not yield significant differences between *PRNP*^{Mut} and *PRNP*^{WT} (*Figure* 50A). Clinical symptoms in *PRNP*^{Mut} patients did not affect anti-PrP^{C} autoantibody levels when compared to asymptomatic *PRNP*^{Mut} patients (*Figure* 50B), neither did p.129 polymorphisms (*Figure* 50C). No gender-specific effects were observable (*Figure* 51D). When correlating the age at phlebotomy with anti-PrP^{C} autoantibody titers, the titers of *PRNP*^{Mut} patients significantly decreased during aging (Pearson $r=-0.41$, $p<0.01$) while those of *PRNP*^{WT} patients remained stable (*Figure* 51E), independent of age per groups at baseline (*Table* 5). A second phlebotomy was performed in n<20 *PRNP*^{Mut} patients (due to data protection of *PRNP*^{Mut} patients the exact number cannot be disclosed). Comparison of titers did not yield a significant change (paired, two-tailed T-test, *Figure* 51F).

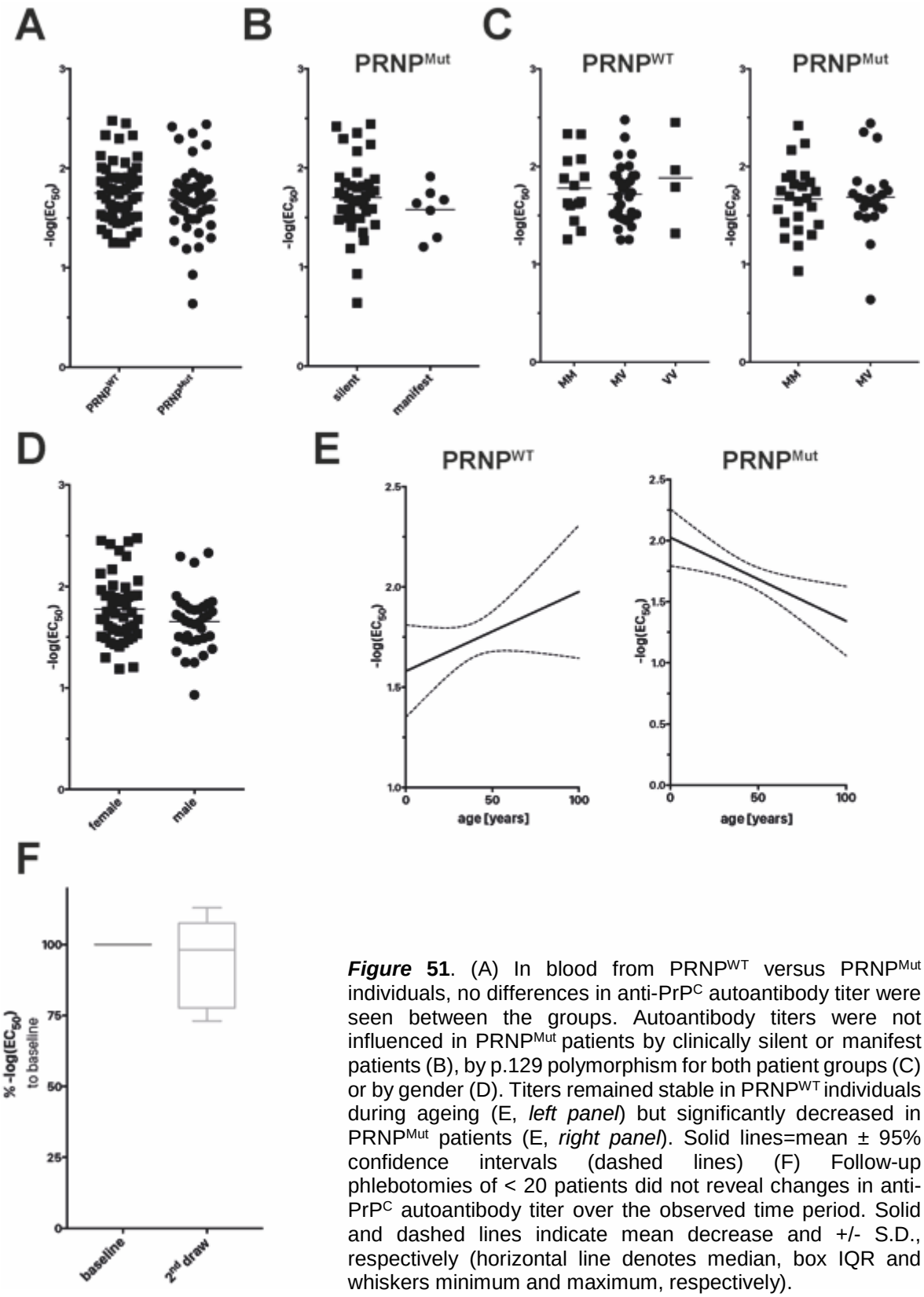

***Figure* 51**. (A) In blood from PRNP^{WT} versus PRNP^{Mut} individuals, no differences in anti-PrP^{C} autoantibody titer were seen between the groups. Autoantibody titers were not influenced in PRNP^{Mut} patients by clinically silent or manifest patients (B), by p.129 polymorphism for both patient groups (C) or by gender (D). Titers remained stable in PRNP^{WT} individuals during ageing (E, *left panel*) but significantly decreased in PRNP^{Mut} patients (E, *right panel*). Solid lines=mean ± 95% confidence intervals (dashed lines) (F) Follow-up phlebotomies of < 20 patients did not reveal changes in anti-PrP^{C} autoantibody titer over the observed time period. Solid and dashed lines indicate mean decrease and +/- S.D., respectively (horizontal line denotes median, box IQR and whiskers minimum and maximum, respectively).

Anti-PrP^{C} autoantibodies in CIDP patients

Prnp$^{0/0}$ mice suffer from chronic demyelinating polyneuropathy (Nuvolone et al. 2016; Bremer et al. 2010; Kuffer et al. 2016), similar to chronic inflammatory demyelinating polyneuropathy (CIDP), a rare neuropathy seen in human patients, the etiology of which remains largely elusive (Hanewinckel, Ikram, and Van Doorn 2016). If antibodies in human blood were to sequester soluble PrP^{C}, inadequate pro-myelinating signaling of GPR126 would lead to a *Prnp*$^{0/0}$-like, demyelinating phenotype. I have received n = 100 plasma samples from CIDP patients from a variety of hospitals in France (Jerome Devaux, CNRS, Marseille). The median age of the patients was 60 years (inter-quartile range 49-68), n=35 patients were of female gender. Control groups included patients with autoimmune polyendocrinopathy candidiasis ectodermal dystrophy (APECED), also called autoimmune polyendocrine syndrome type 1 (APS1), a rare autoimmune disease caused by mutations in the autoimmune regulator (AIRE) gene (Kisand and Peterson 2011). In APS-1 patients, AIRE mutations lead to a failure to eliminate autoreactive T cell pools with the subsequent development of autoimmunity (Kisand and Peterson 2011). These patients display a broad autoantibody profile against many antigens (Hayday 2013). Guillain-Barré Syndrome (GBS) is an acute peripheral neuropathy and often considered to be the acute counterpart of CIDP (Wijdicks and Klein 2017). Lastly, patients with systemic lupus erythematosis (SLE) suffer from a chronic autoimmune syndrome sharing pathogenic features with CIDP patients, e.g. terminal complement activation (Quast et al. 2016).

Anti-PrP^{C} autoantibody titers did not significantly correlate with patient age (*Figure* 52A) or gender (*Figure* 52B). Autoantibody titers showed good inter-assay correlation when testing blood on plates with directly absorbed rhPrP$_{23\text{-}231}$ versus Streptavidin-linked hPrP-AT$_{biotin}$ (Spearman's r = 0.55, 95% confidence interval 0.37-0.69, p<0.001, *Figure* 52C). When testing patient blood from CIDP patients against unbiotinylated rhPrP$_{23\text{-}231}$, CIDP patients exhibited a strong reactivity compared to unselected hospital patients from the University Hospital of Zurich (p<0.001, mean -log$_{10}$(EC$_{50}$) 1.87 ± 0.33 CIDP vs. 1.38 ± 0.22 UHZ controls, two-tailed, unpaired, t-test, *Figure* 53A). CIDP autoantibody titers were not different from SLE patients,

but significantly elevated to APS1, GBS, Sepsis, *PRNP*^{Mut} patients and their *PRNP*^{WT} family counterparts (*Figure* 53B). As any strong reactivity could be due to artificial polyreactivity of the blood samples, I tested n=42 CIDP patient blood samples against biotinylated, pyroglutamylated $A\beta_{3\text{-}17}$ ($pE_{3\text{-}17}$, a gift from Prof. H.-U. Demuth, (Nussbaum et al. 2012)) as well as against Streptavidin, biotin, BSA and uncoated plates alone to exclude unspecific binding

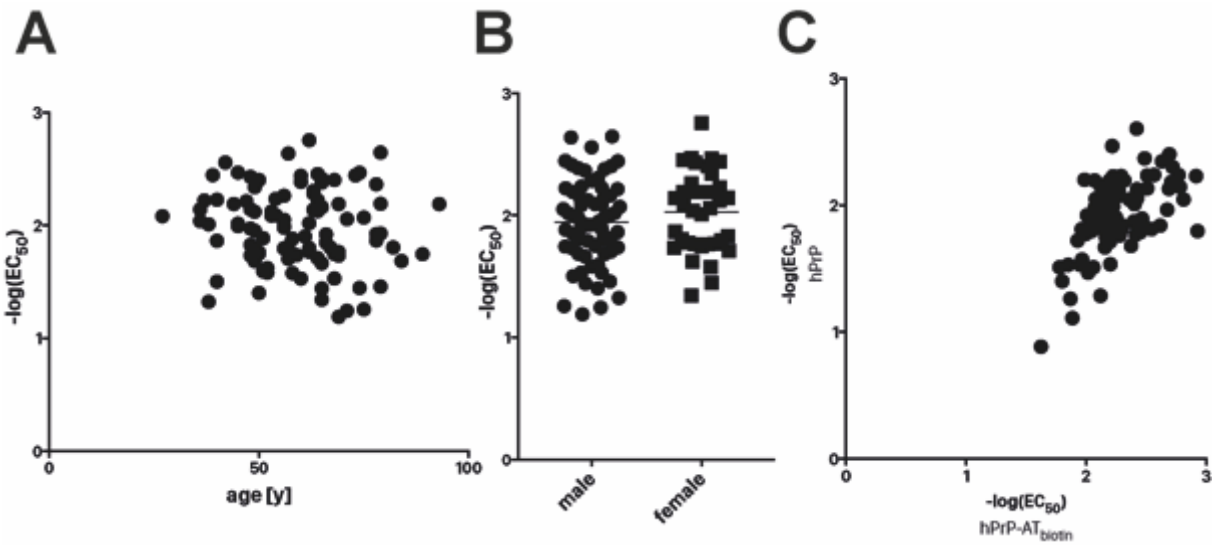

***Figure* 52**. No correlation was seen between the age of CIDP patients and anti-PrP^C autoantibody titer (A), nor did I see a difference in antibody titers in regards to gender of the patients (B). (C) When correlating titers in two different assays, i.e. directly absorbed $rhPrP_{23\text{-}231}$ versus Streptavidin-linked $hPrP\text{-}AT_{biotin}$, a good correlation was observed (Spearman's r=0.55, p<0.001).

(*Figure* 53C). Binding of CIDP blood samples against $hPrP\text{-}AT_{biotin}$ was significantly stronger than all other conditions tested (p<0.001, $hPrP\text{-}AT_{biotin}$ versus all other conditions, one-way ANOVA with Dunnett's post hoc test, *Figure* 53C). Lastly, I tested total IgG levels in CIDP, SLE, APS1, 2, 4 and UZH patients, herein, no significant differences were seen (*Figure* 53D).

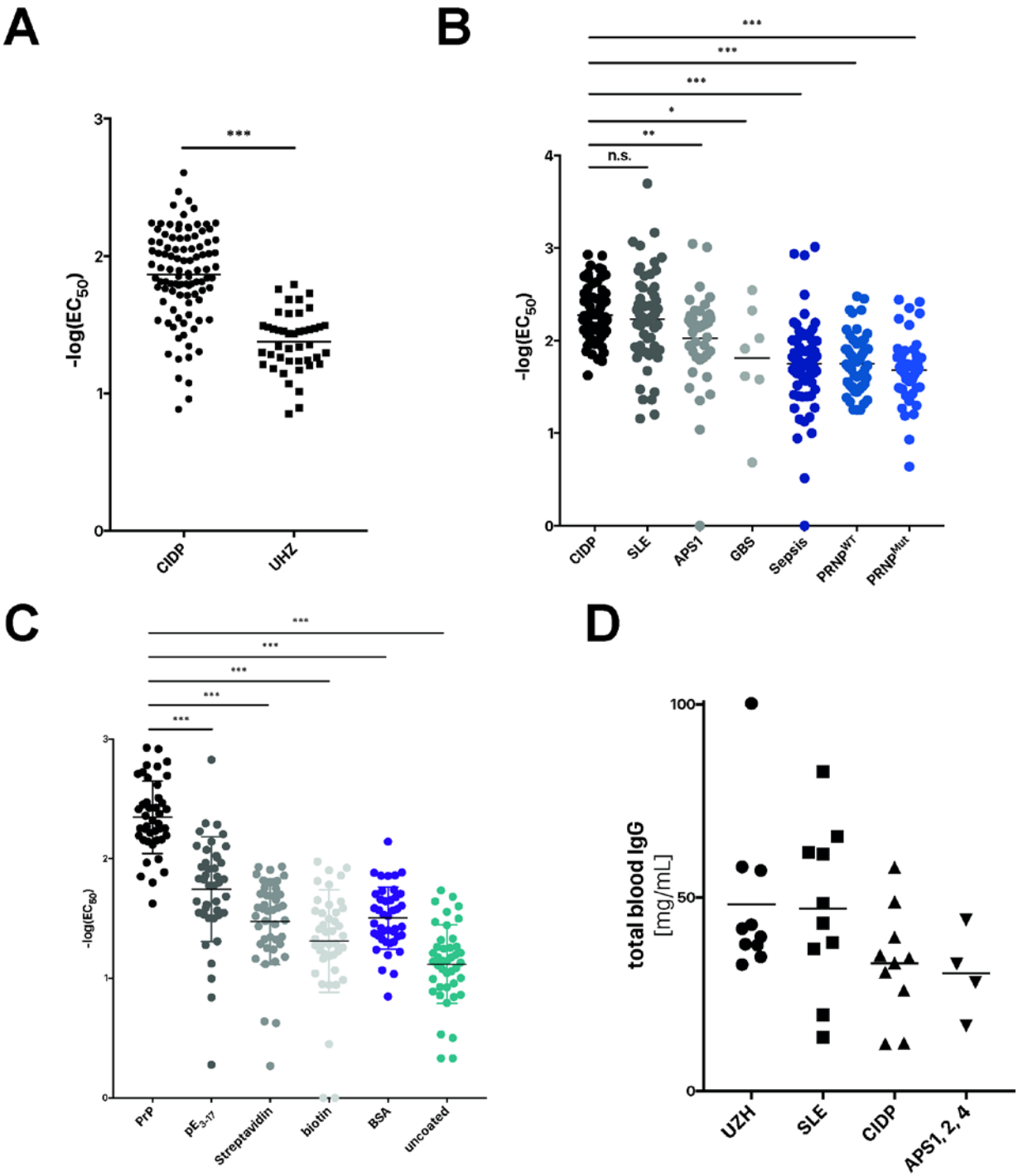

***Figure* 53**. (A) CIDP patients show strong anti-PrP^{C} reactivity compared to patients randomly selected from the University Hospital of Zurich, *** p<0.001, two-tailed, unpaired t-test. (B) CIDP patients showed significantly elevated anti-PrP^{C} autoantibody titers compared to patients suffering from APS1, GBS, Sepsis as well as PRNP^{Mut} mutation carriers and their PRNP^{WT} family members. No significant difference is seen between SLE and CIDP patients. N.s. not significant, * p<0.05, ** p<0.01, *** p<0.001, one-way ANOVA with Dunnett's post hoc test. (C) Reactivity of CIDP blood is significantly higher when compared to the biotinylated protein pE$_{3\text{-}17}$, as well as against Streptavidin, biotin and BSA alone and when compared to uncoated test plates *** p<0.001, one-way ANOVA with Dunnett's post hoc test. (D) No significant differences are observed in total IgG levels from randomly selected UZH patients, as well as SLE, CIDP and APS1, 2, 4 patients.

Discussion and Outlook

I have successfully established an enzyme-linked immunosorbent assay (ELISA) to detect anti-PrP^C autoantibodies in human blood. Herein, recombinantly expressed, site-specificy biotinylated hPrP-AT_{biotin} is immobilized via Streptavidin to microwell test plates (*Figure* 43B), as antigens directly absorbed to polystyrene plates are more prone to denaturation (Kim and Herr 2013). Humanized versions of the monoclonal anti-PrP^C antibodies POM1 and POM2 served as positive controls (*Figure* 43A). Importantly, the assay was able to detect all human IgG_{1-4} isoforms (*Figure* 45).

Genetic prion diseases (gPrD) are rare, neurodegenerative diseases that rely on the autosomal-dominant inheritance of mutations in the ORF of the PrP^C coding gene *PRNP* probably le. Although gPrD patients carry a mutated version of PrP^C throughout their lifetime, they usually become clinically manifest at a later age, indicative of protective factors (Takada and Geschwind 2013). Anecdotal reports of successfully treated cases of gPrD and other prion diseases have been published. However, randomized, controlled, double-blind clinical trials of patients with prion disease have hitherto failed to yield therapeutic compounds (Geschwind et al. 2013; Geschwind 2014). It has recently been found that PrP^C-GD antibody-mediated toxicity is exerted through the engagement of PrP^C-FT, as no toxicity was observed in mice expressing a shortened variant of the PrP^C-FT (Sonati et al. 2013). Importantly, blockade of the FT by antibodies is beneficial in three models of prion toxicity, e.g. toxic GD antibodies, prion infection, and mice expressing a toxic PrP variant (Sonati et al. 2013; Herrmann et al. 2015), implicating the FT as the PrP-effector module of neuronal death. But the role of PrP^C in inducing cellular neurotoxicity might not be restricted to prion disease. Several reports have suggested the potential of antibodies against PrP^C to prevent Aβ-mediated toxicity *in vitro* and *in vivo* (Chung et al. 2010; Resenberger et al. 2011; Klyubin et al. 2014).

Importantly, naturally occurring monoclonal antibodies represent novel therapeutic molecules for neurologic disorders such as multiple sclerosis, Parkinson's disease, AD, amyotrophic lateral sclerosis. Naturally occurring antibodies have potentially functional activity

with higher safety profile and are reactive to self-proteins, altered self-components, or foreign antigens. It is postulated that human autoantibodies targeting misfolded pathogenic proteins serve as surveillance molecules to eliminate toxic aggregates before they can elicit a deleterious response (Szabo, Relkin, and Weksler 2008). Such antibodies might neutralize the activity of oligomers and/or facilitate the clearance of deposited aggregates via microglia uptake. A successful example of human-derived antibodies is represented by Aducanumab (currently in phase III clinical trial), targeting a conformation epitope of aggregated Aβ and derived from healthy, aged donors who were cognitively normal (Sevigny et al. 2016). At early phases of clinical trial is HIgM22, targeting myelin and oligodendrocytes and promoting central nervous system repair in animal studies (Wootla et al. 2015).

In this study, I have established a workflow from screening the blood from gPrD patients to bait-gated, single-cell sorting of cognate memory B-cells that I plan to use for sequence extraction and production of endogenous, affinity-maturated antibodies (*Figure* 48). Unfortunately, I was not able to detect any differences in anti-PrP^{C} autoantibody titers between gPrD patients and *PRNP*^{WT} family members. Furthermore, no significant association was found between gender, clinically silent or manifest gPrD patients or over time. Of note, gPrD patients exhibited decreased anti-PrP^{C} autoantibody titers than did their *PRNP*^{WT} counterparts independent of age – suggesting a gPrD-specific effect rather than age-dependent immunosencesce. In rodent models of gPrD, mutated prion protein forms birefringent amyloid and proteinase K resistant PrP^{Sc} (Hsiao et al. 1994). One could speculate that anti-PrP^{C} autoantibodies in gPrD patients bind to pathologically aggregated PrP^{Sc} preventing neurological symptoms to occur. Over time, the immune system is overwhelmed by the amount of PrP^{Sc} produced and patients become symptomatic.

It will be interesting to find out whether gPrD and control patients target different epitopes of PrP^{C}. As disease-causing mutations predominantly occur in PrP^{C}-GD, one might speculate that these mutations lead to generation of “neo”-epitopes that cause autoimmunity. Furthermore, I am planning to test the blood of gPrD patients for autoantibodies against aggregated forms of PrP^{C} (Swietnicki et al. 2000). In a last step, one could think of testing the

patient's autoreactivity against recombinant, human, mutated prion protein, although the biosafety implications are rather worrisome.

In the second part of this chapter, I have begun to investigate the possibility of disease-causing, anti-PrP^C autoantibodies in CIDP patients. CIDP is a rare, chronic neuropathy of uncertain etiology (Hanewinckel, Ikram, and Van Doorn 2016). Antibodies against a plethora of nodal and paranodal proteins have been suggested to be involved in CIDP pathogenesis, such as neurofascin 140 and 155, contactin-1 and contactin-associated protein 1, although the disease still lacks trackable biomarkers (Delmont et al. 2017). In my investigations, CIDP patients showed strong responses against native and biotinylated PrP^C, in addition, anti-PrP^C autoantibody titers were significantly higher than those in the "acute" form of CIDP, i.e., Guillain-Barré syndrome as well as other chronic inflammatory states such as sepsis and the monogenic autoimmune disease APS (*Figure* 53A+B). The CIDP signal was specific to PrP^C as CIDP blood reacted significantly less to a fragment of pyroglutamylated Aβ (pE_{3-17}), the anti-pE_{3-17} reactivity was only slightly higher than the IgG immuneresponse against streptavidin, biotin and BSA alone (*Figure* 53C). SLE patients share pathogenic pathways with CIDP patients, such as a dysregulated complement system (Quast et al. 2016). In my assay, the anti-PrP^C autoantibody titers of SLE were similar to those of CIDP patients (*Figure* 53B). Although not significant, probably due to the low number of patients tested, IgG levels were around 30% higher in SLE patients (*Figure* 53D) possibly leading to an overall higher anti-IgG reactivity.

Rigorous studies in *Prnp*$^{0/0}$ mice of different genetic backgrounds have established a chronic demyelinating polyneuropathy to represent a true phenotype of animals lacking PrP^C. After several months, *Prnp*$^{0/0}$ animals develop characteristic walking disturbances that manifest in typical demyelinating changes in peripheral nerves, such as macrophage invasion, breakdown of myelin proteins (Bremer et al. 2010). These changes were not caused by neuron-specific, but Schwann cell-specific knock-out of PrP^C suggesting a receptor in need of PrP^C or fragment thereof to exert pro-myelinating functions (Bremer et al. 2010). Recently, the G-protein coupled receptor Adgrg6/GPR126 has been demonstrated to depend on functional

PrP^C signaling to maintain myelin integrity (Kuffer et al. 2016). PrP^C is binding through its N-terminal polybasic stretch KKRPKPG to GPR126, in fact, a 27 aa, the KKRPKPG-containing PrP_{23-50} fragment was sufficient to induce cAMP responses via GPR126 in zebrafish (Kuffer et al. 2016).

What is the possible pathogenic mechanism of anti-PrP^C autoantibodies in CIDP patients? In human blood, PrP^C is most abundantly found in the plasma fraction (MacGregor et al. 1999) and – independent of the organ - subjected to α- (at aa 110/111) and β-cleavage (at the C-terminus of PrP^C-OR) yielding PrP^C-FT fragments accessible to GPR126-mediated, pro-myelinating signaling. One might speculate that an increased prevalence of anti-PrP^C autoantibodies, preferably to N-terminus of PrP^C, could sequester pro-myelinating signals resulting in a functional *Prnp*$^{0/0}$. If this were true, systemic administration of PrP_{23-50} would provide an immediate treatment option for CIDP patients.

To strengthen my hypothesis, I plan to perform epitope mapping on CIDP autoantibodies by ELISA using truncated PrP^C fragments, amongst others PrP^C-FT and PrP^C-GD. Further experiment such as competition of autoantibody reactivity by addition of recombinant prion protein to blood samples and cell-based assays are planned to validate the presence of anti-PrP^C autoantibodies in CIDP patients. Blood from a second CIDP patient cohort is needed to cross-validate my findings. Although the CIDP samples investigated here come from different centers across France, possible confounders in sample preparation could lead to a sampling bias. Lastly, I believe the gold standard to verify the presence of anti-PrP^C autoantibodies in CIDP patients is their cloning from cognate memory B-cells as presented in *Figure* 48, purification and subsequent injection into rodents in order to elicit a CIDP-like syndrome.

Materials and Methods

Animals and PCR genotyping

Prnp$^{0/0}$ (ZH1) and *Tga*20$^{+/+}$ mice were generated on a mixed 129Sv/Bl6 background, *Prnp*$^{0/0}$ (ZH3) mice were generated on a pure C57BL/6J background (Aller et al. 2003; Büeler et al. 1992; Fischer et al. 1996; Nuvolone et al. 2016). F1 generation animals were used for further ex Embryos for injection of *thy1* driven YFP expression were obtained from matings between (C57BL6/J and CBA) F1 hybrids and transgenic founders were backcrossed to C57BL6/J mice resulting in the YFP16 mouse line (Feng et al. 2000). A 2-primer PCR was used to genotype the YFP allele (primers oIMR1258 and oIMR1260, see appendix a)). All animal studies were performed in accordance with local ethics guidelines and with permission by the responsible institutional animal care committee, namely the Animal Welfare Committee of the Canton of Zurich (permit numbers 200/2007, 41/2012, 90/2013 and ZH040/2015).

Animal survival study, inoculation of prions and scFvPOM1-treated brain tissue

Prion inoculations were performed under isofluorane anesthesia and, mice were monitored every other day after prion inoculations. Scrapie was diagnosed when ataxia, limb weakness, front leg paresis or rolling were observable and mice were subsequently euthanized by CO_2 inhalation. At necropsy, brains were halved either snap-frozen in liquid N_2 or fixed in 4% formalin. The time elapsed from prion inoculation to the terminal stage of disease was defined as incubation time for the survival study. All brain and COCS homogenates were diluted in 0.32 M sucrose in demineralized water before inoculation. 3 months-old *tga20* mice were inoculated in the right frontal lobe at 1% (36 µg protein in 30 µL, corresponding to 3 x 10^6 LD_{50} units, *high dose*) and 0.0001% (3.6 ng protein per animal, corresponding to 3 x 10^2 LD_{50} units, *low dose*) of RML6 homogenate, and 1% (18 µg protein in 30 µL) of COCS homogenate. The protein concentrations in brain homogenates used for inoculation are in agreement with

previously reported protein concentrations of infectious and non-infectious brain homogenates (Basu et al. 2007). No unexpected deaths were observed during the animal experiments reported.

Antibodies

POM monoclonal antibodies were created as described in (Polymenidou et al. 2008). Single-chain variable fragment antibodies of POMs were created through purification of inclusion bodies from *E. coli* on a Ni-NTA column as reported in (Sonati et al. 2013). Fab_2POM fragments were generated through pepsin digestion and purified on a protein A column as described in (Sonati et al. 2013). Purified, mutagenized scFvPOM1 antibodies were generously provided by Luca Varani (Institute of Biomecial Research, Bellinzona).

For creation of humanized POM1 and POM2 antibodies (hPOM1 and hPOM2), murine variable light chains were ordered as *gBlocks* (IDT) gene fragments and PCR amplified using Q5 high-fidelity DNA polymerase (New England Biolabs) according to the manufacturer's guidelines prior to restriction enzyme digestion. Variable + constant heavy chains were ordered in *EcoRV* cloning sites in pUC57-Kan expression vectors (Genscript, see sequences below). Heavy and light chain gene blocks included a Kozak initiation sequence and a IL-2 signal peptipe for efficient secretion. Gene blocks of the heavy chain were modified by inclusion of a L234A and L235A mutation ("LALA") in the constant heavy region 2 and contained a C-terminal 6xHis-Tag. PCR-amplified products were excised from agarose gels and double digested with the restriction enzymes *AgeI* and *BsiWI* (variable light chain) and *EcoRV* and *MscI* (heavy chain). For antibody expression, digested light and heavy chain vectors were inserted into the corresponding restriction sites of pFUSE2.CLIg-hK (light chain) and pFUSE2.CHIg-hG1 (heavy chain, both Invivogen) yielding the plasmids pFUSE2.CLIg-hK.POM1, pFUSE2.CLIg-hK.POM2, pFUSE2.CHIg-hG1.POM1 and pFUSE2.CHIg-hG1.POM2. Prior to insertion of the heavy chain gene block, a site-directed mutagenesis was performed at the $MscI_{2594}$ restriction cleavage site of pFUSE2.CHIg-hG1 using QuikChange II Site-Directed Mutagenesis Kit (Agilent) with primers MscI(2594)-fwd and MscI(2594)-rev (see appendix a)) according to the

manufacturer's guidelines. HEK293(*Prnp*$^{0/0}$) monolayer cells were transfected using Lipofectamine 2000 (Invitrogen) in plain OptiMEM medium (Invitrogen) with the corresponding immunoglobulin light and heavy chain expression plasmids at a ratio of light:heavy=3:2 according to the manufacturer's guidelines. Medium was changed 24 h after transfection to standard culture medium. 48 h after transfection, pFUSE2 transfected cells were selected using 5 µg/ml Blasticidin (Invitrogen) and 50 µg/ml Zeocin (Invitrogen). Prior to medium collection for antibody purification, FBS in culture medium was exchanged by Ultra-low IgG FBS and Ultra-low IgG FBS content in culture medium was sequentially decreased to 0% with every medium change (i.e. 10 % -> 5 % -> 1 % -> 0 %). HEK293(*Prnp*$^{0/0}$) supernatants were stored at -20°C until purification. Affinity chromatography was performed on protein G resin using ÄKTA protein purification system ÄKTAprime (GE Life Sciences), antibody elution was undertaken using 0.2 M glycine, pH=2.7. Antibody eluates were pooled and protein concentration was determined using bicinchoninic acid assay (Pierce). Purity of antibodies was determined using SDS-PAGE gel stained with InstaBlue^{TM} Ultrafast Protein Stain (Sigma-Aldrich) and SilverXpress Silver Staining Kit (Thermo Fisher Scientific) according to the manufacturer's guidelines. For detection of correct human IgG-Fc expression, 50 ng of purified antibody were loaded on SDS-PAGE in the presence and in the absence of 200 mM Dithiothreitol (DTT) and blotted onto a nitrocellulose membrane. Human IgG-Fc was detected by a goat anti-human IgG Fcγ-specific HRP-conjugated polyclonal anti-IgG antibody (1:4'000, Jackson ImmunoResearch).

Cell lines and generation of stable cell lines

The human embryonic kidney cell line HEK293 was purchased by ATCC. The HEK293 *PRNP*$^{0/0}$ cell line clone #H1 was generously provided by Mario Hermann. The CAD5 cell line is a prion-susceptible subclone (Mahal et al. 2007) of Cath.a-differentiated cells (Qi et al. 1997) and was generously provided by Charles Weissmann.

For CRISPR/Cas9-aided generation of CAD5 knock-out cells, mouse *Prnp* sgRNA was designed using the web-based tools http://crispr.mit.edu/ and

http://zifit.partners.org/ZiFiT/CSquare9GetOligos.aspx (last access on May 15th 2017). The sgRNA expression plasmid MLM3636 was a gift from Keith Joung (Addgene plasmid # 43860, www.addgene.org). For annealing of single-stranded DNA oligomers of sgRNA (Oligo4 F and Oligo4 R, sequences are listed in appendix a)) for subsequent cloning into the MLM3636 plasmid the following ligation reaction was prepared: 10 µl Oligo4 F [100 µM], 10 µl Oligo4 R [100 µM], 10 µL of NEB Buffer 2.1 (New England Biolabs), 70 µl ddH_2O. Reaction mix was heated for 4 min at 95°C on a heating block ThermoStat (Eppendorf), then the heating block was turned off and the reaction was allowed to proceed for 30 min on the block and was then put at 4°C. Golden Gate assembly (Engler, Kandzia, and Marillonnet 2008) was used in order to clone the double-stranded DNA Oligomers into the MLM3636 plasmid, using the following reaction:

amount	*name*
150 ng	MLM3636 plasmid
1 µl	double-stranded oligomer ligation mix
2 µl	NEB T4 ligase buffer (New England Biolabs)
13.25 µl	ddH_2O
1 µl	Esp3I (New England Biolabs)
1 µl	T4 ligase (New England Biolabs)

This reaction was put on a thermocycler using the following conditions:

temperature	*duration*	*cycles*
37°C	5 min	10 x
16°C	10 min	
37°C	15 min	
80°C	5 min	

The ligated plasmid MLM3636(sgRNA$_{m\textit{Prnp}}$) was subsequently transformed into DH5α chemically competent *E. coli* cells (Invitrogen) and plasmid purification was undertaken using Plasmid Maxi Kit (Qiagen). CAD5 cells were co-transfected using the MLM3636(sgRNA$_{m\textit{Prnp}}$) plasmid and the hCas9 plasmid (hCas9 was a gift from George Church, Addgene plasmid # 41815, (Mali et al. 2013)) dissolved in Lipofectamine 2000 (Invitrogen). After selection of transfected cells with Geneticin (Invitrogen), single colonies were picked and expanded. For sequencing, DNA was extracted from cells using DNeasy Blood & Tissue Kit (Qiagen). PCR amplification with Q5 high-fidelity DNA polymerase was undertaken using the primers Prn-ko F1 and P10 rev. After PCR clean-up using NucleoSpin Gel and PCR Clean-up kit (Macherey-Nagel), blunt-end PCR fragments were cloned into Zero Blunt TOPO PCR Cloning Kit (Thermo Fisher Scientific) and Sanger Sequencing (Microsynth) was performed to identify mutated *Prnp* sequences. Western Blot and ELISA was undertaken to confirm *Prnp*$^{0/0}$ as described below. Unless mentioned otherwise, clone #C12 was used for all experiments.

Generation of stably transfected CAD5 cells with the murine *Prnp* mutants R207A, Q211E and R207C-I138C was done based on CAD5 *Prnp*$^{0/0}$ cells (clone #C12). The pcDNA3.1(+) plasmid harboring *Prnp* (pcDNA3.1-*Prnp*$_{WT}$) between the *EcoRI* and *XhoI* restriction sites was a gift from Valeria Eckhardt. Generation of PrP$_{R207A}$, PrP$_{Q211E}$ and PrP$_{R207C\text{-}I138C}$ was undertaken using one-step (R207A, Q211E) or two-step (R207C-I138C) site-directed mutagenesis with the QuikChange II Site-Directed Mutagenesis Kit (Agilent) according to the manufacturer's guidelines. Empty and *Prnp*-expressing pcDNA3.1(+) plasmid variants were transfected into CAD5 *Prnp*$^{0/0}$ using Lipofectamine 2000 (Invitrogen) according to the manufacturer's guidelines. Cells were selected with 0.5 mg/ml of Geneticin (Invitrogen) for at least 14 days prior to experiments.

pCAG.SypI-hPrP-IRES-GFP was a gift from Vijay Chandrasekar, pCAG.DsRed was a gift from Connie Cepko (Addgene plasmid # 11151, (Matsuda and Cepko 2004)). Prior to transfection, pCAG.SypI-hPrP-IRES-GFP and pCAG.DsRed were linearized by AgeI restriction enzyme digestion (New England Biolabs). Transfection into HEK293 cells was performed using linearized pCAG.SypI-hPrP-IRES-GFP and pCAG.DsRed plasmids mixed with Lipofectamine

2000. Selection of brightest GFP- or DsRed-expressing cells, respectively, was undertaken by operator-based sorts on a FACSAria III 5L (BD Biosciences) at the Flow Cytometry Facility at the University of Zurich.

HEK293 cells were maintained in DMEM/F12 medium (Invitrogen) with 10% fetal bovine serum (Invitrogen), 1% GlutaMAX (Invitrogen) and 1% Penicillin/Streptomycin (Invitrogen). CAD5 cells were maintained in OptiMEM, phenol-red free medium (Invitrogen) with 10% fetal bovine serum (Invitrogen), 1% GlutaMAX (Invitrogen) and 1% Penicillin/Streptomycin (Invitrogen). Cell lines were kept in a standard cell incubator (37°C, 5% CO_2, 95% humidity) and the culture medium was exchanged three times weekly.

Chemicals

All chemicals were purchased from Sigma-Aldrich unless stated otherwise. All DNA oligonucleotides were synthesized by Microsynth.

Enzyme-linked immunosorbent assay (ELISA)

ELISAs were performed in multi-well plates, namely 384-well Spectraplates HB (Perkin Elmer). For the detection of non-avidin linked, directly absorbed proteins, 1 µg of protein was dissolved per 1 ml of PBS and 20 µl of the PBS-protein solution was coated per well at 4°C overnight. Plates were washed three times in in PBS + 0.1% Tween-20 (0.1% PBS-T) and 80 µl per well of 5% skim milk (Migros) in 0.1% PBS-T was added to block nonspecific reactivity. After 2 h incubation at room temperature, blocking solution was discarded and blood samples were added usually at 1:100 starting dilutions (or as stated) in 1% skim milk in 0.1% PBS-T and incubated for 1.5 h at 37°C. Plates were washed five times and secondary anti-human IgG antibody (goat anti-human IgG Fcγ-specific HRP-conjugated polyclonal anti-IgG antibody (1:4'000, Jackson ImmunoResearch)) or anti-mouse IgG antibody (polyclonal HRP-conjugated goat anti-mouse IgG (1:4'000, Jackson ImmunoResearch)) and incubated for 1 h at room temperature. Plates were washed again 3 times in 0.1% PBS-T and 20 µl of the chromogenic HRP substrate 3,3', 5,5;-tetramethylbenzidine (TMB, Life Technologies) was added in each

well, after 5 minutes of incubation at room temperature, chromogenic reaction was stopped by addition of 20 µl of 0.5 M H_2SO_4 and absorbance was read at λ=450 nm on a EnVision plate reader (Perkin Elmer). When coupling proteins through a biotin-avidin linker, 20 µl of the avidin-based protein was absorbed per plate well at 1 µg per 1 ml of PBS overnight at 4°C. The plate was washed three times with 0.1% PBS-T and blocked for 1 hour with 5% TopBlock (Fluka) in 0.1% PBS-T at room temperature. The biotinylated protein was added in molar excess dissolved in 0.1% PBS-T and incubated for 1 h at room temperature. The plate was washed three times in 0.1% PBS-T, further blocking with skim milk and addition of samples and antibodies was undertaken as described above.

For measuring PrP^C levels from cell and OCS lysates, 384-well Spectraplates HB were coated with 400 ng/ml POM1 (or POM19) in PBS at 4°C overnight. Plates were washed three times in 0.1% PBS-T and blocked with 80 µl per well of 5% skim milk in 0.1% PBS-T for 1.5 h at room temperature. Blocking buffer was discarded and samples and controls were added dissolved in 1% skim milk in 0.1% PBS-T for 1 h at 37°C. 2-fold dilutions of $_{rmPrP23-230}$, starting at a dilution of 100 ng/ml in 1% skim milk in 0.1% PBS-T were used as calibration curve. Biotinylated POM2 (or biotinylated POM3) was used to detect PrP^C (200 ng/ml in 1% skim milk in 0.1% PBS-T), biotinylated antibody was detected with Streptavidin-HRP (1:1'000 in 1% skim milk in 0.1% PBS-T BD Biosciences). Chromogenic reaction and reading of plates was performed as described above. Unknown PrP^C concentrations were interpolated from the linear range of the calibration curve.

The Human IgG ELISA Kit (Abcam, ab100547) was used to measure whole IgG levels in human blood.

Fluorescence-activated cell sorting

Cell monolayers were detached by scraping in 1 mM EDTA in PBS and spun down for 5 min at 800 x g. Cells were washed twice in FACS buffer (PBS with 3% FBS and 1 mM EDTA), counted and resuspended at concentrations of at least $1x10^6$ cells per 100 µl. The following primary antibodies were added for 30 min at 4°C in the dark: PE-conjugated monoclonal

mouse anti-human CD19 clone HIB19 (BD Biosciences), PerCP-Cy™5.5-conjugated monoclonal mouse anti-human IgD clone IA6-2 (BD Biosciences). When creating tetramers of BrilliantViolet421-Streptavidin (BV421-SA, BD Biosciences) with biotinylated human PrP-Avitag ($hPrP\text{-}AT_{biotin}$), a ratio of 1:4 of BV421-SA:$hPrP\text{-}AT_{biotin}$ was mixed at room temperature for 1 h. Tetramer solution was spun down at 23'000 x g for 10 min, and 0.35 µg of complex were added per reaction for 30 min at 4°C. Viable cells were visualized by incubating cells with Live/Dead® near-IR dead cell stain kit (Thermo Fisher Scientific). Cells were washed twice in FACS buffer for 5 min at 800 x g. FACS was performed using LSR II Fortessa (BD Biosciences).

Immunohistochemistry and NeuN morphometry

Organotypic slices were washed twice in PBS and fixed in 4% formalin for at least 2 days at 4°C. Membrane inserts were washed and incubated for 1 h in blocking buffer (0.05% vol/vol Triton X-100 and 3% vol/vol goat serum dissolved in PBS) and incubated with primary antibodies diluted in blocking buffer at 4°C for 3 d. Primary antibodies used were as follows: Alexa-488-conjugated mouse anti-neuronal nuclei (NeuN) monoclonal antibody clone A60 (1.6 µg/ml, Millipore), polyclonal rabbit anti-GFAP (1:1'000, DAKO), rat anti-mouse F4/80 clone CI:A3-1 (1:1'000, Bio-Rad). Fluorescent detection of primary antibodies was undertaken using Alexa-conjugated secondary antibodies and counterstained with 4,6-diamidino-2-phenylindole (DAPI, 1 mg/ml) or Hoechst 33342 (H33342, 10 µg/ml). For NeuN morphometry, images were recorded at 10x magnification on a fluorescence microscope (BX-61, Olympus) equipped with a cooled black&white CCD camera. NeuN images were acquired at identical exposure times, and the area of immunoreactivity was determined by morphometry with image analysis software analySIS v5.0 (Soft Imaging System) using identical grey-scale threshold settings for identifying positive pixels.

Glass bottom µ-slide chamber slides (Ibidi) were used to image cell monolayers. For staining of membranal epitopes, cells were washed twice in PBS and fixed with 4% formalin for 30 min at room temperature. For staining of intracellular epitopes, cells were washed twice in PBS

and fixed in ice-cold acetone for 30 min. Cells were again washed twice and blocked for 1 h at room temperature with 10% goat serum (DAKO) and 5% bovine serum albumin (BSA) in PBS. Blocking buffer was discarded and anti-PrP mouse monoclonal POM primary antibodies were added at 1:1'000 in PBS overnight at 4°C diluted in PBS with 1% BSA. Cells were washed twice in PBS and fluorescent Alexa-conjugated secondary antibodies were added at 1:1'000 in PBS with 1% BSA and incubated for 1 h at room temperature. Cells were washed twice in PBS and nuclei were counterstained with DAPI (1mg/ml) in PBS for 5 minutes at room temperature. Imaging of cells was done after another two washes in PBS.

For live imaging of HEK *PRNP*$^{0/0}$ cells transfected with pCAG.SypI-hPrP-IRES-GFP (HEK$_{PrP\text{-}GFP}$) and HEK *PRNP*$^{0/0}$ cells transfected with pCAG.DsRed (HEK-*Prnp*$^{0/0}{}_{DsRed}$), cells were plated in 1:1 ratio and human plasma was diluted 1:50 into OptiMEM (Invitrogen). Cells were incubated for 30 min at 37°C, 5% CO_2 for with OptiMEM-plasma and then washed three times in PBS. Cells were fixed using 4% formalin for 30 min and washed twice with PBS. Blocking, secondary antibodies and counterstainings were performed as described above.

For immunohistochemistry of mice brains, prion-inoculated, formalin-fixed tissues were incubated in concentrated formic acid to inactivate prions, following by embedding in paraffin, sectioning of paraffin tissue (2 µm) and staining with hematoxylin and eosin (H&E). Deparaffinized sections were stained with primary antibodies as follows: polyclonal rabbit anti-GFAP (1:300; DAKO), rabbit anti-Iba1 (1:1'000; Wako), monoclonal mouse anti-PrP^{Sc} clone SAF-84 (1:200; SPI bio). Sections were developed with IVIEW DAB Detection kit (Ventana) and were then counterstained with hematoxylin as described. Representative images were acquired using the digital camera UC30 (Olympus).

In vitro bioassay

In vitro assessment of prion propagation was performed with subclones of the murine neuroblastoma cell line CAD5 as described before (Enari, Flechsig, and Weissmann 2001). Herein, the cells were exposed to 0.001% RML6 (12 ng in 1 mL), 0.001% non-infectious brain homogenate (NBH, 11 ng in 1 mL) and 0.001% scFvPOM1- or scFvPOM1+recPrP$_{23\text{-}230}$ COCS

homogenate (6 ng in 1 mL). Prions were allowed to propagate for 3 days followed by a 1:7 split, with three further 3-day growth periods and 1:7 splits. Cells were harvested, lysed in PBS with 1% Triton-X 100, phosSTOP™ Phosphatase Inhibitor Cocktail (Roche), cOmplete™ Mini Protease Inhibitor Cocktail (Roche).

Live-imaging based neuronal cell quantification

Z-stacks were recorded in Δz steps as indicated and automated stitching was performed by LAS AF (Leica) or Fv10i-LIV (Olympus) software. Merged YFP$^+$ CA1 z-stacks were imported into IMARIS software (Bitplane) for quantification of absolute YFP-positive hippocampal CA1 pyramidal neuron number. IMARIS *Spots* function with automatically determined black&white thresholds was used for automated neuron cell detection with subsequent manual adjustment for falsely labeled neurons. Correlation of blinded semi-automated counting through 2 readers in untreated YFP16 HOCS yielded a Pearson's r=0.91 (n=6, 95% CI 0.38 - 0.99, p=0.01). YFP$^+$ slices were randomly assigned to treatment groups; absolute cell numbers between treatment groups did not differ at baseline and are expressed as percentage of baseline counts per slice. Colocalization of YFP/NeuN double stained neurons on immunohistochemistry was determined using Colocalization Threshold for ImageJ.

Live-imaging confocal microscopy

PTFE-membranes with attached OCS were excised and placed in a glass bottom petri dish (MatTek) with 1.5 mL of organotypic slice culture medium. Live-imaging of fluorescently labeled OCS for quantification of hippocampal CA1 pyramidal neurons or CGL neurons was undertaken using a Fluoview Fv10i CLSM (Olympus) using a 10x dry objective (NA 0.4) at 2x optical zoom or a SP5 confocal microscopy (Leica) using a 10x dry objective (NA 0.4 at 1.7x optical zoom. Laser intensities were kept constant across treatment groups during imaging.

Patients and blood samples

Ethics approval for patient studies was given by the local institutional review board (IRB), e.g. the Cantonal Ethics Committee of Zurich (KEK-ZH). These patients gave blood during their hospital stay at the University Hospital Zurich (UHZ) for diagnostic purposes (application number KEK-ZH 2015-0561). For genetic prion disease (gPrD), CIDP and APECED patients, IRB approval was given to further re-use their biological specimen obtained by external collaborators (application number KEK-ZH 2015-0514). For gPrD, CIDP and APECED patients, all participants have signed an informed consent according to their local jurisdiction and local IRB approvals are in place, where applicable.

In the UHZ patient cohort, blood was tested only from patients who signed an informed consent for secondary use of diagnostic specimen for research purposes ("Generalkonsent 2.0"). Physical interventions on UHZ patients were only performed during routine diagnostics and no additional blood was drawn for the purpose of this study. For gPrD, APECED and CIDP patients, phlebotomies were performed by qualified medical personnel (medical doctors, nurses) according to their local jurisdiction. No physical interventions were performed on Swiss gPrD patients (blood from one Swiss gPrD patient is included and IRB approval for this patient was given under the application number KEK-ZH 2015-0561).

Pharmacological treatment of OCS

Antibody treatment was initiated 10-14 days after dissection of OCS and was re-added with every medium change. Under live-imaging conditions, treatments were initiated and/or re-added after imaging with every medium change. When combined with recPrP, antibodies were pre-incubated at 4°C for 1 hour with recPrP before administration.

Preparation of organotypic slice cultures

400 µm thick HOCS were prepared from 5-7 day-old pups and 350 µm thick COCS were prepared from 9-12 day-old pups according to previously published protocols (Stoppini, Buchs,

and Muller 1991; Falsig and Aguzzi 2008). Herein, animals were decapitated and the brains were immediately transferred into ice-cold Geys balanced salt solution (i.e. NaCl [137 mM], KCl [5 mM], Na_2HPO_4 [0.845 mM], $CaCl_2 \cdot 2H_2O$ [1.5 mM], KH_2PO_4 [0.66 mM], $MgSO_4 \cdot 7H_2O$ [0.28 mM], $MgCl_2 \cdot 6H2O$ [1.0 mM] and $NaHCO_3$ [2.7 mM]) with 33.33 mM glucose and 1 mM of the glutamate receptor antagonist kynurenic acid. The activation of the Thy1.2 expression cassette in neural tissue exhibits diverse variations depending amongst others on age, region and cell type (Porrero et al. 2010). Hence, only fluorescent brains were dissected for slices cultures despite the appearance of an YFP-allele on genotyping. Usually, 4-6 HOCS and 6-9 COCS were plated per PTFE-coated cell culture insert (Millipore) in organotypic slice culture medium. Cultures were kept in a standard cell incubator (37°C, 5% CO_2, 95% humidity). OCS culture medium was exchanged three times weekly.

PRNP genotyping

PRNP genotyping from gPrD patients was performed using a modified version of the DNeasy Blood & Tissue Kit (Qiagen). 20 µl of PK (600 mAU/ml) and 200 µl of guanidine hydrochloride (GdnHCl) with 1% Triton-X100 at pH=5.0 were added to 200 µl of anticoagualted blood, vortexed thoroughly and incubated for 24 h at room temperature. 200 µl EtOH (96-100%) were added to the reaction and the rest of the DNA purification was performed according to the manufacturer's guidelines. The primer pair *PRNP*_up and *PRNP*_low (see also *appendix a*)) was used in combination with Q5 high-fidelity DNA polymerase to amplify the open reading frame from exon 2 of *PRNP*. Sanger sequencing was performed at the Department of Molecular Pathology (Institute of Surgical Pathology, University Hospital Zurich). Sequencing traces were aligned to reference DNA from the Reference Sequence (RefSeq) Database (O'Leary et al. 2016) using CLC Main Workbench (Qiagen).

Recombinant proteins

Bacterial expression of mouse and human recPrP and fragments thereof was performed as described in (Zahn, von Schroetter, and Wuthrich 1997; Hornemann et al. 2009; Sonati et al.

2013; Kuffer et al. 2016). For generation of hPrP-AT$_{biotin}$, a synthetic gene fragment (*gBlock*, IDT, see sequence in *appendix b*)) was designed harboring a N-terminal 6xHistidine-Tag followed by full-length human PrP$_{23-231}$ linked by a GSGS-linker to the Avitag®-coding sequence (GLNDIFEAQKIEWHE, (Fairhead and Howarth 2015)). The hPrP-AT gene fragment was PCR amplified (primers hPrP-ATgbl_5' and hPrP-ATgbl_5', see also *appendix a*)) and DNA was excised and purified from the agarose gel using NucleoSpin Gel and PCR Clean-up kit (Macherey-Nagel). Cloning of hPrP-AT *gBlock* was done into the *BamHI* and *EcoRI* sites of a modified pREST-A-mini-T vector described in (Sonati et al. 2013) yielding pRSET-A-mini-T.hPrP-AT. The plasmid pBirAcm (Avidity) containing the biotin ligase birA was used for *in vivo* biotinylation of hPrP-AT. Lysogeny broth (LB) agar containing 50 µg/ml Carbenicillin and 30 µg/ml Chloramphenicol were plated with BL21 DE3 pLySs chemically competent E. coli *(Invitrogen)* co-transfected with pRSET-A-mini-T.hPrP-AT and pBirAcm and incubated overnight at 37°C. A single colony was picked and grown at 37°C overnight in LB liquid medium ("pre-culture") containing 50 µg/ml Carbenicillin and 30 µg/ml Chloramphenicol. For protein expression, the pre-culture was diluted 1:20 in 2xYT medium (16 g Tryptone, 10 g Yeast, 5 g NaCl dissolved in 1 l ddH_2O) supplemented with 50 µg/ml Carbenicillin, 30 µg/ml Chloramphenicol and 50 mM D-biotin and incubated at 25°C. When the optical density at λ=600 nm (OD_{600}) reached 0.6 - 1.0, 1 mM of Isopropyl-β-D-thiogalactopyranosid (IPTG), and the cells were grown overnight at 25°C. For expression tests, cells were subsequently spun down at 23'000 x g for 5 min and 1 ml of cell equivalents of OD_{600}=0.8 was lysed in NuPAGE LDS Sample Buffer (Thermo Fisher) in the presence and absence of 200 mM DTT. For large-scale protein purification, hPrP-AT$_{biotin}$ was purified on a Ni-Nitrilotriacetic acid (Ni-NTA) column as already described (Hornemann et al. 2009; Zahn, von Schroetter, and Wuthrich 1997). Purified protein was visualized using SDS-PAGE gels stained with InstaBlue (Sigma) and correct biotinylation was tested in Western Blot using Streptavidin-HRP (Abcam).

Custom peptide synthesis of PrP fragments PrP$_{106-126}^{A117V}$ (KTNMKHMAGAA**V**AGAVVGGLG) and PrP$_{106-126}^{scrambled}$ (NGAKALMGGHGATKVMVGAAA) was performed by EZbiolabs.

Statistical analyses

Statistical tests were performed as indicated and computed by GraphPad Prism 7 (GraphPad). GraphPad Prism 7, SPSS (IBM) and MATLAB (MathWorks) were used for data visualization. For statistical determination of differences in variance, an F-test of equality of variances was used. All data are given as mean ± S.D. unless stated otherwise.

Three-dimensional neuron modeling and computation of time-lapse neuronal loss

All computations from live-imaging derived data were performed using SPSS (IBM) and custom-written scripts in MATLAB (MathWorks). For three-dimensional visualization of neurons, x/y/z coordinates of YFP-positive CA1 pyramidal neurons were exported from IMARIS *Spots* and visualized using the *plot3*-function for MATLAB. The same neuronal three-dimensional point clouds were used for slice-based calculations of cell-to-encompassing YFP-positive volume ratios through application of a convex hull function (i.e. the *convhull*-function in MATLAB), where each neuron of a YFP^+-slice is assigned a coefficient that is eventually used to compute a weighted average of all neuronal coefficients in three-dimensional space. For re-construction of time-lapse neuronal loss, I chose 9 putatively suitable curve estimation models with one regression coefficient (*Table 1*). Relative quality of estimated models was calculated using Akaike's Information Criteria (AIC) corrected for finite sample sizes (AICc):

$$AIC = n * \ln(RSS / n) + 2k$$

$$AICc = AIC + \frac{2k(k+1)}{n-k-1}$$

where n = number of data points, RSS = residual sum of squares, k = number of parameters in the statistical model.

The best candidate model was chosen by its smallest difference in AICc values when compared to other AICc values, Δ_i:

$$\Delta_i = AICc_i - \min AICc$$

where $AICc_i$ is AICc for model i and $\min AICc$ is the minimum AIC value of all models.

Western blot

OCS were washed twice in PBS and scraped off the membrane using sterile PBS per slice, spun down at 1'000 x g for 5 min, followed by homogenization in lysis buffer (0.5% Triton-X 100, phosSTOP™ Phosphatase Inhibitor Cocktail (Roche), cOmplete™ Mini Protease Inhibitor Cocktail (Roche) in PBS) using the TissueLyser LT (Qiagen) at 50 Hz for 2 min. For PNGaseF digestion, 20 µg of samples were processed using a commercially available kit (New England Biolabs). Protein concentration of samples was determined using a bicinchoninic acid assay (Pierce Biotechnology). For determination of PrP^{Sc}, cell homogenates were digested with 5 µg/mL, *Tga20* COCS and C57BL/6 whole brain homogenates were digested with 25 µg/mL Proteinase K (Roche) at a final volume of 20 µL in PBS for 30 minutes at 37°C. *Tga20* whole brain homogenates were digested with 50 µg/mL PK at a final volume of 20 µL in PBS for 45 minutes at 37°C. Loading buffer was added and samples were boiled at 95°C for 5 minutes to deactivate PK. Western blotting was performed using the monoclonal anti-PrP antibody POM1 as described before (Herrmann et al. 2015). For SDS-PAGE analysis, protein samples from OCS homogenates (10-20 µg per lane) were diluted in 20 µL of PBS and were separated using a 12% Bis-Tris polyacrylamide gel or for higher molecular weight proteins on a 4–12% gradient gel (NuPAGE, Invitrogen) with subsequent blotting onto a nitrocellulose membrane. Membranes were blocked with 5% wt/vol Top-Block (Fluka) in Tris-buffered saline supplemented with Tween (150 mM NaCl, 10 mM Tris HCl, 0.05% Tween 20 (vol/vol)) for 30 minutes and incubated with primary antibodies in 1% Top-Block. Primary antibodies used were as follows: mouse monoclonal IgG_1 raised against PrP^C POM1 (400 ng/ml, see (Polymenidou et al. 2008)), monoclonal rabbit anti-ATF4 clone D4B8 (1:1'000, Cell Signalling Technologies), monoclonal rabbit anti-CHOP clone D46F1 (1:1'000, Cell Signalling Technologies), monoclonal mouse anti-gp91[phox] (833 ng/ml, BD Biosciences), polyclonal rabbit anti-NeuN (1:1'000, Abcam), monoclonal mouse anti-actin clone C4 (1:10'000, Chemicon), mouse monoclonal anti-GAPDH clone 6C5 (200 ng/ml, Millipore). Secondary antibodies used were

horseradish peroxidase (HRP)-conjugated goat anti-rabbit IgG (1:10’000, Chemicon) and HRP-conjugated goat anti-mouse IgG (1:10’000, Jackson ImmunoResearch). Blots were developed using Luminata Crescendo Western HRP substrate (Millipore) and visualized using the Stella chemilumniscence detection system (Raytest). Protein levels were normalized to actin and/or GAPDH as loading control and analyzed semi-quantitatively using the QuantityONE software (Bio-Rad).

Appendix

a) Primer DNA and sgRNA sequences

Name (forward/reverse)	**Sequence 5' -> 3'**
Genotyping of YFP16 animals	
oIMR1258 (forward)	TCT GAG TGG CAA AGG ACC TTA GG
oIMR1260 (reverse)	CGC TGA ACT TGT GGC CGT TTA CG
Creation of CAD5 Prnp$^{0/0}$	
sgRNA	TCA GTC ATC ATG GCG AAC CT
Oligo 4 F (forward)	ACA CCG CAG TCA TCA TGG CGA ACC TG
Oligo 4 R (reverse)	AAA ACA GGT TCG CCA TGA TGA CTG CG
Prn-ko F1 (forward)	TGC AGG TGA CTT TCT GCA TTC TGG
P10 rev (reverse)	GCT GGG CTT GTT CCA CTG ATT ATG GGT AC
MscI$_{2594}$ restriction enzyme site mutagenesis of pFUSE2.CH-Ig1	
MscI(2594)-fwd (forward)	CGG CAC TGG TCA ACT TCG CCA TGA TGG CTC CTC C
MscI(2594)-rev (reverse)	GGA GGA GCC ATC ATG GCG AAG TTG ACC AGT GCC G
PCR amplification of hPOM1- and hPOM2-variable chain gene blocks	
POM1 variable light (forward)	ATA TAA CCG GTG CCA CCA TGT ACA GGA
POM1 variable light (reverse)	TAT ATC GTA CGA CGT TTC AGC TCT AGC TTG GT
POM2 variable light (forward)	ATA TAA CCG GTG CCA CCA TGT ACA GGA T

POM2 variable light (reverse)	TAT ATC GTA CGT TTG ATT TCC AGC TTG GTA CCT CC
Generation of hPrP-AT$_{biotin}$	
hPrP-ATgbl_5' (forward)	ATA TAT GGA TCC AAG AAA CGC CCT AAA C
hPrP-ATgbl_3' (reverse)	ATA TAT GAA TTC TCA TTA TTC ATG CCA CTC GA

b) Gene blocks DNA sequences

Name	Sequence 5' -> 3'
hPOM1	
Variable light chain	ACCGGTGCCACCATGTACAGGATGCAACTCCTGTCTTGCATTGC ACTAAGTCTTGCACTTGTCACGAATTCGGATATTGTGCTGACCCA ATCTCCAGCCATCCTGTCTGTGAGTCCAGGAGAAAGAGTCAGTTT CTCCTGCAGGGCCAGTCAGAACATTGGCACAAGCATACACTGGT ATCAGCAAAGAACAAATGAATCTCCAAGGCTTATCATAAAGTATG CTTCTGAGTCTATCTCTGGGATCCCTTCCAGGTTTAGTGGCAGTG GATCAGGGACAGATTTTACTCTTAGCATCAACAGTGTGGAGTCTG AAGATATTGCAGATTATTACTGTCAACAAAGTAATACCTGGCCGT ACACGTTCGGAGGGGGGACCAAGCTAGAGCTGAAACGTCGTAC G
Variable + constant heavy chain	GATATCGCCACCATGTACAGGATGCAACTCCTGTCTTGCATTGCA CTAAGTCTTGCACTTGTCACGAATTCGCAGGTCCAGCTCCAGCAA TCTGGGACTGAGCTTGTGATGCCTGGGGCTTCAGTGAAGATGTC CTGCAAGGCTTCTGGCTACACATTCACTGACTACTGGATGCACTG GGTGAAGCAGAGGCCTGGACAAGGCCTTGAGTGGATCGGATCG ATTGATCCTTCTGATAGTTATACTAGTCACAATGAAAAGTTCAAGG GCAAGGCCACATTGACTGTAGACGAATCCTCCAGCACAGCCTAC ATGCAGCTCAGCAGCCTGACATCTGAGGACTCTGCGGTCTATTT CTGTTCAAGATCCGGCTACGGATATTATGCTATGGAGTACTGGG GTCAAGGAACCTCAGTCACCGTCTCCTCGGCTAGCACCAAGGGC CCATCGGTCTTCCCCCTGGCACCCTCCTCCAAGAGCACCTCTGG GGGCACAGCGGCCCTGGGCTGCCTGGTCAAGGACTACTTCCCC GAACCGGTGACGGTGTCGTGGAACTCAGGCGCCCTGACCAGCG

	GCGTGCACACCTTCCCGGCTGTCCTACAGTCCTCAGGACTCTAC TCCCTCAGCAGCGTGGTGACCGTGCCCTCCAGCAGCTTGGGCA CCCAGACCTACATCTGCAACGTGAATCACAAGCCCAGCAACACC AAGGTGGACAAGAAAGTTGAGCCCAAATCTTGTGACAAAACTCAC ACATGCCCACCGTGCCCAGCACCTGAAGCAGCCGGGGGACCGT CAGTCTTCCTCTTCCCCCCAAAACCCAAGGACACCCTCATGATCT CCCGGACCCCTGAGGTCACATGCGTGGTGGTGGACGTGAGCCA CGAAGACCCTGAGGTCAAGTTCAACTGGTACGTGGACGGCGTG GAGGTGCATAATGCCAAGACAAAGCCGCGGGAGGAGCAGTACA ACAGCACGTACCGTGTGGTCAGCGTCCTCACCGTCCTGCACCAG GACTGGCTGAATGGCAAGGAGTACAAGTGCAAGGTCTCCAACAA AGCCCTCCCAGCCCCCATCGAGAAAACCATCTCCAAAGCCAAAG GGCAGCCCCGAGAACCACAGGTGTACACCCTGCCCCCATCCCG GGAGGAGATGACCAAGAACCAGGTCAGCCTGACCTGCCTGGTC AAAGGCTTCTATCCCAGCGACATCGCCGTGGAGTGGGAGAGCAA TGGGCAGCCGGAGAACAACTACAAGACCACGCCTCCCGTGCTG GACTCCGACGGCTCCTTCTTCCTCTACAGCAAGCTCACCGTGGA CAAGAGCAGGTGGCAGCAGGGGAACGTCTTCTCATGCTCCGTGA TGCATGAGGCTCTGCACAACCACTACACGCAGAAGAGCCTCTCC CTGTCTCCGGGTAAACATCACCATCACCATCACTGATGGCCA
hPOM2	
Variable light chain	ACCGGTGCCACCATGTACAGGATGCAACTCCTGTCTTGCATTGC ACTAAGTCTTGCACTTGTCACGAATTCGGATATTGTGATGACACA GTCTCACAAATTCATGTCCACTTCAGTAGGAGACAGGGTCAGCAT CACCTGCAAGGCCAGTCAGGATGTGGGTACTGCTCTAGCCTGGT ATCAACAGAAACCAGGGCAATCTCCTAAACTACTGATTTACTGGG CATCCACCCGGCACACTGGAGTCCCTGATCGCTTCACAGGCAGT GGATCTGGGACAGATTTCACTCTCACCATTAGCAATGTGCAGTCT GAAGACTTGTCAGATTATTTCTGTCAGCAATATAGCAGCTATCCG ACGTTCGGTGGAGGTACCAAGCTGGAAATCAAACGTACG
Variable + constant heavy chain	GATATCGCCACCATGTACAGGATGCAACTCCTGTCTTGCATTGCA CTAAGTCTTGCACTTGTCACGAATTCGGAGGTAAAGCTTCAGGAG TCTGGAGGTGAGGTGGTAAGGCCTGGGACTTCAGTGAAGGTGTC CTGCAAGGCTTCTGGATATGCCTTCACTAATTACTTAATAGAGTG GGTAAAGCAGAGGCCTGGACAGGGCCTTGAGTGGATTGGAGTG ATTAATCCTGGAAGTGGTGATACTAACTACAATGAGAAGTTCAAG GGCAAGGCAACACTGACTGCAGACAAGTCCTCCAGCACTGCCTA

	TATGCAGCTCAACAGCCTGACATCTGATGACTCTGCGGTCTATTT CTGTGCAAGATCAGGGGTAGCTGCCCCTTATTACTATGCTATGGA CTACTGGGGTCAAGGAACCTCAGTCACCGTCTCCTCGGCTAGCA CCAAGGGCCCATCGGTCTTCCCCCTGGCACCCTCCTCCAAGAGC ACCTCTGGGGGCACAGCGGCCCTGGGCTGCCTGGTCAAGGACT ACTTCCCCGAACCGGTGACGGTGTCGTGGAACTCAGGCGCCCT GACCAGCGGCGTGCACACCTTCCCGGCTGTCCTACAGTCCTCAG GACTCTACTCCCTCAGCAGCGTGGTGACCGTGCCCTCCAGCAGC TTGGGCACCCAGACCTACATCTGCAACGTGAATCACAAGCCCAG CAACACCAAGGTGGACAAGAAAGTTGAGCCCAAATCTTGTGACA AAACTCACACATGCCCACCGTGCCCAGCACCTGAAGCAGCCGG GGGACCGTCAGTCTTCCTCTTCCCCCCAAAACCCAAGGACACCC TCATGATCTCCCGGACCCCTGAGGTCACATGCGTGGTGGTGGAC GTGAGCCACGAAGACCCTGAGGTCAAGTTCAACTGGTACGTGGA CGGCGTGGAGGTGCATAATGCCAAGACAAAGCCGCGGGAGGAG CAGTACAACAGCACGTACCGTGTGGTCAGCGTCCTCACCGTCCT GCACCAGGACTGGCTGAATGGCAAGGAGTACAAGTGCAAGGTCT CCAACAAAGCCCTCCCAGCCCCCATCGAGAAAACCATCTCCAAA GCCAAAGGGCAGCCCCGAGAACCACAGGTGTACACCCTGCCCC CATCCCGGGAGGAGATGACCAAGAACCAGGTCAGCCTGACCTG CCTGGTCAAAGGCTTCTATCCCAGCGACATCGCCGTGGAGTGGG AGAGCAATGGGCAGCCGGAGAACAACTACAAGACCACGCCTCC CGTGCTGGACTCCGACGGCTCCTTCTTCCTCTACAGCAAGCTCA CCGTGGACAAGAGCAGGTGGCAGCAGGGGAACGTCTTCTCATG CTCCGTGATGCATGAGGCTCTGCACAACCACTACACGCAGAAGA GCCTCTCCCTGTCTCCGGGTAAACATCACCATCACCATCACTGAT GGCCA
Generation of hPrP-AT$_{biotin}$	
hPrP-AT	ATATATGGATCCAAGAAACGCCCTAAACCGGGAGGGTGGAATAC AGGTGGTAGCCGTTACCCCGGGCAAGGAAGCCCGGGGGGTAAT CGTTACCCTCCTCAAGGCGGGGGTGGATGGGGCCAACCCCATG GCGGGGGTTGGGGCCAGCCGCATGGTGGAGGTTGGGGCCAAC CTCATGGAGGCGGGTGGGGTCAGCCGCACGGAGGAGGCTGGG GGCAGGGAGGCGGCACACACTCCCAATGGAATAAACCCAGTAA GCCCAAAACCAATATGAAGCATATGGCTGGAGCAGCAGCGGCAG GGGCCGTTGTTGGGGGACTGGGGGGTTATGTTCTTGGATCAGC CATGTCCCGCCCCATCATTCACTTTGGGTCTGATTATGAAGACCG

	CTACTATCGTGAAAATATGCACCGTTACCCCAACCAAGTCTACTA TCGCCCGATGGACGAGTACAGCAATCAGAACAACTTTGTTCACG ACTGCGTGAACATTACAATTAAACAGCACACTGTCACCACTACAA CCAAAGGGGAGAATTTTACCGAAACTGATGTCAAGATGATGGAG CGTGTCGTGGAACAGATGTGCATCACTCAATATGAGCGTGAATC CCAAGCATATTACAAACGTGGTAGCGGTTCGGGCAGTGGTCTGA ACGACATCTTCGAGGCCCAGAAAATCGAGTGGCATGAATAATGA GAATTCATATAT

References

Aguzzi, A., B. A. Barres, and M. L. Bennett. 2013. 'Microglia: scapegoat, saboteur, or something else?', *Science*, 339: 156-61.

Aguzzi, A., F. Baumann, and J. Bremer. 2008. 'The prion's elusive reason for being', *Annu Rev Neurosci*, 31: 439-77.

Aguzzi, A., and J. Falsig. 2012. 'Prion propagation, toxicity and degradation', *Nat Neurosci*, 15: 936-9.

Aguzzi, A., and F. L. Heppner. 2000. 'Pathogenesis of prion diseases: a progress report', *Cell Death Differ*, 7: 889-902.

Aguzzi, A., and C. Weissmann. 1997. 'Prion research: the next frontiers', *Nature*, 389: 795-8.

Aller, M.I., A. Jones, D. Merlo, M. Paterlini, A.H. Meyer, U. Amtmann, S. Brickley, H.E. Jolin, A.N. McKenzie, H. Monyer, M. Farrant, and W. Wisden. 2003. 'Cerebellar granule cell Cre recombinase expression', *Genesis*, 36: 97-103.

Alper, T., W. A. Cramp, D. A. Haig, and M. C. Clarke. 1967. 'Does the agent of scrapie replicate without nucleic acid?', *Nature*, 214: 764-6.

Antonyuk, S. V., C. R. Trevitt, R. W. Strange, G. S. Jackson, D. Sangar, M. Batchelor, S. Cooper, C. Fraser, S. Jones, T. Georgiou, A. Khalili-Shirazi, A. R. Clarke, S. S. Hasnain, and J. Collinge. 2009. 'Crystal structure of human prion protein bound to a therapeutic antibody', *Proc Natl Acad Sci U S A*, 106: 2554-8.

Arosio, P., M. Vendruscolo, C. M. Dobson, and T. P. Knowles. 2014. 'Chemical kinetics for drug discovery to combat protein aggregation diseases', *Trends Pharmacol Sci*, 35: 127-35.

Ashe, K. H., and A. Aguzzi. 2013. 'Prions, prionoids and pathogenic proteins in Alzheimer disease', *Prion*, 7: 55-9.

Atarashi, R., K. Sano, K. Satoh, and N. Nishida. 2011. 'Real-time quaking-induced conversion: a highly sensitive assay for prion detection', *Prion*, 5: 150-3.

Ayrolles-Torro, A., T. Imberdis, J. Torrent, K. Toupet, I. V. Baskakov, G. Poncet-Montange, C. Gregoire, F. Roquet-Baneres, S. Lehmann, D. Rognan, M. Pugniere, J. M. Verdier, and V. Perrier. 2011. 'Oligomeric-induced activity by thienyl pyrimidine compounds traps prion infectivity', *J Neurosci*, 31: 14882-92.

Baral, P. K., B. Wieland, M. Swayampakula, M. Polymenidou, M. H. Rahman, N. N. Kav, A. Aguzzi, and M. N. James. 2012. 'Structural studies on the folded domain of the human prion protein bound to the Fab fragment of the antibody POM1', *Acta Crystallogr D Biol Crystallogr*, 68: 1501-12.

Basu, S., M. L. Mohan, X. Luo, B. Kundu, Q. Kong, and N. Singh. 2007. 'Modulation of proteinase K-resistant prion protein in cells and infectious brain homogenate by redox iron: implications for prion replication and disease pathogenesis', *Mol Biol Cell*, 18: 3302-12.

Beck, E., P. M. Daniel, W. B. Matthews, D. L. Stevens, M. P. Alpers, D. M. Asher, D. C. Gajdusek, and C. J. Gibbs, Jr. 1969. 'Creutzfeldt-Jakob disease. The neuropathology of a transmission experiment', *Brain*, 92: 699-716.

Berry, D. B., D. Lu, M. Geva, J. C. Watts, S. Bhardwaj, A. Oehler, A. R. Renslo, S. J. DeArmond, S. B. Prusiner, and K. Giles. 2013. 'Drug resistance confounding prion therapeutics', *Proc Natl Acad Sci U S A*, 110: E4160-9.

Bittner, T., S. Burgold, M. M. Dorostkar, M. Fuhrmann, B. M. Wegenast-Braun, B. Schmidt, H. Kretzschmar, and J. Herms. 2012. 'Amyloid plaque formation precedes dendritic spine loss', *Acta Neuropathol*, 124: 797-807.

Blattler, T., S. Brandner, A. J. Raeber, M. A. Klein, T. Voigtlander, C. Weissmann, and A. Aguzzi. 1997. 'PrP-expressing tissue required for transfer of scrapie infectivity from spleen to brain', *Nature*, 389: 69-73.

Bolton, D. C., M. P. McKinley, and S. B. Prusiner. 1982. 'Identification of a protein that purifies with the scrapie prion', *Science*, 218: 1309-11.

Brandner, S., S. Isenmann, A. Raeber, M. Fischer, A. Sailer, Y. Kobayashi, S. Marino, C. Weissmann, and A. Aguzzi. 1996. 'Normal host prion protein necessary for scrapie-induced neurotoxicity', *Nature*, 379: 339-43.

Bredesen, D. E., R. V. Rao, and P. Mehlen. 2006. 'Cell death in the nervous system', *Nature*, 443: 796-802.
Bremer, J., F. Baumann, C. Tiberi, C. Wessig, H. Fischer, P. Schwarz, A. D. Steele, K. V. Toyka, K. A. Nave, J. Weis, and A. Aguzzi. 2010. 'Axonal prion protein is required for peripheral myelin maintenance', *Nat Neurosci*, 13: 310-8.
Brown, P., and R. Bradley. 1998. '1755 and all that: a historical primer of transmissible spongiform encephalopathy', *BMJ*, 317: 1688-92.
Bueler, H., A. Aguzzi, A. Sailer, R. A. Greiner, P. Autenried, M. Aguet, and C. Weissmann. 1993. 'Mice devoid of PrP are resistant to scrapie', *Cell*, 73: 1339-47.
Büeler, H.R., M. Fischer, Y. Lang, H. Bluethmann, H.P. Lipp, S.J. DeArmond, S.B. Prusiner, M. Aguet, and C. Weissmann. 1992. 'Normal development and behaviour of mice lacking the neuronal cell-surface PrP protein', *Nature*, 356: 577-82.
Busche, M. A., G. Eichhoff, H. Adelsberger, D. Abramowski, K. H. Wiederhold, C. Haass, M. Staufenbiel, A. Konnerth, and O. Garaschuk. 2008. 'Clusters of hyperactive neurons near amyloid plaques in a mouse model of Alzheimer's disease', *Science*, 321: 1686-9.
Caspi, S., M. Halimi, A. Yanai, S. B. Sasson, A. Taraboulos, and R. Gabizon. 1998. 'The anti-prion activity of Congo red. Putative mechanism', *J Biol Chem*, 273: 3484-9.
Chesebro, B., R. Race, K. Wehrly, J. Nishio, M. Bloom, D. Lechner, S. Bergstrom, K. Robbins, L. Mayer, J. M. Keith, and et al. 1985. 'Identification of scrapie prion protein-specific mRNA in scrapie-infected and uninfected brain', *Nature*, 315: 331-3.
Chung, E., Y. Ji, Y. Sun, R. J. Kascsak, R. B. Kascsak, P. D. Mehta, S. M. Strittmatter, and T. Wisniewski. 2010. 'Anti-PrPC monoclonal antibody infusion as a novel treatment for cognitive deficits in an Alzheimer's disease model mouse', *BMC Neurosci*, 11: 130.
Cohen, S. I., M. Vendruscolo, C. M. Dobson, and T. P. Knowles. 2012. 'From macroscopic measurements to microscopic mechanisms of protein aggregation', *J Mol Biol*, 421: 160-71.
Collinge, J., and A. R. Clarke. 2007. 'A general model of prion strains and their pathogenicity', *Science*, 318: 930-6.
Creutzfeldt, H.G. 1920. 'Über eine eigenartige herdförmige Erkrankung des Zentralnervensystems (vorläufige Mitteilung)', *Zeitschrift für die gesamte Neurologie und Psychiatrie*, 57: 1-18.
Crick, F. 1970. 'Central dogma of molecular biology', *Nature*, 227: 561-3.
Cuillé, J., and P.L. Chelle. 1936. 'La maladie dite “tremblante” du mouton; est-elle inoculable?', *Comptes Rendus de l'Académie des Sciences*, 203.
Delmont, E., C. Manso, L. Querol, A. Cortese, A. Berardinelli, A. Lozza, M. Belghazi, P. Malissart, P. Labauge, G. Taieb, N. Yuki, I. Illa, S. Attarian, and J. J. Devaux. 2017. 'Autoantibodies to nodal isoforms of neurofascin in chronic inflammatory demyelinating polyneuropathy', *Brain*.
Enari, M., E. Flechsig, and C. Weissmann. 2001. 'Scrapie prion protein accumulation by scrapie-infected neuroblastoma cells abrogated by exposure to a prion protein antibody', *Proc Natl Acad Sci U S A*, 98: 9295-9.
Engler, C., R. Kandzia, and S. Marillonnet. 2008. 'A one pot, one step, precision cloning method with high throughput capability', *PLoS One*, 3: e3647.
Ertmer, A., S. Gilch, S. W. Yun, E. Flechsig, B. Klebl, M. Stein-Gerlach, M. A. Klein, and H. M. Schatzl. 2004. 'The tyrosine kinase inhibitor STI571 induces cellular clearance of PrPSc in prion-infected cells', *J Biol Chem*, 279: 41918-27.
Fairhead, M., and M. Howarth. 2015. 'Site-specific biotinylation of purified proteins using BirA', *Methods Mol Biol*, 1266: 171-84.
Falsig, J., and A. Aguzzi. 2008. 'The prion organotypic slice culture assay--POSCA', *Nat Protoc*, 3: 555-62.
Falsig, J., C. Julius, I. Margalith, P. Schwarz, F. L. Heppner, and A. Aguzzi. 2008a. 'A versatile prion replication assay in organotypic brain slices', *Nat Neurosci*, 11: 109-17.
Falsig, J., C. Julius, I. Margalith, P. Schwarz, FL. Heppner, and A. Aguzzi. 2008b. 'A versatile prion replication assay in organotypic brain slices', *Nat Neurosci*, 11: 109-17.

Falsig, J., T. Sonati, U. S. Herrmann, D. Saban, B. Li, K. Arroyo, B. Ballmer, P. P. Liberski, and A. Aguzzi. 2012. 'Prion pathogenesis is faithfully reproduced in cerebellar organotypic slice cultures', *PLoS Pathog*, 8: e1002985.
Fang, C., T. Imberdis, M. C. Garza, H. Wille, and D. A. Harris. 2016. 'A Neuronal Culture System to Detect Prion Synaptotoxicity', *PLoS Pathog*, 12: e1005623.
Feng, G., R. H. Mellor, M. Bernstein, C. Keller-Peck, Q. T. Nguyen, M. Wallace, J. M. Nerbonne, J. W. Lichtman, and J. R. Sanes. 2000. 'Imaging neuronal subsets in transgenic mice expressing multiple spectral variants of GFP', *Neuron*, 28: 41-51.
Feraudet, C., N. Morel, S. Simon, H. Volland, Y. Frobert, C. Creminon, D. Vilette, S. Lehmann, and J. Grassi. 2005. 'Screening of 145 anti-PrP monoclonal antibodies for their capacity to inhibit PrPSc replication in infected cells', *J Biol Chem*, 280: 11247-58.
Fischer, M., T. Rülicke, A. Raeber, A. Sailer, M. Moser, B. Oesch, S. Brandner, A. Aguzzi, and C. Weissmann. 1996. 'Prion protein (PrP) with amino-proximal deletions restoring susceptibility of PrP knockout mice to scrapie', *EMBO J*, 15: 1255-64.
Fraenkel-Conrat, H., and R. C. Williams. 1955. 'Reconstitution of Active Tobacco Mosaic Virus from Its Inactive Protein and Nucleic Acid Components', *Proc Natl Acad Sci U S A*, 41: 690-8.
Frontzek, K., R. Moos, E. Schaper, L. Jann, G. Herfs, D. R. Zimmermann, A. Aguzzi, and H. Budka. 2015. 'Iatrogenic and sporadic Creutzfeldt-Jakob disease in 2 sisters without mutation in the prion protein gene', *Prion*, 9: 444-8.
Fuhrmann, M., G. Mitteregger, H. Kretzschmar, and J. Herms. 2007. 'Dendritic pathology in prion disease starts at the synaptic spine', *J Neurosci*, 27: 6224-33.
Gabizon, R., M. P. McKinley, D. Groth, and S. B. Prusiner. 1988. 'Immunoaffinity purification and neutralization of scrapie prion infectivity', *Proc Natl Acad Sci U S A*, 85: 6617-21.
Gajdusek, D. C., C. J. Gibbs, and M. Alpers. 1966. 'Experimental transmission of a Kuru-like syndrome to chimpanzees', *Nature*, 209: 794-6.
Gajdusek, D. C., and V. Zigas. 1957. 'Degenerative disease of the central nervous system in New Guinea; the endemic occurrence of kuru in the native population', *N Engl J Med*, 257: 974-8.
Gerlai, R. 1996. 'Gene-targeting studies of mammalian behavior: is it the mutation or the background genotype?', *Trends Neurosci*, 19: 177-81.
Geschwind, M. D. 2014. 'Doxycycline for Creutzfeldt-Jakob disease: a failure, but a step in the right direction', *Lancet Neurol*, 13: 130-2.
Geschwind, M. D., A. L. Kuo, K. S. Wong, A. Haman, G. Devereux, B. J. Raudabaugh, D. Y. Johnson, C. C. Torres-Chae, R. Finley, P. Garcia, J. N. Thai, H. Q. Cheng, J. M. Neuhaus, S. A. Forner, J. L. Duncan, K. L. Possin, S. J. Dearmond, S. B. Prusiner, and B. L. Miller. 2013. 'Quinacrine treatment trial for sporadic Creutzfeldt-Jakob disease', *Neurology*, 81: 2015-23.
Gibbs, C. J., Jr., D. C. Gajdusek, D. M. Asher, M. P. Alpers, E. Beck, P. M. Daniel, and W. B. Matthews. 1968. 'Creutzfeldt-Jakob disease (spongiform encephalopathy): transmission to the chimpanzee', *Science*, 161: 388-9.
Giordano, G., S. Hong, E. M. Faustman, and L. G. Costa. 2011. 'Measurements of cell death in neuronal and glial cells', *Methods Mol Biol*, 758: 171-8.
Goni, F., E. Knudsen, F. Schreiber, H. Scholtzova, J. Pankiewicz, R. Carp, H. C. Meeker, R. Rubenstein, D. R. Brown, M. S. Sy, J. A. Chabalgoity, E. M. Sigurdsson, and T. Wisniewski. 2005. 'Mucosal vaccination delays or prevents prion infection via an oral route', *Neuroscience*, 133: 413-21.
Gordon, W. S. 1946. 'Advances in veterinary research', *Vet Rec*, 58: 516-25.
Griffith, J. S. 1967. 'Self-replication and scrapie', *Nature*, 215: 1043-4.
Hanewinckel, R., M. A. Ikram, and P. A. Van Doorn. 2016. 'Peripheral neuropathies', *Handb Clin Neurol*, 138: 263-82.
Hayday, A., Krohn, K., Ranki, A., Peterson, P., Kisand, K., Stuart, E., Macagno, A. 2013. "Method of isolating human antibodies." In.

Head, M. W., H. M. Yull, D. L. Ritchie, J. P. Langeveld, N. A. Fletcher, R. S. Knight, and J. W. Ironside. 2013. 'Variably protease-sensitive prionopathy in the UK: a retrospective review 1991-2008', *Brain*, 136: 1102-15.
Heikenwalder, M., M. O. Kurrer, I. Margalith, J. Kranich, N. Zeller, J. Haybaeck, M. Polymenidou, M. Matter, J. Bremer, W. S. Jackson, S. Lindquist, C. J. Sigurdson, and A. Aguzzi. 2008. 'Lymphotoxin-dependent prion replication in inflammatory stromal cells of granulomas', *Immunity*, 29: 998-1008.
Heppner, F. L., C. Musahl, I. Arrighi, M. A. Klein, T. Rulicke, B. Oesch, R. M. Zinkernagel, U. Kalinke, and A. Aguzzi. 2001. 'Prevention of Scrapie Pathogenesis by Transgenic Expression of Anti-Prion Protein Antibodies', *Science*, 294: 178-82.
Herrmann, U. S., T. Sonati, J. Falsig, R. R. Reimann, P. Dametto, T. O'Connor, B. Li, A. Lau, S. Hornemann, S. Sorce, U. Wagner, D. Sanoudou, and A. Aguzzi. 2015. 'Prion infections and anti-PrP antibodies trigger converging neurotoxic pathways', *PLoS Pathog*, 11: e1004662.
Hessell, A. J., L. Hangartner, M. Hunter, C. E. Havenith, F. J. Beurskens, J. M. Bakker, C. M. Lanigan, G. Landucci, D. N. Forthal, P. W. Parren, P. A. Marx, and D. R. Burton. 2007. 'Fc receptor but not complement binding is important in antibody protection against HIV', *Nature*, 449: 101-4.
Hochgrafe, K., and E. M. Mandelkow. 2013. 'Making the brain glow: in vivo bioluminescence imaging to study neurodegeneration', *Mol Neurobiol*, 47: 868-82.
Hornemann, S., B. Christen, C. von Schroetter, D. R. Perez, and K. Wuthrich. 2009. 'Prion protein library of recombinant constructs for structural biology', *FEBS J*, 276: 2359-67.
Hsiao, K. K., D. Groth, M. Scott, S. L. Yang, H. Serban, D. Rapp, D. Foster, M. Torchia, S. J. Dearmond, and S. B. Prusiner. 1994. 'Serial transmission in rodents of neurodegeneration from transgenic mice expressing mutant prion protein', *Proc Natl Acad Sci U S A*, 91: 9126-30.
Imberdis, T., J. T. Heeres, H. Yueh, C. Fang, J. Zhen, C. B. Rich, M. Glicksman, A. B. Beeler, and D. A. Harris. 2016. 'Identification of Anti-prion Compounds using a Novel Cellular Assay', *J Biol Chem*, 291: 26164-76.
Jakob, A.M. 1921. 'Über eigenartige Erkrankungen des Zentralnervensystems mit bemerkenswertem anatomischen Befunde', *Zeitschrift für die gesamte Neurologie und Psychiatrie*, 64: 147-228.
Jarrett, J. T., and P. T. Lansbury, Jr. 1993. 'Seeding "one-dimensional crystallization" of amyloid: a pathogenic mechanism in Alzheimer's disease and scrapie?', *Cell*, 73: 1055-8.
Jendroska, K., F. P. Heinzel, M. Torchia, L. Stowring, H. A. Kretzschmar, A. Kon, A. Stern, S. B. Prusiner, and S. J. DeArmond. 1991. 'Proteinase-resistant prion protein accumulation in Syrian hamster brain correlates with regional pathology and scrapie infectivity', *Neurology*, 41: 1482-90.
Julius, C., G. Hutter, U. Wagner, H. Seeger, V. Kana, J. Kranich, P. C. Klohn, C. Weissmann, G. Miele, and A. Aguzzi. 2008. 'Transcriptional stability of cultured cells upon prion infection', *J Mol Biol*, 375: 1222-33.
Karapetyan, Y. E., G. F. Sferrazza, M. Zhou, G. Ottenberg, T. Spicer, P. Chase, M. Fallahi, P. Hodder, C. Weissmann, and C. I. Lasmezas. 2013. 'Unique drug screening approach for prion diseases identifies tacrolimus and astemizole as antiprion agents', *Proc Natl Acad Sci U S A*, 110: 7044-9.
Kim, D., and A. E. Herr. 2013. 'Protein immobilization techniques for microfluidic assays', *Biomicrofluidics*, 7: 41501.
Kisand, K., and P. Peterson. 2011. 'Autoimmune polyendocrinopathy candidiasis ectodermal dystrophy: known and novel aspects of the syndrome', *Ann N Y Acad Sci*, 1246: 77-91.
Klein, M. A., P. S. Kaeser, P. Schwarz, H. Weyd, I. Xenarios, R. M. Zinkernagel, M. C. Carroll, J. S. Verbeek, M. Botto, M. J. Walport, H. Molina, U. Kalinke, H. Acha-Orbea, and A. Aguzzi. 2001. 'Complement facilitates early prion pathogenesis', *Nat Med*, 7: 488-92.

Klöhn, P.C., M. Farmer, J.M. Linehan, C. O'Malley, M. Fernandez de Marco, W. Taylor, M. Farrow, A. Khalili-Shirazi, S. Brandner, and J. Collinge. 2012. 'PrP antibodies do not trigger mouse hippocampal neuron apoptosis.', *Science*, 335: 52.
Klyubin, I., A. J. Nicoll, A. Khalili-Shirazi, M. Farmer, S. Canning, A. Mably, J. Linehan, A. Brown, M. Wakeling, S. Brandner, D. M. Walsh, M. J. Rowan, and J. Collinge. 2014. 'Peripheral administration of a humanized anti-PrP antibody blocks Alzheimer's disease Abeta synaptotoxicity', *J Neurosci*, 34: 6140-5.
Knowles, T. P., C. A. Waudby, G. L. Devlin, S. I. Cohen, A. Aguzzi, M. Vendruscolo, E. M. Terentjev, M. E. Welland, and C. M. Dobson. 2009. 'An analytical solution to the kinetics of breakable filament assembly', *Science*, 326: 1533-7.
Korth, C., B. C. May, F. E. Cohen, and S. B. Prusiner. 2001. 'Acridine and phenothiazine derivatives as pharmacotherapeutics for prion disease', *Proc Natl Acad Sci U S A*, 98: 9836-41.
Kovacs, G. G., and H. Budka. 2008. 'Prion diseases: from protein to cell pathology', *Am J Pathol*, 172: 555-65.
———. 2010. 'Distribution of apoptosis-related proteins in sporadic Creutzfeldt-Jakob disease', *Brain Res*, 1323: 192-9.
Kovacs, G. G., P. Gasque, T. Strobel, E. Lindeck-Pozza, M. Strohschneider, J. W. Ironside, H. Budka, and M. Guentchev. 2004. 'Complement activation in human prion disease', *Neurobiol Dis*, 15: 21-8.
Kristiansen, M., P. Deriziotis, D. E. Dimcheff, G. S. Jackson, H. Ovaa, H. Naumann, A. R. Clarke, F. W. van Leeuwen, V. Menendez-Benito, N. P. Dantuma, J. L. Portis, J. Collinge, and S. J. Tabrizi. 2007. 'Disease-associated prion protein oligomers inhibit the 26S proteasome', *Mol Cell*, 26: 175-88.
Kuffer, A., A. K. Lakkaraju, A. Mogha, S. C. Petersen, K. Airich, C. Doucerain, R. Marpakwar, P. Bakirci, A. Senatore, A. Monnard, C. Schiavi, M. Nuvolone, B. Grosshans, S. Hornemann, F. Bassilana, K. R. Monk, and A. Aguzzi. 2016. 'The prion protein is an agonistic ligand of the G protein-coupled receptor Adgrg6', *Nature*, 536: 464-8.
Kurt, T. D., C. Bett, N. Fernandez-Borges, S. Joshi-Barr, S. Hornemann, T. Rulicke, J. Castilla, K. Wuthrich, A. Aguzzi, and C. J. Sigurdson. 2014. 'Prion transmission prevented by modifying the beta2-alpha2 loop structure of host PrPC', *J Neurosci*, 34: 1022-7.
Kuwahara, C., A. M. Takeuchi, T. Nishimura, K. Haraguchi, A. Kubosaki, Y. Matsumoto, K. Saeki, Y. Matsumoto, T. Yokoyama, S. Itohara, and T. Onodera. 1999. 'Prions prevent neuronal cell-line death', *Nature*, 400: 225-6.
Kuwata, K., N. Nishida, T. Matsumoto, Y. O. Kamatari, J. Hosokawa-Muto, K. Kodama, H. K. Nakamura, K. Kimura, M. Kawasaki, Y. Takakura, S. Shirabe, J. Takata, Y. Kataoka, and S. Katamine. 2007. 'Hot spots in prion protein for pathogenic conversion', *Proc Natl Acad Sci U S A*, 104: 11921-6.
Lalancette-Hebert, M., D. Phaneuf, G. Soucy, Y. C. Weng, and J. Kriz. 2009. 'Live imaging of Toll-like receptor 2 response in cerebral ischaemia reveals a role of olfactory bulb microglia as modulators of inflammation', *Brain*, 132: 940-54.
Lawson, V. A., C. L. Haigh, B. Roberts, V. B. Kenche, H. M. Klemm, C. L. Masters, S. J. Collins, K. J. Barnham, and S. C. Drew. 2010. 'Near-infrared fluorescence imaging of apoptotic neuronal cell death in a live animal model of prion disease', *ACS Chem Neurosci*, 1: 720-7.
Le Pichon, C. E., M. T. Valley, M. Polymenidou, A. T. Chesler, B. T. Sagdullaev, A. Aguzzi, and S. Firestein. 2009. 'Olfactory behavior and physiology are disrupted in prion protein knockout mice', *Nat Neurosci*, 12: 60-9.
Leopoldt, J.G. 1759. 'Nützliche und auf die Erfahrung gegründete Einleitung zu der Landwirthschaft: Fünf Theile. Mit Kupfer und Baurissen', *Berlin und Glogau, Günther*.
Li, J., S. Browning, S. P. Mahal, A. M. Oelschlegel, and C. Weissmann. 2010. 'Darwinian evolution of prions in cell culture', *Science*, 327: 869-72.
Llorens, F., I. Lopez-Gonzalez, K. Thune, M. Carmona, S. Zafar, O. Andreoletti, I. Zerr, and I. Ferrer. 2014. 'Subtype and regional-specific neuroinflammation in sporadic creutzfeldt-jakob disease', *Front Aging Neurosci*, 6: 198.

Lu, D., K. Giles, Z. Li, S. Rao, E. Dolghih, J. R. Gever, M. Geva, M. L. Elepano, A. Oehler, C. Bryant, A. R. Renslo, M. P. Jacobson, S. J. Dearmond, B. M. Silber, and S. B. Prusiner. 2013. 'Biaryl amides and hydrazones as therapeutics for prion disease in transgenic mice', *J Pharmacol Exp Ther*, 347: 325-38.

Luk, K. C., V. Kehm, J. Carroll, B. Zhang, P. O'Brien, J. Q. Trojanowski, and V. M. Lee. 2012. 'Pathological alpha-synuclein transmission initiates Parkinson-like neurodegeneration in nontransgenic mice', *Science*, 338: 949-53.

Lyahyai, J., R. Bolea, C. Serrano, E. Monleon, C. Moreno, R. Osta, P. Zaragoza, J. J. Badiola, and I. Martin-Burriel. 2006. 'Correlation between Bax overexpression and prion deposition in medulla oblongata from natural scrapie without evidence of apoptosis', *Acta Neuropathol*, 112: 451-60.

MacGregor, I., J. Hope, G. Barnard, L. Kirby, O. Drummond, D. Pepper, V. Hornsey, R. Barclay, H. Bessos, M. Turner, and C. Prowse. 1999. 'Application of a time-resolved fluoroimmunoassay for the analysis of normal prion protein in human blood and its components', *Vox Sang*, 77: 88-96.

Mahal, S. P., C. A. Baker, C. A. Demczyk, E. W. Smith, C. Julius, and C. Weissmann. 2007. 'Prion strain discrimination in cell culture: the cell panel assay', *Proc Natl Acad Sci U S A*, 104: 20908-13.

Maley, F., R. B. Trimble, A. L. Tarentino, and T. H. Plummer, Jr. 1989. 'Characterization of glycoproteins and their associated oligosaccharides through the use of endoglycosidases', *Anal Biochem*, 180: 195-204.

Mali, P., L. Yang, K. M. Esvelt, J. Aach, M. Guell, J. E. DiCarlo, J. E. Norville, and G. M. Church. 2013. 'RNA-guided human genome engineering via Cas9', *Science*, 339: 823-6.

Mallucci, G., A. Dickinson, J. Linehan, P. C. Klohn, S. Brandner, and J. Collinge. 2003. 'Depleting neuronal PrP in prion infection prevents disease and reverses spongiosis', *Science*, 302: 871-4.

Manson, J. C., A. R. Clarke, M. L. Hooper, L. Aitchison, I. McConnell, and J. Hope. 1994. '129/Ola mice carrying a null mutation in PrP that abolishes mRNA production are developmentally normal', *Mol Neurobiol*, 8: 121-7.

Matsuda, T., and C. L. Cepko. 2004. 'Electroporation and RNA interference in the rodent retina in vivo and in vitro', *Proc Natl Acad Sci U S A*, 101: 16-22.

May, B. C., A. T. Fafarman, S. B. Hong, M. Rogers, L. W. Deady, S. B. Prusiner, and F. E. Cohen. 2003. 'Potent inhibition of scrapie prion replication in cultured cells by bis-acridines', *Proc Natl Acad Sci U S A*, 100: 3416-21.

McKinley, M. P., D. C. Bolton, and S. B. Prusiner. 1983. 'A protease-resistant protein is a structural component of the scrapie prion', *Cell*, 35: 57-62.

Mead, S., J. Uphill, J. Beck, M. Poulter, T. Campbell, J. Lowe, G. Adamson, H. Hummerich, N. Klopp, I. M. Ruckert, H. E. Wichmann, D. Azazi, V. Plagnol, W. H. Pako, J. Whitfield, M. P. Alpers, J. Whittaker, D. J. Balding, I. Zerr, H. Kretzschmar, and J. Collinge. 2012. 'Genome-wide association study in multiple human prion diseases suggests genetic risk factors additional to *PRNP*', *Hum Mol Genet*, 21: 1897-906.

Merz, P. A., R. A. Somerville, H. M. Wisniewski, L. Manuelidis, and E. E. Manuelidis. 1983. 'Scrapie-associated fibrils in Creutzfeldt-Jakob disease', *Nature*, 306: 474-6.

Meyer, S., M. Woodward, C. Hertel, P. Vlaicu, Y. Haque, J. Karner, A. Macagno, S. C. Onuoha, D. Fishman, H. Peterson, K. Metskula, R. Uibo, K. Jantti, K. Hokynar, A. S. Wolff, Apeced patient collaborative, K. Krohn, A. Ranki, P. Peterson, K. Kisand, and A. Hayday. 2016. 'AIRE-Deficient Patients Harbor Unique High-Affinity Disease-Ameliorating Autoantibodies', *Cell*, 166: 582-95.

Meyer-Luehmann, M., J. Coomaraswamy, T. Bolmont, S. Kaeser, C. Schaefer, E. Kilger, A. Neuenschwander, D. Abramowski, P. Frey, A. L. Jaton, J. M. Vigouret, P. Paganetti, D. M. Walsh, P. M. Mathews, J. Ghiso, M. Staufenbiel, L. C. Walker, and M. Jucker. 2006. 'Exogenous induction of cerebral beta-amyloidogenesis is governed by agent and host', *Science*, 313: 1781-4.

Meyer-Luehmann, M., T. L. Spires-Jones, C. Prada, M. Garcia-Alloza, A. de Calignon, A. Rozkalne, J. Koenigsknecht-Talboo, D. M. Holtzman, B. J. Bacskai, and B. T. Hyman.

2008. 'Rapid appearance and local toxicity of amyloid-beta plaques in a mouse model of Alzheimer's disease', *Nature*, 451: 720-4.
Michel, B., A. Ferguson, T. Johnson, H. Bender, C. Meyerett-Reid, B. Pulford, A. von Teichman, D. Seelig, J. H. Weis, G. C. Telling, A. Aguzzi, and M. D. Zabel. 2012. 'Genetic depletion of complement receptors CD21/35 prevents terminal prion disease in a mouse model of chronic wasting disease', *J Immunol*, 189: 4520-7.
Moda, F., C. Vimercati, I. Campagnani, M. Ruggerone, G. Giaccone, M. Morbin, L. Zentilin, M. Giacca, I. Zucca, G. Legname, and F. Tagliavini. 2012. 'Brain delivery of AAV9 expressing an anti-PrP monovalent antibody delays prion disease in mice', *Prion*, 6: 383-90.
Moore, R. C., I. Y. Lee, G. L. Silverman, P. M. Harrison, R. Strome, C. Heinrich, A. Karunaratne, S. H. Pasternak, M. A. Chishti, Y. Liang, P. Mastrangelo, K. Wang, A. F. Smit, S. Katamine, G. A. Carlson, F. E. Cohen, S. B. Prusiner, D. W. Melton, P. Tremblay, L. E. Hood, and D. Westaway. 1999. 'Ataxia in prion protein (PrP)-deficient mice is associated with upregulation of the novel PrP-like protein doppel', *J Mol Biol*, 292: 797-817.
Moreno, J. A., M. Halliday, C. Molloy, H. Radford, N. Verity, J. M. Axten, C. A. Ortori, A. E. Willis, P. M. Fischer, D. A. Barrett, and G. R. Mallucci. 2013. 'Oral treatment targeting the unfolded protein response prevents neurodegeneration and clinical disease in prion-infected mice', *Sci Transl Med*, 5: 206ra138.
Moreno, J. A., H. Radford, D. Peretti, J. R. Steinert, N. Verity, M. G. Martin, M. Halliday, J. Morgan, D. Dinsdale, C. A. Ortori, D. A. Barrett, P. Tsaytler, A. Bertolotti, A. E. Willis, M. Bushell, and G. R. Mallucci. 2012. 'Sustained translational repression by eIF2alpha-P mediates prion neurodegeneration', *Nature*, 485: 507-11.
Morita-Fujimura, Y., M. Fujimura, M. Kawase, K. Murakami, G. W. Kim, and P. H. Chan. 1999. 'Inhibition of interleukin-1beta converting enzyme family proteases (caspases) reduces cold injury-induced brain trauma and DNA fragmentation in mice', *J Cereb Blood Flow Metab*, 19: 634-42.
Negro, A., C. Ballarin, A. Bertoli, M. L. Massimino, and M. C. Sorgato. 2001. 'The metabolism and imaging in live cells of the bovine prion protein in its native form or carrying single amino acid substitutions', *Mol Cell Neurosci*, 17: 521-38.
Nicoll, A. J., C. R. Trevitt, M. H. Tattum, E. Risse, E. Quarterman, A. A. Ibarra, C. Wright, G. S. Jackson, R. B. Sessions, M. Farrow, J. P. Waltho, A. R. Clarke, and J. Collinge. 2010. 'Pharmacological chaperone for the structured domain of human prion protein', *Proc Natl Acad Sci U S A*, 107: 17610-5.
Nussbaum, J. M., S. Schilling, H. Cynis, A. Silva, E. Swanson, T. Wangsanut, K. Tayler, B. Wiltgen, A. Hatami, R. Ronicke, K. Reymann, B. Hutter-Paier, A. Alexandru, W. Jagla, S. Graubner, C. G. Glabe, H. U. Demuth, and G. S. Bloom. 2012. 'Prion-like behaviour and tau-dependent cytotoxicity of pyroglutamylated amyloid-beta', *Nature*, 485: 651-5.
Nuvolone, M., M. Hermann, S. Sorce, G. Russo, C. Tiberi, P. Schwarz, E. Minikel, D. Sanoudou, P. Pelczar, and A. Aguzzi. 2016. 'Strictly co-isogenic C57BL/6J-*Prnp*-/- mice: A rigorous resource for prion science', *J Exp Med*, 213: 313-27.
O'Leary, N. A., M. W. Wright, J. R. Brister, S. Ciufo, D. Haddad, R. McVeigh, B. Rajput, B. Robbertse, B. Smith-White, D. Ako-Adjei, A. Astashyn, A. Badretdin, Y. Bao, O. Blinkova, V. Brover, V. Chetvernin, J. Choi, E. Cox, O. Ermolaeva, C. M. Farrell, T. Goldfarb, T. Gupta, D. Haft, E. Hatcher, W. Hlavina, V. S. Joardar, V. K. Kodali, W. Li, D. Maglott, P. Masterson, K. M. McGarvey, M. R. Murphy, K. O'Neill, S. Pujar, S. H. Rangwala, D. Rausch, L. D. Riddick, C. Schoch, A. Shkeda, S. S. Storz, H. Sun, F. Thibaud-Nissen, I. Tolstoy, R. E. Tully, A. R. Vatsan, C. Wallin, D. Webb, W. Wu, M. J. Landrum, A. Kimchi, T. Tatusova, M. DiCuccio, P. Kitts, T. D. Murphy, and K. D. Pruitt. 2016. 'Reference sequence (RefSeq) database at NCBI: current status, taxonomic expansion, and functional annotation', *Nucleic Acids Res*, 44: D733-45.
Oesch, B., D. Westaway, M. Walchli, M. P. McKinley, S. B. Kent, R. Aebersold, R. A. Barry, P. Tempst, D. B. Teplow, L. E. Hood, and C. Weissmann. 1985. 'A cellular gene encodes scrapie PrP 27-30 protein', *Cell*, 40: 735-46.

Peretz, D., R. A. Williamson, K. Kaneko, J. Vergara, E. Leclerc, G. Schmitt-Ulms, I. R. Mehlhorn, G. Legname, M. R. Wormald, P. M. Rudd, R. A. Dwek, D. R. Burton, and S. B. Prusiner. 2001. 'Antibodies inhibit prion propagation and clear cell cultures of prion infectivity', *Nature*, 412: 739-43.

Perrier, V., J. Solassol, C. Crozet, Y. Frobert, C. Mourton-Gilles, J. Grassi, and S. Lehmann. 2004. 'Anti-PrP antibodies block PrPSc replication in prion-infected cell cultures by accelerating PrPC degradation', *J Neurochem*, 89: 454-63.

Perrier, V., A. C. Wallace, K. Kaneko, J. Safar, S. B. Prusiner, and F. E. Cohen. 2000. 'Mimicking dominant negative inhibition of prion replication through structure-based drug design', *Proc Natl Acad Sci U S A*, 97: 6073-8.

Polymenidou, M., R. Moos, M. Scott, C. Sigurdson, Y. Z. Shi, B. Yajima, I. Hafner-Bratkovic, R. Jerala, S. Hornemann, K. Wuthrich, A. Bellon, M. Vey, G. Garen, M. N. James, N. Kav, and A. Aguzzi. 2008. 'The POM monoclonals: a comprehensive set of antibodies to non-overlapping prion protein epitopes', *PLoS One*, 3: e3872.

Poncet-Montange, G., S. J. St Martin, O. V. Bogatova, S. B. Prusiner, B. K. Shoichet, and S. Ghaemmaghami. 2011. 'A survey of antiprion compounds reveals the prevalence of non-PrP molecular targets', *J Biol Chem*, 286: 27718-28.

Porrero, C., P. Rubio-Garrido, C. Avendano, and F. Clasca. 2010. 'Mapping of fluorescent protein-expressing neurons and axon pathways in adult and developing Thy1-eYFP-H transgenic mice', *Brain Res*, 1345: 59-72.

Prusiner, S. B. 1982. 'Novel proteinaceous infectious particles cause scrapie', *Science*, 216: 136-44.

Prusiner, S. B., M. P. McKinley, K. A. Bowman, D. C. Bolton, P. E. Bendheim, D. F. Groth, and G. G. Glenner. 1983. 'Scrapie prions aggregate to form amyloid-like birefringent rods', *Cell*, 35: 349-58.

Puig, B., and I. Ferrer. 2001. 'Cell death signaling in the cerebellum in Creutzfeldt-Jakob disease', *Acta Neuropathol*, 102: 207-15.

Qi, Y., J. K. Wang, M. McMillian, and D. M. Chikaraishi. 1997. 'Characterization of a CNS cell line, CAD, in which morphological differentiation is initiated by serum deprivation', *J Neurosci*, 17: 1217-25.

Quast, I., C. W. Keller, F. Hiepe, B. Tackenberg, and J. D. Lunemann. 2016. 'Terminal complement activation is increased and associated with disease severity in CIDP', *Ann Clin Transl Neurol*, 3: 730-5.

Radde, R., T. Bolmont, S. A. Kaeser, J. Coomaraswamy, D. Lindau, L. Stoltze, M. E. Calhoun, F. Jaggi, H. Wolburg, S. Gengler, C. Haass, B. Ghetti, C. Czech, C. Holscher, P. M. Mathews, and M. Jucker. 2006. 'Abeta42-driven cerebral amyloidosis in transgenic mice reveals early and robust pathology', *EMBO Rep*, 7: 940-6.

Reimann, R. R., T. Sonati, S. Hornemann, U. S. Herrmann, M. Arand, S. Hawke, and A. Aguzzi. 2016. 'Differential Toxicity of Antibodies to the Prion Protein', *PLoS Pathog*, 12: e1005401.

Rensing, N., Y. Ouyang, X. F. Yang, K. A. Yamada, S. M. Rothman, and M. Wong. 2005. 'In vivo imaging of dendritic spines during electrographic seizures', *Ann Neurol*, 58: 888-98.

Resenberger, U. K., A. Harmeier, A. C. Woerner, J. L. Goodman, V. Muller, R. Krishnan, R. M. Vabulas, H. A. Kretzschmar, S. Lindquist, F. U. Hartl, G. Multhaup, K. F. Winklhofer, and J. Tatzelt. 2011. 'The cellular prion protein mediates neurotoxic signalling of beta-sheet-rich conformers independent of prion replication', *EMBO J*, 30: 2057-70.

Sakaguchi, S., S. Katamine, N. Nishida, R. Moriuchi, K. Shigematsu, T. Sugimoto, A. Nakatani, Y. Kataoka, T. Houtani, S. Shirabe, H. Okada, S. Hasegawa, T. Miyamoto, and T. Noda. 1996. 'Loss of cerebellar Purkinje cells in aged mice homozygous for a disrupted PrP gene', *Nature*, 380: 528-31.

Sanders, D. W., S. K. Kaufman, S. L. DeVos, A. M. Sharma, H. Mirbaha, A. Li, S. J. Barker, A. C. Foley, J. R. Thorpe, L. C. Serpell, T. M. Miller, L. T. Grinberg, W. W. Seeley, and M. I. Diamond. 2014. 'Distinct tau prion strains propagate in cells and mice and define different tauopathies', *Neuron*, 82: 1271-88.

Schatzl, H. M., L. Laszlo, D. M. Holtzman, J. Tatzelt, S. J. DeArmond, R. I. Weiner, W. C. Mobley, and S. B. Prusiner. 1997. 'A hypothalamic neuronal cell line persistently infected with scrapie prions exhibits apoptosis', *J Virol*, 71: 8821-31.
Scheltens, P., K. Blennow, M. M. Breteler, B. de Strooper, G. B. Frisoni, S. Salloway, and W. M. Van der Flier. 2016. 'Alzheimer's disease', *Lancet*, 388: 505-17.
Seifert, M., S. Jahn, J. Schwab, W. Docke, H. D. Volk, and R. von Baehr. 1992. 'Lymphocyte surface marker expression on hybridomas secreting human monoclonal antibodies', *Hum Antibodies Hybridomas*, 3: 86-92.
Senisterra, G. A., and P. J. Finerty, Jr. 2009. 'High throughput methods of assessing protein stability and aggregation', *Mol Biosyst*, 5: 217-23.
Sevigny, J., P. Chiao, T. Bussiere, P. H. Weinreb, L. Williams, M. Maier, R. Dunstan, S. Salloway, T. Chen, Y. Ling, J. O'Gorman, F. Qian, M. Arastu, M. Li, S. Chollate, M. S. Brennan, O. Quintero-Monzon, R. H. Scannevin, H. M. Arnold, T. Engber, K. Rhodes, J. Ferrero, Y. Hang, A. Mikulskis, J. Grimm, C. Hock, R. M. Nitsch, and A. Sandrock. 2016. 'The antibody aducanumab reduces Abeta plaques in Alzheimer's disease', *Nature*, 537: 50-6.
Shmerling, D., I. Hegyi, M. Fischer, T. Blattler, S. Brandner, J. Gotz, T. Rulicke, E. Flechsig, A. Cozzio, C. von Mering, C. Hangartner, A. Aguzzi, and C. Weissmann. 1998. 'Expression of amino-terminally truncated PrP in the mouse leading to ataxia and specific cerebellar lesions', *Cell*, 93: 203-14.
Sigurðsson, B. 1954. 'Rida, a chronic encephalitis of sheep: With general remarks on infections which develop slowly and some of their special characteristics', *British Veterinary Journal*, 110: 341-54.
Silva, A. C., and N. A. Bock. 2008. 'Manganese-enhanced MRI: an exceptional tool in translational neuroimaging', *Schizophr Bull*, 34: 595-604.
Singh, S., and N. Joshi. 2017. 'Astrocytes: inexplicable cells in neurodegeneration', *Int J Neurosci*, 127: 204-09.
Siso, S., B. Puig, R. Varea, E. Vidal, C. Acin, M. Prinz, F. Montrasio, J. Badiola, A. Aguzzi, M. Pumarola, and I. Ferrer. 2002. 'Abnormal synaptic protein expression and cell death in murine scrapie', *Acta Neuropathol*, 103: 615-26.
Solforosi, L., J. R. Criado, D. B. McGavern, S. Wirz, M. Sanchez-Alavez, S. Sugama, L. A. DeGiorgio, B. T. Volpe, E. Wiseman, G. Abalos, E. Masliah, D. Gilden, M. B. Oldstone, B. Conti, and R. A. Williamson. 2004. 'Cross-linking cellular prion protein triggers neuronal apoptosis in vivo', *Science*, 303: 1514-6.
Sonati, T., R. R. Reimann, J. Falsig, P. K. Baral, T. O'Connor, S. Hornemann, S. Yaganoglu, B. Li, U. S. Herrmann, B. Wieland, M. Swayampakula, M. H. Rahman, D. Das, N. Kav, R. Riek, P. P. Liberski, M. N. James, and A. Aguzzi. 2013. 'The toxicity of antiprion antibodies is mediated by the flexible tail of the prion protein
', *Nature*.
Sorce, S., M. Nuvolone, A. Keller, J. Falsig, A. Varol, P. Schwarz, M. Bieri, H. Budka, and A. Aguzzi. 2014. 'The role of the NADPH oxidase NOX2 in prion pathogenesis', *PLoS Pathog*, 10: e1004531.
Steele, A. D., S. Lindquist, and A. Aguzzi. 2007. 'The prion protein knockout mouse: a phenotype under challenge', *Prion*, 1: 83-93.
Stoppini, L., P. A. Buchs, and D. Muller. 1991. 'A simple method for organotypic cultures of nervous tissue', *J Neurosci Methods*, 37: 173-82.
Suzuki, K., S. Hata, Y. Kawabata, and H. Sorimachi. 2004. 'Structure, activation, and biology of calpain', *Diabetes*, 53 Suppl 1: S12-8.
Swietnicki, W., M. Morillas, S. G. Chen, P. Gambetti, and W. K. Surewicz. 2000. 'Aggregation and fibrillization of the recombinant human prion protein huPrP90-231', *Biochemistry*, 39: 424-31.
Sydow, A., A. Van der Jeugd, F. Zheng, T. Ahmed, D. Balschun, O. Petrova, D. Drexler, L. Zhou, G. Rune, E. Mandelkow, R. D'Hooge, C. Alzheimer, and E. M. Mandelkow. 2011. 'Tau-induced defects in synaptic plasticity, learning, and memory are reversible in transgenic mice after switching off the toxic Tau mutant', *J Neurosci*, 31: 2511-25.

Szabo, P., N. Relkin, and M. E. Weksler. 2008. 'Natural human antibodies to amyloid beta peptide', *Autoimmun Rev*, 7: 415-20.
Tada, M., A. Takeuchi, M. Hashizume, K. Kitamura, and M. Kano. 2014. 'A highly sensitive fluorescent indicator dye for calcium imaging of neural activity in vitro and in vivo', *Eur J Neurosci*, 39: 1720-8.
Takada, L. T., and M. D. Geschwind. 2013. 'Prion diseases', *Semin Neurol*, 33: 348-56.
Tamguney, G., K. P. Francis, K. Giles, A. Lemus, S. J. DeArmond, and S. B. Prusiner. 2009. 'Measuring prions by bioluminescence imaging', *Proc Natl Acad Sci U S A*, 106: 15002-6.
Tatzelt, J., N. Maeda, M. Pekny, S. L. Yang, C. Betsholtz, C. Eliasson, J. Cayetano, A. P. Camerino, S. J. DeArmond, and S. B. Prusiner. 1996. 'Scrapie in mice deficient in apolipoprotein E or glial fibrillary acidic protein', *Neurology*, 47: 449-53.
Telling, G. C., M. Scott, J. Mastrianni, R. Gabizon, M. Torchia, F. E. Cohen, S. J. DeArmond, and S. B. Prusiner. 1995. 'Prion propagation in mice expressing human and chimeric PrP transgenes implicates the interaction of cellular PrP with another protein', *Cell*, 83: 79-90.
Wang, K. K. 2000. 'Calpain and caspase: can you tell the difference?', *Trends Neurosci*, 23: 20-6.
Watts, J. C., K. Giles, S. K. Grillo, A. Lemus, S. J. DeArmond, and S. B. Prusiner. 2011. 'Bioluminescence imaging of Abeta deposition in bigenic mouse models of Alzheimer's disease', *Proc Natl Acad Sci U S A*, 108: 2528-33.
Webb, T. E., S. Pal, D. Siddique, D. C. Heaney, J. M. Linehan, J. D. Wadsworth, S. Joiner, J. Beck, S. J. Wroe, V. Stevenson, S. Brandner, S. Mead, and J. Collinge. 2008. 'First report of Creutzfeldt-Jakob disease occurring in 2 siblings unexplained by *PRNP* mutation', *J Neuropathol Exp Neurol*, 67: 838-41.
White, A. R., P. Enever, M. Tayebi, R. Mushens, J. Linehan, S. Brandner, D. Anstee, J. Collinge, and S. Hawke. 2003. 'Monoclonal antibodies inhibit prion replication and delay the development of prion disease', *Nature*, 422: 80-3.
Wijdicks, E. F., and C. J. Klein. 2017. 'Guillain-Barre Syndrome', *Mayo Clin Proc*, 92: 467-79.
Wootla, B., J. O. Watzlawik, A. E. Warrington, N. J. Wittenberg, A. Denic, X. Xu, L. R. Jordan, L. M. Papke, L. J. Zoecklein, M. L. Pierce, S. H. Oh, O. H. Kantarci, and M. Rodriguez. 2015. 'Naturally Occurring Monoclonal Antibodies and Their Therapeutic Potential for Neurologic Diseases', *JAMA Neurol*, 72: 1346-53.
Wu, B., A. J. McDonald, K. Markham, C. B. Rich, K. P. McHugh, J. Tatzelt, D. W. Colby, G. L. Millhauser, and D. A. Harris. 2017. 'The N-terminus of the prion protein is a toxic effector regulated by the C-terminus', *Elife*, 6.
Wulf, M. A., A. Senatore, and A. Aguzzi. 2017. 'The biological function of the cellular prion protein: an update', *BMC Biol*, 15: 34.
Yarden, Y., and Gabi Tarcic. 2013. *Vesicle trafficking in cancer* (Springer: New York).
Yun, S. W., A. Ertmer, E. Flechsig, S. Gilch, P. Riederer, M. Gerlach, H. M. Schatzl, and M. A. Klein. 2007. 'The tyrosine kinase inhibitor imatinib mesylate delays prion neuroinvasion by inhibiting prion propagation in the periphery', *J Neurovirol*, 13: 328-37.
Zahn, R., C. von Schroetter, and K. Wuthrich. 1997. 'Human prion proteins expressed in Escherichia coli and purified by high-affinity column refolding', *FEBS Lett*, 417: 400-4.
Zeng, L. H., L. Xu, N. R. Rensing, P. M. Sinatra, S. M. Rothman, and M. Wong. 2007. 'Kainate seizures cause acute dendritic injury and actin depolymerization in vivo', *J Neurosci*, 27: 11604-13.
Zimmer, E. R., M. J. Parent, A. C. Cuello, S. Gauthier, and P. Rosa-Neto. 2014. 'MicroPET imaging and transgenic models: a blueprint for Alzheimer's disease clinical research', *Trends Neurosci*, 37: 629-41.

Acknowledgments

I thank Adriano Aguzzi for giving me time, equipment and inspiration to do experimental research.

Simone Hornemann, Silvia Sorce, Tiziana Sonati and Jeppe Falsig Petersen have provided great scientific support during my thesis.

I am grateful for Valeria Eckhardt and Daniel Kirschenbaum's friendship during my time in and outside the lab.

Elisabeth Rushing and Herbert Budka were fantastic supervisors during my neuropathological training who gave me space to continue my research but also broadened my horizon scientifically and personally.

Marco Bardelli and Luca Varani have continuously supported my work with a never-ending supply of reagents. Petra Schwarz and Rita Moos have given me the luxury of a 24/7 animal and antibody service.

The following people have further significantly – either personally or scientifically or both – enhanced the time during my PhD thesis (in arbitrary order): Caihong Zhu, Bei Li, Asvin Lakkaraju, Uli Herrmann, Mario Hermann, Daiji Sakata, Mirka Epskamp, Tina Kottharatil, Georg Meisl, Mario Nuvolone, Elke Schaper, Flavio Vasella, Marie-Angela Wulf, Alexander Küffer, Musa Hadzere, Alexander von Hoyningen, Adrian Müllner, Henning Leske, Veronika Kana, Agnes Lau, Claudia Scheckel, Marco Losa, Manfredi Carta, Renier Myburgh, Cesar Nombela Arrieta, Manuela Pfammatter, Ahmet Varol, Mirzet Delic, Regina Reimann, Marc Emmenegger, Sergey Yakushev, Tracy O'Connor, Badmavady Segarane, Paolo Dametto..

My PhD thesis was funded by the career development award "Forschungskredit 'Candoc'" from the University of Zurich as well as a research grant by the Theodor Ida Herzog-Egli Stifung.

There are dozens other people who were very helpful as well but I probably forgot to mention: please do not take it personally.

I thank my parents and my sister and my in-laws for being there in times of good and bad.

I thank my wife Victoria – this could not have worked without you.

Curriculum vitae

Given names: Karl Joachim
Family name: Frontzek
Date of birth: June 17th 1984
Citizen of Germany and Poland, married, no children

EDUCATION AND ACADEMIC DEGREES

02'2013-08'2017	Ph.D. degree (Dr. sc. nat), M.D./Ph.D. program at the University of Zurich (CH), Institute of Neuropathology
02'2013-08'2014	M.D. degree (Dr.med.), University of Basel (CH), Institute of Endocrinology
2011	License to practice medicine in Germany and Switzerland
2004-2010	University of Goettingen (D) Medical School

POSITIONS

2011-now	Resident in Neuropathology, University Hospital Zurich
2007-2011	Scientific Assistant, University of Goettingen (D), Laboratory of Molecular Gynecology

PROFESSIONAL MEMBERSHIPS

2013-now	German Society of Pathology

HONORS&GRANTS

2016	Research grant, Theodor Ida Herzog-Egli Stufung
2016	1st student prize, Latsis Symposium on Personalized Medicine
2015	Dissertation prize, University of Basel Medical School
2012-2013	Career development award, University of Zurich
2012	Young Investigator Award, European Stroke Organisation